TECHNICAL DIGEST
1995

OPTICAL AMPLIFIERS AND THEIR APPLICATIONS

15–17 JUNE 1995
DAVOS, SWITZERLAND

1995 TECHNICAL DIGEST SERIES
VOLUME 18

SPONSORED BY
OPTICAL SOCIETY OF AMERICA

DISCLAIMER NOTICE

THIS DOCUMENT IS BEST QUALITY AVAILABLE. THE COPY FURNISHED TO DTIC CONTAINED A SIGNIFICANT NUMBER OF PAGES WHICH DO NOT REPRODUCE LEGIBLY.

CONFERENCE EDITION

Summaries of the papers
presented at the topical meeting

OPTICAL AMPLIFIERS AND THEIR APPLICATIONS

15 June 1995, Davos, Switzerland

1995 Technical Digest Series
Volume 18

SPONSORED BY
Optical Society of America

COSPONSORED BY
IEEE/Lasers and Electro-Optics Society

IN COOPERATION WITH
European Physical Society: Quantum Electronics & Optics Division
European Optical Society
Swiss Physical Society

PARTIAL SUPPORT PROVIDED BY
Hewlett Packard and Corning, Inc.

2010 Massachusetts Avenue NW
Washington DC 20036-1023

Articles in this publication may be cited in other publications. To facilitate access to the original publication source, the following form for the citation is suggested:

Name of Author(s), "Title of Paper," in *Optical Amplifiers and their Applications*, Vol. 18, 1995 OSA Technical Digest Series (Optical Society of America, Washington DC, 1995), pp. xx-xx.

Optical Society of America

ISBN

Conference Edition	1-55752-405-X
Postconference Edition	1-55752-406-8
(Note: Postconference Edition includes postdeadline papers.)	
1995 Technical Digest Series	1-55752-368-1

Library of Congress Catalog Card Number

Conference Edition	95-68682
Postconference Edition	95-68683

Printed in the U.S.A.

Contents

Agenda of Sessions v
ThA Plenary Session 1
ThB Amplified Systems 7
ThC Pump Lasers 21
ThD Poster Session 31
ThE Amplifier Characterization 91
FA Semiconductor Devices and Functional Circuits 109
FB High-Rate and Short Pulse Systems 127
FC Amplifier Performance and Characteristics 149
FD Planar Waveguides 175
SaA Alternative Fiber Amplifiers 185
SaB WDM Networks and Systems 203
SaC Nonlinearities in Semiconductor Optical Amplifiers 225
Key to Authors and Presiders 247

OPTICAL AMPLIFIERS AND THEIR APPLICATIONS 1995
TECHNICAL PROGRAM COMMITTEE

GENERAL CHAIRS

William J. Miniscalco, *GTE Laboratories, Inc., U.S.A.*
Ikuo Mito, *NEC Corporation, Japan*
John J. O'Reilly, *University College London, U.K.*

EUROPEAN CHAIR

Hans Melchior, *Swiss Federal Institute of Technology, Switzerland*

PROGRAM CHAIRS

Robert Jopson, *AT&T Bell Laboratories, U.S.A.*
Kristian Stubkjaer, *Technical University of Denmark, Denmark*
Masuo Suyama, *Fujitsu Ltd., Japan*

SUBCOMMITTEE 1: FIBER AND ACTIVE WAVEGUIDES

Yasutake Ohishi, *NTT, Japan, Subcommittee Chair*
Douglas Baney, *Hewlett Packard, U.S.A.*
Steven Frisken, *Photonic Technologies Pty. Ltd., Australia*
Thierry Georges, *CNET, France*
Stephen Grubb, *AT&T Bell Laboratories, U.S.A.*
Kevin Malone, *NIST, U.S.A.*
Mark Newhouse, *Corning, Inc., U.S.A.*
Masayuki Nishimura, *Sumitomo, Japan*
Bo Pedersen, *NKT Research Center, Denmark*
Akira Wada, *Fujikura, Japan*
Tim Whitley, *BT Laboratories, U.K.*
Michael Zervas, *University of Southampton, U.K.*

SUBCOMMITTEE 2: SEMICONDUCTOR DEVICES AND FUNCTIONAL CIRCUITS

Mats Gustavsson, *LM Ericsson, Sweden, Subcommittee Chair*
Shigehisa Arai, *Tokyo Institute of Technology, Japan*
Francois Brillouet, *Alcatel Alsthom Recherche, France*
Tatsuo Kunii, *Oki Electric Industry Company, Japan*
Shinya Sasaki, *Hitachi, Japan*
Wayne Sharfin, *Lasertron, U.S.A.*
Luuk F. Tiemeijer, *Philips, The Netherlands*
Kerry J. Vahala, *California Institute of Technology, U.S.A.*
Hans G. Weber, *Heinrich-Hertz-Institut, Germany*
Jay M. Wiesenfeld, *AT&T Bell Laboratories, U.S.A.*

SUBCOMMITTEE 3: SYSTEMS AND NETWORKS

Neal Bergano, *AT&T Bell Laboratories, U.S.A., Subcommittee Chair*
Stephen B. Alexander, *Ciena Corporation, U.S.A.*
Jan Conradi, *Telecommunications Research Laboratories, Canada*
Noboru Edagawa, *KDD R&D Laboratories, Japan*
K. Emura, *NEC, Japan*
Evan Goldstein, *Bellcore, U.S.A.*
Masahiko Jinno, *NTT, Japan*
Sonny Johansson, *Ellemtel Telecom Systems Lab., Sweden*
Paul R. Morkle, *STC Submarine Systems, U.K.*
Michael G. Taylor, *BNR Europe Ltd., U.K.*

WEDNESDAY
14 JUNE 1995

FOYER

18:00–20:00
Registration

THURSDAY
15 JUNE 1995

FOYER

8:00–17:30
Registration/Speaker Check-in

THEATERSAAL

9:00–9:15
Opening Remarks
John O'Reilly, *University College London, U.K.*
Hans Melchior, *Swiss Federal Institute of Technology, Switzerland*

9:15–10:30
ThA • Plenary Session
Ikuo Mito, *NEC Corporation, Japan, Presider*

9:15 (Plenary)
ThA1 • Towards all-optical networks, John E. Midwinter, *Univ. College London, U.K.* Ever since the impressive properties of the EDFA were first reported, it has been recognized that the possibility exists that optical transmission might move beyond point-to-point or point-to-few-point transport to something much more exciting. In parallel, there has been much debate on the possibilities of "photonic switching," carrying the clear implication that photonics was soon to challenge electronics. Today we witness two lines of development for optical transport exploiting TDM and WDM, each having its limitations. The talk will compare these two approaches and discuss where each appears to fit within the evolving broadband network scenario. **(p. 2)**

10:00 (Invited)
ThA2 • Status and perspectives in optical amplifier standardization, Pietro Di Vita, *CSELT, Italy.* Optical amplifiers standardization activities are reviewed with reference to characterization parameters, integration in transmission system, and network aspects, with indications of the perspectives of development. **(p. 3)**

FOYER

10:30–11:00
Coffee Break/Exhibit

THEATERSAAL

11:00–12:30
ThB • Amplified Systems
Evan Goldstein, *Bellcore, U.S.A., Presider*

11:00 (Invited)
ThB1 • Deployment of fiber amplifier systems, Giorgio Grasso, *Pirelli Cavi S.p.A., Italy.* Details of the terrestrial installations of a 2.5 Gbit/s SONET line in U.S.A. and a 2.5 Gbit/s S.D.H. network in Italy are given together with the feedback from a one-year field operation of more than 1000 optical amplifiers. In addition, the present deployment plans for multiwavelength and single wavelength line amplifiers are presented. **(p. 8)**

11:30
ThB2 • Possibility for upgrade of the first installed optical amplifier system, R. A. Jensen, D. G. Duff, J. J. Risko, C. R. Davidson, *AT&T Bell Laboratories.* We demonstrate the potential to operate an installed undersea optical amplifier system at higher bit rates with only terminal modifications. Our results suggest acceptable transmission performance at data rates of up to 15.0 Gb/s using WDM techniques on an installed system designed to operate with a single NRZ channel at 2.5 Gb/s. **(p. 9)**

11:45
ThB3 • 120-channel AM-VSB signal transmission by two-wavelength multiplexing through gain flattened hybrid erbium-doped fiber amplifier, Masayuki Shigematsu, Motoki Kakui, Masayuki Nishimura, *Sumitomo Electric Industries, Ltd., Japan.* By using a hybrid EDFA with a flat gain over 17 nm, two-wavelength multiplexed AM-VSB signals were successfully transmitted without significant degradation of distortions. **(p. 13)**

12:00 (Invited)
ThB4 • Ultra-high-capacity amplified WDM lightwave systems, A. H. Gnauck, *AT&T Bell Laboratories.* Capacity upgrades in lightwave systems can be accomplished by increasing single-channel bit rates and by wavelength-division multiplexing (WDM) high-speed channels. This paper outlines the technical challenges facing amplified lightwave systems which incorporate WDM techniques to increase system capacity. It also reviews recent experiments which have pushed the throughput of an amplified optical-fiber link to one-third terabit/s. **(p. 17)**

12:30–14:00
Lunch Break (on your own)

THEATERSAAL

14:00–15:00

ThC • Pump Lasers

Heinz Meier, *IBM Zurich Laboratory, Switzerland, Presider*

14:00 (Invited)

ThC1 • New developments in 980-nm pump lasers, Wayne F. Sharfin, *Lasertron.* Recent advances in package and chip designs which result in increased power and spectral stability of 980-nm pump lasers for erbium-doped fiber amplifiers will be reviewed. The latest reliability data from devices operating in the field will also be discussed. **(p. 22)**

14:30

ThC2 • Near-ideal diffraction-limited beam from a 970-nm high-power angled-facet tapered semiconductor optical amplifier, S. H. Cho, S. Fox, S. A. Merritt, P. J. S. Heim, B. Gopalan, S. Kareenahalli, V. Vusirikala, C. E. C. Wood, M. Dagenais, *Univ. Maryland.* An angled-facet tapered semiconductor optical amplifier operating at 970 nm producing 2.6 W quasi-cw mode and 1.9 W cw with less than 5 mW coupled input power is reported. This amplifier is shown to produce a near-ideal diffraction-limited beam, with a beam quality factor M^2 of approximately 1.1. **(p. 24)**

14:45

ThC3 • 1.02-μm pump laser diodes with high power above 300 mW into single mode fiber, Mitsuru Sugo, Jiro Temmyo, Teruhiko Nishiya, Eiichi Kuramochi, Toshiaki Tamamura, *NTT Opto-Electronics Laboratories, Japan.* New 1.02-μm strained InGaAs pump laser diodes with small-divergence angles exhibit high coupling efficiency and high power above 300 mW into single-mode fiber. **(p. 28)**

CONGRESS CENTRE FOYER

15:00–16:15

ThD • Poster Session

ThD1 • Gain spectrum flattening of erbium-doped fiber amplifier using tapered fiber filter, A. V. Belov, E. M. Dianov, V. I. Karpov, A. V. Kurkov, V. N. Protopopov, M. Yu. Tsvetkov, *Fiber Optics Research Center, Russia;* A. N. Guryanov, V. F. Khopin, *Institute of Chemistry of High-Purity Substances, Russia;* W. H. Choe, S. J. Kim, *Samsung Advanced Institute of Technology, Korea.* Erbium-doped fiber amplifier with a newly developed fiber tapered filter showed a flat gain of 30 dB ± 1.5 dB in a spectral region of 35 nm. **(p. 32)**

ThD2 • Gain-peak-wavelength controllable erbium-doped fiber amplifier for long-haul WDM transmission, Youichi Fukada, Hideki Maeda, Yasutaka Ichihashi, *NTT Optical Network Systems Laboratories, Japan.* We propose a gain-peak-wavelength controllable erbium-doped fiber amplifier for cascaded use. The gain-peak-wavelength can shift from 1553 to 1557 nm under constant gain operation. **(p. 36)**

ThD3 • Full suppression of channel output power co-dependence in amplifiers, demonstrated in a two-wavelength system, Moira Stewart, Richard Epworth, *BNR Europe Limited, U.K.* A novel amplifier topology is described which suppresses channel co-dependence using gratings. Results are presented and compared to conventional amplifiers and benefits for networks discussed. **(p. 40)**

ThD4 • 1-W output power all-fiber laser-based Tm^{3+}-doped fluoride fiber, P. Bousselet, A. Marquant, F. Chiquet, I. Riant, J. L. Beylat, *Alcatel Alsthom Recherche, France.* Using an all-fiber architecture, 1W of output power has been obtained with a thulium-doped fluoride fiber laser. **(p. 44)**

ThD5 • EDFA gain equalization with fiber filter for WDM systems, Eric Saint Georges, *T. J. Watson IBM Research Center.* A complex fiber filter can achieve gain equalization, associated with SNR flatness over the whole EDFA bandwidth (more than 30 nm) and constant gain over a wide range of input power. Choice of the filter and simulation results are discussed. **(p. 48)**

ThD6 • Spectroscopic properties of Nd^{3+}-doped fluoride crystals for amplification at 1.3 μm, V. B. Sigachev, T. T. Basiev, M. E. Doroshenko, V. V. Osiko, A. G. Papashvili, *General Physics Institute, Russia.* For a number of neodymium-doped fluoride crystals both with regular and disordered structure the Judd-Ofelt analysis of absorption spectra has been performed, and fluorescence and lasing spectra were studied in order to reveal most promising materials for optical amplification in a 1.3-μm telecommunication window. **(p. 52)**

ThD7 • Optimization of bandgap wavelength of a semiconductor optical amplifier for cross index modulation at 1.55-μm wavelength, W. Schweiker, R. Schimpe, *Siemens AG, Germany.* The efficiency-spectrum for cross index modulation has been measured. For minimizing the (pump-) power for π-phase change, the wavelength for maximum unsaturated gain should be about 20 nm below the (probe-) wavelength of 1.55 μm. **(p. 56)**

ThD8 • Modeling of a semiconductor optical-amplifier-based nonlinear optical loop mirror for all-optical regeneration, L. Billes, I. Valiente, J. C. Simon, *France Telecom/CNET/LAB/RIO.* Modeling results of a semiconductor optical-amplifier-based nonlinear optical loop mirror are presented, with regard to applications in all-optical regeneration. **(p. 59)**

ThD9 • Receiver characteristics of two-section semiconductor optical amplifier transparent detectors for LANs applications, G. Giuliani, *Univ. Pavia, Italy;* P. Cinguino, V. Seano, *Centro Studi e Laboratori Telecomunicazioni SpA, Italy.* A two-section packaged SOA has been characterized as add-drop transparent receiver for optical LANs with measured receiver sensitivities of –18 dBm at 622 Mbit/s and –26.4 dBm at 155 Mbit/s. **(p. 63)**

ThD10 • Wavefront engineering—a novel antireflection design technique for travelling-wave semiconductor optical amplifiers, Wayne W. Lui, Katsuaki Magari, Kiyoyuki Yokoyama, *NTT Opto-Electronics Laboratories, Japan.* An antireflection design methodology based on wavefront engineering is proposed, which is afforded by a 2D Helmholtz equation solver from which valuable information on the reflected wave is readily extracted. **(p. 67)**

ThD11 • 2.5 Gbit/s transmission over 200 km of dispersion-shifted fiber using a spectrum-sliced fiber amplifier light source, Jung-Hee Han, Jae-Seung Lee, Sang-Soo Lee, Tae-Yeoul Yun, Hyang-Kyun Kim, Chang-Hee Lee, *Optical Transmission Section Electronics and Telecommunications Research Institute, Korea;* Sang-Yung Shin, *Korea Advanced Institute of Science and Technology, Korea.* We demonstrate a single channel 2.5-Gbit/s transmission over 200 km of dispersion-shifted fiber using a spectrum-sliced fiber amplifier light source. **(p. 73)**

ThD12 • Bidirectional transmission to reduce fiber FWM penalty in WDM lightwave systems, C. R. Giles, A. McCormick, *AT&T Laboratories.* Bidirectional transmission allows high WDM channel capacity while lessening deleterious four-wave mixing effects relative to those in unidirectional transmission. In a 4-channel, 2.5-Gbit/s NRZ WDM experiment, FWM degradation in a 100-km dispersion-shifted fiber span was eliminated through the use of bidirectional transmission. **(p. 76)**

ThD13 • Soliton transmission control with semiconductor amplifiers, Antonio Mecozzi, *Fondazione Ugo Bordoni, Italy.* The insertion of filters along a transmission line of negative dispersion in which loss is compensated by semiconductor amplifiers allows the propagation of stable soliton-like waveforms. Pattern effects due to the amplifiers are strongly reduced. **(p. 80)**

ThD14 • 9,000-km WDM transmission of three 2.5-Gbit/s channels covering a 5-nm wavelength range and using no pre-emphasis, S.-H. Huang, X. Y. Zou, A. E. Willner, *Univ. Southern California.* We demonstrate near-error-free optical transmission of three 2.5 Gbit/s WDM channels through 9,000 km of dispersion-shifted fiber by using a recirculating loop. The wide wavelength range of the channels is 5 nm. These channels are transmitted off the 1560-nm peak, and no pre-emphasis of the channels is required. **(p. 84)**

ThD15 • Unregenerated single-channel transmission at 10 Gbit/s over 300-km standard fiber, Bo Foged Jørgensen, Rune J. S. Pedersen, *Technical Univ. Denmark.* We demonstrate experimentally unregenerated single-channel transmission at 10 Gbit/s over the record length of 300.4 km in a 1.55-μm standard single-mode fiber system with two optical in-line amplifiers. **(p. 88)**

THEATERSAAL

16:15–17:30

ThE • Amplifier Characterization

Douglas Baney, *Hewlett Packard Laboratories, U.S.A., Presider*

16:15

ThE1 • Inhomogeneous gain saturation of erbium-doped fiber amplifiers, H. Chou, J. Stimple, *Hewlett-Packard Company.* We demonstrate the characterization of the inhomogeneous gain saturation of an Er-doped fiber amplifier using the time-domain extinction technique. **(p. 92)**

16:30

ThE2 • Noise figure increase of high concentration erbium-doped fiber amplifiers pumped by a 1.48-μm or 0.98-μm laser diode, Hiroji Masuda, Kazuo Aida, *NTT Optical Network Systems Laboratories, Japan.* Noise figure increased from 3.2 dB (4.5 dB) at 500 ppm to 4.2 dB (6.1 dB) at 8,800 ppm with 0.98-μm (1.48-μm) pumping. **(p. 96)**

16:45

ThE3 • Nanosecond kinetics of upconversion process in EDF and its effect on EDFA performance, P. Myslinski, J. Fraser, J. Chrostowski, *National Research Council, Canada.* The experimental study of the dynamics of erbium ion interactions in EDFA is presented. The lifetime of the excited ion pairs/clusters is determined to be about 50 ns, much shorter than currently assumed in the literature. **(p. 100)**

17:00 (Invited)

ThE4 • Reliability of fluoride fibers for use in fiber amplifiers, Kazuo Fujiura, *NTT Opto-Electronics Laboratories, Japan.* With a view to applications in practical optical systems, this paper reviews both the reliability of rare-earth-doped fluoride fibers for use in fiber amplifiers and recent studies on their predicted lifetime in practical environments. **(p. 104)**

18:00–20:00

Conference Banquet

FOYER

8:00–17:30
Registration/Speaker Check-in

THEATERSAAL

9:00–10:30
FA • Semiconductor Devices and Functional Circuits
Francois Brillouet, *Alcatel Alsthom Recherche, France, Presider*

9:00 (Invited)
FA1 • New developments in OEICs, U. Koren, *AT&T Bell Laboratories, U.S.A.* Recent progress in designing semiconductor optical amplifiers as elements in optoelectronic integrated circuits such as WDM transceivers, as well as for FTTL (fiber to the loop) applications is discussed. The incorporation of quantum well amplifiers with polarization insensitivity and broad spectral gain, and the integration of waveguide beam expanders for easier packaging are described. **(p. 110)**

9:30
FA2 • Dynamic effects in integrated 4 × 4 InGaAsP/InP semiconductor optical gate amplifier switch matrices, Lars Gillner, *Ericsson Components AB, Sweden;* Eilert Berglind, *Royal Institute of Technology, Sweden;* Claus Popp Larsen, *L. M. Ericsson A/S, Denmark;* Erland Almström, *Ellemtel Utvecklings-AB, Sweden.* Integrated 4 × 4 InP amplifier gate switch arrays are analyzed with respect to dynamic gain saturation and residual reflections within the chip. Comparison with measurements is made. **(p. 111)**

9:45
FA3 • Polarization-resolved, complete noise characterization of bulk ridge waveguide semiconductor optical amplifiers, Ch. Holtmann, P. A. Besse, H. Melchior, *Swiss Federal Institute of Technology, Switzerland.* A realistic noise figure model for pigtailed SOAs, accounting for polarization imbalances, is presented and applied experimentally in 10°-tilted, antireflection-coated bulk ridge-waveguide SOAs. **(p. 115)**

10:00
FA4 • Polarization independent 1550-nm semiconductor optical amplifier packaged module with 29 dB fiber-to-fiber gain, P. Doussiere, F. Pommerau, R. Ngo, M. Goix, T. Fillion, P. Bousselet, *Alcatel Alsthom Recherche, France;* G. Laube, *Alcatel-SEL Research Center, Germany.* Based on tapered amplifier structure and YAG welding technique a highly performant semiconductor optical amplifier packaged module is reported. **(p. 119)**

10:15
FA5 • Performance of cascaded 1300-nm QW laser amplifiers in 10 Gbit/s long-haul NRZ transmission, Jean G. L. Jennen, *Eindhoven Univ. Technology, The Netherlands;* Luuk F. Tiemeijer, Coen T. H. F. Liedenbaum, John J. E. Reid, *Philips Optoelectronics Centre, The Netherlands;* Hugo de Waardt, *PTT Research, The Netherlands.* 10-Gbit/s long-haul 1300-nm NRZ transmission using QWLA repeaters is analyzed numerically. Using a recent 200-km experiment as calibration, extention to 450 km is discussed. **(p. 123)**

FOYER

10:30–11:00
Coffee Break/Exhibit

THEATERSAAL

11:00–12:30
FB • High-Rate and Short Pulse Systems
Neal Bergano, *AT&T Bell Laboratories, U.S.A., Presider*

11:00 (Invited)
FB1 • Soliton transmission with sliding-frequency guiding filters: progress toward 100 Gbit/s over transoceanic distances, P. V. Mamyshev, L. F. Mollenauer, *AT&T Bell Laboratories, U.S.A.* The technique of sliding-frequency guiding filters has enabled extremely robust, error-free transmission at single channel rates of 10 to 20 Gbit/s, over distances often approaching the circumference of the earth. Soliton transmission using filters has also enabled 40 Gbit/s, in the form of an 8 × 5 Gbit/s WDM transmission over 9600 km. We describe problems and progress toward extension of filtered soliton transmission to many WDM channels at 10 Gbit/s each. **(p. 128)**

11:30
FB2 • Soliton transmission at high bit rates through distributed erbium-doped fibers, Christian Lester, Karsten Rottwitt, *Technical Univ. Denmark;* Kent Bertilsson, Peter A. Andrekson, *Chalmers Univ. Technology, Sweden;* Mark A. Newhouse, A. J. Antos, *Corning, Inc., U.S.A.* The utility of distributed erbium-doped fibers for soliton transmission is studied. Stable soliton propagation over a span with a 90-km pump station separation is demonstrated. **(p. 132)**

11:45
FB3 • Optical filtering technique for suppressing nonlinear pulse distortion caused by long transmission distance, Ken-ichi Suzuki, Katsumi Iwatsuki, Shigendo Nishi, *NTT Optical Network Systems Laboratories, Japan.* We demonstrate the nonlinear pulse transmission near the zero dispersion wavelength with optical filtering to suppress the pulse distortion at the trailing edge. While the pulses move to the anomalous dispersion region, the dispersive wave at the pulse trailing edge remains around the normal dispersion region, and thus can be removed by optical filtering. **(p. 136)**

12:00
FB4 • 10-Gbit/s signal transmission in a 1600-km line employing distributed erbium-doped fiber to suppress the nonlinear effect, H. Kawakami, T. Kataoka, *NTT Optical Network Systems Laboratories, Japan.* We propose a new in-line amplifier system that suppresses the nonlinear effect. A 10-Gbit/s signal transmission in a 1600 km was demonstrated. **(p. 140)**

12:15
FB5 • Long-haul transmission using actual optical amplifier submarine cable systems, Toshio Kawazawa, Koji Goto, Tomohiro Otani, Haruo Abe, Masando Tanaka, Hitoshi Yamamoto, Hiroharu Wakabayashi, *KDD Submarine Cable Systems Department, Japan.* We have successfully conducted the 5.3-Gbit/s optical signal error-free transmission over 4,000 km with 85 km optical amplifier spacing and 11,300 km with 60 km spacing, respectively. **(p. 144)**

12:30–14:00
Lunch Break (on your own)

THEATERSAAL

14:00–15:30
FC • Amplifier Performance and Characteristics
Michael N. Zervas, *Southampton University, U.K., Presider*

14:00
FC1 • A low-cost intrinsically low-distortion EDFA design for AM-CATV applications with a wide input power and wavelength range, F. W. Willems, J. C. van der Plaats, *AT&T Network Systems Nederland B.V., The Netherlands;* D. J. DiGiovanni, M. J. Andrejco, P. Wysocki, J. Aspell, *AT&T Bell Laboratories.* We present a 980-nm pumped low-cost EDFA design for AM-CATV applications with intrinsic low distortion and noise-figure over a wide input power and wavelength range using optimized erbium-doped fiber. **(p. 150)**

14:15
FC2 • AC gain tilt variations with gain compression in erbium-doped fiber amplifiers, J. Nilsson, S. J. Kim, S. H. Lee, W. H. Choe, *Samsung Advanced Institute of Technology, Korea.* We have measured AC gain tilt changes resulting from gain variations in erbium-doped fiber amplifiers. The result agrees with a theoretical expression in some wavelength ranges, but not in others. **(p. 154)**

14:30
FC3 • Novel configuration for low-noise and wide-dynamic-range Er-doped fiber amplifier for WDM systems, Y. Sugaya, S. Kinoshita, T. Chikama, *Fujitsu Laboratories Ltd., Japan.* We propose a two-stage novel configuration of an EDFA for WDM systems, which achieves gain flatness and low noise with a wide input dynamic range. **(p. 158)**

14:45
FC4 • Single-stage booster amplifier with two 980-nm pumps stabilized by fiber gratings, G. R. Jacobovitz-Veselka, P. Wysocki, A. M. Vengsarkar, T. Erdogan, V. Mizrahi, J. Borick, *AT&T Bell Laboratories;* S. W. Granlund, *AT&T Bell Laboratories STC.* We present a co- and counter-propagating 980-nm pumped Er-doped fiber booster amplifier, which does not require isolators or temperature control to stabilize the pumps. **(p. 162)**

15:00
FC5 • Suppression of residual amplitude modulation using highly saturated erbium-doped fiber amplifiers, P. B. Hansen, L. Eskildsen, J. Alphonsus, D. Truxal, *AT&T Bell Laboratories.* A highly saturated fiber amplifier with a 25-kHz response is employed to reduce a 3.5-dB power penalty from residual amplitude modulation due to wavelength dithering to only 0.2 dB. **(p. 166)**

15:15
FC6 • Polarization-maintaining erbium-doped optical fiber amplifier, T. Sakai, K. Himeno, S. Okude, A. Wada, R. Yamauchi, *Fujikura Ltd., Japan.* A polarization-maintaining EDF with a PANDA structure has been developed. Gain more than 30 dB is achieved with an extinction ratio better than 30 dB. **(p. 170)**

FOYER

15:30–16:00
Coffee Break/Exhibit

THEATERSAAL

16:00–17:00
Product Presentations

THEATERSAAL

17:00–17:45
FD • Planar Waveguides
Kevin Malone, *NIST, U.S.A., Presider*

17:00 (Invited)
FD1 • The erbium-doped planar amplifiers: from laboratory to local loop, Martin Hempstead, *Univ. Southampton, U.K.* The status of research into planar erbium-doped waveguide amplifiers, highlighting the challenges and prospects through examination of a typical application is reviewed. **(p. 176)**

17:30
FD2 • Ion-exchanged waveguide amplifier in erbium-doped glass for broadband communications, Patrice Camy, Pascale Laborde, Christian Lerminiaux, *Corning Europe Inc., France;* José E. Román, Martin Hempstead, *Univ. Southampton, U.K.* We discuss the fabrication, characterization, and modeling of planar erbium-doped amplifiers realized as ion-exchanged waveguides in glass. **(p. 181)**

17:45–20:00
Dinner Break

THEATERSAAL

20:00
Rump Session

SATURDAY
17 JUNE 1995

FOYER

8:00–15:30
Registration/Speaker Check-in

THEATERSAAL

8:45–10:30
SaA • Alternative Fiber Amplifiers
Thierry Georges, *France Telecom, Presider*

8:45 (Invited)
SaA1 • 1.3-μm cascaded Raman amplifiers, Stephen G. Grubb, *AT&T Bell Laboratories, U.S.A.* A novel cascaded Raman resonator approach has been used to utilize high-power, fiber-coupled pump sources in the 1-μm region to amplify signals at 1.3 μm in germanosilicate fibers. Gains of 40 dB and output powers of +24.6 dBm have been achieved. The first successful digital transmission test of a 1.3-μm Raman amplifier has also been completed. **(p. 186)**

9:15
SaA2 • Raman amplifier for 1.3 μm on the base of low-loss high-germanium-doped silica fibers, E. M. Dianov, A. A. Abramov, M. M. Bubnov, A. V. Shipulin, S. L. Semjonov, A. G. Schebunjaev, *General Physics Institute, Russia;* A. N. Guryanov, V. F. Khopin, *Institute of Chemistry of High-Purity Substances, Russia.* A 1.3-μm Raman amplifier based on the low-loss high-germanium-doped silica fibers with gain coefficients comparable to the same ones of the conventional Pr-doped fluoride fiber amplifiers is reported. **(p. 189)**

9:30
SaA3 • Fiber optical parametric amplifier operating near zero-dispersion wavelength, N. Kagi, T. K. Chiang, L. G. Kazovsky, *Stanford Univ.;* M. E. Marhic, *Northwestern Univ.* We investigated theoretically and experimentally the gain spectrum and the saturation characteristics of a fiber optical parametric amplifier operating near zero-dispersion wavelength. **(p. 193)**

9:45
SaA4 • High-power 1.48-μm cascaded Raman laser in germanosilicate fibers, S. G. Grubb, T. Strasser, W. Y. Cheung, W. A. Reed, V. Mizrahi, T. Erdogan, P. J. Lemaire, A. M. Vengsarkar, D. J. DiGiovanni, D. W. Peckham, *AT&T Laboratories;* B. H. Rockney, *Polaroid Corporation.* We report cw, diode-pumped fiber laser output at 1.48 μm from a multiple-order cascaded Raman laser. An output power of 1.5 W has been obtained when pumping with a diode-pumped Yb^{3+} cladding-pumped fiber laser. **(p. 197)**

10:00 (Invited)
SaA5 • Towards pump-efficient 1.3-μm fiber amplifiers, David N. Payne, R. I. Laming, D. W. Hewak, *Univ. Southampton, U.K.* The route to pump-efficient 1.3-μm fiber amplifiers depends on the development of new host glasses having carefully tailored properties. Progress on amplifiers based on a range of new glasses doped with Nd, Pr, or Dy is reviewed, together with prospects for the future. **(p. 200)**

FOYER

10:30–11:00
Coffee Break/Exhibit

THEATERSAAL

11:00–12:30
SaB • WDM Networks and Systems
Paul Morkle, *STC Submarine Systems, U.K., Presider*

11:00 (Invited)
SaB1 • Wavelength-division multiplexed networks, Hiromu Toba, Kazuhiro Oda, Kyo Inoue, *NTT Optical Network Systems Laboratories, Japan.* WDM-based transport network configurations are reviewed and major technological issues that determine network scale are described. A recently developed WDM ring network test bed is also reported. **(p. 204)**

11:30
SaB2 • Effect of amplifier gain shape on optical nonlinearity penalties, Fabrizio Forghieri, R. W. Tkach, A. R. Chraplyvy, J. A. Nagel, *AT&T Bell Laboratories.* Optical nonlinearity penalties in a long-haul WDM system with non-flat-gain amplifiers are investigated by computer simulations. It is shown that the benefits of using pre-emphasis can be limited by optical nonlinearities. **(p. 208)**

11:45
SaB3 • Suppression of Raman cross talk in WDM systems, Fabrizio Forghieri, R. W. Tkach, A. R. Chraplyvy, *AT&T Bell Laboratories.* A technique based on power equalization at amplifiers is shown to relax the capacity limitation due to stimulated Raman scattering in wavelength-division-multiplexed transcontinental optical networks by an order of magnitude. **(p. 212)**

12:00
SaB4 • Optimum gain equalization for WDM in-line multistage amplifier systems, Mitsunori Fukutoku, Kazuhiro Oda, Hiromu Toba, *NTT Optical Network Systems Laboratories, Japan.* We propose a simple method for optimizing amplifier gain equalization focusing on the position of gain equalizers and pre-emphasis of the input signal power. **(p. 216)**

12:15
SaB5 • 8 × 10 Gbit/s repeaterless transmission over 150 km of dispersion-shifted fiber using fluoride-based amplifiers, B. Clesca, S. Artigaud, L. Pierre, J.-P. Thiery, *Alcatel Alsthom Recherche, France.* Using wideband power and preamplifiers, repeaterless 8 × 10 Gbit/s transmission is performed over 150 km of dispersion-shifted fiber with limited four-wave mixing penalty. **(p. 220)**

12:30–14:00
Lunch Break (on your own)

THEATERSAAL

14:00–15:45
SaC • Nonlinearities in Semiconductor Optical Amplifiers
Luuk F. Tiemeijer, *Philips Optoelectronics Center, The Netherlands, Presider*

14:00 (Invited)
SaC1 • Applications of high-speed nonlinearities of semiconductor amplifiers, R. J. Manning, D. A. O. Davies, A. D. Ellis, D. M. Patrick, *BT Laboratories, U.K.* We describe advances in the development of a high-speed all-optical regenerator made entirely from semiconductor amplifiers. **(p. 226)**

14:30

SaC2 • Femtosecond pulse amplification and cross-phase modulation in semiconductor laser amplifiers—theory and experiment, A. Dienes, J. P. Heritage, M. Y. Hong, *UC–Davis;* P. J. Delfyett, *Univ. Central Florida.* Amplification and cross-phase modulation experiments in two different semiconductor laser amplifiers are reported and explained by our model, which includes fast nonlinearities and gain dispersion. **(p. 230)**

14:45

SaC3 • Saturation and gain dispersion effects on four-wave mixing in semiconductor laser amplifiers, I. Koltchanov, S. Kindt, K. Petermann, *Institut für Hochfrequenztechnik, Germany;* S. Diez, R. Ludwig, R. Schnabel, H. G. Weber, *Heinrich-Hertz-Institut für Nachrichtentechnik, Germany;* R. Schimpe, G. Kristen, *Siemens AG, Germany.* FWM experiments in a wide range of input powers (30 dB) and detunings (5 THz) are explained by a new analytical theory including the gain difference of the participating waves and the nonproportionality of the nonlinear susceptibility and the gain(s). **(p. 234)**

15:00 (Invited)

SaC4 • Wavelength conversion using interferometric structures containing semiconductor optical amplifiers, B. Mikkelsen, T. Durhuus, C. Joergensen, S. L. Danielsen, R. J. S. Pedersen, K. E. Stubkjaer, *Technical Univ. Denmark.* The principle of operation of wavelength converters based on interferometric structures employing SOAs as optical phase shifters is discussed. Results for monolithic integrated structures such as Mach–Zehnder and Michelson interferometers are presented. **(p. 238)**

15:30

SaC5 • Optical buffering at 10 Gbit/s employing a monolithically integrated all-optical interferometric Michelson wavelength converter, S. L. Danielsen, B. Mikkelsen, C. Joergensen, T. Durhuus, K. E. Stubkjaer, *Technical Univ. Denmark.* Optical cell buffering at 10 Gbit/s is accomplished with a novel simple multi-wavelength fiber loop memory technique. It is based on wavelength conversion by a monolithically integrated Michelson interferometer employing semiconductor optical amplifiers. **(p. 242)**

15:45–16:15

Coffee Break

16:15–18:15

Postdeadline Paper Session

18:15–18:30

Closing Remarks

William Miniscalco, *GTE Laboratories, Inc., U.S.A.*

Plenary Session

ThA 9:15-10:30
Theatersaal

Ikuo Mito, *Presider*
NEC Corporation, Japan

Toward All-Optical Networks

John E. Midwinter
University of College London
Torrington Place, London, England, U.K.

Ever since the impressive properties of the EDFA were first reported, it has been recognized that the possibility exists that optical transmission might move beyond point-to-point or point-to-few-point transport to something much more exciting. In parallel, there has been much debate on the possibilities of "photonic switching," carrying the clear implication that photonics was soon to challenge electronics. Today we witness two lines of development for optical transport exploiting TDM and WDM, each having its limitations. The talk will compare these two approaches and discuss where each appears to fit within the evolving broadband network scenario.

STATUS AND PERSPECTIVES IN OPTICAL AMPLIFIERS STANDARDISATION

Pietro Di Vita

CSELT
Via Reiss Romoli 274 - Torino - Italy
Tel. +39 11 228 5278 - Fax: +39 11 228 5085

1. Introduction

The rapid development occurred in the last years in the field of Optical Amplifiers (OAs) urged soon a proper standardisation. In particular, since the beginning, it was recognised that a consistent development of norms concerning both OAs and their applications (particularly regarding transmission systems) represents a key condition for a rational evolution of telecommunication networks employing this new component. In this respect OA standardisation activities, started in the proper National and International Committees more than four years ago, were and are still pushed by two basic motivations. The first one rises from the need to establish the requirements necessary to guarantee uniform functional characteristics of the different components, thus ensuring their compatibility in the various assemblages. The second one comes from the need to specify those aspects ensuring a proper integration of OAs in the telecommunication networks.

Due to the rapid development of OAs and related applications, the standardisation in this field requires a judicious progressive setting of norms, balancing the market needs and the exigency of avoiding possible distortions of further progress.

OA standardisation developed so far mainly concern Optical Fibre Amplifiers (OFAs), and in particular Erbium-doped (silica based) fibre amplifiers, which represent a quite consolidated product largely diffused in the market. However, other kinds of OAs (e.g. semiconductor OAs or fluoride glass based OFAs) are not intended to be excluded. Once sufficiently mature, they can be included either in the existing documents or in new dedicated ones.

Two International Standardisation Bodies are currently active on OAs: ITU-T (formerly CCITT), which generally is more oriented toward the applications in the field of telecommunications, and IEC, which is prevalently oriented to the product. These Bodies act at world level and have (formal or informal) liaisons with corresponding regional Bodies (as, e.g., ETSI at European level). In order to avoid inconsistencies as far as possible, ITU-T and IEC have set-up official liaisons which, in the case of OAs, work very effectively. In general, ITU-T issues Recommendations which, although not having the strength of norms, are taken worldwide in the maximum consideration. IEC generally emanates International Standards with the strength of norms for its Country members. Figure 1 shows the structure of ITU-T and IEC Groups involved in OAs standardisation.

Three directions, considered in the subsequent sections, are followed in OAs standardisation: the first consists in providing appropriate definitions and consistent test procedures for the characterisation of OA parameters; the second consists in identifying the specifiable characteristics necessary in the various OA applications; the third is directly related to the introduction of the OAs in the various kinds of transmission networks and includes the specification of allowed value ranges for the relevant parameters.

2. Standardisation of OA relevant parameters

A number of parameters relevant for a proper specification of the functional requirements of OAs from the users point of view were identified. They include both transmission parameters (Gain, Input and output signal power, Noise, Reflectance, Pump leakage and Out-of-band insertion loss parameters); and non-transmissive parameters (Mechanical, Environmental, Safety and Reliability parameters). Their definitions are contained in two ITU-T Recommendations [1, 2] and one draft IEC Generic Specification [3]. Concerning the recommended test methods for these parameters, thanks to an agreement between the ITU-T and IEC OA Groups, they are developed by IEC only while ITU-T refers to the corresponding IEC Documents. Nine IEC Basic Specifications for OFA test methods [4] (concerning Gain, Optical Power, Noise, Pump leakage and Out-of-band insertion loss parameters) have been developed so far and some others are under preparation.

An effort has been produced by ETSI in order to extend all these parameter definitions and test methods from OFAs to semiconductor OAs [5].

3. Specification of OA characteristics

Concerning OAs in general, the following two fundamental classes were identified [2]:

- OA devices (intended as stand-alone OAs), subdivided according to the application in
  - Power Amplifiers; *- Pre-Amplifiers,* *- Line Amplifiers,*
- OA sub-systems (intended as integrated OAs), subdivided in
  - Optically Amplified Transmitters, *- Optically Amplified Receivers.*

A general criterion of specification of OA characteristics is to ensure the maximum possible compatibility with the existing system ITU-T Recommendations [6, 7]. However, such a compatibility is possible in principle for OA devices only (with a possible restriction on the operating wavelength range), provided that the OA devices inserted along an optical path shall be considered between the reference points S and R defined in ITU-T Recommendations for line terminals and regenerators [6, 7], as shown in the scheme of Fig. 2. (Note that the input and output characteristics of the OA device shall be specified at the reference points R' and S', before and after the OA device, respectively).

For OA sub-systems, on the contrary, the integration with the transmitter or the receiver imply that the internal connection is proprietary and cannot be specified. Consequently, a reference point S (R) only can be defined for the specification of the output (input) characteristics of an optically amplified transmitter (receiver), after (before) the OA, as shown in Figure 3. The compatibility with existing ITU-T Recommendations on line systems is therefore much more difficult, and this urged the preparation, still in progress, of following new ITU-T Recommendations on line systems using OAs (provisional denomination):

- G.SCS (for optically amplified single-channel long distance line systems),
- G.MCS (for optically amplified multi-channel long distance line systems),
- G.LON (for the functional characteristics of optically amplified interoffice line systems)
- G.OASS (for optically amplified submarine line systems).

Finally, a minimum list of relevant parameters to be specified for each category of OA devices or sub-systems is either already provided (by ITU-T [2]) or under preparation (by IEC, in the form of future OFA Blank Detail Specifications).

4. Specification of OAs in optical networks

The standardisation of those aspects directly related to the introduction of the OAs in the various kinds of transmission networks has started recently. In particular ITU-T is preparing a Recommendation (provisionally denominated G.OA3) on application-related aspects of OA devices and sub-systems which should address transmission, maintenance, optical safety and environmental conditions (e.g. climatic and EMC/ESD) aspects as well as the allowed value ranges for generic parameters of OA devices (e.g. power and wavelength value ranges).

The possible "secondary" effects induced by OAs on optical fibre systems shall also be considered, including optical non-linearities, polarisation and chromatic dispersion, noise accumulation, etc., and indicating the onset conditions, the limitations imposed to the transmission and how to overcome these limitations.

Those aspects more specific to each kind of system applications are being developed in the mentioned ITU-T Recommendations G.SCS, G.MCS, G.LON and G.OASS. Different approaches will be considered for systems which include or do not include line OAs, due the substantial differences in the OA supervision systems (for monitoring purposes, alarm transfer, etc.). However, the standardisation of the supervisory channel for line OAs is currently strongly debated and various positions (e.g. considering in-band or out-of-band channels, supervisory channel information capacity, actual set of supervisory signal, etc.) are being confronted.

Concerning the introduction of OAs in optical access networks, ETSI developed recently a Standard about this kind of networks [8], suggesting some useful normative criteria of insertion of OA devices and sub-systems in this case.

6. Conclusions

In the current globalisation of the economy, Telecom operators and manufacturers need to deploy common solutions. In this scenario the role of standardisation is fundamental. This is particularly true for OAs, a new component which has introduced an authentic revolution in the already recent technology of optical communications. Standardisation will have a key relevance in the development of OAs in the transmission networks as well as in the innovative applications that they make possible.

According to the status of OA standardisation outlined in this paper, it is evident that a considerable amount of work has been done leading to a number of consolidated documents. The aspect of identification of the key characterising OA parameters has been abundantly developed, while the one concerning the OA characteristics is going to be fulfilled. However, additional work is still needed, particularly for the development of norms concerning the introduction of the OAs in the various networks: activities in this direction are in progress.

References

1. ITU-T Recommendation G.661 (1993) *Definition and test methods of the relevant generic parameters of OFAs*
2. ITU-T Recommendation G.662 (1995) *Generic characteristics of OFA devices and sub-systems*
3. IEC Document 1291-1 (Draft 1995) *Generic specification - OFAs*
4. IEC Documents 1290 Series (Draft 1995) *Basic specifications for OFA test methods*
5. ETSI European Telecommunication Standard DE/TM-1034 (Draft 1995) *Relevant generic characteristics of OA devices and sub-systems*

6. ITU-T Recommendation G.955 (1993) *Digital line systems based on the 1 544 kbit/s and the 2 048 kbit/s hierarchy on optical fibre cables*
7. ITU-T Recommendation G.957 (1995) *Optical interfaces for equipments and systems relating to the synchronous digital hierarchy*
8. ETSI European Telecommunication Standard DE/TM-1009 (Draft 1995) *Optical distribution network for optical access network*

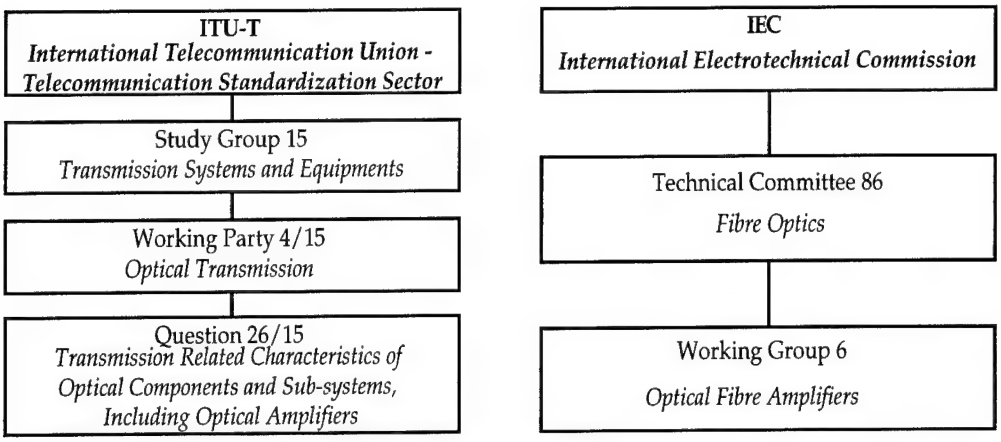

Figure 1- Structure of ITU-T and IEC Groups for OA Standardisation

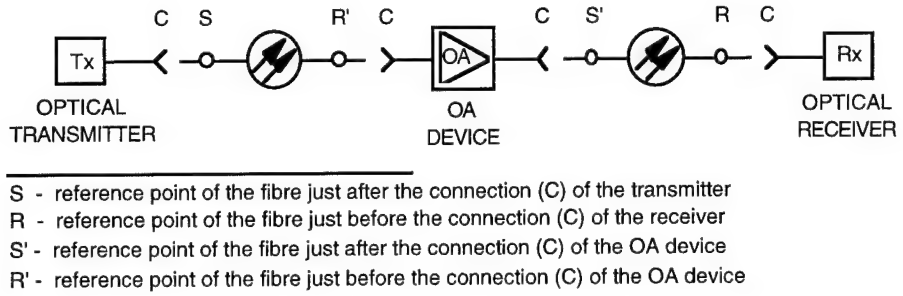

Figure 2 - Scheme of insertion of an OA device

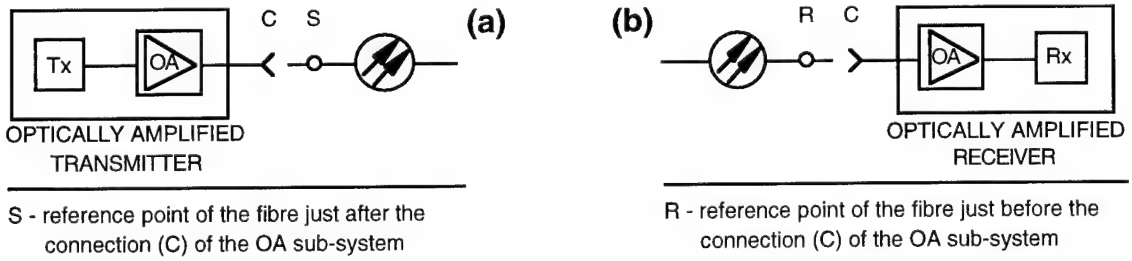

Figure 3 - Scheme of insertion of OA sub-systems: (a) Optically amplified transmitter, (b) Optically amplified receiver

Thursday, June 15, 1995

Amplified Systems

ThB 11:00-12:30
Theatersaal

Evan Goldstein, *Presider*
Bellcore, U.S.A.

Deployment of Fiber Amplifier Systems

Giorgio Grasso
Pirelli Cables Corp.
Wiale Sarca 202, Milano, Italy 20126

Details of the terrestrial installations of a 2.5 Gbit/s SONET line in U.S.A. and a 2.5 Gbit/s S.D.H. network in Italy are given together with the feedback from a one-year field operation of more than 1000 optical amplifiers. In addition, the present deployment plans for multiwavelength and single wavelength line amplifiers are presented.

Possibility For Upgrade Of The First Installed Optical Amplifier System

R. A. Jensen, D. G. Duff, J. J. Risko, and C. R. Davidson

AT&T Bell Laboratories, Crawfords Corner Road, Holmdel NJ 07733
Tel (908)-949-1024 fax (908)-949-2031 raj2@hogpa.att.com

1. Introduction

We demonstrate the potential to operate an installed undersea optical amplifier system at higher bit rates with only terminal modifications. Our results suggest acceptable transmission performance at data rates of up to 15.0 Gb/s using WDM techniques on an installed system designed to operate with a single NRZ channel at 2.5 Gb/s.

This paper reports the results of field measurements done on the 2100 km optically amplified segment of the Columbus-II undersea system, which is the worlds longest commercially operating optically amplified system. Wavelength Division Multiplexing (WDM) and single channel transmission experiments were done at 2100 and 4200 km.

2. Overview of the Columbus-2B Segment

The Columbus-2B segment connects West Palm Beach, FL and Magen's Bay, Saint Thomas, USVI. The 2100 km segment contains two fiber pairs and 26 repeaters with an average span length of 80 km. Each line pair operates with a 2.5 Gb/s NRZ single channel at 1558.5 nm. The nominal repeater output power is about +5.0 dBm with a gain of 18.0 dB and average noise figure of 5.7 dB.

To reduce the impairments caused by non-linearities a dispersion management scheme is used. The segment consists of dispersion shifted fiber with an average λ_0 of about 1560.5 nm with 4 short sections of conventional fiber for dispersion compensation at roughly equal intervals along the line. The cumulative dispersion at the signal wavelength is approximately zero after each compensating fiber.

4. Results of Transmission Experiments

The 2100 km transmission experiments were done with the undersea plant in its normal service configuration. The system performance was determined using Q measurements[1]. (A Q measurement of 15.6 dB corresponds to a Bit Error Ratio (BER) of about 10^{-9} while a Q of 19.0 dB corresponds to a BER of about 10^{-19}.) Table 1 compares the 2100 km measurements and simulations for both single and multi-channel WDM.

The 2100 km channel results show that virtually error free transmission was measured at 5.0 Gb/s using a single 5.0 Gb/s channel, at 10.0 Gb/s using 2 X 5.0 Gb/s channels, and at 15.0 Gb/s using 3 X 5.0 Gb/s channels.

Columbus-2B Line Pair 1 2100 km Results Summary			
Number of Channels X Bit Rate per Channel	Total Bit Rate (Gb/s)	Measured Average Q (dB)	Simulated Average Q (dB)
1 X 2.5 Gb/s	2.5	25.7	25.9
1 X 5.0 Gb/s	5.0	22.5	23.0
2 X 5.0 Gb/s	10.0	21.6	21.1
3 X 5.0 Gb/s	15.0	19.0	20.0

Table 1: 2100 km Results Summary

The 4200 km experiments were done by looping one fiber pair at Magen's Bay. Table 2 compares the 4200 km measurements and simulations for both single and multi-channel WDM.

The 4200 km results show that acceptable 2.5 Gb/s and 5.0 Gb/s long term operation of the segment can be achieved using a single 2.5 Gb/s or 5.0 Gb/s channel. Good transmission performance was also measured for 7.5 Gb/s using 3 X 2.5 Gb/s channels, 10.0 Gb/s using 2 X 5.0 Gb/s and 15.0 Gb/s using 3 X 5.0 Gb/s channels.

A plot of both the 2100 and 4200 km results, expressed as bitrate distance products, is shown in Figure 1. Comparing the WDM results to the single channel results for similar bit rates show the WDM system to have better transmission performance for equivalent overall transmission capacity.

Unequal channel spacing was used for three channel experiment to reduce the effects of four wave mixing interference between channels. Pre-equalization of the input channels was required also to correct for the non-ideal gain characteristics of the amplifier chain.

Columbus-2B Line Pair 1 4200 km Results Summary		
Number of Channels X Bit Rate per Channel	Measured Average Q (dB)	Simulated Average Q (dB)
1 X 2.5 Gb/s	21.0	22.7
1 X 5.0 Gb/s	20.0	19.9
3 X 2.5 Gb/s	18.4	18.0
2 X 5.0 Gb/s	18.3	18.2
3 X 5.0 Gb/s	17.0	17.0

Table 2: 4200 km Results Summary

5. Conclusions

The results of these experiments show the potential to upgrade the 2100 km optically amplified segment of the Columbus-II undersea system to bitrates of up to 10.0 Gb/s and possible higher. The simulation results agree closely with the measured results. The results of the 4200 km measurements (double pass through the segment) indicate the potential to upgrade even longer systems with this repeater spacing.

For system viability, the results have to be analyzed in the context of impairment budgets which take into account aging, repair and other impairments. The higher capacity configurations may require the use of Forward Error Correction (FEC). FEC can be used to improve average system Q factor margin by more than 4.0 dB. The results confirm that the initial promise of optical amplifier systems as being "light pipes" with vast capabilities is being fulfilled.

---

[1] N. S. Bergano F. W. Kerfoot and C. R. Davidson, "Margin Measurements in Optical Amplifier Systems," *IEEE Photonics Technology Letters*, vol. 5, no. 3, March 1993.

FIGURE 1: COLUMBUS-2B EXPERIMENTAL RESULTS

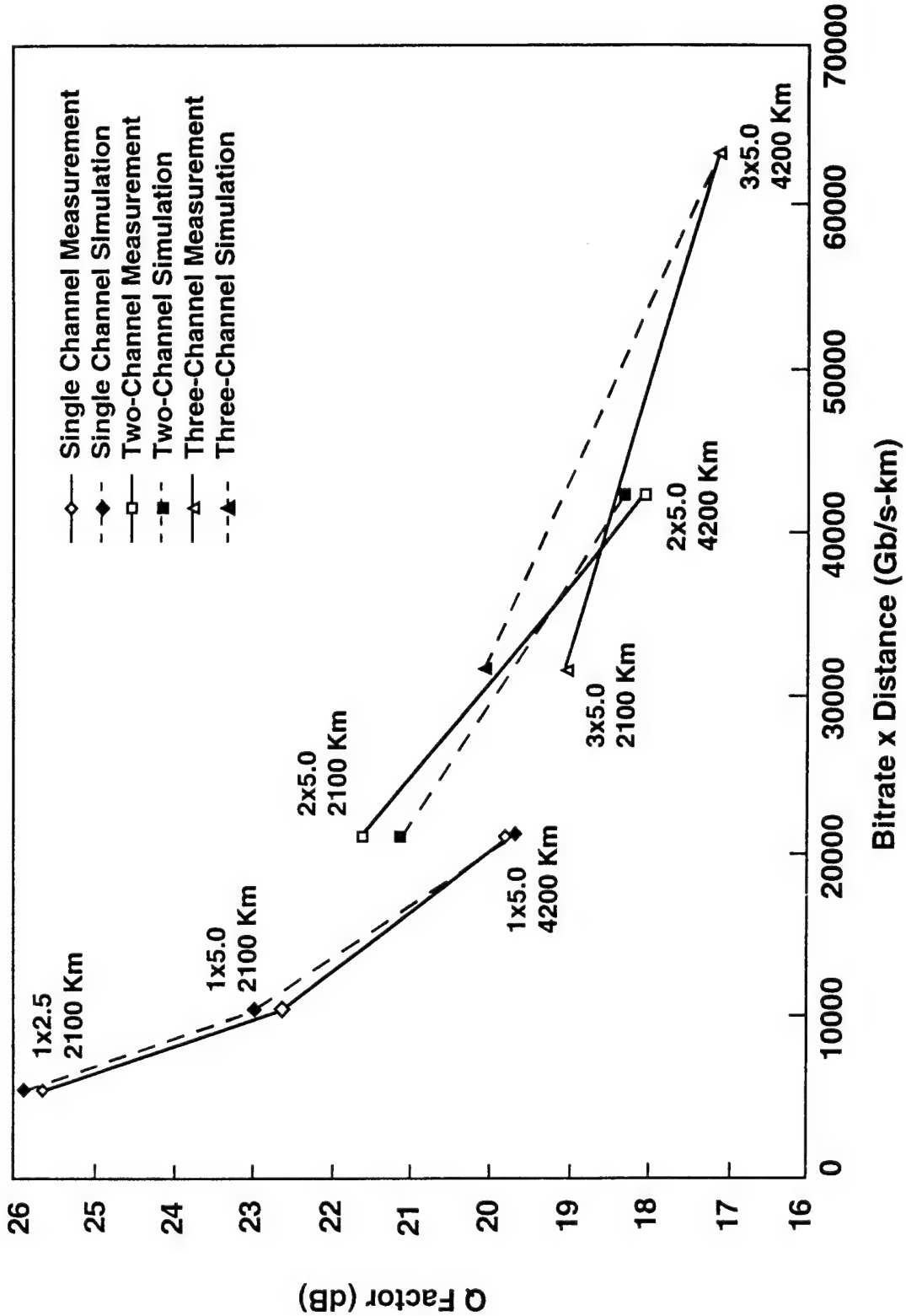

120 channel AM-VSB Signal Transmission by 2 Wavelength Multiplexing through Gain Flattened Hybrid Erbium-doped Fiber Amplifier

Masayuki Shigematsu, Motoki Kakui and Masayuki Nishimura

Sumitomo Electric Industries, Ltd.

1, Taya-cho, Sakae-ku, Yokohama, 244, JAPAN
Tel. +81-45-853-7171 Fax. +81-45-851-1557

In optical analog transmission systems using the erbium-doped fiber amplifier (EDFA), its spectral gain tilt is known to induce signal distortions in combination with laser chirping[1]. We have proposed a hybrid EDFA which consists of serially cascaded EDFs with different glass compositions and shown that the hybrid EDFA realizes a flat spectral gain(low distortion) without sacrificing an output power even after multi-stage amplification[2].

In this paper, we introduce a newly developed hybrid EDFA which realizes a flat gain profile in a wider wavelength range over 17nm. This EDFA employs a serially cascaded aluminum and phosphorus (Al-P) co-doped EDF and aluminum (Al) co-doped EDF[3]. We apply this type of EDFA to wavelength division multiplexed(WDM) optical analog transmission and demonstrate, for the first time, that 2 wavelength multiplexed 120 channel AM-VSB (amplitude-modulated vestigial side-band) signals can be amplified and transmitted with no significant degradation of signal distortions.

We have evaluated the locked-inversion(LI) spectral gain curves[4] of Al co-doped(#1), Al non-doped(#2) and Al-P co-doped(#3) EDFs with almost the same structural parameters. Small signal gain was measured with a probe signal when the main signal power launched into the EDFs was around +3dBm, satisfying the LI condition. Figure 1 shows the measured LI gain curves for a main signal wavelength of 1552nm. The effective fiber length[2] at 1.55μm($\alpha_{1.55}$xL) was 50dB for Fibers #1 and #2, and 40dB for Fiber #3. It should be noted that the Al-P co-doped EDF has a shortest gain peak wavelength, which is located around 1545nm. When Fibers #1 and #3 are serially cascaded (Type II), a flat gain profile is expected in a wavelength range from 1545 to 1560nm, which is significantly wider than that of cascaded Fibers #1 and #2 (Type I)[2].

Figure 2 shows the measured gain tilt for various types of EDF. The gain flatness was well improved in Type II over a wider wavelength range than that of Type I as expected. The gain tilt for Type II was found to be within ±0.1dB/nm over 17nm. Such a flat gain in a wider wavelength range has produced the

possibility of WDM analog transmission.

We have further optimized the fiber lengths of Type II for 2 channel WDM analog transmission. The gain curve and gain tilt measured with 2 main signals (1552 and 1558nm) simultaneously launched are shown in Fig.3. The total effective fiber length and input signal power were 45dB and +1.4dBm each. As seen in Fig.3, the gain tilt was almost zero at both 1552 and 1558nm.

To confirm the effectiveness of this hybrid EDFA for WDM analog transmission, 2 WDM 120 channel AM-VSB signal transmission experiment has been conducted. The experimental setup is shown in Fig.4. 1552 and 1558nm DFB-LDs with output power about +9dBm were used as transmitters. Each transmitter was modulated by 60 channel AM-VSB scheme with a modulation index per channel of 4%. The two signals were multiplexed through a 3dB coupler and simultaneously amplified by the hybrid EDFA. Then, the 1552nm signal was extracted by using a band pass filter (BPF). The received signal power was set to be 0dBm by a variable attenuator.

Figure 5 shows the configuration of the hybrid EDFA. The hybrid EDF was bidirectionally pumped by two 1.48μm pump LD modules with a total power of 140mW. The total effective fiber length was 55dB so that an output power around +18dBm was achieved.

Figure 6 shows the carrier to noise ratio(CNR), the composite second order distortion(CSO) and the composite triple beat noise(CTB) measured at the 1st, 29th and 60th channels at each position indicated as A-C in Fig.4. With the help of the newly developed BPF which had a flat transmittance around the peak wavelength and a high extinction ratio of 24dB at the adjacent signal wavelength, no degradation of CNR or CSO was observed at both positions A and B after passing through the BPF. It is also noted that no significant degradation of the signal distortions was observed after the amplification (position C). The noise figure of the EDFA calculated from the measured CNR was about 10dB.

In summary, we have newly developed a hybrid EDFA for WDM analog transmission. We have demonstrated, for the first time, that 2 WDM 120 channel AM-VSB signals can be amplified and transmitted with no significant degradation of signal distortions.

References

[1] C. Y. Kuo et al., IEEE Photon. Technol. Lett., Vol.3, No.9, pp829-831 (1992)
[2] M. Shigematsu et al., OAA'94, FD-2 (1994)
[3] T. Kashiwada et al., OFC'95, TuP1 (1995)
[4] S. L. Hansen et al., IEEE Photon.Technol.Lett.,Vol.4,No.4,pp409-411 (1993)

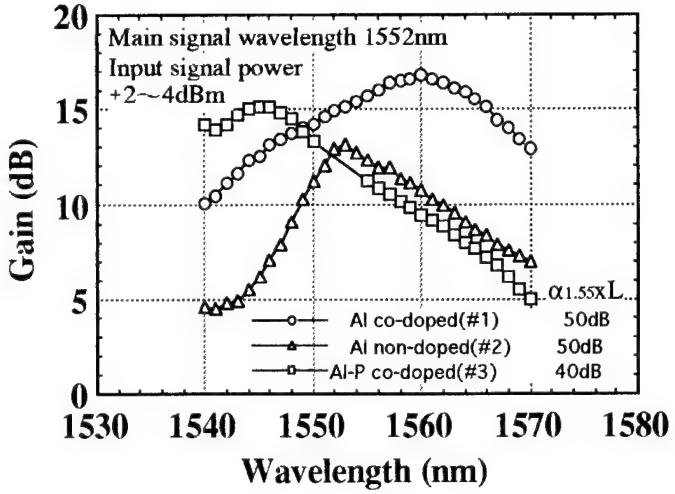

Fig.1 LI gain curves of EDFs with various glass compositions

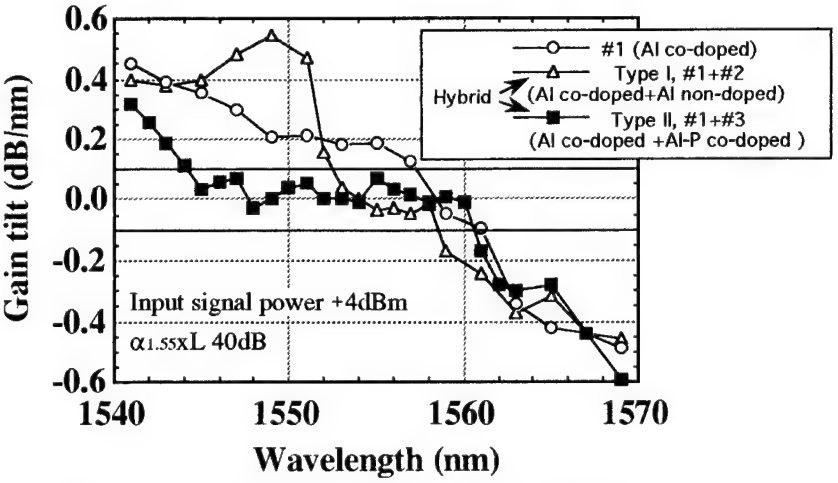

Fig.2 Gain tilt for various types of EDF

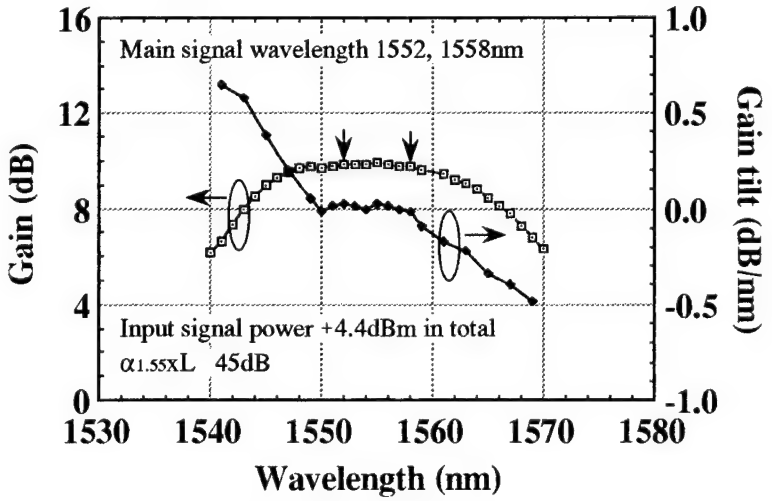

Fig.3 LI gain curve and gain tilt of hybrid EDF Type II for 2 main signals

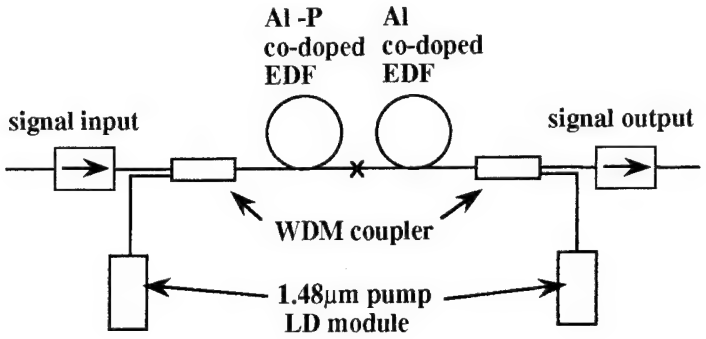

Fig.4 Configuration of hybrid EDFA

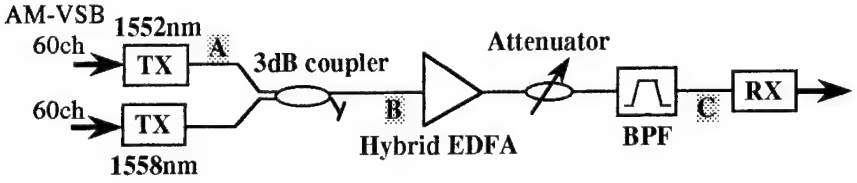

Fig.5 Experimental setup

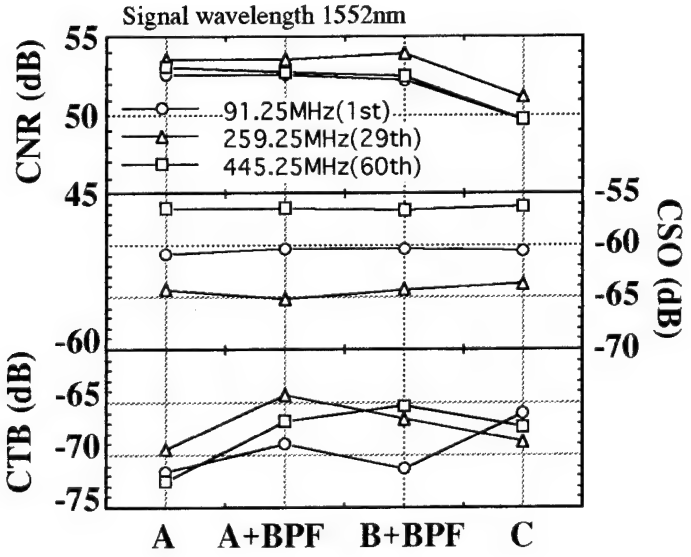

Fig.6 Experimental results of WDM transmission

Ultra-High-Capacity Amplified WDM Lightwave Systems

A.H. Gnauck
AT&T Bell Laboratories
Crawford Hill Laboratory
Holmdel, NJ 07733-0400

The trend in lightwave transmission systems is towards higher bit rates, higher powers, longer span lengths, and the incorporation of optical amplifiers to replace regenerators. This trend brings with it a number of technical challenges. Optical fibers present limitations due to loss, dispersion, and nonlinearities. Optical amplifier performance is constrained by parameters such as bandwidth, gain magnitude and flatness, output power, and noise figure. In general, capacity upgrades can be accomplished by increasing single-channel bit rates [1,2], and by wavelength-division multiplexing (WDM) high speed channels [3]. Both strategies can be implemented simultaneously. This paper outlines the technical challenges facing amplified lightwave systems which incorporate WDM techniques to increase system capacity. It also reviews recent WDM experiments, which have pushed the throughput of an amplified optical-fiber link to one-third terabit/s [4].

Commercial lightwave transmission systems now operate at 2.5 Gb/s, and 10-Gb/s systems are nearing deployment. Optical-amplifier repeaters are already in service. At any point in the evolution of single-channel systems, upgrading by WDM appears to be a natural and flexible solution to the need for greater capacity. This is largely due to the availability of erbium-doped fiber amplifiers (EDFAs), which provide gain over tens of nanometers of optical bandwidth in the 1.55-μm-wavelength region. EDFAs can amplify many channels without significant crosstalk, due to their slow gain dynamics. Impressively, a two-stage amplifier has exhibited gain of 50 dB and near-theoretical noise figure of 3.1 dB [5]. Power amplifiers have surpassed 500 milliwatts in output power [6]. The most significant remaining problem for long-haul WDM applications is gain variation as a function of wavelength. Adjustment of the channel input powers, or pre-equalization, can counteract gain variations to some extent [7]. Gain equalizers (filters) have also been demonstrated [8]. These could be placed at amplifier sites. However, the best solution would be the design of broadband amplifiers with flat gain profiles. Thus far, improved flatness has been obtained with erbium-doped fluoride-based fiber amplifiers [9] and EDFAs which have been co-doped with aluminum and phosphorus [10].

The performance of systems that use optical amplifiers as repeaters is characterized by optical signal-to-noise ratio (SNR). This dictates the minimum optical power that must be launched into

each fiber span. Therefore, the effects of fiber nonlinearities such as stimulated Raman scattering (SRS), stimulated Brillouin scattering (SBS), self-phase modulation (SPM) and cross-phase modulation (CPM), and four-photon mixing (FPM) must be addressed in system design [11]. Stimulated Raman scattering removes power from shorter-wavelength signals and adds it to longer-wavelength signals. Channel pre-emphasis at the transmitter and channel-equalization filters at the repeaters are remedies to degradation caused by SRS. Stimulated Brillouin scattering leads to a backward-propagating component and forward component that is clamped in power with additional noise. The threshold power for SBS is approximately +10 dBm (average power) for an on-off-keyed (OOK) optical channel, but can be increased substantially by broadening the optical carrier. Self-phase modulation, cross-phase modulation, and four-photon mixing arise from the nonlinear refractive index of optical fiber (Kerr nonlinearity). SPM and CPM broaden the optical spectrum of modulated light propagating in fiber. In SPM a single channel broadens its own spectrum, while in CPM the modulation in one channel broadens the spectrum of another channel. Pulse distortion can result when this spectral broadening is combined with either chromatic dispersion or optical filtering. Four-photon mixing occurs when channels at different wavelengths interact via the nonlinear refractive index to produce mixing products. This mixing is especially deleterious when products fall at the channel wavelengths, as is the case with channels that are equally spaced (in frequency). FPM requires optical phase matching, and can be suppressed by locally avoiding dispersion of magnitude less than about 1-2 ps/nm/km. Larger channel spacing also reduces the effect, but at the cost of limiting the number of channels that can be accomodated by optical amplifiers.

Recent system experiments demonstrate some of the solutions to the limitations imposed by optical nonlinearities. SRS is as yet only a minor problem, and has been controlled by signal pre-emphasis [12]. As previously mentioned, SBS suppression is usually required for OOK transform-limited data at power levels above 10 milliwatts. However, nonuniformity in the germanium concentration of fiber increases the Brillouin linewidth and, consequently, the SBS threshold [13]. This effect can be as large as several dB. When it is required, SBS suppression is accomplished through spectral broadening of the optical carrier. Typically this is done by frequency-dithering the laser source. Another method is to add external phase modulation. Launched average powers above 200 milliwatts have been demonstrated in this way [14].

In high-speed WDM systems, the combined requirements of low dispersion and substantial power in a number of channels can lead to severe four-photon-mixing penalties. A recent WDM experiment demonstrates what can happen when a simplistic approach is taken in system design [15]. The system involved eight channels, each operating at 10 Gb/s (8×10Gb/s). The channels were equally spaced at 1.6 nm apart, and the fiber dispersion zero fell between channels two and

three. The fiber length was 137 km. As the launched power was raised, the bit-error rate (BER) was recorded for channel three, the channel most affected by FPM. The error rate dropped until the launched power per channel reached -1 dBm (BER = 10^{-6}). At this point, the error rate began to increase due to interference from mixing products. Unequal channel spacing was then applied, such that the frequency slots dedicated to channels were free of mixing products. A BER of less than 10^{-9} was thereby achieved for launched powers per channel from +1 dBm to +8 dBm. For launched powers per channel above +7 dBm, performance again degraded due to signal depletion as significant power was transferred to the mixing waves. This experiment demonstrates a possible upgrade path for installed systems containing fibers with dispersion zeros near the signal wavelengths. For new systems, an alternative approach is to use dispersion management, wherein the overall dispersion is low, but individual fiber segments exhibit dispersion of greater than 1-2 ps/nm/km. An 8 × 10-Gb/s experiment employed fibers with dispersion of -2.5 ps/nm/km concatenated with shorter lengths of conventional fiber having dispersion of 16 ps/nm/km, to achieve 240-km transmission [16]. A similar dispersion map was used in a circulating loop configuration to transmit eight 5-Gb/s channels over 8000 km [17]. A 17 × 20-Gb/s experiment used approximately equal lengths of fibers having dispersion values of +2.5 and -2.5 ps/nm/km to attain 150-km transmission [4]. It is important to note that installed systems which utilize conventional single-mode fiber (dispersion of approximately 17 ps/nm/km at 1.55-μm wavelength) may be upgraded to operate at higher bitrates by adding lengths of dispersion-compensating fiber, which exhibit large negative dispersion. Such systems will, by default, be dispersion-managed. Already, 1000-km transmission has been attained in a 16 × 10-Gb/s demonstration [18], and 232-km transmission has been achieved in an 8 × 20-Gb/s experiment [19]. This second system is unique in that the compensating fiber had both negative dispersion and negative dispersion slope. The negative dispersion slope partially compensated for the dispersion slope of the transmission fiber. This feature may allow for more channels and higher per-channel bitrates in future systems.

REFERENCES

1. K. Hagimoto et al., "Ultra-high-speed modulation technology for IM/DD systems," *European Conf. Opt. Comm. 1993*, paper MoC1.4, p. 9, 1993.
2. S. Kawanishi et al., "200-Gbit/s, 100-km TDM transmission using supercontinuum pulses with prescaled PLL timing extraction and all-optical demultiplexing," *Opt. Fiber Comm. Conf. 1995*, postdeadline paper PD28, 1995.
3. T. Li, "The impact of optical amplifiers on long-distance lightwave communications," Proceedings of the IEEE **81**, pp. 1568-1579, 1993.
4. R. W. Tkach et al., "One-third terabit/s transmission through 150 km of dispersion-managed fiber," *European Conf. Opt. Comm. 1994*, postdeadline paper, 1994.
5. R. I. Laming et al., "Erbium-doped fiber amplifier with 54 dB gain and 3.1 dB noise figure," IEEE Photonics Technol. Lett. **4**, pp. 1345-1347, 1992.

6. S. G. Grubb et al., "+24.6 dBm output power Er/Yb codoped optical amplifier pumped by diode-pumped Nd:YLF laser," Electron. Lett. **28**, pp. 1275-1276, 1992.

7. A. R. Chraplyvy et al., "End-to-end equalization experiments in amplified WDM lightwave systems," IEEE Photonics Technol. Lett. **5**, pp. 428-429, 1993.

8. K. Oda, et al., "128 channel, 480 km FSK-DD transmission experiment using 0.98 μm pumped erbium-doped fibre amplifiers and a tunable gain equaliser," Electron. Lett. **30**, pp. 982-984, 1994.

9. B. Clesca et al., "Multiwavelength gain flatness assessment of fluoride-based fibre amplifiers using a circulating loop," Electron. Lett. **30**, pp. 1308-1309, 1994.

10. T. Kashiwada et al., "Gain-flattened optical-fiber amplifiers with a hybrid Er-doped-fiber configuration for WDM transmission," *Opt. Fiber Comm. Conf. 1995*, paper TuP1, 1995.

11. A. R. Chraplyvy, "Limitations on lightwave communications imposed by optical-fiber nonlinearities," IEEE J. Lightwave Tech. **8**, p. 1548, 1990.

12. A. R. Chraplyvy et al., "1420-km transmission of sixteen 2.5-Gb/s channels using silica-fiber-based EDFA repeaters." IEEE Photonics Technol. Lett. **6**, pp. 1371-1373, 1994.

13. X. P. Mao et al., "Stimulated Brillouin threshold dependence on fiber type and uniformity." IEEE Photonics Technol. Lett. **4**, p. 66, 1992.

14. P. B. Hansen et al., "2.488-Gb/s unrepeatered transmission over 529 km using remotely pumped post- and pre-amplifiers, forward error correction, and dispersion compensation," *Opt. Fiber Comm. Conf. 1995*, postdeadline paper PD25, 1995.

15. F. Forghieri et al., "Repeaterless transmission of eight channels at 10 Gb/s over 137 km (11 Tb/s-km) of dispersion-shifted fiber using unequal channel spacing," IEEE Photonics Technol. Lett. **6**, pp. 1374-1376, 1994.

16. A. R. Chraplyvy et al., "8 x 10 Gb/s transmission through 280 km of dispersion-managed fiber," IEEE Photonics Technol. Lett. **5**, p. 1233, 1993.

17. N. S. Bergano et al., "40 Gb/s WDM transmission of eight 5 Gb/s data channels over transoceanic distances using the conventional NRZ modulation format," *Opt. Fiber Comm. Conf. 1995*, postdeadline paper PD19, 1995.

18. K. Oda et al., "16-channel × 10-Gbit/s optical FDM transmission over 1000 km conventional single-mode fiber employing dispersion-compensating fiber and gain equalization," *Opt. Fiber Comm. Conf. 1995*, postdeadline paper PD22, 1995.

19. A. H. Gnauck, et al., "Transmission of 8 20-Gb/s channels over 232 km of conventional fiber," *Opt. Fiber Comm. Conf. 1995*, postdeadline paper PD23, 1995.

Pump Lasers

ThC 14:00-15:00
Theatersaal

Heinz Meier, *Presider*
IBM Zurich Laboratory, Switzerland

New Developments in 980nm Pump Lasers

W. F. Sharfin, L. A. Scheffel, S. D. Conover, C. R. Ó Cochláin

Lasertron
23 Fourth Avenue
Burlington, Massachusetts 01803
617-272-6462 Phone
617-229-8193 Fax

Commercial erbium-doped fiber amplifiers (EDFAs) are pumped by semiconductor lasers at either 980nm or 1480nm wavelength. Although 980nm pumping offers the well-known advantages of lower noise, greater gain-slope efficiency, and lower power consumption, until recently concerns about catastrophic optical mirror damage (COMD) have limited the use of 980nm pump lasers in telecom applications. Reliability data from field deployment of 980nm-pumped EDFAs in an 2.5 Gb/s long-distance fiber link between Salt Lake City and Chicago has shown that the facet passivation technology developed for GaAs-based lasers at IBM has successfully prevented front-facet COMD of the pumps. The results of over 4 million device hours of operation were recently presented by Pirelli and Lasertron at OFC '95 in San Diego [1]. The measured failure rate at a chip power of 150mW corresponds to about 1000 FITs over 25 years. Recent data on Lasertron modules have also shown an increased threshold for failures associated with electrical overstress (EOS); greater than four times normal operating powers. Updated data (greater than 6 million device hours) on facet and EOS failures will be presented.

Increasing commercial demand for higher pump-module power has stimulated improvements in fiber-coupling efficiency and changes in device design. The use of new fiber-lensing techniques has recently increased the coupling efficiency from about 50% to greater than 65% in Lasertron modules with single-mode fiber pigtails.

Fiber-coupled power greater than 1W is anticipated from the development of a fiber-pigtailed module incorporating a high-power semiconductor device with a laterally tapered active region. The active region is tapered or flared so that the beam spreads laterally to reduce the power density at the output facet. Recent work at MIT Lincoln Laboratory [2] and SDL [3] has shown that several watts of power can be obtained in a near-diffraction-limited beam from a device consisting of an index-guided region combined with a section that is flared to 0.2mm wide at the front facet. The phase-front of the beam from a laterally tapered laser or amplifier is highly astigmatic; a longer tapered region permits higher output power but has proportionately greater astigmatism. As the beam emerges from the front facet the phase-front is curved in the lateral plane and flat in the guided, transverse plane. The lateral intensity profile of the beam more closely resembles a top-hat than a Gaussian function. Despite these characteristics, close to 60% coupling efficiency into a single-mode fiber has been demonstrated in benchtop experiments at Lincoln Laboratory [4] and SDL

[5], resulting in greater than 1W of coupled power. Schemes for fiber-coupling tapered devices will be discussed.

1. G. Grasso et al., in *Conference on Optical Fiber Communication*, 1995 Technical Digest Series, Vol. 8, (Optical Society of America, Washington, D.C., 1995), p. 232.

2. J. N. Walpole et al., Appl. Phys. Lett., **61**, 740 (1992).

3. D. Welch et al., IEEE Photon. Tech. Lett., **5**, 297 (1993).

4. J. C. Livas et al., in *Conference on Optical Amplifiers and Their Applications*, 1994 Technical Digest Series, Vol. 14, (Optical Society of America, Washington, D.C., 1994) p. 29.

5. F. Shum et al., in *Conference on Optical Fiber Communication*, 1995 Technical Digest Series, Vol. 8, (Optical Society of America, Washington D.C., 1995), paper PD13.

Near-Ideal Diffraction-Limited Beam from a 970 nm High-Power Angled-Facet Tapered Semiconductor Optical Amplifier

S.H. Cho, S.Fox, S.A. Merritt, P.J.S Heim, B. Gopalan, S.Kareenahalli, V.Vusirikala, C.E.C Wood* and M. Dagenais

University of Maryland
Department of Electrical Engineering and
Joint Program for Advanced Electronic Materials
College Park, MD 20742.
Phone: (301) 405 - 3684 Fax : (301) 314 - 9281

** Laboratory for Physical Sciences,*
8050, Greenmead Drive,
College Park, MD 20742

Tapered semiconductor laser amplifiers have been one of the most successful approaches for producing high optical power in a diffraction limited beam [1-4]. Until now, this work has been done using anti-reflection coated normal incidence laser facets. In this paper, we report on the use of angle-facet tapered laser amplifiers to produce multi-watts of optical power in a near ideal diffraction-limited beam. Previous work on tapered angled facet amplifiers [5] has been geared toward low power operation. When combined with a dissipating grid on the unpumped region of the amplifier, the angled-facet structure leads to several new advantages for high power applications. These include: (i) a reduction of the effective reflectivity which results in less gain competition with the forward propagating signal, (ii) a reduction of filamentation formation, and (iii) a reduction of the reflected amplified signal at the input facet, which increases the catastrophic optical damage threshold. Angled facets can also be used in combination with anti-reflection coatings, easing the stringent requirements on the anti-reflection coating.

We report here on the production of 2.6 W in a quasi-CW mode and 1.9 W CW at 970 nm with less than 5 mW coupled input power. These results are obtained with a near-ideal, diffraction-limited beam with a beam quality factor M^2 of 1.1. Ultra low thermal impedances of 1.5 °C/W are obtained using a new die mounting technique. By adjusting the wavelength, the amplifier can be used to pump erbium doped fiber amplifiers.

The angled-facet tapered optical amplifier,shown in Fig.1, consists of a tapered index-guided waveguide angled 7^0 to the cleaved facets. The optical waveguide is an AlGaAs-GaAs GRINSCH structure with a single 9 nm InGaAs quantum well centered in the active region. The input waveguide width is 8 μm, the output width is 150 μm, and the device length is 2 mm. Due to the angled-facet structure, reflections from the facets are fed back as a small angle relative to

the signal propagation direction. A self-aligned dissipating grid [6] is positioned on the unpumped region to prevent oscillation outside the gain region. The grid efficiently prevents oscillations at normal incidence to the cleaved facets. Each facet was also AR coated [7] for more efficient power extraction and to further increase the threshold current..

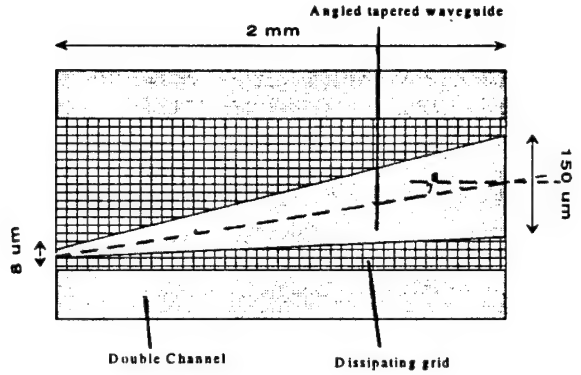

Fig.1 Top view of the angled-facet tapered amplifier

Particular care was taken to mount this device using our recently developed void-free technique for reliably mounting the amplifier die epitaxy-side down [8]. Our method is based on the controlled interdiffusion of a 2.0 μm Sn layer evaporated on a copper heat sink with a 2.5 μm layer of In evaporated on the epitaxial side of the wafer to generate a near-eutectic alloying beneath the die. After In coating, the wafer is patterned photolithographically to create cleaving and dicing lines in the In layer. The absolute thermal resistance is as low as 1.5 °C/W and specific thermal resistances of 4×10^{-3} K-cm^2/W are reproducibly obtained. Results obtained for 4 mW of coupled optical input power are shown in Fig.2. More than 2.6 W were obtained in the pulsed mode with a slope efficiency of 0.7 W/A. The CW results closely reproduced the pulsed result, with only a small decrease in the slope efficiency. More than 1.9 W CW were obtained, before the onset of catastrophic optical damage.

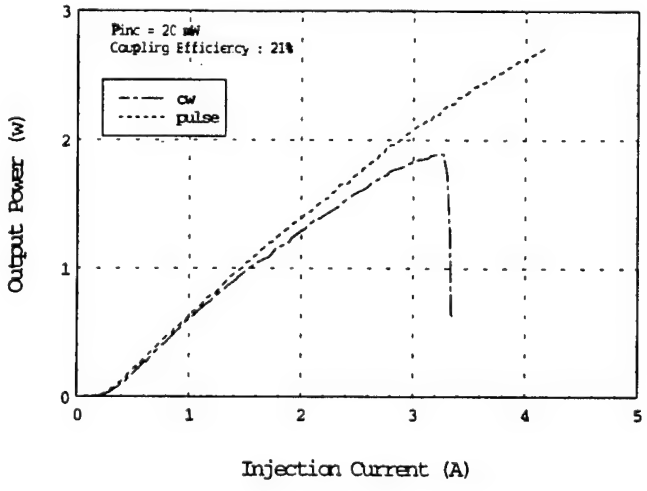

Fig.2 Optical Power Vs. Injection current for both CW and pulsed operation

The lateral near- field pattern at a quasi-CW output power of 1.2 W is shown in Fig.3. From the near-field and far-field measurements, a beam quality factor of $M^2 \cong 1.1$ [9] is extracted, which indicates that the beam is nearly Gaussian. This result is obtained by truncating the very small wings of the near-field profile. More than 97% of the power is in the main beam. The transverse near-field was also measured (Fig.4) and was found to have the same value of M^2, once again indicating a very high quality beam.

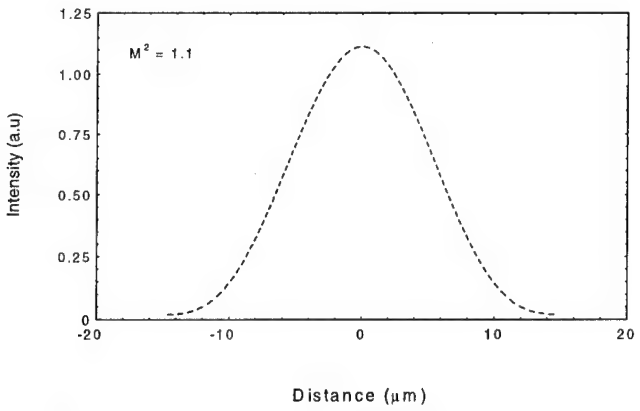

Fig.3 Near field pattern in the lateral direction

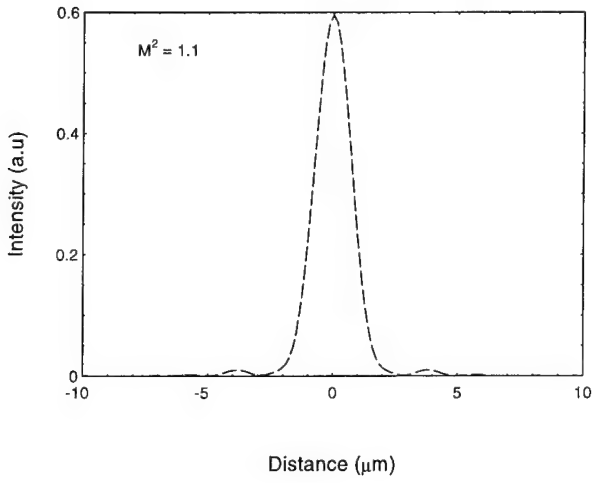

Fig.4 Near field pattern in the transverse direction

Similar M^2 values were obtained at different currents and injection levels. Values of M^2 varying from 1.5 to 1.7 have previously been reported for similar tapered laser amplifiers [2]. Therefore, our results demonstrate a significant improvement towards obtaining near-ideal, diffraction-limited Gaussian beams.

In our experiment, the coupled input beam was not appropriately mode matched to the input waveguide and therefore a coupling efficiency of only 21% was deduced by back biasing the amplifier structure. By improving the coupling efficiency, we expect that substantially higher powers can be obtained. In addition, by widening the input aperture from 8 μm to 100 μm,

higher output powers should be obtainable. These experiments are presently ongoing in our laboratory.

In conclusion, more than 2.6 W quasi-CW and 1.9 W CW were obtained at 970 nm from a tapered angled-facet semiconductor amplifier with only 4 mW of coupled input power. Near ideal beam quality factors $M^2 \cong 1.1$ were determined indicating the diffraction limited nature of the output beam. Ultra-low thermal impedances (1.5 ^{o}C/W) were obtained using a new die mounting technique that ensures a high level of uniformity.

REFERENCES:

[1] J.N.Walpole, E.S.Kintzer, S.R.Chinn, C.A.Wang, and L.J.Missaggia, "High-power strained-layer InGaAs/AlGaAs tapered traveling wave amplifier", Appl. Phys. Lett., Vol. 61, No. 7, pp. 740-742, 1992.

[2] S.O'Brien, D.F.Welch, R.A.Parke, D.Mehuys, K.Dzurko, R.J.Lang, R.Waarts and D.Scifres,"Operating characteristics of a high-power monolithically integrated flared amplifier master oscillator power amplifier", IEEE J. Quantum Electronics, Vol. 29, No. 22, pp. 2052-2057, 1993.

[3] P.S.Yeh, I.-F.Wu, S.Jiang, and M.Dagenais, "High-power high gain monolithically integrated preamplifier / power amplifier", Electron. Lett., Vol. 29, No. 22, pp. 1981-1983, 1993.

[4] L.Goldberg, D.Mehuys, M.R.Surette and D.C.Hall, "High-power, near-diffraction-limited large-area traveling-wave semiconductor amplifier", IEEE J. Quantum Electron., Vol. 29, No. 6, pp. 2028-2043, 1993.

[5] C.E.Zah, R.Bhat, S.G.Menokal, N.Andreakis, F.Favire, C.Caneau, M.A.Koz, and T.P.Lee," 1.5 μm GaInAsP Angled-facet Flared-Waveguide Traveling-Wave Laser Amplifiers"' IEEE Photonics Technol. Lett., 2, pp. 46-47, 1990.

[6] P.Sophia Yeh, I-Fan Wu, Peter Heim, Scott Meritt, Shijun Jiang, Colin Wood, and Mario Dagenais," Self-Aligned Dissipating grid for High-Powered Tapered Semiconductor Amplifiers", in Conference on Lasers and Electro-Optics, Vol. 8., 1994 OSA Technical Digest series (Optical Society of America, Washington, D.C., 1994), pp. 232-233.

[7] I-Fan Wu, Isabelle Ryan, Jean-Marc Verdiell, and Mario Dagenais," Real-Time In Situ Monitoring of Antireflection Coatings for Semiconductor Laser Amplifiers by Ellipsometry", IEEE Photonics Technol. Lett., 4, pp. 991-993, 1992; I-Fan Wu, J.B. Dottelis, and Mario Dagenais," Real-Time In Situ Ellipsometric Control of Antireflection Coatings for Semiconductor Laser Amplifiers using SiO_x", J. Vac. Sci. Technol., A11, pp. 2398-2406, 1993.

[8] S.A.Meritt, P.J.S.Heim, S.Cho, and M.Dagenais," A Reliable Die Attach Method for High-Power Semiconductor Lasers and Optical Amplifiers", to appear in 45th Electronic Components and Technology Proceedings, Las Vegas, May 21-24, 1995.

[9] A.E.Siegman, " New Developments in Laser Resonators", SPIE Vol. 1224, pp. 2-14, 1990.

1.02-μm pump laser diodes with high power above 300 mW into single mode fiber

Mitsuru Sugo, Jiro Temmyo, Teruhiko Nishiya, Eiichi Kuramochi and Toshiaki Tamamura
NTT Opto-electronics Laboratories,
3-1 Morinosato-Wakamiya, Atsugi, Kanagawa, 243-01 Japan
Tel. +81(462)40-3262
Fax. +81(462)40-4305

INTRODUCTION: Currently the most promising candidate for a practical 1.3-μm fiber amplifier is the praseodymium-doped fluoride fiber amplifier (PDFFA). However the low quantum efficiency of the 1.3-μm band stimulated transition of the present PDFFA requires high power pump lasers. The first commercial prototype PDFFA module appeared in the market place last year [1]. This module uses a high power Nd:YLF laser pumped with a semiconductor laser diode (LD). Furthermore, a PDFFA module pumped by 1.02-μm strained InGaAs quantum well LDs consisted of four LD modules [2]. In order to achieve a low cost and low power consumption PDFFA module, a higher power and more reliable 1.02-μm LD module is required. Here, we report high-power 1.02-μm strained InGaAs/AlGaAs LDs with small divergence angles for a LD module.

LASER STRUCTURE: Figure 1 shows a schematic compositional profile of the new LDs. The InGaAs/AlGaAs double quantum well (DQW) LD structures basically consist of separate confinement heterostructures (SCH) with guiding layers, but contain low refractive index layers (400-nm-thick) between the cladding and guiding layers. The low refractive index layers expand the vertical spot size and increase the vertical confinement factor per well. Differences in the refractive index between the low refractive index layer and cladding layer were chosen to be in the order of 0.01. The AlGaAs cladding lasers have an advantage in controllability of refractive index over InGaP cladding lasers. The aluminum compositions of all AlGaAs layers were chosen to be lower than 30 %. The designed epitaxial structures were grown by low pressure metalorganic vapor phase epitaxy (MOVPE).

Ridge waveguide structures were formed using high-resolution electron beam lithography and electron cyclotron resonance reactive-ion etching [3]. These technologies enable us to precisely control ridge widths and etching depths which are responsible for horizontal mode stability. The ridge width was 2 μm and cavity length 900 μm. An anti-reflecting film (4 %) and a high reflecting film (90 %) were coated onto the front and rear facets, respectively.

LASER PERFORMANCE: The expansion of vertical spot size results in the reduction of the divergence angle. Figure 2(a) shows the typical far-field patterns of the new LDs with the

low refractive index layers. For comparison, those of the usual LDs are also shown in Fig. 2(b) [4]. The vertical divergence angle of 17 degrees for the new LDs with the low refractive index layers was smaller than that of 24 degrees for the usual LDs; whereas the horizontal divergence angle was 13 degrees for the new LDs.

The new LDs exhibited high LD performance, that is, the threshold current was around 20 mA, the slope efficiency was around 1.0 W/A and the characteristic temperature was around 135 K. For the usual LDs, on the other hand, the reduction of divergence angle increases the threshold current and decreases the characteristic temperature because of decreasing confinement factor [4].

The reduction of the divergence angle, reducing the divergence beam aspect ratio to 1.3, produces a high coupling efficiency above 65 % for laser-to-single mode fiber (SMF) coupling. Figure 3 shows light-current (L-I) characteristics in free-space and in a SMF. We used a single aspheric lens for laser-to-SMF coupling. Kink free L-I characteristics comes from the mode stability of the new LDs even at high driving current. A maximum output power above 300 mW in the SMF was achieved above a driving current of 500 mA.

One of the most important points for strained InGaAs pump LDs is reliability. A preliminary aging test for the new LDs has been performed at 50 °C and a constant power of 100 mW in free space. No prescreening was performed. 8 LDs out of a total of 11 exhibited stable operation over 2500 hours. The other LDs showed initial increases in operating current during the first several hundred hours. These LDs with the initial degradation can be eliminated after the first 200-hour operation. These results confirm that the new LDs are as reliable as usual strained InGaAs pump LDs.

CONCLUSION: We have demonstrated new 1.02-μm strained InGaAs pump lasers with high coupling efficiency and high power above 300 mW into single mode fiber. The results open the way for the development of a low cost and low power consumption PDFFA module pumped with a single 1.02-μm LD module.

References

[1] Fake, M., Lawrence, E.P., and Simmons, T.J., In Proc OFC '94, ThF2, San Jose, USA, 1994.

[2] Shimizu, M., Kanamori, T., Temmyo, J., Wada, M., Yamada, M., Terunuma, Y., Ohishi, Y., and Sudo, S., *IEEE Phot. Tech. Lett.*, vol. 5, no. 6, pp. 654-657, 1993.

[3] Nishiya, T., Kuramochi, E., Sugo, M., Shimizu, M., Temmyo, J., and Tamamura, T., In Proc OFC '95, ThC4, San Diego, USA, 1995.

[4] Temmyo, J., and Shimizu, M., *IEE. Electron. Lett.*, vol. 30, no. 24, pp. 2046-2047, 1994.

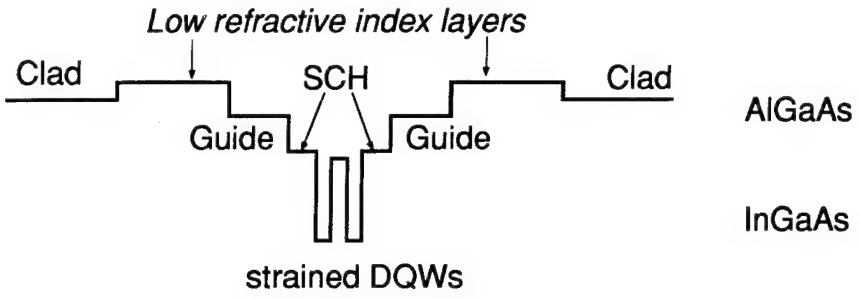

Fig. 1 Schematical compositional profile of new LDs with low refractive index layers.

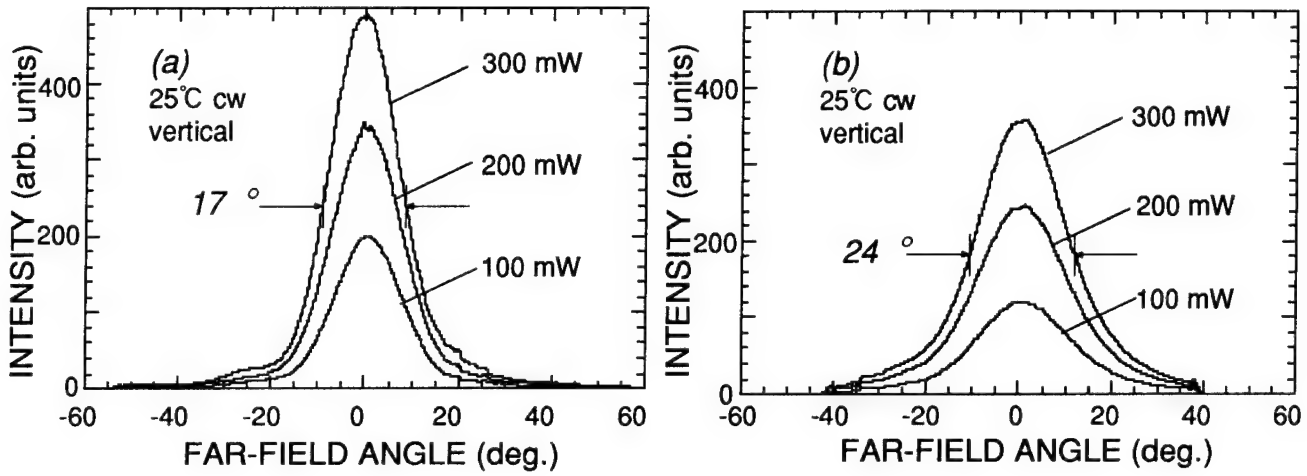

Fig. 2 Typical vertical far-field patterns of new LDs with low refractive index layers (a) and of usual LDs (b).

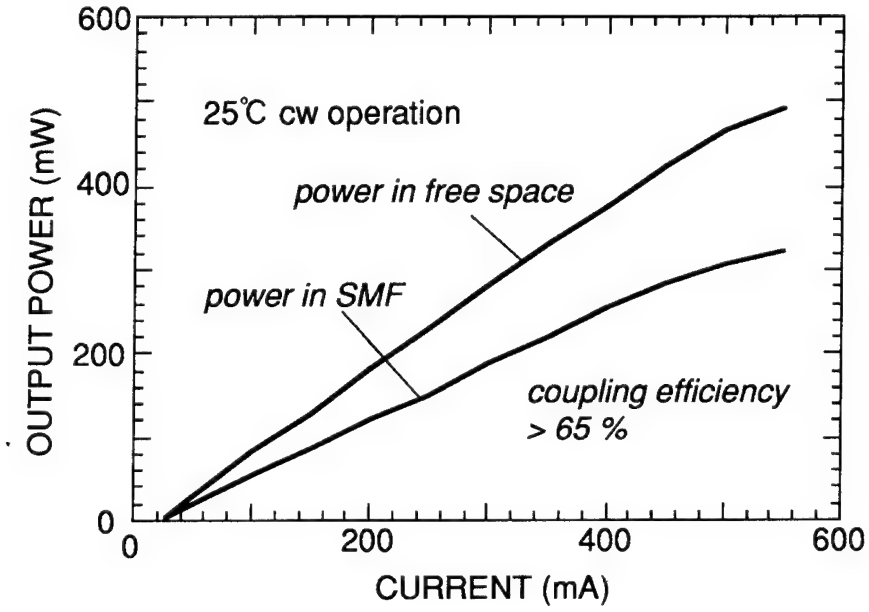

Fig. 3 Light-current characteristics of new LDs with low refractive index layers in free space and in a single mode fiber (SMF). A single aspheric lens is used for coupling.

Poster Session

ThD 15:00-16:15
Congress Centre Foyer

GAIN SPECTRUM FLATTENING OF ERBIUM-DOPED FIBER AMPLIFIER USING TAPERED FIBER FILTER.

A.V.Belov, E.M.Dianov, V.I.Karpov, A.V.Kurkov, V.N.Protopopov, M.Yu.Tsvetkov, *Fiber Optics Research Center, Russian Academy of Sciences, 38 Vavilov St. 177932, Moscow, Russia, FAX:095/135-81-39.*
A.N.Guryanov, V.F.Khopin, *Institute of Chemistry of High-Purity Substances, Russian Academy of Sciences, Tropinin St. 49, Nizhnii Novgorod 603600, Russia.*
W.H.Choe, S.J.Kim, *Samsung Advanced Institute of Technology, P.O.Box 111, Suvon, Korea 440-600.*

Introduction

Erbium-doped fiber amplifiers with broad and flat gain spectrum are very promising in long-haul telecommunications with WDM and analog video transmission systems. The most broad and smooth gain spectrum can be achieved by incorporating a high quantity of aluminum into a glass-host matrix of EDF [1]. However, in case of a small input signal regime in high gain 980 nm-pumped EDFA, the difference between the gain near the peak of 1532 nm and the gain at long wavelength region is still as high as 8-12 dB. Further flattening of gain spectrum can be achieved by inserting of band-stop or notch filters tuned to the peak gain into the EDFA. Recently several approaches have been proposed for creating passive filters: mechanical deformation of the fiber to couple fundamental and leaky modes [2], etching of grating at the surface of D-fiber [3], the use of twin-core fiber filter [4], or photoinduced fiber grating [5], or WDM coupler [6].

This paper reports on incorporating of a newly developed fiber tapered filter into an EDFA to achieve a broad and flat gain spectrum. The proposed filter has the following advantages: fiber compatibility and low additional loss, simplicity of fabrication, and polarisation insensitivity as a result of its axial symmetry. Low insertion loss at pump wavelength near 980 nm allows to insert the filter into the middle of the EDF to suppress a build-up of an amplified spontaneous emission near 1532 nm.

Filter fabrication

Tapered fiber filter (TFF) is made on the equipment used for manufacturing of fused fiber couplers. The single-mode fiber sample is locally heated and pulled forming a typical biconical taper structure. The excitation of additional higher-order modes depends on the refractive index profile and the fiber taper geometry [7]. In the taper a

power coupling between the fundamental and higher order modes takes place. The mode distribution of power in the filter output is defined by propagation constants of these modes and by the length of the taper waist.

During the tapering, the power oscillations corresponding to the coupling of the first order mode to higher order mode occur. The number of oscillations at the wavelength of 1532 nm is counted. The process of tapering is stopped when the transmission of the filter at 1532 nm falls to minimum after N^{th} oscillation. To create the filter with spectral selectivity suitable for EDFA gain flattening, the value of N should be 29-31. The attenuation at the wavelength of the minimum transmission depends on the refractive index profile of a single mode fiber and can be adjusted to within of ±2 dB by the change of tapering conditions. The single-mode fiber with depressed cladding was applied for the preparation of a tapered filter. This fiber had the ratio of deposited cladding to core radius of about 2.5, refractive index difference of +0.02 and -0.005 for the core and deposited cladding, respectively, and the cut-off wavelength of 920 nm. Transmission spectra of the TFF optimised for the gain flattening are shown in Fig.1a,b. The insertion loss estimated at 1550 nm was 0.4 dB. N deviation of ±1 leads to negligible change in the spectral selectivity, which gives the flexibility in attaining of the minimum insertion loss at the pump wavelength. Transmission spectrum of the filter in the pump region shows the minimum loss at 976 nm (Fig.1b). Insertion loss measured at pump wavelength of 978 nm was less than 0.3 dB.

Gain flattening experiment

Alumino-germano-silicate host erbium-doped fiber made by MCVD-solution technique was applied to make the EDFA with flat gain spectrum. The concentration of erbium ions estimated from absorption spectrum was 230 ppm. Aluminum concentration was increased up to 5 wt.% to achieve broad and smooth gain spectrum. The fiber had effective refractive index difference of 0.026, cut -off wavelength of 0.81 μm and confinement of erbium-ion distribution of 0.5. Gain spectra of EDFA were investigated using the set-up shown in Fig.2. Pump light at 978 nm from a Ti:Sapphire laser and signal light from Erbium-doped fiber laser were combined in a WDM coupler and launched into the amplifier. The pump power was stabilised by electro-optical modulator with a feedback through two WDM couplers. An EDF laser used as signal source was the feature of the set-up. In the laser aluminum-codoped fiber with length of 60 meters was pumped by LD at 980 nm. The signal wavelength was tuned by diffraction grating with 600 lines/mm. The endface of the EDF with Fresnel reflection of 4% formed the output mirror. A spectral linewidth of the laser was narrower than 0.1 nm inside the total tuneable region from 1526 nm to 1566 nm. The level of the

amplified spontaneous emission, measured in 1nm bandwidth, was -45 dB relative to the power in the laser mode.

The gain spectrum of the EDF with length of 13 meters, measured with the input signal of -30 dBm and the input pump power of 40 mW is shown in Fig.3 (curve a). The gain of more than 30 dB at the total spectral region broader than 35 nm due to high aluminum concentration was obtained; nevertheless the difference of gain at 1532 nm and 1555 nm was still ~10 dB.

To flatten the gain spectrum, the TFF with transmission shown in Fig.1 was spliced into the middle of the EDF. The gain measurements were carried out under the same conditions as for the reference EDFA. As seen from the curve b in Fig.3, the gain peak near 1532 nm is totally suppressed. Inside the band from 1526 nm to 1561 nm the average value of the gain is 30 dB ±1.4 dB. The gain value of the EDFA with TFF at 1555 nm exceeds the reference gain by 1 dB. Taking into account that at this wavelength the total attenuation in the TFF including splices was 0.9 dB, it becomes evident that the increasing of the gain in both sections of the EDFA due to rejection of the part of the ASE exceeds 1.9 dB.

Fig.4 shows the gain of the EDFA with the midway TFF versus the pump power measured with the input signal of -30 dBm at 1532 nm and 1555 nm. When the pump power is changed from 25 mW to 45 mW the difference in gain at these wavelengths does not exceed 3 dB. At the pump power of 40 mW the gain remains uniform with variations of ±1.5 dB, if the input signal is increased from -40 dBm to -25 dBm.

In conclusion, the authors present flat gain EDFA with a midway tapered fiber filter. Low insertion loss of the filter at the wavelength beyond the absorption peak and at the pump wavelength makes it very attractive for the creating of an all-fiber flat gain amplifier.

References:

1.T.Kashiwada et al., in Optical Amplifiers and Their Applications Technical Digest, 1993, vol. 14 (OSA, Washington, D. C., 1993), p.104.

2.M.Tachibana et al., IEEE Photonics Technol. Lett., vol.3, no.2, p.118, (1991).

3.M.Wilkinson et al., Electron. Lett., vol 28, no 2, 131 (1992).

4.G.Grasso, in Proc. Conference on Optical Fiber Communications, OFC'91, OSA, Washinghton, D.C., paper FA3, (1991).

5.R.Kashyap et al., Electron. Lett., vol 29, no 2, p.154 (1993).

6.R.G.Smart et al., Electron. Lett., vol 3, no 19, p.50 (1994).

7.A.C.Boucouvalas, G.Georgiou, IEE Proc., Pt.J, v.133, no 6, p.385, (1986).

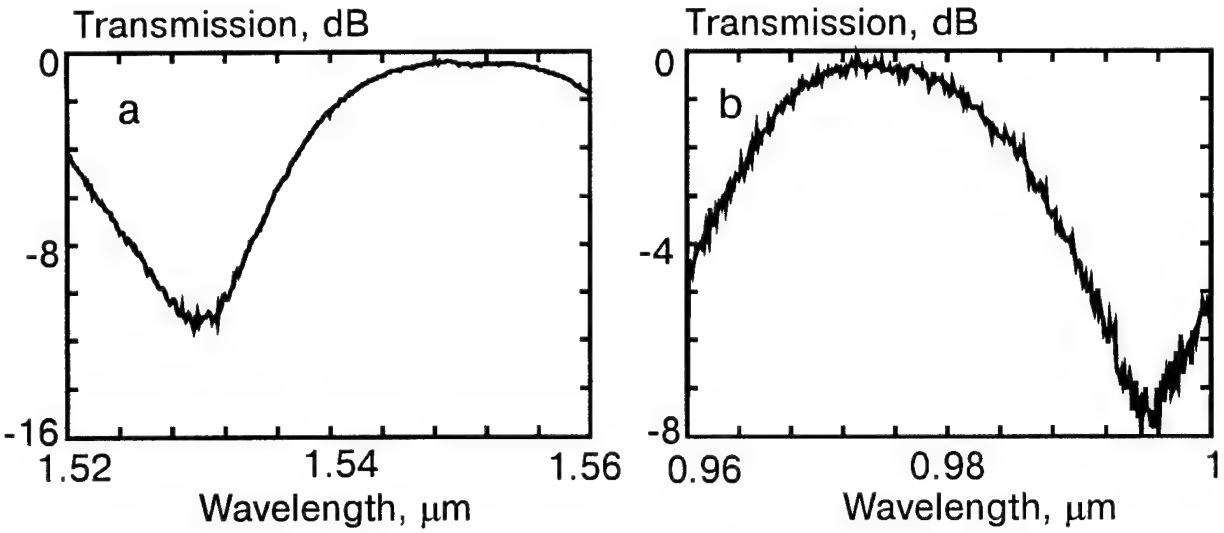

Fig.1. Transmission of the tapered fiber filter at signal (a) and pump (b) spectral regions.

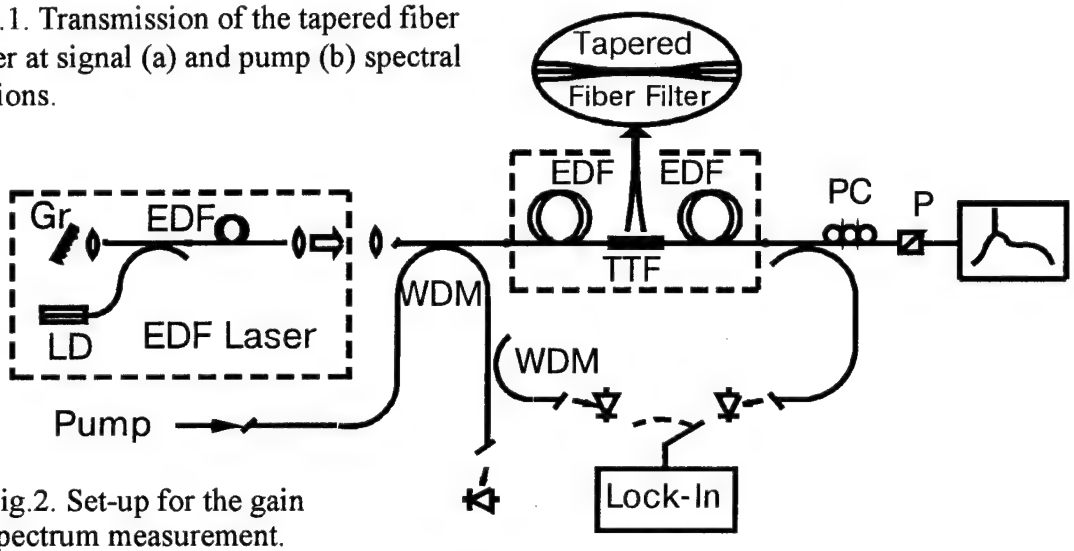

Fig.2. Set-up for the gain spectrum measurement.

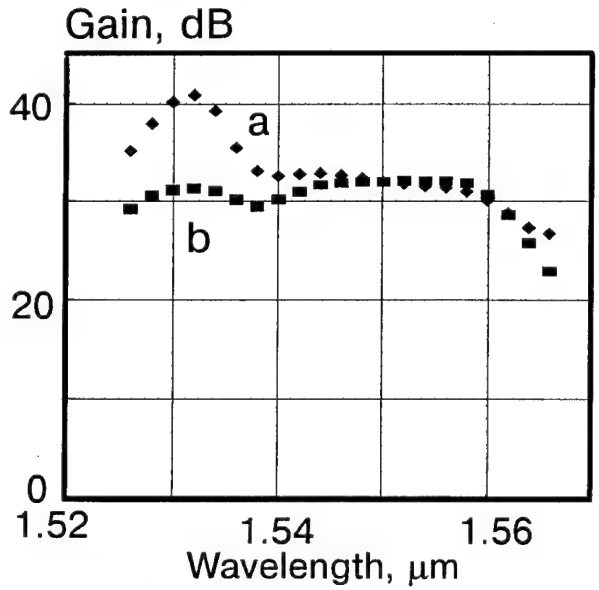

Fig.3. Gain spectrum with (b) and without (a) midway TFF.

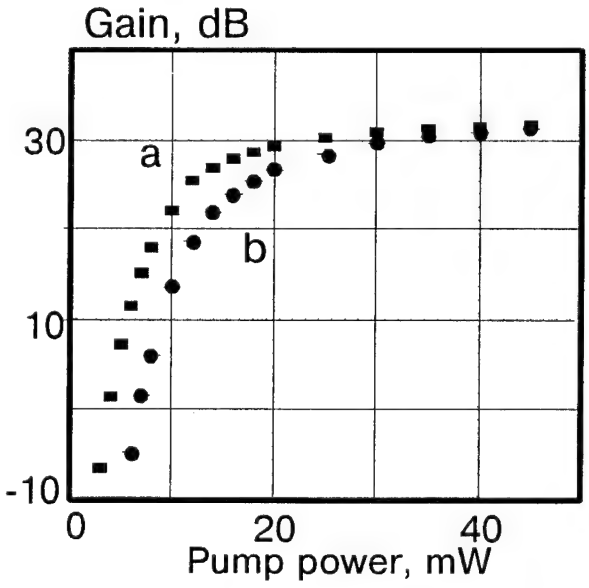

Fig.4. Gain of EDFA with midway filter at 1555 nm (a) and 1532 nm (b).

Gain-Peak-Wavelength Controllable Erbium-Doped Fiber Amplifier for Long-Haul WDM Transmission

Youichi FUKADA, Hideki MAEDA, and Yasutaka ICHIHASHI
NTT Optical Network Systems Laboratories
1-2356 Take, Yokosuka-shi, Kanagawa-ken, Japan
Telephone: +81 468 59 4086
Facsimile: +81 468 59 3396

I. Introduction

One important requirement for long-haul WDM signal transmission over cascaded Er-doped fiber amplifiers (EDFAs) is signal power equalization [1]. Broadening the EDFA gain-spectrum is effective to equalize signal power [1, 2, 3]. Another technique is to make the gain-peak wavelength (GPW) of EDFA coincide with the distribution-center wavelength (DCW) of the WDM signals. In the case of non-cascaded EDFA use, GPW control is achieved by an EDFA with two amplifying sections, whose Er-doped fiber (EDF) type are the same [4]. However, in long-haul transmission with many cascaded EDFAs, GPW is fixed by EDF type, EDF length and operating gain, and it is independent of pump wavelength, pump power, signal power, and EDFA configuration [5].

We propose here a GPW controllable EDFA for cascaded use. This EDFA has two amplifying sections that employ different types of EDF. Then, GPW variation is 4 nm under constant gain operation. Experimental results of GPW control are shown using a gain- and noise figure-spectrum measuring technique proposed in this letter.

II. Gain- and Noise Figure-Spectrum Measuring Set-up

Fig. 1 shows the new gain- and noise figure-spectrum measuring set-up. The EDFA under test forms a loop with a coupler, an AOM switch (AOM 1), and a variable optical attenuator. Part of the EDFA output light is extracted from the loop by the coupler, and measured by an optical spectrum analyzer (OSA). For gating measurement, an AOM switch (AOM 2) is placed between the coupler and the OSA. While AOM 1 is open, the EDFA output spectrum $A_\infty(\nu)$ satisfies the following expression.

$$A_\infty(\nu) = G(\nu) \cdot L \cdot A_\infty(\nu) + h\nu \cdot G(\nu) \cdot F(\nu) \qquad (1)$$

Where, L, h, and ν are loop-loss, Plank's constant, and lightwave frequency, respectively. $G(\nu)$ and $F(\nu)$ are gain- and noise figure-spectrum of the EDFA under test. The EDFA output spectrum $A_0(\nu)$ obtained when AOM 1 is closed is written as follow.

$$A_0(\nu) = h\nu \cdot G(\nu) \cdot F(\nu) \qquad (2)$$

$G(\nu)$ and $F(\nu)$ are obtained as follow.

$$G(\nu) = (1/L)\cdot \{1 - A_0(\nu) / A_\infty(\nu)\} \quad (3)$$

$$F(\nu) = (L/h\nu)\cdot \{A_\infty(\nu) \cdot A_0(\nu)\} / \{A_\infty(\nu) - A_0(\nu)\} \quad (4)$$

$A_0(\nu)$ can be measured by synchronously gating AOM 1 and 2 (Fig. 1).

We measured the gain- and noise figure-spectrum of a conventional EDFA. Loop loss was 20.0 dB. The GPW λ_{gp} and total input power were 1552.0 nm and -16.1dBm, respectively (Fig. 2(a)). Fig. 2(b) plots $G(\nu)$ and $F(\nu)$. To confirm our measurement method, we also measured the gain of the EDFA using WDM signals ($\{\lambda_1+\lambda_2+\lambda_3+\lambda_4\}/4$ = 1552.0 nm, 3 nm spacing, total input power -16.1dBm) (Fig. 2(b)). The gain profiles coincide within 0.2 dB, thus confirming the effectiveness of the proposed measurement method.

III. GPW Control Experiment

The GPW controllable EDFA (Fig. 3) has two amplifying sections. The first section employs a 20m long EDF (type 1----Er^{3+}: 850 ppmw, Al^{3+}: 17,500 ppmw) and the second a 12 m long EDF (type 2----Er^{3+}: 800 ppmw); they are pumped independently. A long-wave-pass-filter (LWPF) at the EDFA's output suppresses ASE at 1530 nm.

Gain spectrum was examined using the proposed measurement method. Loop loss was 10.0 dB to simulate a long-haul transmission system with 50 km EDFA spacing. With the EDFA output power held at 6 dBm, we changed the power of pump 1 and 2 (P_1, P_2). The GPW shifted from 1553 nm (P_1=23.1 mW, P_2=41.5 mW) to 1557 nm (P_1=111.6 mW, P_2=0.0 mW) (Fig. 4). The Noise Figure also changed from 5 dB to 9 dB. The reason for this degradation was lightwave absorption in the first amplifying section when pump power P_1 was small. Noise figure degradation will be improved by increase in number of amplifier section and decrease in EDF length of each section.

IV. Conclusion

We proposed a GPW controllable EDFA suitable for long-haul WDM transmission. The EDFA under constant gain operation exhibited 4 nm GPW shift simply by changing the power of pump 1 and 2. If each pump power are is optimized, power of WDM signals can be equalized.

Acknowledgment

The authors would like to thank Dr. M. Aiki for fruitful suggestions and Dr. I. Kobayashi for his encouragement.

References

[1] E. L. Goldstein, V. da Silva, L. Eskildsen, M. Andrejco, and Y. Silberberg, "Inhomogeneously broadened fiber-amplifier cascade for wavelength-multiplexed systems," IEEE Photon. Technol. Lett., vol. 5, pp. 543-545, 1993.

[2] E. L. Goldstein, L. Eskildsen, G. K. Chang, M. Z. Iqubal, C. Lin, "Self-Regulating WDM Amplifier Module for Scalable Lightwave Networks," OAA '94, FA-2, 1994.

[3] J. Y. Pan, A. F. Elrefaie, R. E. Wagner, and M. Ali, "Fiber-Amplifier Cascades with Equalization Employing Mach-Zender Optical Filters in Multiwavelength Systems," OAA '94, FA-3, 1994.

[4] H. Nakamura, S. Ichino, H. Hayakawa, and H. Ogoshi, "CSO distortion suppression by gain spectrum control of cascaded EDFAs," OAA '94, FB-2, 1994.

[5] P. F. Wysocki, J. R. Simpson, D. Lee, "Gain peaking in EDFAs," OFC '94, FA-4, 1994.

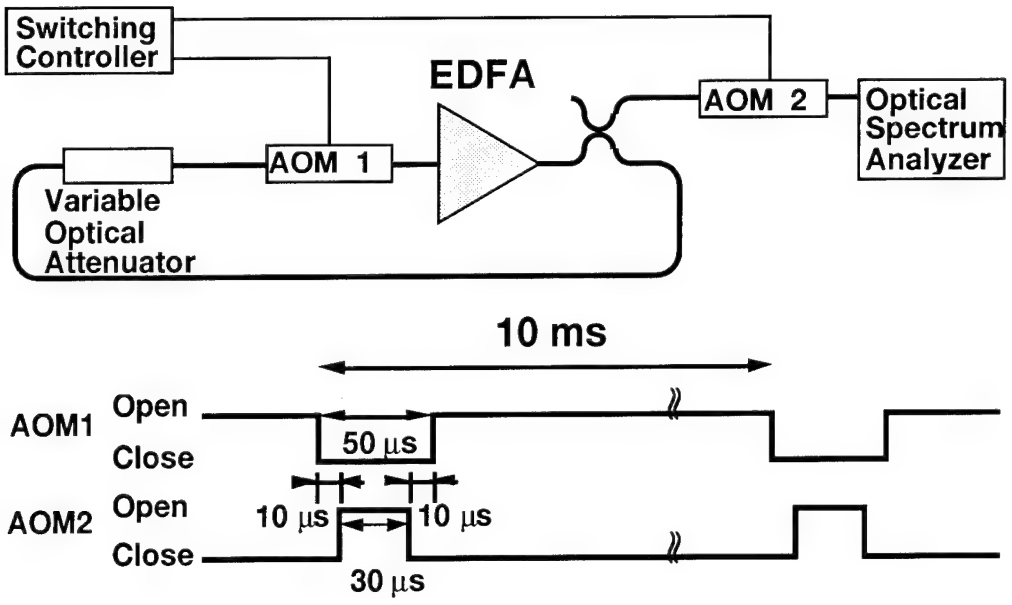

Fig. 1 Gain- and Noise Figure-Spectrum Measuring Set-up in Loop Configuration, and AOM Control Time Chart

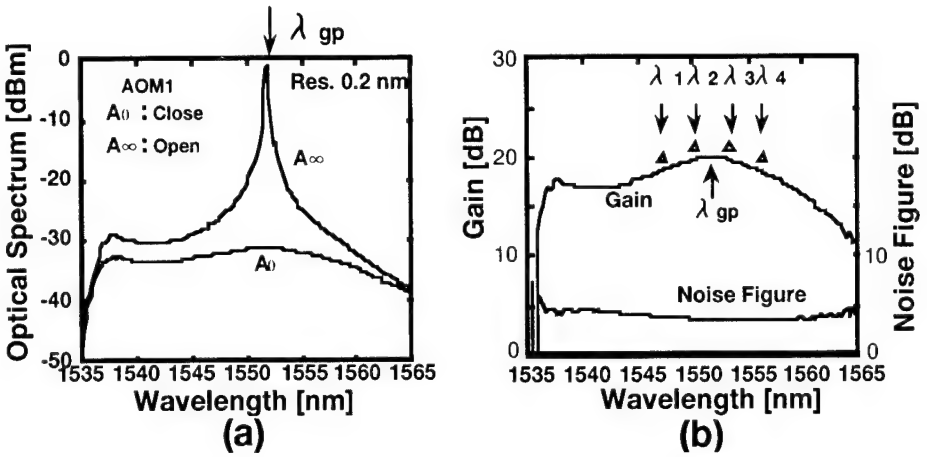

Fig. 2 (a) EDFA Output Optical Spectrum with Loop Configuration (λ_{gp}:gain peak wavelength)

(b) Gain and Noise Figure Spectrum Measured with Loop Configuration

(Δ: gain measured with 4 ch WDM signals($\lambda_{1,2,3,4}$)
$(\lambda_1+\lambda_2+\lambda_3+\lambda_4)/4 = \lambda_{gp}$)

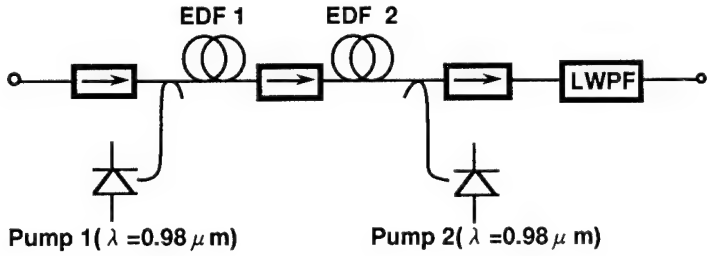

Fig. 3 GPW Controllable EDFA Configuration

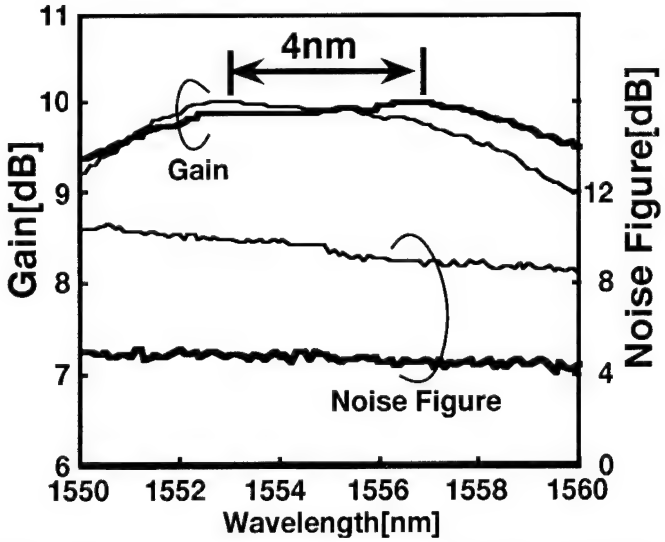

Fig.4 Gain and Noise Figure of GPW Controllable EDFA Measured in Loop Configuration

—— P_1= 111.6 mW, P_2= 0.0 mW

—— P_1= 23.1 mW, P_2= 41.5 mW

Full Suppression of Channel Output Power Co-dependence in Amplifiers, demonstrated in a Two Wavelength System.

Moira Stewart, Richard Epworth
BNR Europe Limited
London Road, Harlow, Essex, CM17 9NA, U.K.
Tel : (01279) 403698
Fax : (01279) 402115

Introduction

As the demand for higher capacity transmission systems continues, Wavelength Division Multiplexing (WDM) looks more attractive. It avoids the problems of higher speed transmission by using multiple lower speed channels on the same fibre. However there are challenges involved in moving to multiple wavelength, not least in the Optical Amplifier itself. Homogeneous broadening within the amplifier is what provides gain over a continous range of wavelengths, but it fundamentally links the output powers of the channels to one another. This co-dependence is unattractive in real WDM networks which will use wavelength switching to route channels and thus need complete independence. In this paper we show a novel use of photo-refractive gratings to break this dependence.

Background

Optical Amplifiers have established themselves as key components in the all optical network. They avoid the need to transfer back to the electrical domain. For single wavelengths the natural saturation characteristics gives constant power output. This feature is especially useful in amplified systems where the loss between amplifiers varies.

As already stated Optical Amplifiers can provide gain over a continuos wavelength range from 1520-1570nm. This is due to the homogeneous broadening of the Stark Levels in the $^4I_{15/2}$ and $^4I_{13/2}$ energy levels which are inhomogenous. The channel co-dependence is caused both by the homogeneous broadening where wavelengths are sharing photons from the same level and also by the different levels being pumped from the same source, therefore the population inversion of all transitions are interlinked. This leads to two problems:-

Problem 1:- The gain spectrum can be flattened for particular input power conditions. In a system the span loss between amplifiers varies, the input power changes and thus gain required from the amplifier changes to compensate. However the resulting gain change is not the same at every wavelength, as is shown in Figure 1. This shows the gain spectra of an amplifier for different span losses, note the non uniformity especially in the 1530nm region. If this effect was concatenated through several amplifiers the channel at 1530nm would disappear into the noise and be undetectable.

Problem 2:- Ideally each channel in a system is required to have output power which is fixed and independent of the powers of the other channels. As the gain spectrum of the amplifiers is dependent on the total input power of the amplifier, removing one channel will increase the gain of the others as the amplifier comes out of saturation.

Unfortunately, these effects are most pronounced at the extremes of the gain spectrum between 1530nm and 1560nm. If the WDM channels are limited to the 1540nm to 1560nm region (solutions using densely spaced WDM within this region have been reported in Reference 1), the effect of problem 1 is reduced but problem 2 still remains and practical laser tolerances and multiplexer/demultiplexer specifications limit their use in today's network.

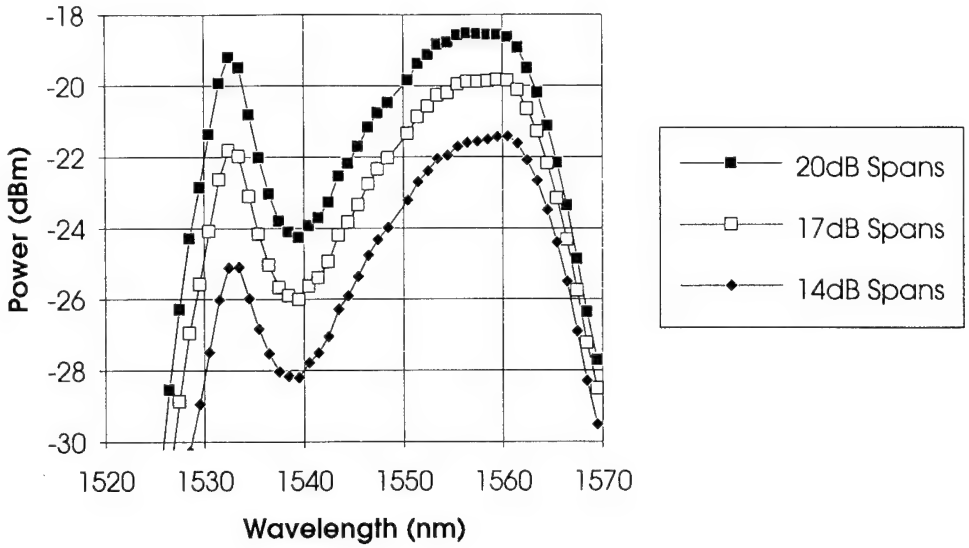

Figure 1 Effect of varying Span Losses

Two Wavelength Solution to Both Problems

Consider the topology in Figure 2a. a two wavelength amplifier at 1533nm and 1557nm. The wavelengths are split at A, amplified completely separately by amplifiers 1 and 2, and recombined at B. Each amplifier is separately controlled and its saturation is dependent on one wavelength only. This topology breaks the co-dependence between the channels. The difference in gain between the two channel with different span losses, is also reduced by equalising the saturation characteristics of the amplifiers at the two wavelengths by optimising the Erbium fibre length and the pump power. This topology closely resembles a Mach-Zehnder Interferometer and coherent interference can occur if there is insufficient isolation between the arms.

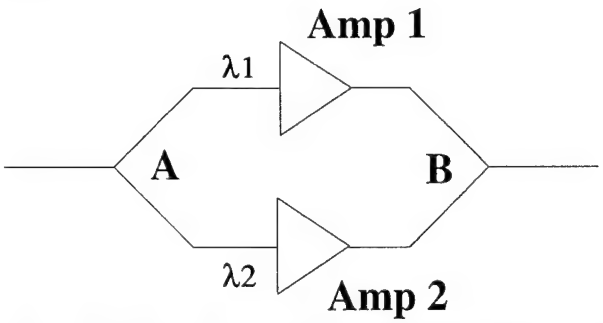

Figure 2a Simple Two Wavelength Amplifier

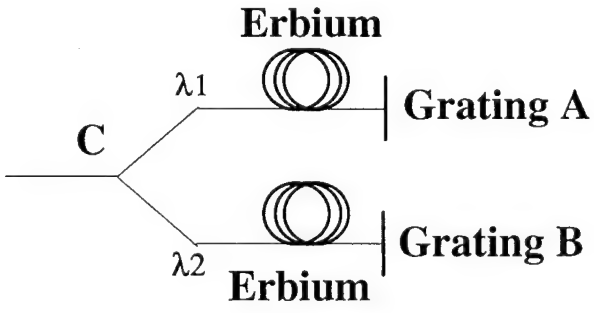

Figure 2b Two Wavelength Amplifier using Gratings

Fibre Gratings can provide high isolation with precise spectral responses (reference 2), so they have been explored to produce a practical solution to the above problems. Figure 2b also shows the topology of an amplifier constructed at BNR using two gratings. Grating A had a pass band of 2nm around 1533nm and grating B had a pass band of 4nm around 1557nm. In this topology the component at C separates input and output signals and could provide wavelength selectivity. For example a circulator and a Wavelength Division multiplexer could be used. If the gratings provide sufficient isolation between their pass and stop bands a wavelength selective device may not be necessary and a 3dB splitter could be used at C. In this

amplifier both wavelengths travel in each arm to the grating, but only one returns. The gain in the forward and reverse directions is the same and clamped by the power in the reverse direction as it is the largest signal in the fibre.

Results and Discussion

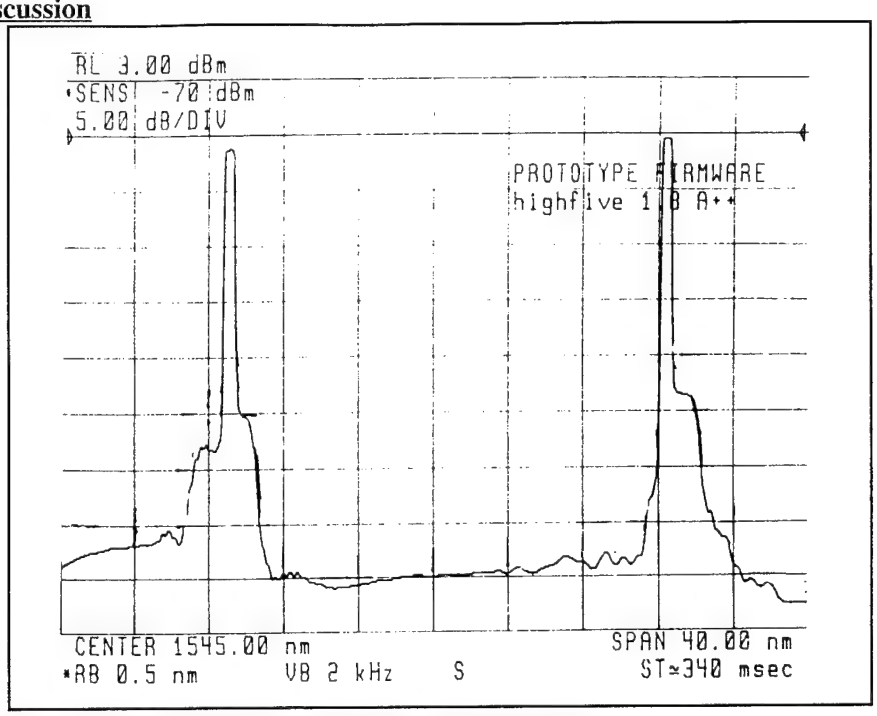

Figure 3 Spectrum of Two Wavelength Amplifier with Gratings

Figure 3 shows the spectrum of an amplifier using gratings. Note that the gratings have provided significant noise reduction away from the signal. The noise around the signal reveals the shapes of the gratings. Table 1 compares the results of the grating amplifier with those of a conventional amplifier.

Conventional Amplifier				Independent Channel Grating Amplifier			
Effect of Span Loss on Gain (Change in Gain/Change in Span Loss)		Effect of Channel Dropping on Gain		Effect of Span Loss on Gain (dB/dB)(Change in Gain/Change in Span Loss)		Effect of Channel Dropping on Gain (dB)	
on 1533nm	on 1557nm	no 1533nm	no 1557nm	on 1533nm	on 1557nm	no 1533nm	no 1557nm
1.7dB/dB	0.8dB/dB	+0.4dB	+2.9dB	0.9 +/-*	0.9 +/-*	+0.4 +/-*	+0.4 +/-*

Table 1 Amplifier Results

The effect of span loss is shown with units dB/dB, this is how much the gain at this wavelength changes when the required gain changes by 1dB. The effect of channel dropping shows the change in gain of one channel when the other is removed. Use of the fibre gratings vastly reduces gain tilt and channel co-dependence in a two channel amplifier.

Measurements of the Independent Channel Grating Amplifier exhibited some variations indicated in table 1 as +/-*, the gain changed by up to +/-0.4dB. This instability is due to coherent interference between the two paths. The level of this interference is dependent on the small-signal gain of the 'wrong' path of the

amplifier and on the isolation provided by the gratings (side mode suppression). This was measured to be 30dB for each grating at its 'wrong' wavelength; the 1557nm grating was replaced with second grating with a side mode suppression of 40dB and the variation reduced to +/-0.1dB (but only for a pass band of 1.5nm). From calculations it was deduced that a total isolation of 53dB would produce 1% uncertainty and these levels of suppression should be possible with appodising (reference 2).

System Implications

The ability to independently control the 1530 and 1550nm areas of the amplifier gain spectrum hold great potential in several areas of Optical Transmission. Optical rings are being implemented in many networks and protection is an important area in the implementation of these networks. To provide full protection in a single wavelength ring, the same number of fibres are required for protection as for normal transmission, doubling the fibre requirement and leading to fibre redundancy. Using a different wavelength for the each direction will remove the need for extra fibres, as shown as discussed in references 3 and 4. Under normal conditions each fibre supports only one wavelength but when a break occurs both wavelengths can travel down each fibre with no interference, ie redundancy now occurs in wavelength not fibre.

In small rings this can be easily implemented and causes no problems. Larger networks, however may use optical amplifiers between nodes to maintain signal level. If conventional amplifiers are used, the channel co-dependence will mean that the introduction of a second wavelength onto the fibre will affect the output of the existing wavelength, possibly reducing its performance. If Grating Amplifiers are introduced this channel co-dependence is broken and the existing channel is unaffected by the introduction of a second.

These amplifiers may also be useful in the trunk network where the introduction of multiple wavelength systems is imminent. Network users generally don't need to provide multiple wavelengths all at once but will need to add wavelengths as demand for capacity increases. They don't want the performance of existing wavelengths to be degraded. In addition, span loss variations and uncertainties cause gain tilt if conventional amplifiers are used, penalising performance. The solution used at present involves padding the spans to the worst case loss and designing the amplifiers for this loss. With these amplifiers, span loss padding may not be necessary and the reach of the system would be increased.

Conclusion

The incorporation of fibre photo-refractive gratings into Optical Amplifiers has broken the channel co-dependence in a two Channel WDM system. It has also introduced an additional degree of freedom whereby the saturation characteristic of each channel can be individually controlled thus removing gain tilt problems. This amplifier removes both of the WDM system problems highlighted in this paper. Broadening the pass band of the grating at 1557nm would allow extra transmission wavelengths independent of the channel at 1530nm, giving extra value to networks outlined in reference 1. This type of amplifier could be implemented in both optical ring networks and the trunk network to enhance performance.

Acknowledgements

The authors would like to thank BNR for permission to publish this work and H Rourke for providing the gratings. Sections of this paper have been published by the I.E.E.

References

1. Gnauck, A.H., "160Gbit/s (8x20GBit/s DM) 300km transmission with 50km amplifier spacing and span-by-span dispersion reversal", Elect. Lett. vol. 30 (**15**), 1994, pp. 1241-1243
2. H Rourke et al, "Development of special grating components for WDM application", IEE Collloquium on Optical Fibre Gratings and Their Applications, London, Jan 1995.
3. Goldstein, E., "Multiwavelength Fiber-Amplifier Cascades for Networks", OFC'94, TuI4, pp39.
4. Elrefaie, A.F., "Fiber-Amplifier Cascades with Gain Equalization in Multiwavelength Unidirectional Inter-Office Ring Networks", IEEE Photon.Technol. Lett., vol. 5, No.9, pp. 1026-1028, 1993.

1W Output Power All-Fiber Laser Based Tm^{3+}-Doped Fluoride Fiber

P. Bousselet, A. Marquant, F. Chiquet, I. Riant and J. L. Beylat

Alcatel Alsthom Recherche, Route de Nozay, 91460 Marcoussis, France
Tel : 33.1.64.49.19.61 Fax : 33.1.64.49.18.65

Introduction

Recent publications have improved the transmission length of repeaterless systems at 2.5 Gbit/s. To this date, fiber spans in excess of 400 km have been achieved [1]. One of the important parameters used to increase the distance of repeaterless systems or to increase the output power of erbium-doped fiber amplifiers [2] is the available power at 1480 nm. This paper deals with the demonstration of a Thulium-Doped Fluoride Fiber Laser (TDFFL), pumped with a 1064 nm Nd:YAG laser, and which allows a high output power at 1480 nm.

Figure 1 presents the schematic representation of the electronic energy levels and transitions of Tm^{3+} [3], and shows the 1480 nm radiative transition from $^3H_4$ to $^3F_4$ levels, along with the lifetime of each level in fluoride glass fiber. With a silica glass fiber, the short lifetime of the $^3F_4$ level reduces the population of the $^3H_4$ level. By using a fluoride glass fiber, this lifetime is increased by about a factor of 10 ($\approx$ 10 ms) [4], and an inverted population can be observed between $^3H_4$ and $^3F_4$ levels.

To obtain the 1480 nm transition, Figure 1 shows all the pump wavelength possibilities, and we observe that 0.66 µm and 0.79 µm seem to be the more logical ones. However, some papers have shown that these wavelengths do not allow a good conversion efficiency with the 1480 nm [4,5]. Others have proved that the efficient upconversion pumping wavelength was 1064 nm, owing to the active Excited State Absorption transition between $^3F_4$ and $^3F_2$ levels [6]. The upconversion scheme employed to pump the TDFFL at 1064 nm provides an elegant route to efficiently populate the $^3H_4$ level while simultaneously depopulating the $^3F_4$ level [7].

In agreement with these theoretical conditions, a 1-W CW TDFFL has already been shown in a recent publication [8]. In order to build a laser compatible with the compact sizes and the reliability required by the transmission systems, we present here an all-fiber architecture TDFFL, pumped at 1064 nm.

Experimentation

Figure 2 presents the internal structure of the laser. The pump light source was a 6 W CW TEM_{00} Nd:YAG laser operating at 1064 nm. This level of power is compatible with those obtained with recent LD-pumped Nd:YAG lasers. The coupling efficiency in a single-mode fiber was higher than 50%. The laser cavity was made with a 3-meter Thulium-Doped Fluoride Fiber (TDFF) and closed with two In-Fibre Bragg Gratings (IFBG's).

The ZBLAN single-mode fluoride fiber was elaborated by a casting and overcladding process. The perform and the jacketing tube were prepared from Zr, Hf, Ba, La, Al, Na, Li, Pb and Y commercial pure fluorides and cast by a rotational casting technique [9] in an inert dry atmosphere. The Tm^{3+} content in the core glass is 2000 ppm. The raw materials were mixed and melted in a platinum

crucible in a reactive gas flow and poured into a brass mould. Before the fiber drawing the stretched perform and the overclad tube were mechanically polished, $ZrOCl_2$ chemically etched and ethanol rinsed to optimise mechanical properties. The fiber was drawn in an inert atmosphere and coated with a UV curable polyacrylate polymer. The outer and the core diameters measured by microscopy were respectively 125 µm and 7 µm. The minimum loss, measured by the cut-back method, was 0.19 dB/m at 1380 nm. The reactive index difference Δn was 7.10^{-3} and the cut-off wavelength was 1330 nm.
Figures 3 and 4 show respectively the absorption and the fluorescence spectra measured on the TDFF. These two figures are the physical translation of the Figure 1. A large emission bandwidth around 1470 nm, corresponding to the transition between the $^3H_4$ and $^3F_4$ levels, was observed.

The 1480 nm selection was made by the IFBG's themselves. The IFBG's reflectivities at 1480 nm were 99.8% and 36% for the input and output, respectively. All the other wavelengths, particularly the 1064 nm emission, were transmitted without loss due to the IFBG's. These IFBG's were fabricated by a side holographic exposure in a Ge doped core of an optical fiber, using a 484-nm dye laser frequency doubled by a BBO crystal, and a prism to generate interferences [10]. The 99.8% and 36% IFBG's had spectral bandwidths of 1.2 nm and 0.5 nm, respectively.
To eliminate the 1064 nm residual launched pump power at the output of the TDFFL, and measure only the 1480 nm emission, a grating filter was used. Its characteristics were a -3 dB bandwidth close to 1.3 nm and a rejection efficiency of 40 dB for the other wavelengths (including 1064 nm). We finely evaluated the insertion loss of this filter at 1480 nm and added it to the output power read just after it. So, we could know exactly the 1480 nm power just after the second IFBG.

The difference of fusion temperature between silicate glass fiber and fluoride glass fiber did not allow the use of a splicing adjustment technique but rather a butt joint one. For this experiment, we used butt-joint splicing without index matching glue in order to suppress the reliability problems associated with a high flux.
This technology was compatible with the laser oscillation structure ensured by IFBG's.

Results and discussions

Exactly 1.07-W CW 1480 nm laser light was obtained with this all-fiber design. To get this result, 3-W CW 1064 nm launched pump power was necessary. The slope efficiency was exactly 33.5% and the threshold close to 200 mW. Figure 5 shows the 1480 nm spectral emission after the output filter with 400 mW of launched pump power.

Owing to the good opto-geometrical qualities and the appropriate dimensions of the TDFF core, we were able to launch more than 3 W at 1060 nm without damage in the TDFF and in the butt-joints. To optimize this laser, an index adaptation will be necessary between the silica and fluoride glasses. The threshold and the performance will be better as soon as the intra-cavity losses will be decreased. Also, we will be able to improve this performance by using in-thulium doped fluoride fibre Bragg gratings.

Conclusion

With only 3 W of pump power at 1064 nm, we obtained 1 W of output power at 1480 nm in an all-fiber architecture of a thulium-doped fluoride fiber laser. A threshold of 200 mW and a slope efficiency of 33.5% were observed. This work shows that an upconversion pumping scheme at 1064 nm and an all-fiber architecture can be used to give performance characteristics in excess of conventional 1480 nm-laser diodes.

References

[1] O. Gautheron et al., "407 km, 2.5 Gbits/s repeaterless transmission using an electroabsorption modulator and remotely pumped erbium-doped fiber post-and-pre-amplifiers", in *Tech. Dig. ECOC'94*, Florence, Italy, vol. 4, pp.15, 1994.
[2] P. Bousselet et al., "+25.2 dBm output power from an erbium-doped fiber amplifier with 1.48 mm SMQW laser diode modules", in *OFC'95*, San Diego, USA, Tu J2, Feb. 1995.
[3] M. J. F. Digonnet, "Rare earth doped fiber lasers and amplifiers", fig. 25, pp. 472, M. Decker INC., 1993.
[4] J. Y. Allain et al., "Tunable CW lasing around 0.82, 1.48, 1.88 and 2.35 mm in thulium-doped fluorozirconate fibre", *IEE Electron. Lett.*, vol. 25, n° 24, pp 1660-1662, 1989.
[5] R. Allen et al., "An efficient 1.46 μm thulium fiber laser via cascade process", *IEEE Journal of Quant. Electron.*, vol. 29, n° 2, 1993.
[6] T. Komuka et al., "Efficient upconversion pumping at 1.064 μm of Tm^{3+}- doped fluoride fibre laser operating around 1.47 μm", *IEE Electron. Lett.*, vol. 28, n° 9, pp. 830-832, 1992.
[7] R. M. Percival et al., "Highly efficient 1.064 μm upconversion pumped 1.47 μm thulium-doped fluoride fibre laser", *IEE Electron. Lett.*, vol. 30, n°13, 1994.
[8] Y. Miyajima et al., "1-W CW Tm-doped fluoride fibre laser at 1.47 μm", *IEE Electron. Lett.*, vol. 29,n° 8, pp. 660-661, 1993.
[9] D.C. Tran et al.,"Fluoride glass preforms prepared by rotational casting process", *IEE Electron. Lett.*, vol. 18, pp. 657, 1982.
[10] G. Meltz et al., "Formation of Bragg gratings in optical fibres by a transverse holographic method',*Opt. Lett.*, vol. 14, n° 15, pp. 823-825, 1989.

Fig1 : Electronic energy levels and transitions of Thulium

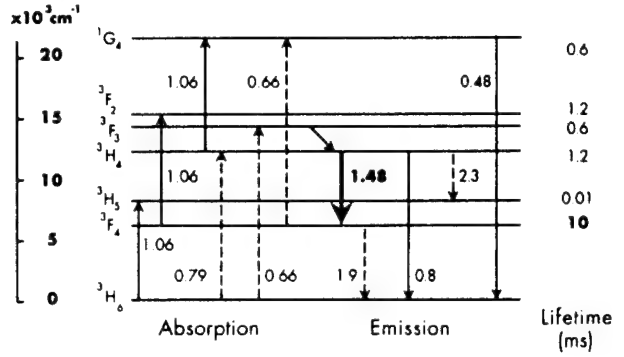

Fig 2 : Experimental set up

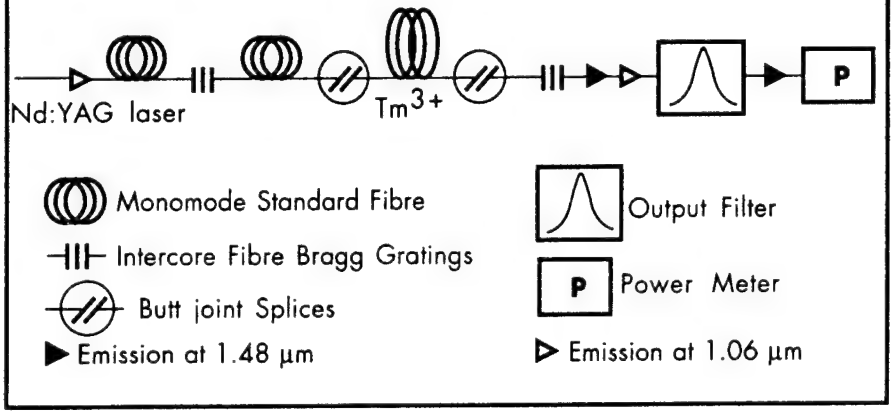

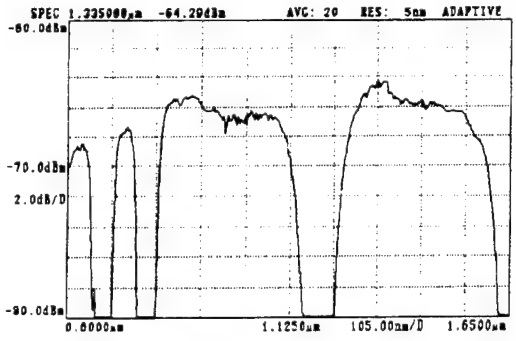

Fig 3 : Absorption spectrum

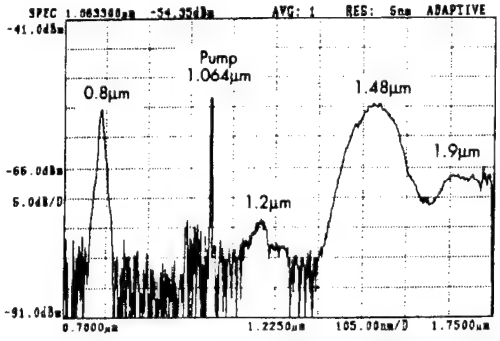

Fig 4 : Fluorescence spectrum

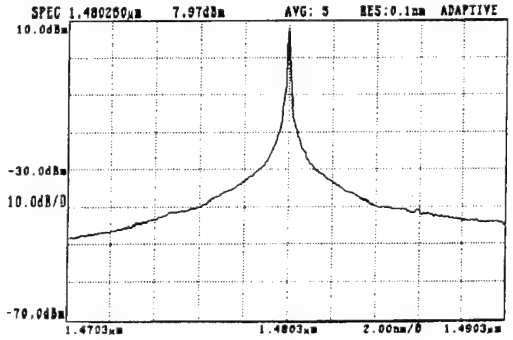

Fig 5 : Laser emission spectrum

EDFA gain equalization with fiber filter for WDM systems

Eric Saint Georges
Advanced Optical Networking Department
T.J. Watson IBM Research Center
P.O. Box 704, Yorktown Heights, New York, NY 10598
Tel (914) 784 6072 Fax (914) 784 6225

Introduction

Erbium doped fiber amplifiers can achieve a high gain over more than 40nm bandwidth. However, they suffer from a non uniformity of the gain, and this is particularly detrimental to WDM applications. As they propagate through a chain of EDFAs, the channels at different wavelengths will accumulate increasing discrepancies between them in terms of gain and SNR. In order to make it possible to chain EDFAs in a WDM environment, the EDFAs should have ideally both a flattened gain and SNR. A method as proposed in [1] and [2] admittedly cannot achieve equalization of both gain and SNR. On the other hand, some EDFAs are optimized for WDM by adjusting the characteristic and length of the fiber and the pump power [3], but in that case they usually show a flattened gain for a small range of input power.

Among various means proposed to achieve gain equalization of the EDFAs is the use of a filter [4], [5]. For that, the Bragg grating technology seems a promising way to easily insert a filter within a fiber with low insertion loss [6], and [7] shows that the technology needed to implement complex fibers should be available soon. The question is then to define the ideal shape of such a filter. This paper discusses the results of simulating such a filter embedded in the fiber.

The shape of the ASE of the EDFA without input signal, is used as the filter attenuation shape, and we show that in addition to a very good equalization of the gain, this method provides two advantages : 1) - SNR flatness, and 2) - The same quality of gain equalization can be achieved over a wide range of input power, by only adjusting the pump power, and the resulting gain is constant, and fully determined by the choice of the filter shape.

We discuss how we determine at what pump power the ASE, which is taken as the basis for the filter shape, should be generated and we show how to optimize the position of the filter in the fiber.

We finally discuss the advantages for WDM systems, of incorporating a feedback loop on the pump power in an EDFA with such a filter, and we show the results obtained when cascading EDFAs implementing this feedback loop.

EDFA Model and fiber parameters

The simulation is based on a spectrally-resolved model developed in [8](pages 25-31), with a Gaussian envelope approximation for the mode envelope, and assuming a step profile E_r^{3+} doping. The fiber parameters used are : a (core radius) $= 2\mu m$, a_0 (doping radius) $= 1.2\mu m$, $NA = 0.2$, $E_r^{3+} density = 362ppm\ (mol)$, τ (fluorescence life time) $= 10.5ms$, σ_a^{peak} (peak absorption cross-section) $= 5.6e^{-25}m^2$, σ_e^{peak} (peak emission cross-section) $= 3.8e^{-25}m^2$. The fiber length is 8 meters, and the EDFA is forward pumped at $1.480\mu m$. The spectral resolution used for the computations is 0.2nm.

Results

The following results were obtained for 32 channels spaced by 1 nm between $1.530\mu m$ and $1.561\mu m$, and with the filter in the center of the fiber (We justify this placement in a further section). Our simulation shows results obtained when using the shape of the ASE as filter attenuation. The question is to choose what pump power is to be used for this ASE shape.

Let's define *F(x)* as the shape of the ASE of the EDFA without input signal when pumped at x dBm, and let's call P_F this pump power.

If we use a *F(12)* filter and if we pump the EDFA at the same 12dBm we can see from Fig. 1(a) that the output of the amplifier shows a relatively flat SNR, but that both gain and ASE are lower in the short wavelength region than in the long wavelength region (The input power is -30dBm per channel, the minimum SNR is 18.9 dBm and the maximum SNR is 20.8dB, while the gain variation is 5dB). Keeping the filter fixed but increasing the pump power eventually achieves both a very good gain equalization and SNR equalization on the whole bandwidth. Fig. 1(b) shows that with a pump power set to 17.24dBm, the gain variation is less than $\pm 0.13dB$ between 1.530μ and 1.560μ, for an input power of -30dBm per channel with a $F(12)$ filter. And the SNR is enhanced (Minimum 19.6dB and maximum 21dB SNR). If the input power (or the number of channels) changes, same level of equalization of the gain and of the SNR can still be achieved by adjusting the pump power. And moreover, the gain stays almost constant, as shown in Fig. 2 which plots the minimum and maximum gain function of the input power (per channel).

For a given $F(x)$ filter, equalization is achieved when the population inversion level of the EDFA is the same as the inversion level obtained when pumping the EDFA at P_F with zero input power. Since the gain depends only on the inversion level, it remains constant if the same population inversion is maintained. Fig. 3 shows how the pump power required for the equalization depends of the input power, for different P_F. The pump power P_F used to defined the filter depends on the maximum input power and the required gain. All the following results are obtained for a $F(10)$ filter. Fig. 4 shows the shape of this filter.

Optimizing the position of the filter

The advantage of having a filter in the middle of the fiber has already been discussed in [5] and [4]. In addition to flattening the gain, it increases the gain in the $1.550\mu m$ region by attenuating the ASE and therefore increasing the efficiency of the amplifier. Our simulation shows that if the filter is located at the beginning of the fiber, the equalization pump power is minimum. Fig. 5 shows how the equalization pump power required for -20dBm input power per channel and a $F(10)$ filter depends on the filter position. If the filter is located at the end of the fiber, the equalization power increases and the gain decreases slightly. From this point of view, the best location is the beginning of the fiber. But in that case, the noise and the gain variations are increased. We found that locating the filter in the middle of the fiber offers a good compromise for the noise, gain, equalization and EDFA efficiency.

EDFA with feedback

A problem that has to be dealt with in WDM systems is that one or more channels may be dropped at any time. This is particularly relevant in networks were drop and insert and dynamic channel allocation are likely to be used. The resultant changes of the number of channels on WDM link modifies the input power of the EDFA. In this case, implementing a feedback loop on the pump power based on monitoring of the output power spectral distribution of the amplifier makes it possible to keep a constant gain in addition to the equalization, independent of the input power, and thus facilitates the management of WDM networks. We simulated a feedback loop achieving the equalization. In our simulation, we implemented a monitoring of the output power of the shortest and longest wavelength channels, the feedback achieving therefore the gain equalization by equalizing these two channels. In order to take into account that in real systems, the different channels may start with slightly different power levels, we can implement more sophisticated monitoring, averaging the whole spectrum, in order to equalize the average channel power. Taking advantage of the fact that the gain is constant when equalization is achieved, another solution is to inject locally a channel at the EDFA input. In this case it is possible to monitor its gain with precision, achieving the gain equalization by stabilizing this gain to the right value. This channel must be in the $1.530\mu m$ peak region, because it is in this region that the power depends the most on the pump and input powers. If a system implements a maintenance channel, this solution can take advantage of it because this channel would need anyhow to be re-injected at each EDFA location.

Cascading EDFAs

We simulated a chain of 20 EDFAs over 2000km, each of them incorporating a $F(10)$ filter and the feedback loop (equalizing the output power of the shortest and longest wavelength channels), each EDFA output being attenuated by 22 dB (emulating 105 km of 0.21dB/km attenuation fiber). The input to the first EDFA consists of 32 channels at -20dBm each. Fig.6 shows the output of the 20th EDFA. The gain variation on the 31nm bandwidth is less than 6.3dB, with a minimum SNR of 14.6dB. The pump power required for the equalization varies along the chain between 18.9dBm and 19.6dBm.

CONCLUSION

We have studied the equalization of the gain of EDFAs using an ideal filter located in the center of the fiber. This filter, in addition to achieving a very good gain equalization over the whole bandwidth of the EDFA, also increases the performance of the amplifier in the $1.550\mu m$, and at the same time achieves SNR flatness and constant gain over a wide input power range by adjusting only the pump power (which is a parameter which can be easily adjusted while the EDFA is in use). Therefore an EDFA with a constant flattened gain over a wide range of input power can be designed, by implementing a feedback loop on the pump power, based on monitoring of the output power spectrum of the EDFA.

ACKNOWLEDGMENT

The author wish to thank P.E. Green, K. Liu and T. Schrans for helpful and stimulating discussions and for their continuous encouragement, and P. Pepeljugoski for his help in using Matlab.

References

[1] A.R. Chraplivy, J.A. Nagel, R.W. Tkach, "Equalization in Amplified WDM Ligthwave Transmission Systems," *IEEE Phot.Tech.Lett.*, vol. 4, No 8, August 1992.

[2] A.R. Chraplivy, R.W. Tkach, K.C. Reichmann, P.D. Magill, J.A. Nagel, "End-to-End Equalization Experiments in Amplified WDM Ligthwave Systems," *IEEE Phot.Tech.Lett.*, vol. 4, No 4, April 1993.

[3] M.A. Ali, A.F. Elrefaie, R.E. Wagner, F. Mendez, J. Pan, S.A. Ahmed "Optimized Performance of Erbium-Doped Fiber Amplifiers in Multi-wavelength Ligthwave Systems," *IEEE Phot.Tech.Lett.*, vol. 6, No 8, August 1994.

[4] C.R. Giles, E. Desurvire, "Modeling Erbium-Doped Fiber Amplifiers," *J. Lightwave Tech.*, vol.9, p. 271-283, (1991).

[5] M. Tachibana, R.I. Laming, P.R. Morkel, D.N. Payne, "Erbium Doped Fiber Amplifiers with Flattened Gain Spectrum," *IEEE Phot.Tech.Lett.*, vol. 3, No 2, February 1991.

[6] R. Kashyap, R, Wyatt, R.J. Campbell, "Wide band gain Flattened Erbium Fiber Amplifier using a Photosensitive Fibre blazed Grating," *Electron. Lett.*, vol. 29, No 2, January 1993.

[7] J. Martin, J. Lauzon, F. Ouellette, "Novel writing technique of long in-fiber Bragg gratings and investigation of the linearly chirped component," *CLEO 94 conference*, paper CWK2 (1994).

[8] E. Desurvire, *Erbium-Doped Fiber Amplifiers. Principles and Applications*, John Wiley, New York, (1994).

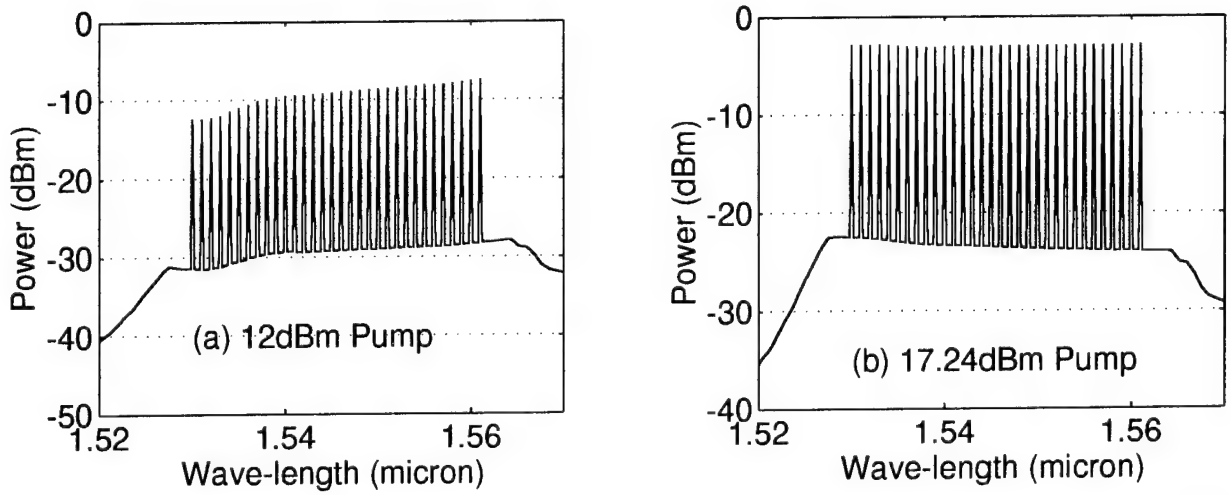

Fig 1. Ouput for 32 channels -30dBm (per chan.) input power, with F(12dbm) filter.

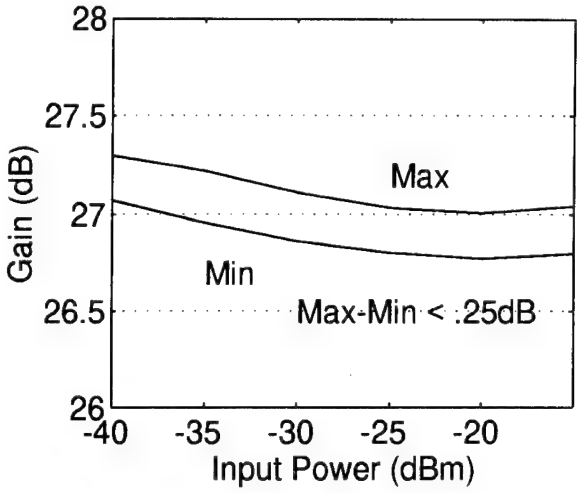

Fig 2. Min & max gain over the 30nm.

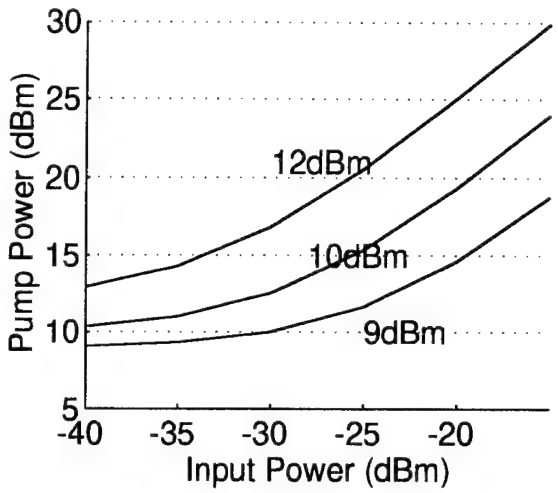

Fig 3. Equalization pump power for PF =9, 10 & 12 dBm.

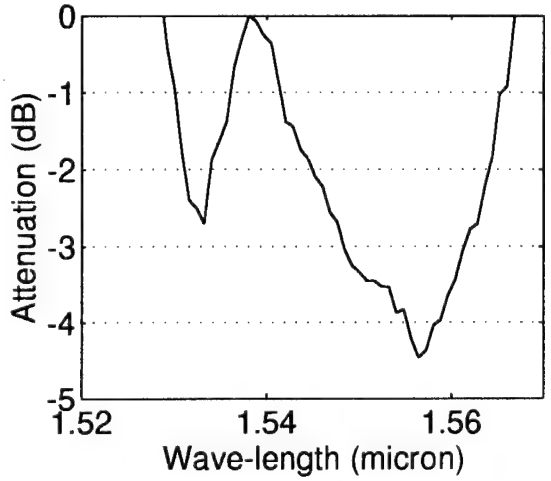

Fig 4. Filter shape for 10dBm PF.

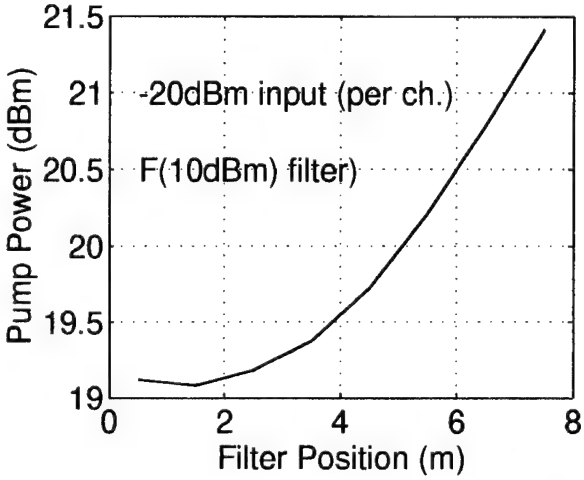

Fig 5. Equalization pump power required as a function of the filter position.

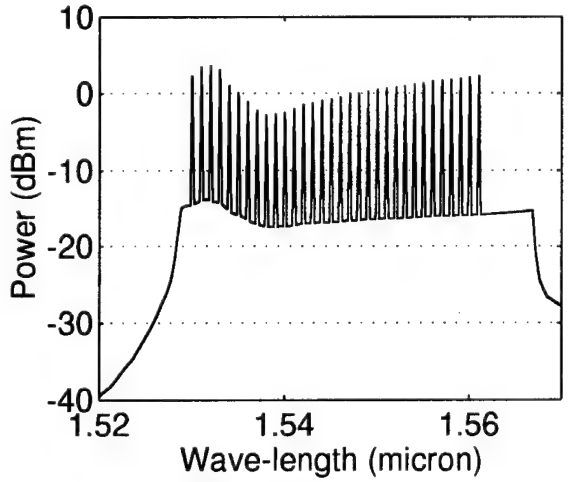

Fig 6. 20th EDFA output.

Spectroscopic properties of Nd^{3+} doped fluoride crystals for amplification at 1.3 μm

V.B. Sigachev, T.T. Basiev, M.E. Doroshenko, V.V. Osiko, A.G. Papashvili

General Physics Institute, Russian Academy of Sciences, Vavilov Street 38, Moscow

Russian Federation, Telephone: (095) 135-03-18, Fax: (095) 135-02-70.

1. INTRODUCTION

A gain medium for 1.3 μm amplifiers of fiber communication networks has to have (a) high and isotropic gain in (1.28-1.32) μm range, and (b) high pumping efficiency at wavelengths of most suitable pump sources (for instance, diode lasers). The utilization of $^4F_{3/2}$-$^4I_{13/2}$ transition of Nd^{3+} ions in crystals and glasses is one of the ways to solve this problem. But two main difficulties have to be overcome for Nd^{3+} doped media. First of all, it is necessary to shift Nd^{3+} emission to the desired spectral position, since the fluorescence of Nd^{3+} ions is usually observed at wavelengths around 1.34 μm. The second obstacle is excited state absorption (ESA) at $^4F_{3/2}$-$^4G_{7/2}$ transition, that can reduce or suppress totally gain at $^4F_{3/2}$-$^4I_{13/2}$ transition.

The goal of this work is to study absorption losses at $^4F_{3/2}$-$^4G_{7/2}$ transition responsible for ESA and emission characteristics (fluorescence and lasing) at $^4F_{3/2}$-$^4I_{13/2}$ transition resposible for gain in a number of Nd^{3+} doped fluoride crystals in order to estimate their applicability to 1.3 μm amplifiers.

2. OBJECTS OF RESEARCH

General analysis of host material influence on shortest emission wavelength near 1.3 μm shows that fluoride crystals and glasses have smaller value of overlapping of RE ion and ligand wave functions, and as a result they have smaller values of nephelauxetic shift, higher energy positions of levels and shorter wavelengths of optical transitions.

The following groups of Nd^{3+}-doped disordered fluoride crystals were grown and studied: a) cubic symmetry crystals of CaF_2, SrF_2, BaF_2, CdF_2 and solid solutions of SrF_2-CaF_2 with fluorite type structure; b) cubic symmetry crystals of SrF_2-LaF_3, CaF_2-YF_3, BaF_2-LaF_3 with yttrofluorite type structure; c) hexagonal symmetry solid solutions of LaF_3-SrF_2, CeF_3-SrF_2 with tysonite type structure; d) cubic symmetry crystal of $5NaF$-$9YF_3$.

The necessity of investigation of disordered crystals or crystalline solid solutions having wide inhomogeneously broadened spectral lines of Nd^{3+} ions is due to requirement of maximum width of gain band and the possibility to realize smooth variations of optical properties of Nd^{3+} ions in solid solutions.

Heterovalent character of Nd^{3+} substitution in studied fluorides results in a variety of charge compensation centers[1,2]. Usually compensation is due to interstitial fluorine ion F_i^-. Different surrounding of Nd^{3+} ions gives rise to their different absorption and fluorescence properties. So, in alkaline earth fluoride crystals MeF_2 (Me^{2+} = Ca^{2+}, Sr^{2+}, Ba^{2+}, Cd^{2+}) Nd^{3+} centers can be divided into single and clustered ones. The single Nd^{3+} ion center composed of Nd^{3+}-F_i pair can have tetragonal (C_{4v}) or trigonal (C_{3v}) local symmetry. The clustered Nd^{3+} centers have rhombic local symmetry (C_s) and composed of two, four and etc. Nd^{3+}-F_i^- pairs. In crystals with yttrofluorite structure clustered rhombic symmetry centers are predominating types of Nd^{3+} centers.

3. RESULTS

To predict gain properties of the crystals the Judd-Ofelt analysis for intensities of Nd^{3+} ion optical transitions was carried out on the basis of measured absorption spectra[3-5]. The set of Ω_2, Ω_4, and Ω_6 intensity parameters have been found for all the studied crystals. Using these data line strength S_{em} of $^4F_{3/2}$-$^4I_{13/2}$ gain transition, and line strength S_{esa} of $^4F_{3/2}$-$^4G_{7/2}$ excited state absorption transition were calculated.

Calculated intensity parameters Ω_t and ratios S_{em}/S_{esa} for some studied fluoride crystals are listed in Table. Results of Judd-Ofelt analysis allow to compare studied groups of crystals in terms of ratio of line strengths for gain and loss transitions from $^4F_{3/2}$ level of Nd^{3+} ion near 1.3 μm wavelength. The highest values of S_{em}/S_{esa} ratio in the range of the 4-5 is realized in alkaline earth fluoride crystals CaF_2, SrF_2, CdF_2 and solid solutions SrF_2-CaF_2 for low enough Nd^{3+} ion concentrations, where high symmetry single-ion Nd^{3+} optical centers predominate over clusters. Therefore these crystals have low Ω_2 and Ω_4 intensity parameters and high Ω_6 intensity parameter. Somewhat lower ratios S_{em}/S_{esa}=3-4.4 are realized in crystals MeF_2-LnF_3:NdF_3 with yttrofluorite type structure, where lower symmetry rhombic optical

centers and their complexes predominate. And at last the smallest S_{em}/S_{esa} ratios varying in the range of the 2.6-3.7 have hexagonal solid solutions of LaF_3-SrF_2:NdF_3 and CeF_3-SrF_2:NdF_3 and cubic solid solution of 5NaF-9YF_3:NdF_3. It should be noted that the ratio S_{em}/S_{esa} for all the studied fluoride crystals except BaF_2 :NdF_3 is higher than that ratio in well known ZBLAN:Nd^{3+} glass, which value does not exceed 2.2 [6].

Fluorescence spectra of MeF_2-LnF_3:NdF_3 and 5NaF-9YF_3:NdF_3 cubic crystals, and Nd^{3+} doped alkaline earth fluorides and (1-x)CaF_2-xSrF_2 solid solutions are shown in Fig. 1-3. For comparison the fluorescence spectrum of Nd^{3+} doped ZBLAN glass is shown in Fig.3. Fluorescence spectra of studied crystals at $^4F_{3/2}$-$^4I_{13/2}$ transition have substantial inhomogeneously broadened shapes (FWHM~ 200-500 cm^{-1}). The nature of the drastic inhomogeneous splitting and broadening of the spectra is the multisite character of Nd^{3+} optical centers. Shortest wavelength fluorescence with maxima in the 1.29-1.32 μm band was observed for tetragonal symmetry Nd^{3+} centers in SrF_2, CaF_2 and CaF_2-SrF_2 solid solutions, and for 5NaF-9YF_3 crystal. For the clustered Nd^{3+} centers in alkaline earth fluorides and for other studied crystals the fluorescence peaks are at wavelengths grater than 1.32 μm, but all the crystals have substantial short wavelength fluorescence side bands in desired 1.28-1.32 μm spectral range.

It should be noted that fluorescence spectra of MeF_2-LnF_3:NdF_3, LnF_3-MeF_2:NdF_3 and 5NaF-9YF_3:NdF_3 solid solutions do not depend considerably on excitation wavelength and Nd^{3+} ions concentration. Different situation realizes for CaF_2 and SrF_2 crystals and their solid solutions. Considerable dependence of fluorescence spectra on excitation wavelength λ_{ex} is the feature of alkaline earth fluoride crystals. Short wavelength fluorescence of tetragonal symmetry centers and long wavelength fluorescence of clustered Nd^{3+} centers is shown in Figs. 2 and 3 respectively.

The fluorescence spectra of tetragonal symmetry centers in CaF_2:NdF_3, SrF_2:NdF_3 crystals and (1-x)CaF_2-xSrF_2:NdF_3 solid solutions are well matched to desired gain band, since three most intensive short wavelength lines are in the 1.29-1.32 μm range. The addition of SrF_2 to CaF_2:NdF_3 results in inhomogeneous broadening of fluorescence lines, but not so dramatic as in the case of LaF_3-SrF_2:NdF_3, CaF_2-YF_3:NdF_3, BaF_2-LaF_3:NdF_3 crystals. Variation of the (1-x)CaF_2-xSrF_2:NdF_3 solid solution composition affects most considerably on the monotonic shift of all lines maxima due to variation of $^4I_{13/2}$ level Stark splitting. Compositions with x=50-70 mol. % of NdF_3possess maximum inhomogeneous broadening of fluorescence lines of tetragonal symmetry centers and have comparatively high Nd^{3+} concentration, up to which this type of centers predominate.

Judd-Ofelt calculation results and measured fluorescence spectra were used to find emission cross section spectra $\sigma_{em}(\lambda)$ for $^4F_{3/2}$-$^4I_{13/2}$ transition and radiative lifetime τ_r of $^4F_{3/2}$ level (see Table), and their product $\sigma_{em}(\lambda)\,\tau_r$ which characterize maximum attainable gain. Emission cross section spectra $\sigma_{em}(\lambda)$ and spectra of $\sigma_{em}(\lambda)\,\tau_r$ product for some crystals are shown in Figs. 4,5. The highest values of product $\sigma_{em}(\lambda)\,x\tau_r=(5\text{-}6)\,x10^{-24}$ cm^2s in 1.3 μm telecommunication window are realized for emission peaks of tetragonal symmetry Nd^{3+} centers in SrF_2 crystal and CaF_2-70%SrF_2 solid solution. For other crystals the $\sigma_{em}(\lambda)\tau_r$ product in 1.28-1.32 μm range vary from about $0.2x10^{-24}$ cm^2s to about $3x10^{-24}$ cm^2s.

Gain properties of studied fluoride crystals were established during the laser experiments. The pump source was free-running alexandrite laser with 100 μs pulse duration and 30 mJ/pulse output energy. Wavelength of alexandrite laser was tuned in the range of 740-755 nm.

Laser oscillation at $^4F_{3/2}$-$^4I_{13/2}$ transition have been realized for SrF_2:0.8%NdF_3 , 48%CaF_2-48%SrF_2:2%NdF_3, and 68.5%SrF_2-30%LaF_3:1.5%NdF_3 crystals. Obtained laser oscillation spectra, shown in Figs. 6,7,confirm that positive gain occurs for these crystals at least at fluorescence maxima. The short wavelength lasing of tetragonal symmetry Nd^{3+} centers and long wavelength laser oscillation of rhombic clustered centers was realized in SrF_2:0.8%NdF_3 crystal for different pump wavelengths (Fig. 7) . Laser oscillation of tetragonal symmetry centers occurred at 1298 nm, 1308 nm, and 1316 nm wavelengths.

CONCLUSION

A number of Nd^{3+} doped fluoride crystals with disordered structure have been studied by means of conventional optical spectroscopy and site selective spectroscopy in order to identify material that can serve as gain medium in 1.3 μm telecommunication window. After these study we conclude that the most promising crystals investigated are cubic disordered fluorides based on (50-70) %SrF_2-(50-30) %CaF_2 solid solutions containing Nd^{3+} optical centers having local tetragonal symmetry. These crystals combine most of the necessary properties, since they possess (a) small value of ESA line strength (S_{em}/S_{esa}~4) , (b) high metastable level lifetime (1.2-1.3 ms), (c) high gain value ($\sigma_{em}(\lambda)\,\tau_r=(5\text{-}6)\,x10^{-24}$ cm^2s) , and (d)

proper fluorescence peak at about 1310 nm wavelength and comparatively wide fluorescence band with about 20 nm FWHM.

ACKNOWLEDGEMENTS

This work was supported in part by AT&T Bell Labs.

REFERENCES

1. V.V.Osiko, Yu.K.Voron'ko, A.A.Sobol, "Spectroscopic investigation of defect structures and Structural transformations in ionic crystals", in Crystals 10, Growth, Properties, and Applications, ed. H.C.Freyherdt, Berlin, Springer-Verlag, pp.37-86, 1984.

2. O.A. Alimov, T.T. Basiev, S.B. Mirov, "Spectral and relaxation characteristics of local electron states of impurities in structurally disordered matrices", in Selective Laser Spectroscopy of Activated Crystals and Glasses, ed. V.V.Osiko, N.Y., Nova Science Publishers, Proceedings of the Institute of General Physics Academy of Sciences of the USSR, vol.9, pp.1-66.

3. B.R.Judd, "Optical absorption intensities of rare earth ions", Phys. Rev., vol.127, pp.750-761, 1962.

4. G.S.Ofelt, "Intensities of crystal spectra of rare-earth ions", J. Chem. Phys., vol.37, pp.511-520, 1962.

5. W.F.Krupke, "Induced-emission cross section in neodymium laser glasses", IEEE J. Quant. Electron., vol. 10, pp.450-457, 1974.

6. J.L. Adam, N. Rigout, E. Denoue, F. Smektala, J. Lucas, "Optical properties of Ba-In-Ga-based fluoride glasses for amplification at 1.3μm", Proc. SPIE, vol. 1581, pp. 155-165, 1991.

Table. Calculated Judd-Ofelt parameters Ω_t (t=2,4,6) and predicted line strengths ratio S_{em}/S_{esa}, spontaneous probability A for $^4F_{3/2}$-$^4I_{13/2}$ transition, radiative τ_r and measured τ_{meas} lifetimes of $^4F_{3/2}$ level in Nd^{3+} doped fluoride crystals

Composition, mol %	Judd-Ofelt parameters, 10^{-20} cm^2			$\frac{S_{em}}{S_{esa}}$	A, s^{-1}	τ_r, μs	τ_{meas}, μs
	Ω_2	Ω_4	Ω_6				
MeF_2-NdF_3 (fluorite type structure)							
99.7%CaF_2:0.3%NdF_3	0.83	0.86	3.34	5.37	145	973	1160
71.5%CaF_2:28%SrF_2:0.5%NdF_3	0.29	1.21	2.22	4.72	98	1190	1260
29.2%CaF_2:70%SrF_2:0.8%NdF_3	0.63	0.77	2.09	4.12	92	1410	1290
99.95%SrF_2:0.05%NdF_3	0.58	0.71	2.05	4.40	91	1460	1350
99.7%CdF_2:0.3%NdF_3	1.26	1.34	4.93	5.16	292	477	
99.7%BaF_2:0.3%NdF_3	0.64	0.23	0.65	1.79	30	4330	
MeF_2-LnF_3-NdF_3 (yttrofluorite type structure)							
96.1%CaF_2:2.3%YF_3:1.6%NdF_3	0.38	2.48	3.79	4.4	164	667	560
88.5%SrF_2:10%LaF_3:1.5%NdF_3	0.56	2.51	3.82	4.0	176	620	490
68.5%SrF_2:30%LaF_3:1.5%NdF_3	0.49	2.85	3.33	3.29	164	602	560
86.6%BaF_2:12.3%LaF_3:1.1%NdF_3	0.33	0.75	1.51	4.17	73	1650	540
LnF_3-MeF_2-NdF_3 (tysonite type structure)							
99%LaF_3:1%NdF_3	0.72	1.95	2.26	2.59	139	705	670
86.5%LaF_3:12%SrF_2:1.5%NdF_3	0.86	2.06	3.42	3.54	202	558	570
99%CeF_3:1%NdF_3	0.94	2.53	3.34	2.93	214	483	330
84.85%CeF_3:13.5%SrF_2:1.65%NdF_3	1.67	2.76	5.78	3.76	349	348	250
5NaF:9YF_3:1%NdF_3	0.78	1.49	2.41	3.13	114	985	870
ZBLAN [6]	2.2	2.82	3.94	2.0			

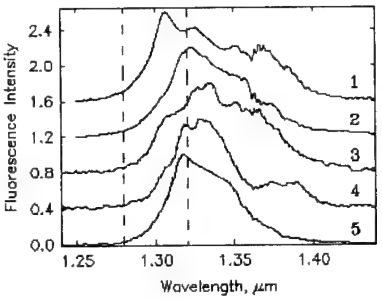

Fig.1

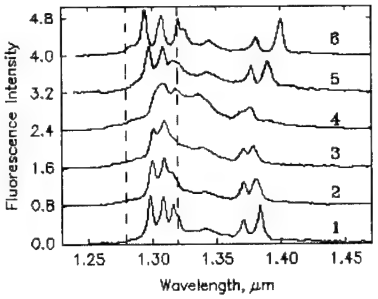

Fig.2

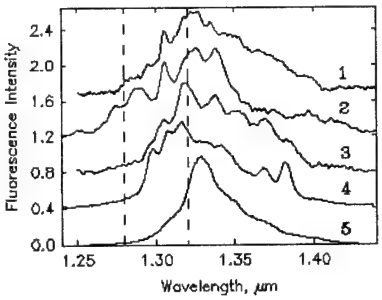

Fig.3

Fig. 1. Room temperature fluorescence spectra of Nd^{3+} ions in 5NaF-9YF3:1%NdF3 (1), 68.5%SrF2:30%LaF3:1.5%NdF3 (2), 96.1%CaF2:2.3%YF3:1.6%NdF3 (3) and 86.6%BaF2: 12.3%LaF3:1.1%NdF3 (4) crystals and ZBLAN glass (5) at 514.5 nm excitation.

Fig. 2. Room temperature fluorescence spectra of 99.2%SrF2:0.8%NdF3 (1), 9.2%CaF2:90%SrF2: 0.8%NdF3 (2), 29.2%CaF2:70%SrF2:0.8%NdF3 (3), 49.2%CaF2:50%SrF2:0.8%NdF3 (4), 71.5%CaF2: 28%SrF2:0.8%NdF3 (5) and 99.7%CaF2:0.3%NdF3 (6) at 514.5 nm excitation with predominating fluorescence of tetragonal symmetry centers.

Fig. 3. Room temperature fluorescence spectra of 93%CaF2:7%NdF3 (1), 97.7%BaF2:0.3%NdF3 (2), 99.7%CdF2:0.3%NdF3 (3) at 514.5 nm excitation and 99.2%SrF2:0.8%NdF3 (4), 49%CaF2:49%SrF2: 2%NdF3 (5) at 752 nm excitation with predominating fluorescence of clustered Nd^{3+} centers.

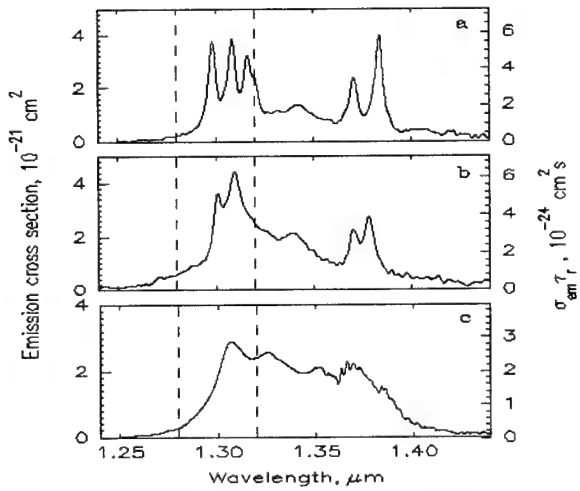

Fig. 4. Stimulated emission cross section spectra and maximum possible gain for SrF2:0.8%NdF3 (a), 29.2%CaF2: 70%SrF2:0.8%NdF3 (b) and 5NaF-9YF3:1%NdF3 (c) crystals.

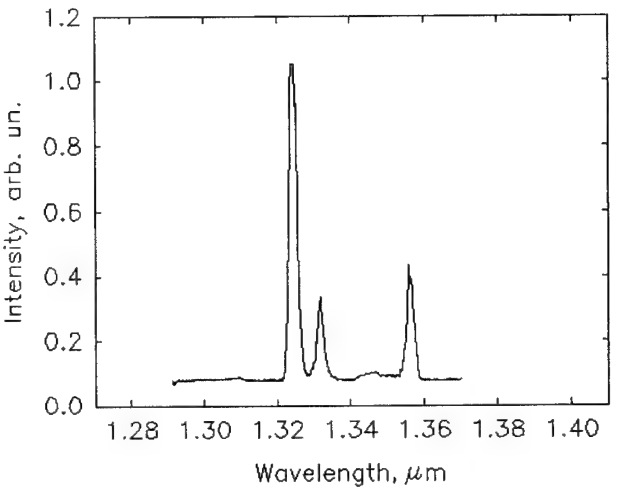

Fig. 6. Laser oscillation spectrum of 68.5%SrF2-30%LaF3: 1.5%NdF3 crystal.

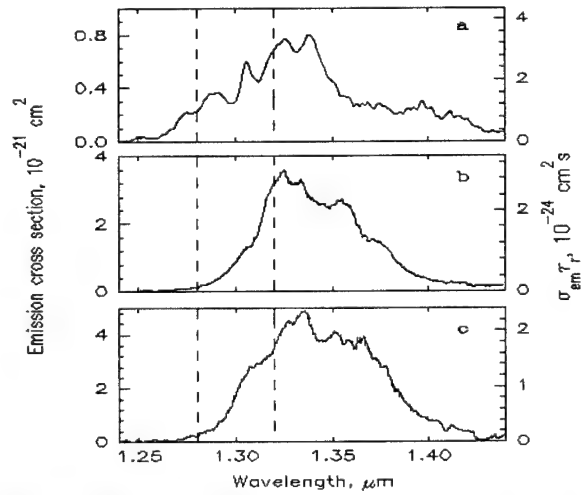

Fig. 5. Stimulated emission cross section spectra and maximum possible gain of BaF2:0.3%NdF3 (a), 68.5%SrF2:30%LaF3:1.5%NdF3 (b) and 96.1%CaF2: 2.3%YF3:1.6%NdF3 (c) crystals.

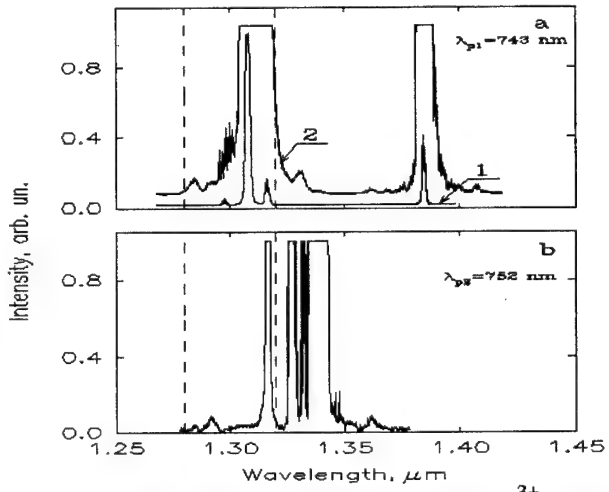

Fig. 7. Laser oscillation spectra of tetragonal symmetry Nd^{3+} centers at 743 nm pump (spectrum 2 was recorded with 1.5 times wider slit compared to spectrum 1) (a) and clustered centers at 752 nm pump (b) in 99.2%SrF2:0.8%NdF3 crystal.

Optimization of Bandgap Wavelength of a Semiconductor Optical Amplifier for Cross Index Modulation at 1.55 µm wavelength

W. Schweiker, R. Schimpe
Siemens AG, Corporate Research and Development, D-81739 Munich, Germany
Tel. +49 89 636 2742, Fax. +49 89 636 3832

Introduction

The semiconductor optical amplifier (SOA) on InP offers a degree of multi-functionality promising for the realization of all-optical functions for future optical networks. SOAs are currently investigated for all-optical switching e.g. in cross-connects of optical frequency multiplex systems. SOA-based frequency converters in an interferometric configuration, as demonstrated by Durhuus et al. [1], have the advantage of high extinction ratio and moderate pump-power requirements. In such arrangements, the pump-pulse induced change in refractive index is the basic mechanism for the signal-conversion from the pump-wavelength to the probe-wavelength. The index-shift causes a phase-shift leading to a variation of the probe-output-power. The maximum extinction is reached for a pump-power change P_π for a phase-shift of π. In this contribution, the dependence of P_π on pump-wavelength and probe-input-power is investigated systematically to optimize the bandgap wavelength of the active material of the frequency converter.

Experimental setup

The investigated device is a 500 µm long buried heterostructure InGaAsP SOA designed for signal amplification at 1.55 µm wavelength.[2] In our experiment, the injection current is 120 mA, which leads to a wavelength of the unsaturated gain maximum of about 1.55 µm. To measure the pump-power-dependence of the refractive index, we used an interferometric setup in bulk-technique with the SOA in the test-arm (fig. 1). The pump signal is generated by a tunable external cavity laser, amplified by an Er-doped fiber

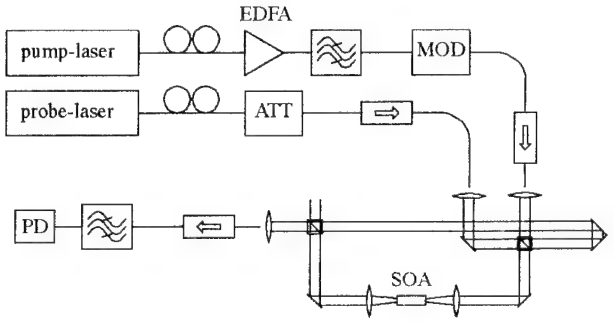

Fig. 1 Experimental setup with Er-doped fiber amplifier (EDFA), modulator (MOD), attenuator (ATT), photodiode (PD), semiconductor optical amplifier (SOA).

amplifier and modulated with an optical modulator. The probe-source is a high-power 1552 nm laser modul. Both probe-powers, P_{ref} in the reference-arm as well as $P_{SOA}(P_{pump})$ in the test-arm, are measured separately before measuring the probe-output-power $P_{out}(P_{pump})$ of the interferometer.

Results and discussion

To obtain values for the change in refractive index $\Delta n(P_{pump})$ with the pump-power, the experimental data for the output-power of the interferometer are fitted, using the following formula:

$$P_{out} = \left| \sqrt{P_{ref}} + \sqrt{P_{SOA}} \cdot \exp\left[i\left(\frac{2\pi}{\lambda} \cdot \Delta n \cdot L + \Phi_0 \right) \right] \right|^2$$

In fig. 2a, a comparision between experimental data for the probe-output-power and the calculated curve for Δn is given, assuming a power-dependence of Δn according to fig. 2b. The equation $\Phi = 2\pi/\lambda\ \Delta n(P_\pi)\ L = \pi$ has been solved to get P_π.

Fig. 3 shows experimental data for P_π versus pump-wavelength, with the probe-wavelength fixed at 1552 nm. A minimum of P_π occurs because of the more pronounced reduction of the carrier concentration near the wavelength of the gain maximum. This minimum shifts towards longer wavelength with increasing optical input-power (i.e. decreasing carrier concentration) because of the corresponding shift of the gain-maximum. High optical input-power is necessary to reduce the gain re-

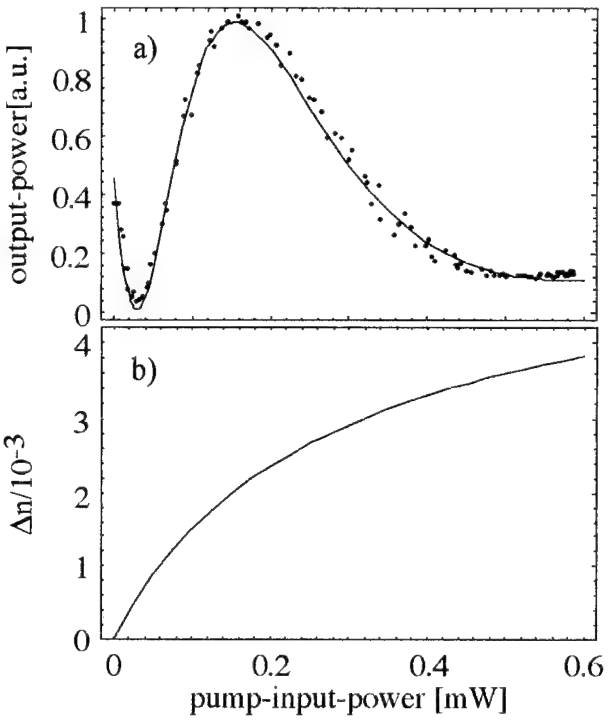

Fig. 2 a) Output-power calculated from eq. 1, assuming the behaviour of Δn, presented in b).

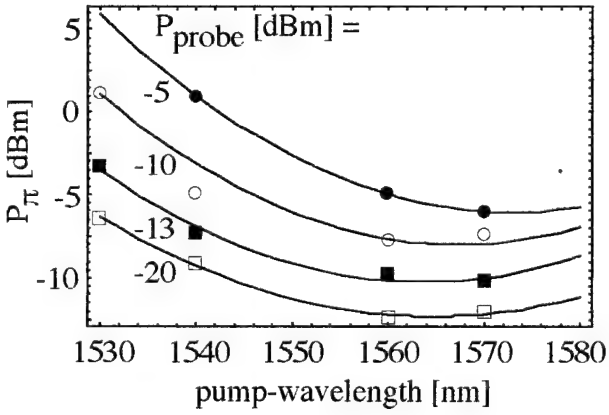

Fig. 3 Dependence of P_π on pump-wavelength with the probe-wavelength fixed at 1552 nm. The injection current is 120 mA, parameter is the probe-input-power. The solid lines are fits to the experimental data to guide the eye.

covery time, which determines the speed of SOA-based wavelength converters [3]. Therefore the shift of the minimum of P_π with increasing input-power has to be considered, when designing a SOA for optical index modulation. Fig. 3 shows that an optimized SOA should have a bandgap wavelength of about 20 to 30 nm below that of our investigated SOA, to compensate for the wavelength-shift of the gain maximum from its unsaturated value of about 1550 nm to its saturated value around 1575 nm at high probe-input-power. More specifically, for a fixed probe-wavelength at 1.55 µm, the unsaturated gain maximum should be around 1.53 µm to obtain minimum values for P_π.

Another effect which should be taken into account when choosing the bandgap wavelength of a converter is the dependence of P_π on the probe-wavelength. Because of the stronger pre-saturation of carrier concentration by the probe-power near the gain maximum, P_π is maximum at the (saturated) gain maximum for a fixed pump-wavelength. But the observed dependence of P_π on the probe-wavelength is weaker than that on pump-wavelength.

For getting maximum extinction ratio the influence of the linewidth-enhancement-factor becomes important. Because this factor increases by lowering the bandgap wavelength [4], a trade-off between P_π and extinction ratio exists.

Conclusion

The choice of the bandgap wavelength of a SOA for frequency conversion in an interferometer is mainly affected by the pump-power dependence of P_π. To reduce P_π the wavelength of the unsaturated gain maximum should be 20 nm to 30 nm below the center probe-wavelength.

Acknowledgement: This work has been supported in part by the German Federal Ministry for Research and Technology (BMFT) under the project Photonik II.

References:

[1] T. Durhuus, C. Joergensen, B. Mikkelsen, K.E.Stubkjaer "Penalty Free All-Optical Wavelength Conversion by SOA's in Mach-Zehnder Configuration" ECOC'93, paper TuC5.2 (1993)

[2] R. Schimpe, B. Bauer, C. Schanen, G. Franz, G. Christen, S. Pröhl "1.5 µm InGaAsP Tilted Buried-Facet Optical Amplifier" CLEO'91, paper CFK5 (1991)

[3] J.M. Wiesenfeld, B. Glance, J.S. Perino, A.H. Gnauck "Wavelength Conversion at 10 Gb/s using a Semicondutor Optical Amplifier" IEEE Photon. Technol. Lett. **5**, pp 1300 (1993)

[4] J.S Perino, J.M Wiesenfeld "Linewidth enhancement factor and chirp for high bit rate semiconductor optical amplifier wavelength converter" CLEO'94, paper CThE1 (1994)

Modelling of a semiconductor optical amplifier based nonlinear optical loop mirror for all-optical regeneration

L. BILLES, I. VALIENTE, J.C. SIMON
FRANCE TELECOM CNET
LAB / RIO
F22307 LANNION Cédex

Introduction

Various applications, such as demultiplexing, clock recovery, or all-optical signal regeneration have been demonstrated using nonlinear optical loop mirrors (NOLM), where the nonlinear effects were either spread over the fiber, due to cross phase modulation, or concentrated on a nonlinear element such as a semiconductor optical amplifier (SOA) undergoing cross gain saturation [1]. This paper addresses the last configuration and its application in all-optical regeneration.

A model of a SOA-based NOLM is presented, taking into account the effects of both cross gain and cross phase saturation on the NOLM transmission characteristics. Main features of a SOA-NOLM all optical regenerator are discussed.

Principle of a SOA-based NOLM

In the device described in figure 1, a low power probe pulse is split by a 3-dB coupler (a) into two waves (E_+ and E_-), which propagate through the loop in opposite directions. Because of the asymmetric position of the SOA, E_- crosses it $\Delta T \ (=2\frac{\Delta x}{c})$ before E_+, where Δx is the optical path length between the middle of the SOA and half the optical length of the loop and c is the light speed in fiber.

In the absence of any pump pulse, probe fields E_+ and E_- see the same gain and phase shifts and recombine after propagation on the input arm of coupler (a). Thus the loop acts as an amplifying mirror. On the contrary, if a high energy pump pulse injected in the loop through coupler (b) reaches the SOA during ΔT, saturating its gain, E_+ and E_- will experience different gain and phase shifts, resulting in a possible constructive recombination of the probe pulse on the output arm of coupler (a), depending on interferences occuring in there.

SOA modelling

The propagation of optical waves through a travelling wave SOA is considered using the slowly varying envelope approximation in a scalar model derived from Agrawal [2]. Auger recombination coefficient and the recombination coefficient for radiative transition and carrier leakage through heterojunctions are present in the carrier density rate equation, as well as a holding beam term, P_{hold}, whose effect is to reduce gain recovery time, as shown in [3]. Probe power is assumed to be sufficiently low to leave the carrier density almost unchanged.

This model provides the dynamics of evolution of SOA gain, which experiences a saturation period while it is crossed by a pump pulse, followed by a recovery period towards

stationary gain. Its numerical solution takes into account propagations in opposite directions through the SOA, including a possible crossing of pump and probe pulses within the amplifier, but it computes gain saturation effects in only the pump direction, for probe pulses shall always satisfy small-signal requirements.

Results on loop modelling

The SOA is placed asymmetrically in the loop, acting as a localized non-linearity. NOLM response is characterized by its transmissivity, defined as :

$$T = \frac{|E_{output}|^2}{|E_{input}|^2}$$

Coupling formulae in (a) lead to the following expression for T :

$$T = \frac{1}{4}\left(G_+ + G_- - 2\sqrt{G_+ G_-}\cos(\Delta\Phi)\right)$$

where $\sqrt{G_+}$ and $\sqrt{G_-}$ are the gains experienced by E_+ and E_- and $\Delta\Phi$ is the additional phase difference between them, caused by the SOA (the minus sign takes into account the π phase shift due to the coupler).

The model of the SOA provides the expressions of G_+ and G_-, as well as $\Delta\Phi$, depending on the degree of asymmetry Δx in the location of the SOA and the temporal interval $\Delta\tau$ between E_p and E_+ ($\Delta\tau = t_+ - t_p$) . Here, t_+ and t_p are the arrival times at the front end of the SOA of E_+ and E_p respectively.

This coupling between gain saturation and phase shift due to the phase-amplitude coupling parameter α allows us to make a global optimization of the loop with regard to physical parameters and also incident waves characteristics.

The transmissivity of the loop is shown in figure 2 for two cases : $\alpha = 6$ (full line curve) and $\alpha = 0$ (dashed line curve).

In the first case, it can be demonstrated that there exists an optimal pump energy, $\mathcal{E}_p^{in} = 0.14\,\mathcal{E}_{sat}$, where $\mathcal{E}_{sat}$ is defined as $\mathcal{E}_{sat} = h\nu A_{eff}/a$, which causes a gain compression of only 4.1 dB, in order to obtain a maximum transmission factor of 0.64 G_{stat}, where G_{stat} = 10.5 dB is SOA stationary gain, without pump pulses ; small-signal gain was 27 dB and P_{hold} = 1 mW. Here a is the differential gain coefficient and A_{eff} the mode effective area.

In these conditions, two transmission windows can be noticed. The main one, where the maximum is reached, will be used for further applications, but a second one does exist, which is unfortunately related to the dynamics of gain recovery. The useful part of the main transmission window is obtained when E_+ enters the SOA after E_p and when E_- leaves the amplifier before crossing the pump. First, its time width is determined by Δx, but it is reduced on its left side by pump pulse time duration and on its right side by the propagation time in the SOA. Then, pump energy and gain recovery time determine transmission variations in this window.

Comparison with the second case ($\alpha = 0$) points out that, for a given optimal gain compression, α parameter drastically enhances transmissivity and greatly improves main window flatness, even if second window relative transmissivity level is higher. Actually, gain compression has been optimized for $\alpha = 6$ case, but in any case, with $\alpha = 0$,

transmissivity is an increasing function of $\mathcal{E}_p^{in}$ with an upper limit less than 0.25 G_{stat} which has to be compared with the previous value of 0.64 G_{stat}.

Application to all-optical regeneration

We have applied this model to the particular case of all-optical regeneration, where data are carried by pump pulses, assuming that an optical clock has been extracted from data stream. These clock pulses are used as probe pulses. The regenerated signal is obtained at the output of the NOLM [4]. Such a configuration also exists in fiber-based devices as described in [5].

Here, the relevant parameters are the data time jitter and intensity variations the loop can absorb. They are directly conditionned by the time width and flatness of the main transmission window. A compromise has nevertheless to be made between time jitter absorption and resistance to intensity variations. Furthermore, pump pulse duration influence on transmission window has been studied and leads to limitations on data duty cycle, due to gain recovery time. This latter parameter also limits data bit rate, since it can generate pattern-dependent effects. However, this does not imply a definitive intrinsic limitation, for the optical holding beam described in [3] can be used in order to shorten gain recovery time.

Hence, in order to obtain a good regeneration, two loops have been cascaded, as can be seen in figure 3 : the transmitted signal exiting the first loop is amplified and launched as a pump into the second loop, while a copy of the optical clock constitutes the probe of the second NOLM.

Improvements on optical eye diagram quality (for a 1 1 1 0 0 0 1 0 1 1 sequence) due to such a configuration are shown in figure 4, for a data stream of 5 Gb/s,with 30 ps FWHM pulses, a 12 dB contrast ratio (contrast ratio is defined as the ratio of "1" and "0" peak powers), a 10 ps time jitter standard deviation and a relative energy noise of 30 % rms deviation (figure 4a). Clock pulses have a 4 ps FWHM duration. The first NOLM is used to absorb data time jitter and provides an unjittered but noisy signal (figure 4b), whereas the second one is designed to suppress residual amplitude variations as much as possible (figure4c).

The influence of low energy pulses in the zeros of data signal is still under study, but contrast ratio may be improved by the association of several loops.

These results clearly show the ability of NOLMs to resynchronize and reshape a jittered signal, provided, at this time, that data duty cycle is lower than 40 % and contrast ratio is better than 10 dB.

References

[1] Kane & al : Appl. Opt. vol 33 n° 29 1994 p 6833-6842
[2] Agrawal & al : IEEE JQE vol 25 n° 11 1989 p 2297-2305
[3] Manning & al : El. Lett. vol 30 n° 15 1994 p 1233-1234
[4] Eiselt & al : El. Lett. vol 29 n° 1 1993 p 107- 109
[5] Jinno : JLT vol 12 n° 9 1994 p 1649-1659

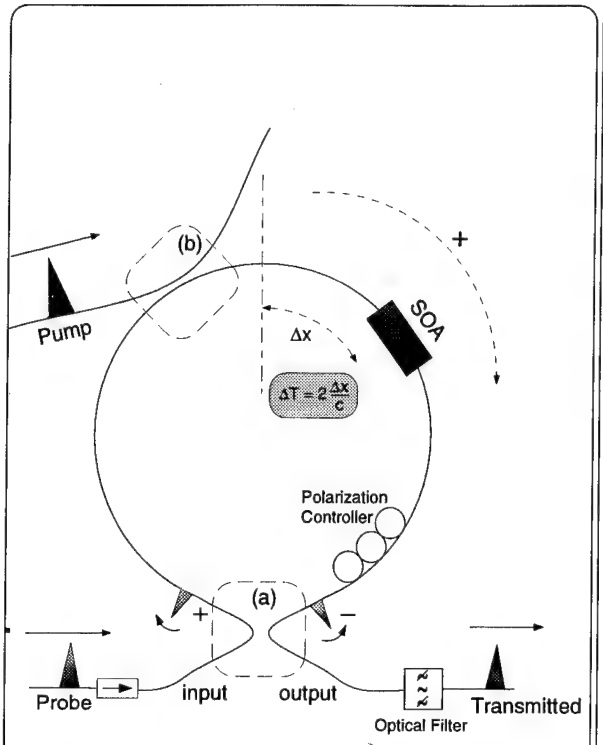

Figure n° 1 : SOA-based NOLM

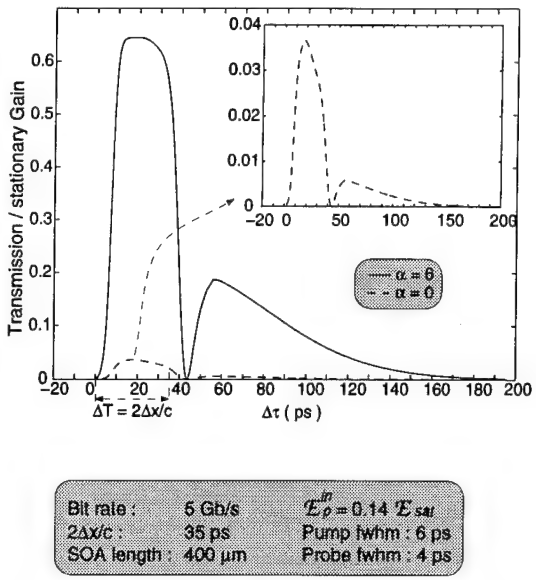

Figure n° 2 : Transmission window

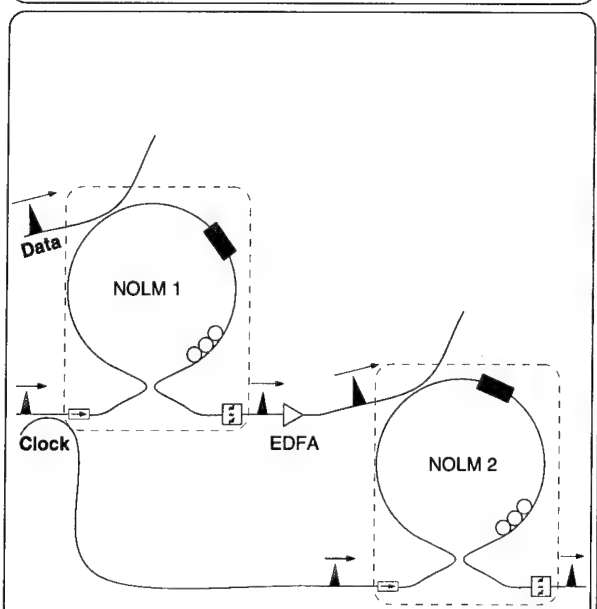

Figure n° 3 : Cascaded loops configuration

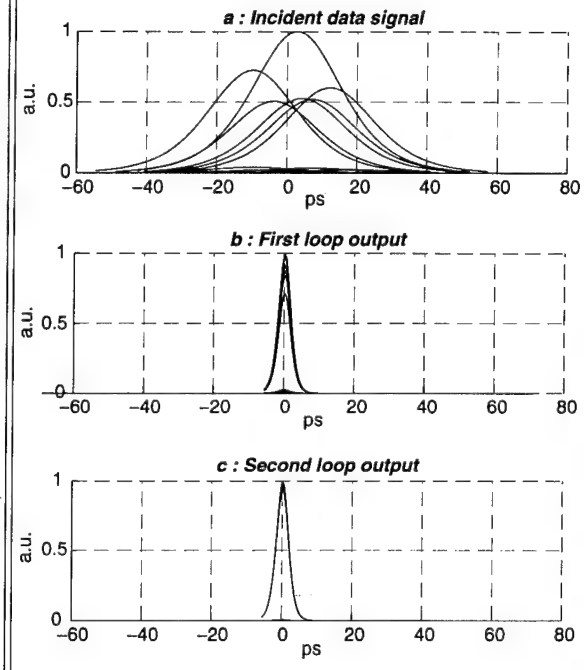

Figure n° 4 : Optical eye diagrams

RECEIVER CHARACTERISTICS OF TWO-SECTION SEMICONDUCTOR OPTICAL AMPLIFIER TRANSPARENT DETECTORS FOR LANS APPLICATIONS.

G. Giuliani*, P. Cinguino, V. Seano

CSELT - Centro Studi e Laboratori Telecomunicazioni SpA
Via G. Reiss Romoli, 274 - 10148 Torino, Italy

**Dipartimento di Elettronica, Università di Pavia, Via Abbiategrasso, 209 - 27100 Pavia, Italy*

Introduction

The application of semiconductor optical amplifiers (SOA) as transparent in-line detectors has been already investigated [1]. A two-sections structure, where the first electrode can provide amplification and/or modulation while the second section operates as non-blocking detector (AMD-SOA), is a convenient approach to be used as add-drop node in photonic packet-switched ring networks [2], with the advantage of an optimisation of the detector section [3]. The features of this network structure are that it can be easily upgraded with the addition of new nodes and that the bit-rate can be increased only for those nodes which require an higher bit-rate without substituting the whole network. With the use of an AMD-SOA read/write node a minimum amount of external electronics is required, therefore reducing cost and complexity of the whole network. For these applications the receiver performances are to be evaluated. For monoelectrode SOA devices Gustavsson *et al.* [4] reported an experimental sensitivity of approximately -25 dBm at 250 Mbit/s while Bertilsson *et al.* [5] reported -27 dBm at 100 Mbit/s. For bi-electrode devices Jørgensen *et al.* [6] have reported a sensitivity of -30.2 dBm at 140 Mbit/s, but using the detector section in the absorbing instead of the amplifying region. In this work we report experimental results at the wavelength of 1530 nm on the receiver characteristics of an AMD-SOA packaged device working at 155 and 622 Mbit/s.

Device characteristics

The AMD-SOA devices are based on a BRS structure with a square InGaAsP active waveguide of 0.4x0.4 μm^2 cross section designed to obtain polarisation insensitive devices [7]. The complete structure was entirely grown by LP-MOCVD and the definition of the active layer was obtained combining reactive ion etching and wet chemical etching. Electrodes separation, with an electrical insulation resistance of 20 KΩ, was achieved by metallisation lift-off and by a InP:p cladding layer etching 0.5 μm close to the InGaAsP active layer. The first amplifying section had a length of 300 μm while the detector section was 100 μm long. The AR coating process was *in-situ* controlled by monitoring both the optical power and the forward voltage of the devices during deposition. The devices were then assembled in a double pig-tailed package. The use of tapered lensed AR-coated fiber pig-tails allowed to obtain fiber-device coupling losses less than 3 dB per facet, while a Peltier cooler and temperature sensor allowed a temperature control better than 0.1°C. High frequency operation was obtained routing the signals to and from the device through SMA connectors, microstripe lines and matching resistors. The devices characterisation showed average fiber-to-fiber gains of 10÷12 dB together with detector responsivities, defined as the ratio of output detected voltage to the optical peak signal power in the input fiber, up to 63 V/W. The gain ripple at the operating currents was less than 3 dB at the working wavelength of 1530 nm while the measured TE/TM dicroism was less than 1 dB. Fig. 1 shows the behaviour of the two sections of the device regarding gain and responsivity. In the left figure the modulator/amplifying section is biased at constant current while the current in the detector section is varied. We note that when the

gain undergoes saturation, due to peak gain detuning, the responsivity has its maximum absolute value, a fact that we consider mainly due to current leakage on the lateral InP omojunctions. The right figure shows a constant increase of both gain and responsivity for increasing modulator current at constant detector current.

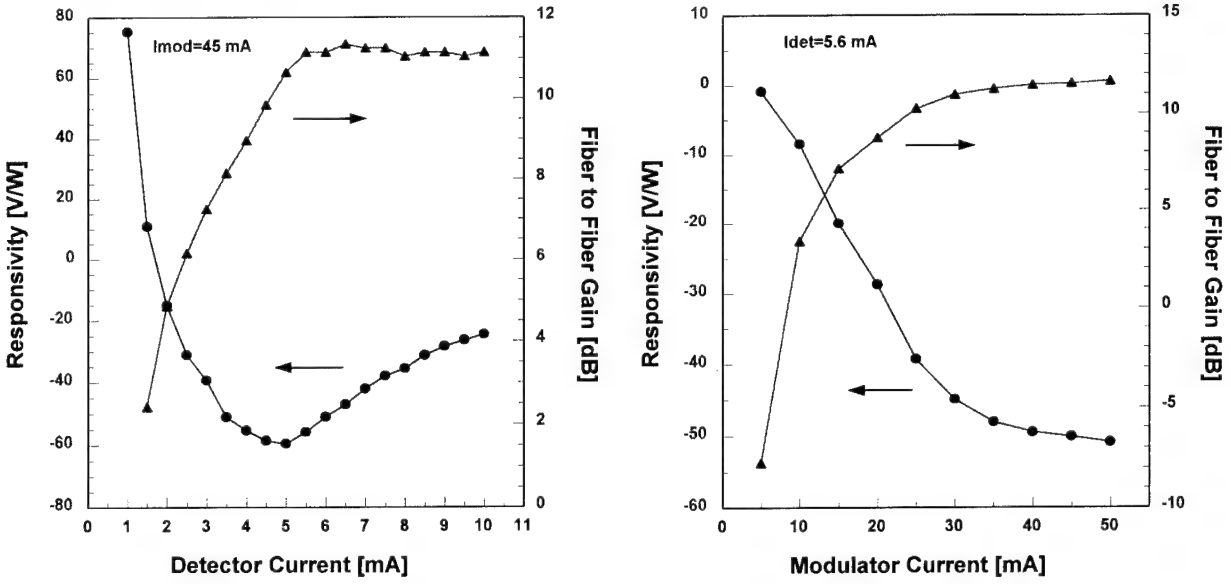

Fig. 1: Responsivity and fiber-to-fiber gain of an AMD-SOA in the two cases of constant modulator current (left) and constant detector current (right).

Experimental results

Bit error rate measurements were carried out using a NRZ format with a PRBS of 2^{23}-1. Light from a tunable laser was amplitude modulated by the transmitter through an external E/O modulator and the detection voltage signal was amplified 60 dB before the decision circuit and BER counter.

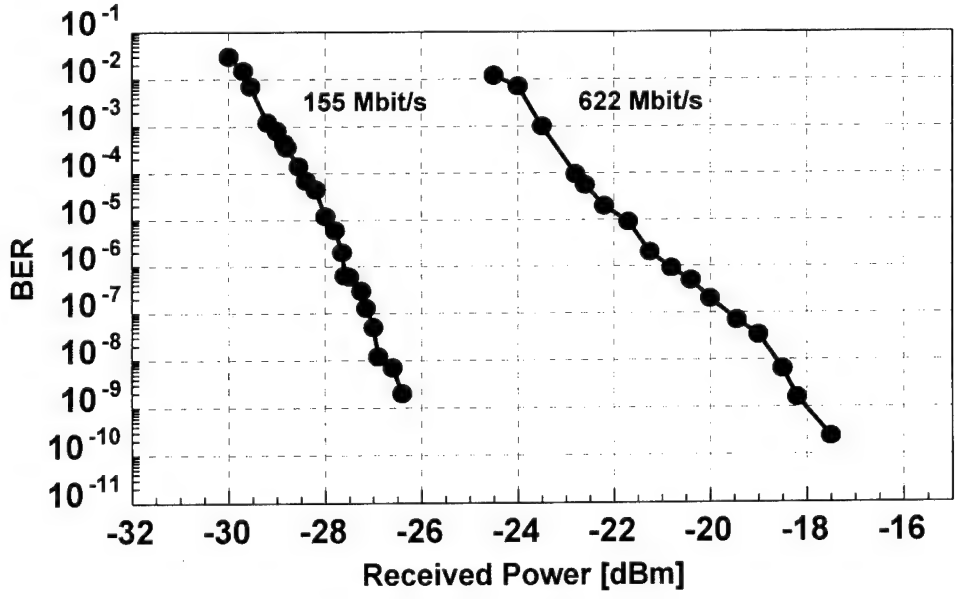

Fig. 2: Measured bit error rates at 622 Mbit/s and 155 Mbit/s.

In Fig. 2 we report BER measurements at 622 Mbit/s and 155 Mbit/s as a function of the power in the input fiber with the AMD-SOA biased at a detector current of 6 mA (622 Mbit/s) and 4 mA (155 Mbit/s) with an amplifier/modulator current of 50 mA. Receiver sensitivities of -18 dBm at 622 Mbit/s and of -26.4 dBm at 155 Mbit/s are obtained for a BER of 10^{-9}. Since the device bandwidth is limited by differential carrier lifetime [4], the bandwidth increases with increasing detector current. Figure 3 reports the current dependence of the bandwidth and responsivity, resulting in a possible bandwidth/responsivity trade-off since the responsivity decreases with increasing current.

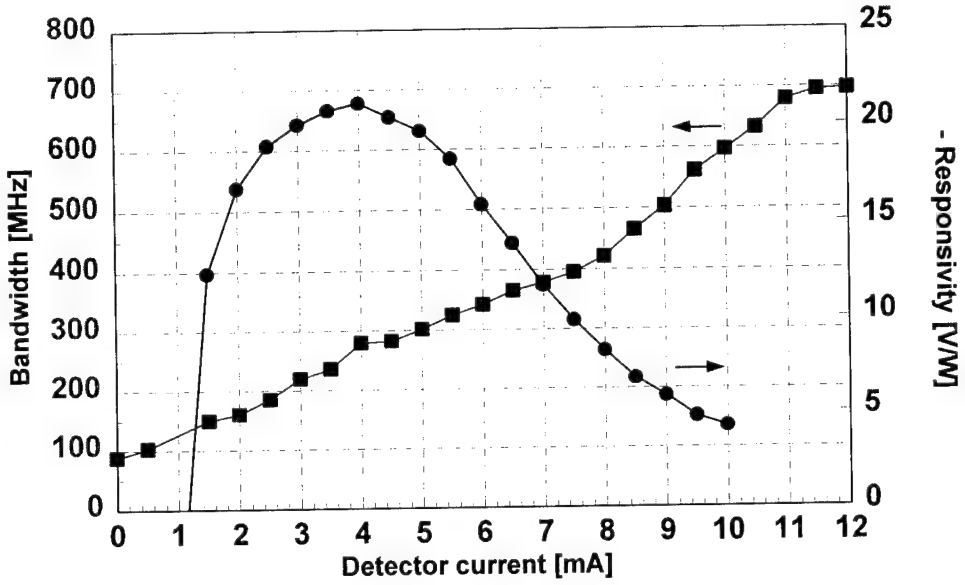

Fig. 3: Measured bandwidth and responsivity as a function of detector current.

To further investigate the system performance of the device we measured the power penalties as a function of several SOA parameters. In Fig. 4 we show the penalty at the two bit rates as a function of the detector bias current.

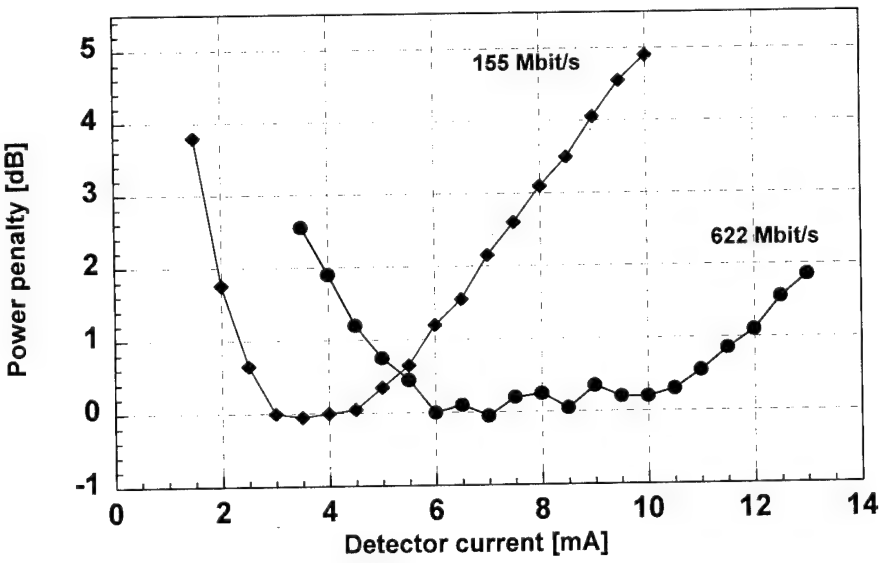

Fig. 4: Measured power penalty as a function of detector current for 155 and 622 Mbit/s.

From the figure we can note that at 622 Mbit/s a trade-off occurs since the decreasing responsivity is compensated by an increasing bandwidth, yielding an optimum operating current range of 6÷10 mA. At 155 Mbit/s the available bandwidth is large enough to determine the optimum operating bias where the responsivity has its maximum. The power penalty due to dicroism is measured to be 1.5 dB at 622 Mbit/s and 1.3 dB at 155 Mbit/s while the penalty due to gain ripple is 4 dB at 622 Mbit/s and 3 dB at 155 Mbit/s. Noise measurements showed that the preamplifier electrical noise power density is 1 dB larger than the device noise power density, suggesting that BER values are 1 dB within device intrinsic noise limit. Furthermore, the device noise does not depend on the input signal power at the considered levels, being primarly due to intrinsic junction voltage fluctuations [8]. Measured values of the device noise power density lie in the range -167.7 ÷ -165.3 dBm/Hz for detector currents 4÷12 mA, indicating that the current dependence of S/N ratio is little affected by the device noise contribution.

Conclusions

The complete characterization of the system performances of a packaged two-sections AMD-SOA at 1.53 μm has been carried out, resulting in a sensitivity of -18 dBm at 622 Mbit/s and of -26.4 dBm at 155 Mbit/s. System power penalties have also been investigated to determine the optimal operating conditions.

Acknowledgements

We like to acknowledge G. Fornuto for material growth, G. Morello for device technology, F. Delpiano and G. Oliveti for device packaging, D. Re for AR deposition, F. Marranzino for assistance, A. Piccirillo for co-ordination support and S. Mottet for discussions.

References

[1] M. Gustavsson, A. Karlsson, L. Thylén, "*Travelling wave semiconductor laser amplifiers detectors*", J. Lightwave Technol., **8**(1990), p. 610

[2] R.M. Fortenberry, Y. Cai, R.S. Tucker, "*Optically trasparent nodes for photonic packet-switched ring networks*", Electron. Lett., **29**(1993), p. 417

[3] R.M. Fortenberry, A.J. Lowery, R.S. Tucker, "*Up to 16 dB improvement in detected voltage using two-section semiconductor optical amplifier detector*", Electron. Lett., **28**(1992), p. 474

[4] M. Gustavsson, L. Thylén, A. Djupsjöbacka, "*System performance of semiconductor laser amplifier detectors*", Electron. Lett., **25**(1989), p. 1375

[5] K. Bertilsson, R. Rörgren, P.A. Andrekson, S.T. Eng "*Characterization of an InGaAsP semiconductor laser amplifier as a multifunctional device*", J. Lightwave Tecnol., **11**(1993), p. 1147

[6] C. Jørgensen, N. Storkfelt, T. Durhuus, B. Mikkelsen, K.E. Stubkjaer, B. Fernier, G. Gelly, P. Doussiere, "*Two-section semiconductor optical amplifier used as an efficient channel dropping node*", IEEE Phot. Technol. Lett., **4**(1992), p. 348

[7] S. Mottet, T. Mercier, M. Le Ligné, A. Le Corre, A. Piccirillo, D. Bertone, E. Dovio, "*Fast semiconductor optical amplifier modulator design*", in *Physical Concepts and Materials for Novel Optoelectronic Device Applications II,* Proc. SPIE Vol. **1985**, p.52, (1993)

[8] C. Harder, J. Katz, S. Margalit, J. Shacham, A. Yariv, "*Noise equivalent circuit of a semiconductor laser diode*", IEEE J. Quant. Electron., **QE-18**(1982), p. 333

Wavefront Engineering - A Novel Antireflection Design Technique for Travelling Wave Semiconductor Optical Amplifiers

Wayne W. Lui, Katsuaki Magari and Kiyoyuki Yokoyama
NTT Opto-electronics Laboratories
3-1 Morinosato, Wakamiya, Atsugi, Kanagawa, Japan.
E-mail address: waynelui @ aecl . ntt . jp

To reduce facet reflectivity in travelling wave (TW) semiconductor optical amplifiers (SOA), the use of antireflection (AR) coating is a well-known technique [1]. As this technique also requires almost exact control of the coating thickness and the refractive index of the coating material, it is not always viable. In an attempt to alleviate this problem, the combination of a window structure [2] with AR coating was proposed. It has been shown recently [3], however, that the window structure is effective only if the window thickness can be controlled to within tenths of a micron -- a precision which is not yet achievable with the current state of processing technology. Until the technological barriers are overcome, these two approaches cannot be considered practical.

A third approach to reduce facet reflectivity is the use of an angled waveguide structure (see Fig.1). Typically, the facet is cleaved at an angle of 7° with respect to the plane of wave propagation. Although substantial reflectivity reduction using this approach has been reported [4], recent theoretical calculation results [1,5] suggest otherwise. To clarify the utility of this approach and to provide a systematic approach for AR design, a two-dimension (2D) simulator based on the numerical solution of the Helmholtz equation

$$\frac{\partial^2 E_y}{\partial x^2} + \frac{\partial^2 E_y}{\partial z^2} - \frac{n^2}{c^2}\frac{\partial^2 E_y}{\partial t^2} = 0 \qquad (1)$$

(for TE mode) has been developed. In this simulator, the Helmholtz equation is solved numerically as an initial value problem, which is time-stepped until a steady-state solution is obtained. A unique feature of this simulator is that reflected waves can easily be obtained, from which reflectivity can be directly extracted. This is important because information on reflected waves is normally difficult to access. In most waveguide simulation tools such as those based on the beam propagation method (BPM), for example, reflected waves are assumed negligible and thus are not taken into consideration. Details of the numerical methods implemented in our simulator are described elsewhere [6,7] and will not be repeated here.

As an illustration, the optical field profile near a non-tilted SOA facet is calculated. The wavelength used in this calculation is 1.3μm, and that the guiding layer is taken to be 0.3μm thick. Furthermore, a CW source is placed at the $z = 1\,\mu m$ plane such that a guided mode wave sinusoidal in time is allowed to propagate in the forward direction from there. The facet in this case is located at $z = 4\,\mu m$ (see Fig.1). In the region where $z < 1\,\mu m$, the simulator is designed such that only reflected wave is permitted there [7]. Absorption boundary conditions [8] are also applied along the boundaries of the simulation region to ensure only reflection from the facet is collected at the $z = 0\,\mu m$ plane. Results of this calculation are shown in Fig.2(a).

A similar calculation is performed for the case where the the facet is tilted at an angle of 7°. The optical field profile is shown in Fig.2(b). Due to diffraction at the facet, the wavefront of the reflected wave, like the transmitted wave, is curved. As a result, part of the reflected wave fall back into the waveguide region and results in a residual reflectivity.

The residual reflectivity R is defined as the ratio of the energy of the reflected wave which couples with the waveguide ξ_{rfl} to the total optical wave energy ξ_{tot} (i.e. $R = \xi_{rfl}/\xi_{tot}$) such that

$$\xi_{rfl} = \frac{\left| \int E_y^{(r)*} E_y^{(i)} dx \right|^2}{\int \left| E_y^{(i)} \right|^2 dx}$$

$$\xi_{tot} = \int \left| E_y^{(i)} \right|^2 dx + \int \left| E_y^{(r)} \right|^2 dx$$

where the superscript (r) denotes the reflected component, and (i) denotes the incident component. Using equation (2), reflectivity as a function of the tilted facet angle is calculated and the results are shown in Fig.3. In the particular case considered in this report, the reflectivity is expected to drop by a factor of 4 if the tilted angle is increased to 10°. Considering the difficulties involved in coupling output light from a tilted facet, it is a dear price to pay for the 6 dB reflectivity reduction in this case.

The idea behind the angled waveguide structure deserves further investigation, however. The proposal is based on the premise that the wavefront of both the transmitted and the reflected waves are, to a good extent, flat. If this assumption is valid, then it is plausible to use a tilted facet to alter the wavefront of (i.e. to deflect) the reflected wave so that it couples poorly with the waveguide, thereby reducing the effective reflectivity. But since the wavefront is not nearly flat, the reflectivity reduction is less effective than expected. Nevertheless, this is one approach by which we meant wavefront engineering.

From calculation results such as shown in Fig.2(a), a wealth of information about the reflected wave is obtained. Knowing what to expect, novel features can be engineered into the waveguide such that a component of the incident wave can be designed to annihilate completely the reflected wave (like with AR coatings), or to deflect it so that it couples poorly with the waveguide (such as the intent of the tilted facet). As an illustration of this approach, one of our proposed structures is shown in Fig.4. In this structure, the purpose of the arch above the waveguide is to modify the wavefront of the incident wave in an asymmetrical manner. By varying the geometry of the arch, the wavefront of the incident wave can be tuned such that the reflectivity is minimized. Fig.5 shows the optical field profile inside of such a structure. In this structure, L = 20μm and the arch takes on the shape of a sine wave with a height of 1μm. As the geometry of the entire structure is not yet optimized, in this particular case, the wavefront of the incident wave is only slightly modified. Deflection of the reflected wave, however, can already be observed. As a result, the effective reflectivity is reduced to 4.7% in this case. Notice that this value is comparable to the 10° tilted facet case. Further optimization of this structure may yield further reduction in reflectivity.

In this report, an antireflection design methodology based on wavefront engineering is proposed. This technique is afforded by a 2D Helmholtz equation solver, from which valuable information on the reflected wave is readily extracted. Further details of this technique and results will be discussed at the presentation.

Finally, the authors would like to thank Dr. J.Yoshida for support and encouragement, and to acknowledge helpful discussions with Drs. K.Kawano and Y.Yoshikuni.

References

[1] Shimada, S. and Ishio, H. (Ed.), *Optical Amplifiers and their Applications*, Chapter 4, John Wiley & Sons, Chichester (1994).
[2] Cha, I. et al, *Electronic Letters*, Vol.25, No.18, pp.1241 (1989).
[3] Lui, W. et al, *IEEE Photonics Technology Letters* (to be published).
[4] Zah, C.E. et al, *Electronic Letters*, Vol.23, No.19, pp.990 (1987).
[5] Hawkins, R.J. et al, *Optical and Quantum Electronics*, Vol.26, p.S207 (1994).
[6] Huang, W.P. et al, *IEEE Photonics Technology Letters*, Vol.3, No.6, p.524 (1991).
[7] Chu, S.T. et al, *Computer Physics Communications*, Vol.68, p.451 (1991).
[8] Mur, G., *IEEE Transactions on Electromagnetic Compatibility*, Vol.EMC-23, No.4 (1981).

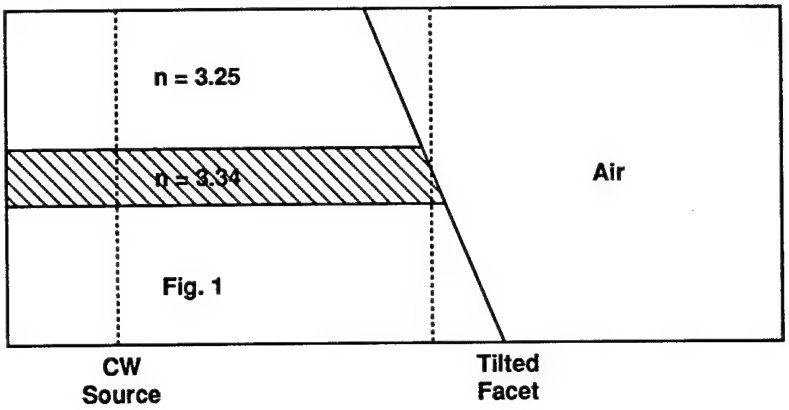

Fig.3 Effective Reflectivity of Tilted Facet

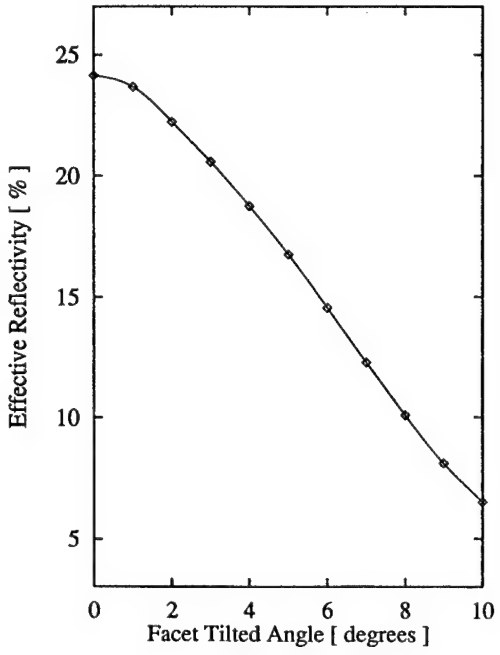

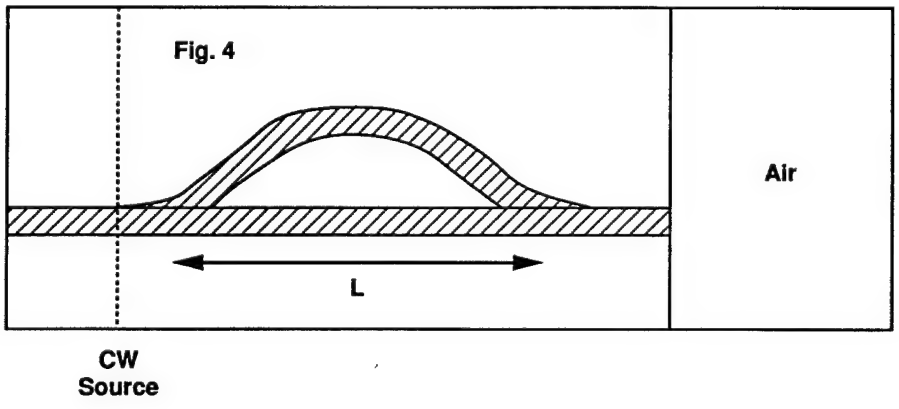

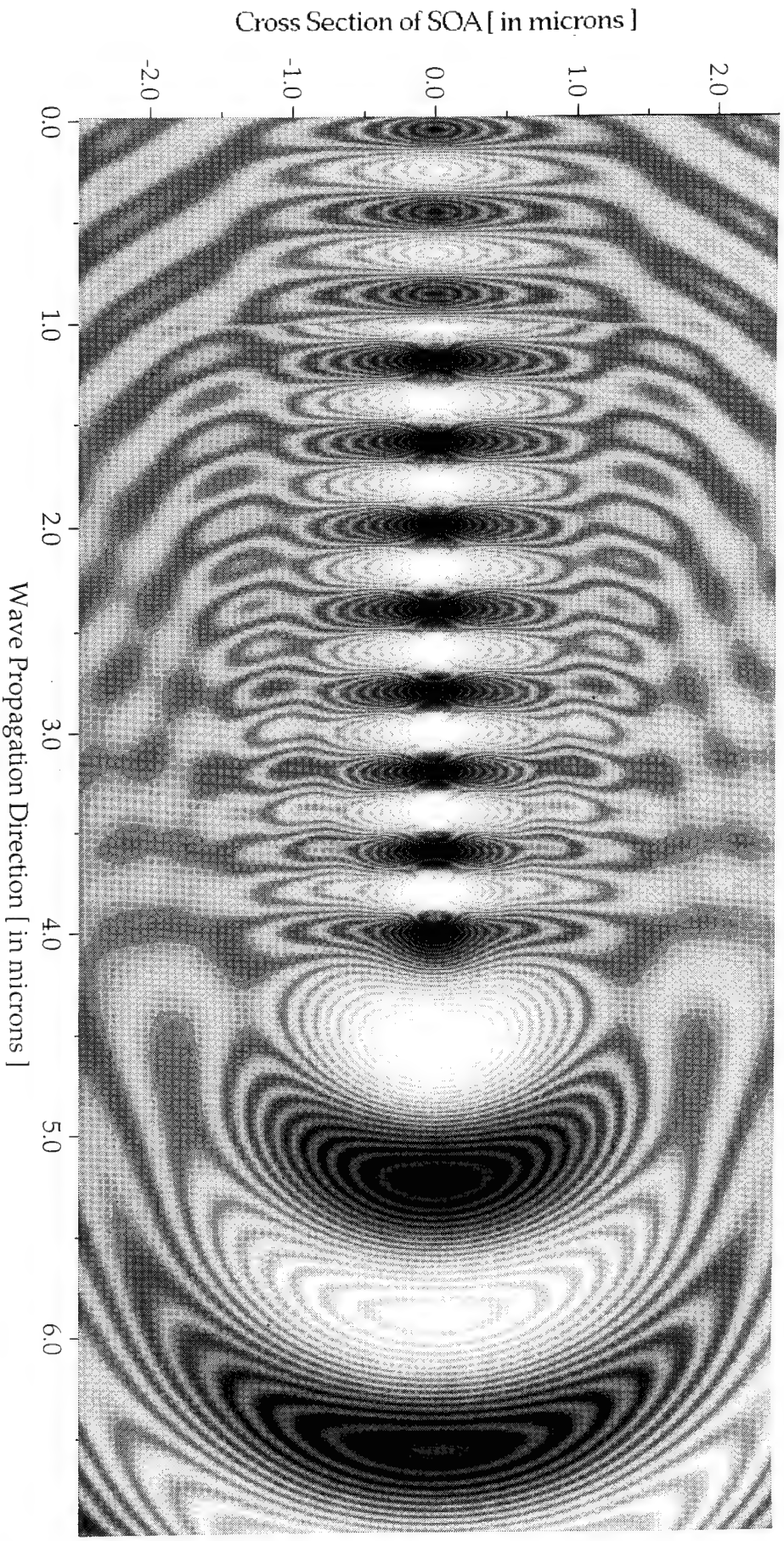

Fig. 2(a)

Optical Field Profile Near Flat Facet

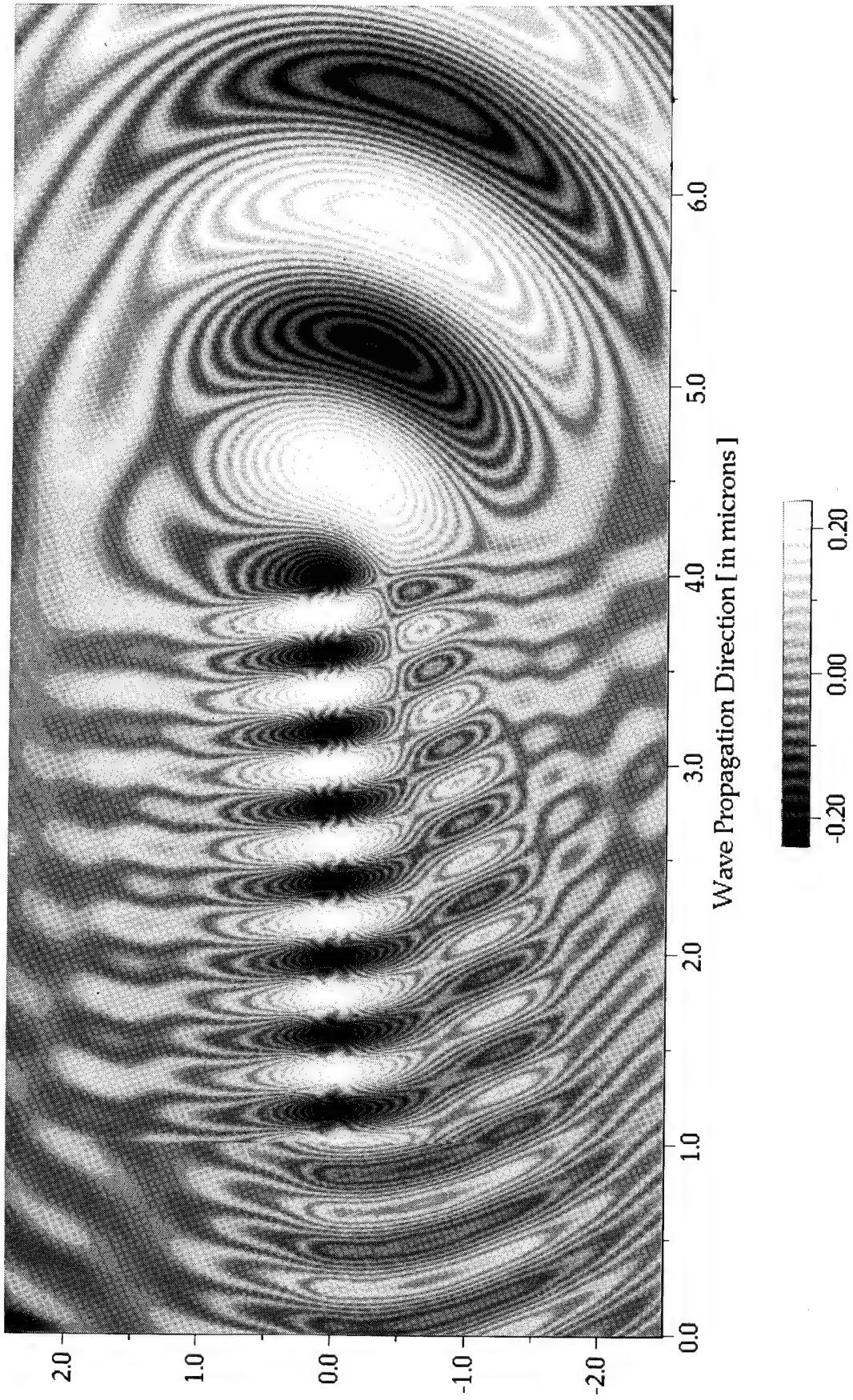

Fig. 2(b)
Optical Field Profile Near the Tilted Facet

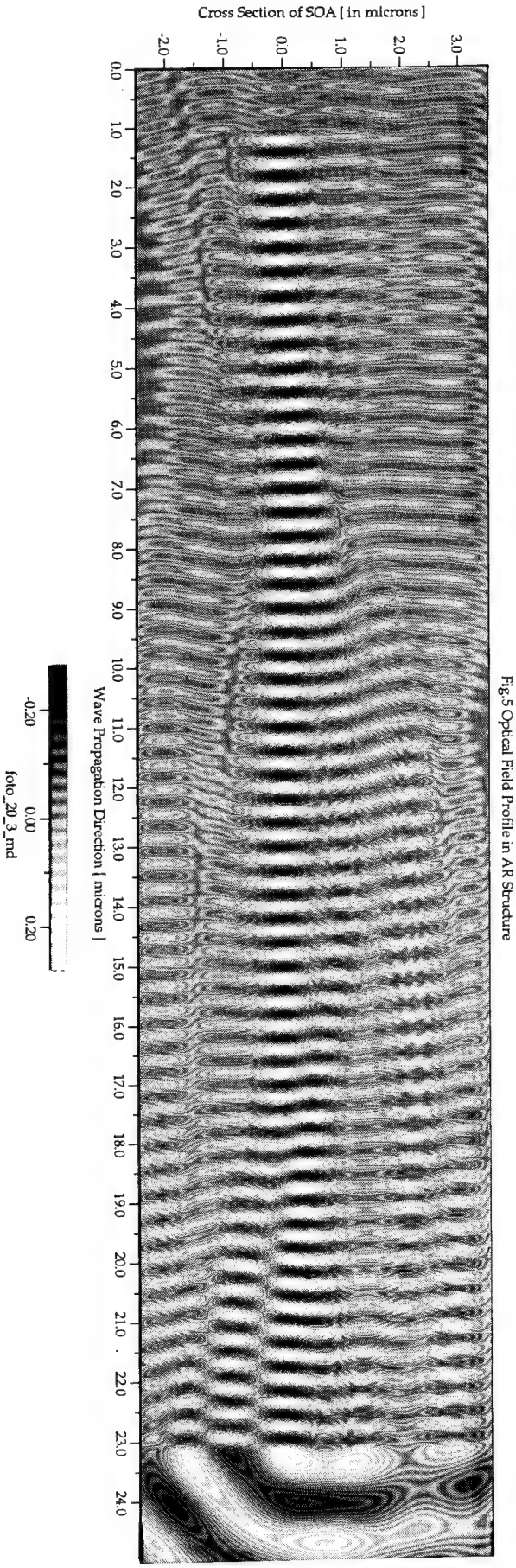

Fig.5 Optical Field Profile in AR Structure

2.5 Gb/s transmission over 200 km of dispersion-shifted fiber using a spectrum-sliced fiber amplifier light source

Jung-Hee Han, Jae-Seung Lee, Sang-Soo Lee, Tae-Yeoul Yun,
Hyang-Kyun Kim , Chang-Hee Lee, and Sang-Yung Shin[+]

Optical Transmission Section Electronics and Telecommunications Research Institute
Yusong P. O. Box 106, Taejon, 305-600, Korea. Phone: 82-42-860-6173, FAX: 82-42-861-5597
[+] Dept. of Electrical Engineering , Korea Advanced Institute of Science and Technology
Yusong-Gu, Kusong-Dong 373-1, Taejon, 305-701, Korea. Phone: 82-42-869-3420, FAX: 82-42-869-3410

I. INTRODUCTION

Spectrum-sliced fiber amplifier light source has been proposed for wavelength division multiplexed (WDM) systems [1,2]. Contrary to coherent laser diodes, its optical channel bandwidth should be sufficiently larger than the transmission bit rate. Thus, its application was focused mainly on local-loop networks limited by the optical fiber dispersion. However, with recently developed dispersion compensation techniques [3], the application area of this incoherent light source can be extended to high bit-rate long-distance communications.

In this paper, setting the center wavelength of a spectrum-sliced channel at the zero-dispersion wavelength of a dispersion-shifted fiber (DSF), we demonstrate a 2.5 Gb/s transmission over 200 km of DSF. To our knowledge, this is the fastest and the longest transmission experiment using incoherent light sources with the bit-rate distance product 500 Gb/s·km [4]. The dispersion penalty was as low as 0.2 dB. No appreciable spectral changes due to fiber four-wave mixing (FWM) were observed after transmission.

II. EXPERIMENTS

Our experimental setup is shown in Fig. 1. Three erbium-doped fiber amplifiers were used (EDFA1, EDFA2, EDFA3). The amplified spontaneous emission (ASE) light from EDFA1 was spectrum-sliced with a tunable optical bandpass filter, BP1. The bandpass filter was tuned at 1557 nm and had a 3 dB bandwidth 1.8 nm. The ASE power was 7 dBm after EDFA1 and -7.1 dBm after BP1. An optical polarizer was used before the $LiNbO_3$ Mach-Zehnder modulator which had a polarization-maintaining fiber pigtail. Its insertion loss and modulation voltage were 3.9 dB and 8 V, respectively.

The spectrum-sliced light was modulated at 2.5 Gb/s with a 2^{23}-1 pseudo-random binary NRZ sequence. The modulated signal was amplified with the optical power amplifier, EDFA2. The optical powers before and after EDFA2 were -20.2 dBm and 7 dBm, respectively. The amplified signal was then launched into a 200 km long DSF. After 110 km, the optical in-line amplifier, EDFA3 was used. The optical powers before and after EDFA3 were -19.8 dBm and 8 dBm, respectively. The zero-dispersion wavelength and dispersion slope of the DSF were 1557 nm and 0.067 ps/km·nm^2, respectively. The total fiber loss was about 48.7 dB including splicing losses.

At the receiver, the received light was filtered again using an optical bandpass filter, BP2. The 3 dB bandwidth of BP2 was about 3 nm. The receiver circuit was composed of an APD-preamplifier, a main amplifier, and a retiming circuit. The 3 dB electrical bandwidth of the receiver was about 1.5 GHz.

III. RESULTS AND DISCUSSIONS

The optical spectrum after BP2 is shown in Fig. 2. The spectral shape was nearly a Gaussian with the 3 dB bandwidth 1.8 nm. After the transmission, no appreciable change was found in the optical spectrum. The eye pattern after 200 km transmission is shown in Fig. 3 measured at -27 dBm. No appreciable degradation was found in the eye opening before and after the transmission. Figure 4 shows the bit error rate (BER) curves. We compare our results with a coherent 1548 nm distributed feedback laser diode (DFB-LD) source. The sensitivity difference was about 4 dB at 10^{-10} BER. The slope change in the BER curve for the received optical power greater than -33 dBm reflects that the dominant noise has changed from the thermal noise to the spontaneous-spontaneous beat noise. After transmission of 200 km DSF, the total power penalty due to the fiber dispersion and the ASE noise from EDFA2 and EDFA3 was less than 0.2 dB.

When the center wavelengths of the optical bandpass filters (BP1 and BP2) were changed to 1560 nm with the same 3 dB bandwidth, the dispersion penalty increased to 1 dB. When the center wavelength was changed to 1550 nm with the same 3 dB bandwidth, we found an error floor near 10^{-8} BER. The total dispersion of DSF at 1550 nm was estimated to be ~110 ps/nm. Thus, our spectrum-sliced ASE light channel can be used for the 200 km DSF transmission at 2.5 Gb/s within the ± 3 nm window from the zero-dispersion wavelength of DSF. Owing to the receiver amplifier saturation , we have used somewhat broad optical filters. The 3 dB optical bandwidth of a Gaussian channel required for the 2.5 Gb/s modulation with an error floor at 10^{-14} BER is about 0.5 nm when both polarizations are used [2]. Therefore, if the receiver circuit is optimized and a polarization-independent modulator is used, the transmission window can be broadened to more than ± 10 nm from the zero-dispersion wavelength.

This spectrum-sliced channel can be used with other coherent light channels in WDM systems. The nonlinear components generated from FWM will be small and spread broadly in spectral domain. Thus, most of the beat noises from FWM can be blocked by the receiver electrical filter [5].

In summary, we have demonstrated a single channel 2.5 Gb/s transmission over 200 km DSF using a spectrum-sliced fiber amplifier light source. The receiver sensitivity was -30 dBm at 10^{-10} BER. The power penalty was as low as 0.2 dB.

ACKNOWLEDGMENT

The authors would like to thank Dr. Chang-Sup Shim and Dr. Man-Seop Lee for their encouragement and support. This work is supported by HAN/B-ISDN project.

REFERENCES

[1] J. S. Lee, Y. C. Chung, and D. J. DiGiovanni, *IEEE Photon. Technol. Lett.*, vol. 5, pp. 1458-1461, 1993.

[2] J. S. Lee *et al.*, *IEEE Photon. Technol. Lett.*, vol. 6, pp. 1035-1038, 1994.

[3] R. M. Jopson, paper THA1, Topical meeting on optical amplifiers and their applications, Aug. 3-5, 1994.

[4] Y. C. Chung *et al.*, *Electronics Lett.*, vol. 30, No. 17, pp. 1427-1428, 1994.

[5] K. Inoue, *IEEE Photon. Technol. Lett.*, vol. 4, No. 11, pp. 1301-1304, 1992.

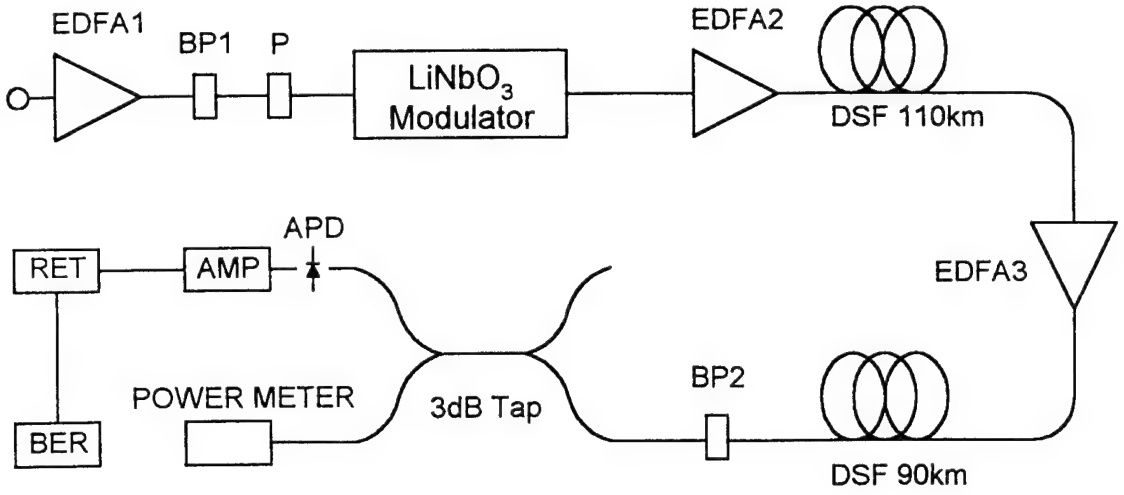

Fig. 1 Experimental setup. BP1 and BP2 : optical bandpass filters. EDFA : erbium-doped fiber amplifier. DSF : dispersion shifted fiber. BER : bit error rate measurement system. P : polarizer. RET : retiming circuit.

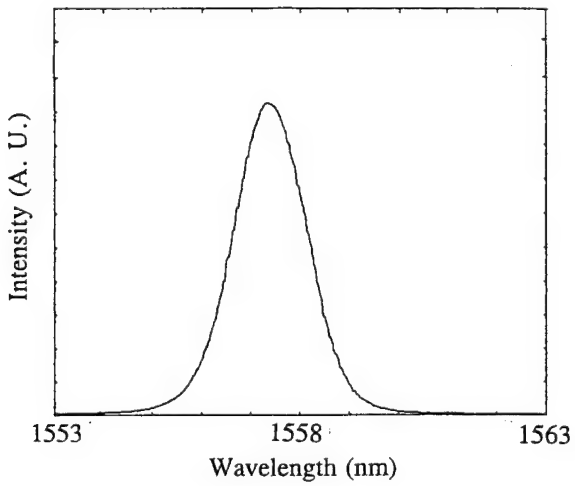

Fig. 2 The ASE spectrum after BP2. The center wavelength and the 3 dB bandwidth were 1557 nm and 1.8 nm, respectively

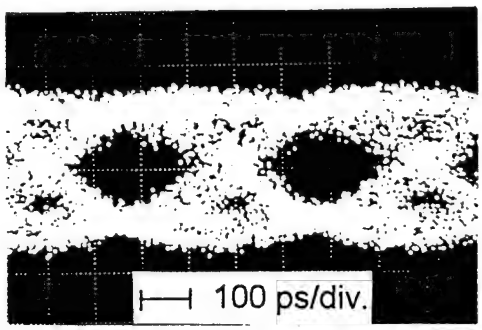

Fig. 3 The eye pattern after the transmission. Received power : -27 dBm.

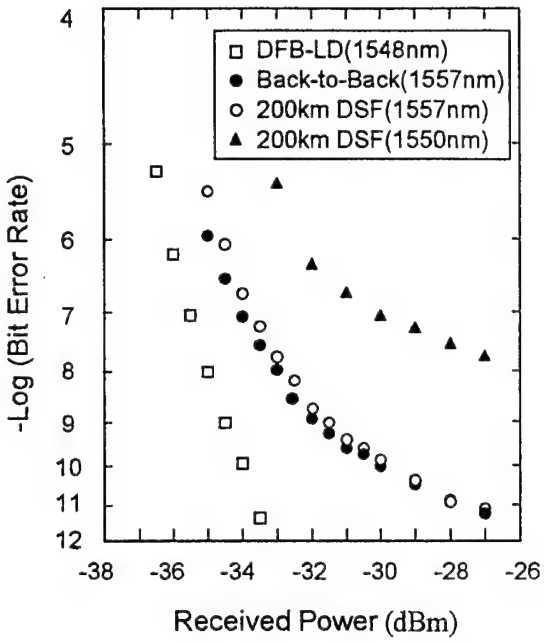

Fig. 4 Measured BER curves. □ : Back-to-Back of the 1548 nm DFB-LD with the same $LiNbO_3$ modulator, ● : Back-to-Back with the channel centered at 1557 nm, ○ : after 200 km transmission with the channel centered at 1557 nm, ▲ : after 200 km transmission with the channel centered at 1550 nm. All the spectrum-sliced channels have nearly the same 3 dB bandwidth after BP2 (~1.8 nm).

Bidirectional Transmission to Reduce Fiber FWM Penalty in WDM Lightwave Systems.

C. R. Giles
A. McCormick

AT&T Bell Laboratories
Crawford Hill Laboratory
Holmdel, NJ 07733-0400 USA
tel: 908-888-7251 e-mail: giles@big.att.com

Introduction

Wavelength-division-multiplexing (WDM) transmission in lightwave systems allows increasing fiber capacity by the simultaneous transmission of multiple channels through a single optical fiber. An example is the recent demonstration of 340 Gb/s transmission over 150 km by wavelength-division multiplexing seventeen 20 Gb/s channels [1]. WDM also enables better network topologies, eases capacity growth, reduces the demands on high-speed electronics, and improves system reliability and robustness.

A significant obstacle in WDM systems is interference caused by nonlinear four-wave mixing (FWM) among the signal channels[2]. The effect worsens with increasing number of channels as the number of FWM products increases by $N^2(N-1)/2$ where N is the number of WDM channels. Methods of reducing FWM penalties include the use of dispersion-managed fiber links [3,4] or unequal spacing of the WDM channels [5]. Here we propose the use of bidirectional transmission [6,7,8] to lessen the impact of FWM where the WDM channels are divided into two groups that simultaneously propagate in opposite directions through the optical fiber.

Results

Our WDM system was comprised of four intensity-modulated NRZ channels equally spaced by 0.8 nm in the 1555 nm gain region of erbium-doped fiber amplifiers. In unidirectional transmission, all channels co-propagate through the fiber and under appropriate phase-match conditions, generate a total of $4^2(4-1)/2=24$ FWM products, many of them overlapping in frequency and interfering with the signal channels. In bidirectional transmission, two channels propagate in each direction, generating only 2 FWM products in each direction, leading to negligible system impairment. Even with more than four channels in a fiber, bidirectional transmission relaxes the design constraints on the other methods of combating FWM.

The experimental setups used to investigate the FWM in unidirectional and bidirectional 4-channel WDM transmission are shown in Figure 1. Three InGaAsP DFB lasers and one tunable external-cavity laser were used as the four externally-modulated sources. The channel wavelength spacing was approximately 0.80 nm and the sources were combined through 3-dB fiber couplers in pairs having 1.60 nm wavelength spacing. Interleaving the wavelengths of the paired channels this way eases the filtering requirements for the channel demultiplexers. The source wavelengths are indicated in the figure; one channel pair was 1554.0-nm and 1555.6-nm and the second channel pair was 1554.8-nm and 1556.4-nm (vacuum wavelengths). The two pairs were each externally modulated at 2.5 Gb/s with a 2^{23}-1 PR bit stream through separate $LiNbO_3$ Mach Zhender modulators.. Erbium-doped fiber amplifiers boosted the channel average power launched into fiber to 8 dBm. The transmission fiber was 100 km of dispersion-shifted fiber that had an average loss of 0.22 dB/km, a mean minimum dispersion wavelength of 1551.8 nm and effective core area of 50 μm^2.

A two-channel demultiplexer and one bidirectional transceiver terminal were constructed using 3-port optical circulators and bandpass fiber gratings [9]. The fiber gratings had 100% reflectivity at the center wavelength, 0.8 nm -3-dB bandwidths and greater than 30 dB adjacent-channel rejection. The bidirectional transceiver terminal used a 3-port circulator to isolate the transmitter and receiver. The reflected and Rayleigh-scattered light from the local transmitters were prevented from reaching the local receiver by inserting 1554.0-nm and 1555.6-nm fiber-grating blocking filters between the transceiver circulator and the two-channel demultiplexer. Insertion loss of the demultiplexer was 2.9 dB to the 1554.8- nm port and 1.8 dB to the second output port. Loss through the transceiver circulator from

transmitter to transmission fiber was 1.1dB Loss through the transceiver circulator from transmission fiber through the two blocking fiber gratings was 2.0 dB.

Optical spectra measured at various points in unidirectional transmission, are shown in Figure 2. All spectra are measured with 0.1 nm resolution. Figure 2(a) shows the optical spectra after 100 km transmission with many of the FWM products generated outside the channels clearly visible. The levels of the FWM products depended upon the relative polarization states of the channels. Turning off the 1554.8 nm channel exposed the interfering FWM product generated by the other channels. Figure 2(b) is an example of spectra at the 1554.8 nm port of the 2-channel demultiplexer, again with and without the 1554.8 nm channel turned on. Severe channel degradation occurred with this level of FWM generation.

Optical spectra measured in the bidirectional transmission experiment are shown in Figure 3. The spectra in Figure 3(a) were measured with the 1554.8-nm and 1556.4-nm channels turned off. The upper spectrum in Figure 3(a) is of the 1554.0-nm and 1555.6-nm channels originating from the bidirectional transceiver, after 100 km transmission. Two weak FWM products are visible. The lower spectrum in Figure 3(a) was measured after the channel blocking filters in the bidirectional transceiver, before the 2-channel demultiplexer. Only Rayleigh backscattered ASE and FWM products passed through the blocking filters. Figure 3(b) shows the spectra also after the blocking filters, but with the 1554.8-nm and 1556.4-nm channels now turned on. The solid line spectrum was measured with the 1554.0-nm and 1555.6-nm channels turned off; the dashed spectrum was measured with all channels of the bidirectional system turned on. The only effect of turning on the 1554.0-nm and 1555.6-nm channels was to *lower* the Rayleigh backscattered ASE by gain-saturating the power amplifier at the bidirectional transceiver. The 1554.8-nm and 1556.6-nm demultiplexed channels are shown in Figure 3(c). The only interference to the 1554.8-nm channel was the -33 dB leakage of the 1556.4 nm channel. Although the fiber gratings blocked the other three channels, the 1556.4-nm demultiplex port included not only 1556.4-nm channel, but ASE originating from the 1554.8/1556.4-nm power amplifier and Rayleigh backscattered ASE from the bidirectional transceiver. The total ASE power at the 1556.4-nm demultiplexer port equaled the 1556.4-nm channel power.

Bit-error rates were measured on the 1554.8-nm channel in the unidirectional and bidirectional transmission configurations. In Figure 4, the hollow data points correspond to measurements in unidirectional transmission. Unidirectional transmission over 100km of one channel (1554.8-nm) or two channels (1554.8-nm and 1556.4-nm), showed no significant degradation of the 1554.8-nm channel receiver sensitivity as compared to the 0-km single-channel (1554.8-nm) receiver sensitivity. However, significant degradation occurred once all four channels were turned on and FWM products interfered with the 1554.8-nm channel. The amount of interference depended upon the relative channel polarizations--the *lowest* obtainable receiver sensitivity penalty was 1.6 dB. In contrast, no degradation of the 1554.8-nm channel was observed in bidirectional transmission. No interfering FWM products overlapped with the 1554.8-nm channel except for the weak Rayleigh backscattered FWM products generated by the 1554.0-nm and 1555.6-nm channels.

Summary

Degradation from four-wave-mixing in 4-channel WDM transmission through dispersion-shifted fiber was eliminated by bidirectional transmission of two pairs of channels. With more than four channels, the channels may be interleaved and propagated in opposite directions such that channels propagating in one direction are unequally spaced in order to reduce FWM interference. The same aggregate capacity as a conventional two-fiber duplex unidirectional WDM transmission system is obtainable by converting both fibers to bidirectional transmission. Bidirectional transmission might be particularly beneficial with very high data rate channels ($\geq$10 Gb/s), where dispersion-shifted fiber is desirable in order to limit the chromatic dispersion penalty.

References

1. A.R. Chraplyvy et al. "One-third terabit/s transmission through 150 km of dispersion-managed fiber," ECOC '94 (Florence) postdeadline paper, 1994.

2. A.R. Chraplyvy, "Limitations on lightwave communications imposed by optical-fiber nonlinearities," IEEE J. Lightwave Tech.., vol. 8, pp. 1548-1557, 1990

3. A.R. Chraplyvy, et al., "8 x 10 Gb/s transmission through 280 km of dispersion-managed fiber," IEEE Photonics Tech.. Lett. p. 1233, 1993.

4. C. Kurtzke, "Suppression of fiber nonlinearities by appropriate dispersion management," IEEE Photonics Tech. Lett p. 1250, 1993.
5. F. Forghieri, et al, "Reduction of four-wave mixing crosstalk in WDM systems using unequally spaced channels," IEEE Photon. Tech. Lett., vol., 6, no. 6, pp 754-756, 1994.
6. J. Haugen, J. Freeman and J. Conradi, "Bidirectional transmission at 622 Mb/s utilizing erbium-doped fiber amplifiers," IEEE Photon. Tech. Lett., vol 4, no. 8, pp 913-916, 1992
7. K. Kannan and S. Frisken, "Unrepeatered bidirectional transmission system over a single fiber using optical fiber amplifiers," IEEE Photon. Tech. Lett., vol. 5, no. 1, pp76-79, 1993
8. W.Y. Gue and Y.K. Chen, "High-speed bidirectional four-channel optical FDM-NCFSK transmission using an Er^{3+}-doped fiber amplifier," IEEE Photon. Tech. Lett. vol. 5, no. 2, pp232-235, 1993
9. G. Meltz, W.W. Morey, and W.H. Glenn, "Formation of Bragg gratings in optical fibers by a transverse holographic method," Opt. Lett., vol. 14, p823, 1989

Figures

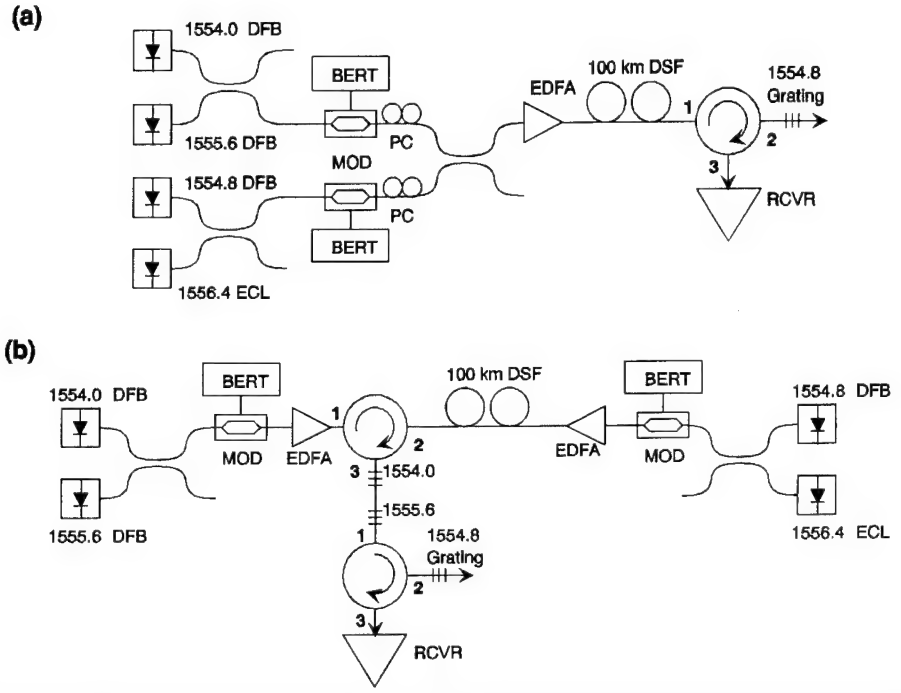

Figure 1. Experiments for (a) unidirectional and (b) bidirectional transmission of 4 NRZ 2.5 Gb/s WDM channels.

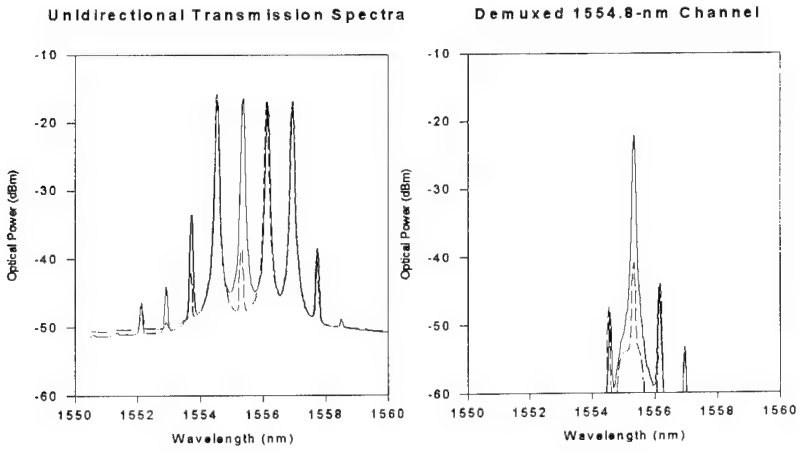

Figure 2. Optical spectra measured for unidirectional transmission after 100 km transmission before and after fiber-grating demultiplexer. Solid lines=all channels on; dashed lines=1554.8-nm channel turned off.

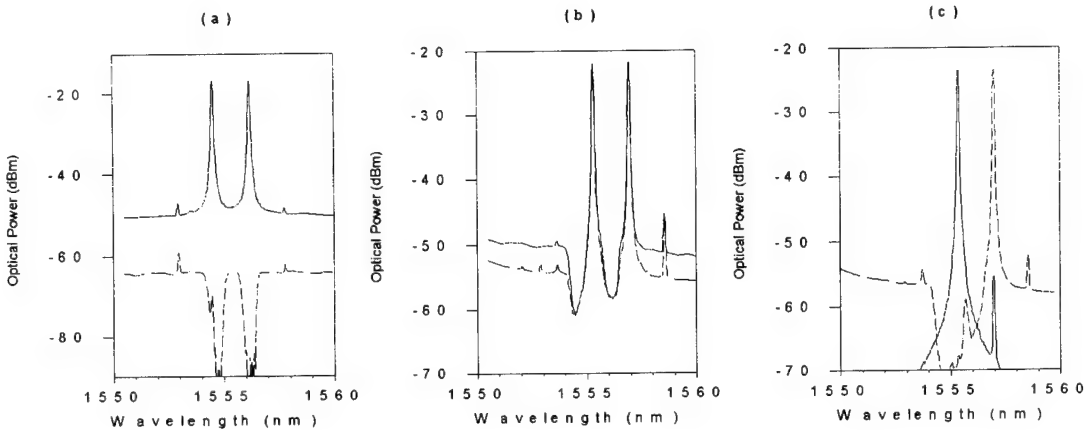

Figure 3. Optical spectra measured in bidirectional transmission. (a) only 1554.0-nm and 1555.6-nm channels on. Solid line is spectrum after 100 km transmission. Dashed line is spectrum after blocking filters at bidirectional transceiver. (b) Optical spectra after blocking filters. Solid line is spectrum with only 1554.8-nm and 1556.4-nm channels on. Dashed line is spectrum with 4 channels on. (c) Optical spectra after 2-channel demultiplexer, 4-channels on. Solid line is spectrum at 1554.8-nm port. Dashed line is spectrum at 1556.4-nm port.

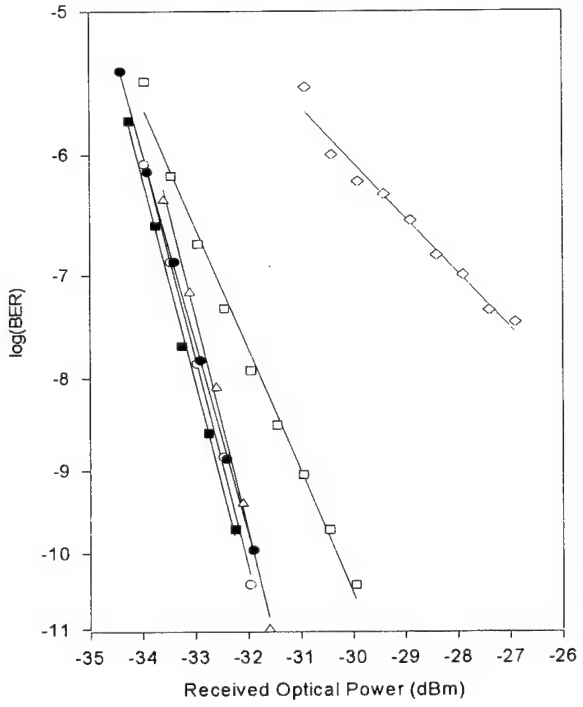

Figure 4. Bit-error-rate curves; ● 0-km; ○ 100-km single channel; (hollow triangle) 100-km unidirectional, 1554.8-nm and 1556.4-nm channels on; □, (hollow diamond) 100-km unidirectional, 4 channels on. Best and worst BER; ■ 100-km bidirectional, 4 channels on.

Soliton Transmission Control with Semiconductor Amplifiers

Antonio Mecozzi

Fondazione Ugo Bordoni

via B. Castiglione 59, I-00142 Roma, Italy

Phone: +39 (6) 5480–2232 Fax: +39 (6) 5480–4402

Semiconductor optical amplifiers have now reached the mature stage. Polarization insensitive devices have been built [1], and fiber-to-fiber noise figure down to 7 dB has been reported for a polarization insensitive device [2]. Semiconductor amplifiers working at 1.3 μm appear as promising candidate for the upgrading to higher bit rates of the existing fiber links made of step index fibers with zero dispersion at 1.3 μm [3]. A problem is still to be solved, however. When pulses are used to carry the information, the short carrier lifetime of the semiconductors (of the order of 200 ps) produces strong pattern effects. The carrier density depleted by a pulse does not recover completely before the following pulse enters the amplifier. This effect is absent in erbium amplifiers, because the long carrier lifetime of erbium ions makes the amplifier sensitive to the average power of the signal over many pulses. Furthermore, the gain-index coupling of semiconductor amplifiers produces chirp of the amplified pulse and a net frequency shift in the GHz range for mW peak power and tens of ps pulses. Since pulses of different power have a different frequency shift, they acquire different speeds if the group-velocity dispersion of the line is different from zero. This enhances the time jitter at the receiver, degrading the bit-error rate. Frequency filtering of solitons has been proven to be a successful method to reduce the frequency and intensity fluctuations in soliton transmission [4]. If control filters are used with semiconductor amplifiers a difficulty arises, however. The nonlinear phase shift induced by the semiconductor amplifiers is of the same order of the nonlinear phase shift due to the fiber. Without filters, the soliton waveform is strongly perturbed both in the frequency and in time domain [3]. With filters, it is not obvious whether a stable waveform will propagate or not. Fortunately, even in the presence of the strong resistive and reactive nonlinearity induced by the semiconductor amplifiers, a stable soliton-like pulse propagates along the line. We will give here the analytical expression of this stable waveform. Beside the existence of stable waveforms, we will show that these soliton-like pulses have many noticeable properties. First of all, the energy of the pulses is set by the amplifier gain only. The area of the pulse (the amplitude times the pulsewidth) is instead independent of the amplifier gain and depends only on the fiber dispersion

and nonlinearity, and on the filter curvature. The most important property is that the frequency offset of the center of the pulse spectrum from the center of the filter band-pass is a function of the pulse area only, it is independent of the pulse energy. Pulses of higher energies have smaller pulsewidths, and consequently higher bandwidths. This pulses have a larger frequency pushing, which is compensated by the stronger effect of the filters on them. Consequently, unlike the case without filters, pulses of different energies have the same center frequency, hence the same speed. This will strongly reduce the pattern effects connected with the use of semiconductor amplifiers.

The equations describing the evolution, path averaged over the amplifier spacing, of a pulse in a fiber in which the loss is compensated by semiconductor amplifiers is

$$\frac{\partial u(z,t)}{\partial z} = \left\{ (\Delta g + i\Delta\psi) + (\Delta t - i\Delta\omega g'') \frac{\partial}{\partial t} + \left(i\frac{\beta''}{2} + \frac{g''}{2} \right) \frac{\partial^2}{\partial t^2} + i\delta r|u(z,t)|^2 - \frac{1-i\alpha}{2\ell}\eta \left(1 - \frac{1}{G}\right) \int_{-\infty}^{t} \frac{dt'}{\tau_s} \exp\left(-\frac{t-t'}{\tau_s}\right) \frac{|u(z,t')|^2}{P_s} \right\} u(z,t). \quad (1)$$

Here, u is the electrical field normalized that $|u|^2$ is the power at the amplifier output, $\ell\Delta g$ is the amplifier excess gain, ℓ is the amplifier spacing, Δt is a time shift, β'' is the group velocity dispersion, g'' is a parameter proportional to the filtering action ($g''\ell$ is the curvature of the parabolic filters inserted at each amplifier position), $\Delta\omega$ is the angular frequency offset of the carrier frequency from the filter center frequency, δ is the nonlinear coefficient, $r = [1 - \exp(-\Gamma\ell)]/(\Gamma\ell)$ is the path average coefficient, Γ is the fiber power loss coefficient, α is the linewidth enhancement factor of the amplifier, $\eta = g/(g - \gamma_{sc})$, g is the amplifier linear gain coefficient, γ_{sc} is the scattering loss coefficient of the amplifier waveguide, $G = \exp[(g-\gamma)L] = \exp(\Gamma\ell)$ is the linear gain of the amplifier, L is the amplifier length, τ_s is the spontaneous lifetime of the semiconductor, P_s is the saturation power of the amplifier. Eq. (1) holds within a first order expansion of the gain saturation of the amplifier. This is a good approximation if

$$\int_{-\infty}^{t} \frac{dt'}{\tau_s} \exp\left(-\frac{t-t'}{\tau_s}\right) \frac{|u(z,t')|^2}{P_s} \ll 1, \quad (2)$$

that is if the average power is below the saturation power of the amplifier and the energy of the isolated pulse is below the amplifier saturation energy $\tau_s P_s$. Let us consider first the case of an isolated pulse. The carrier lifetime τ_s is of the order of 200 ps. For soliton transmission at bit rates of 10 GBit/s, pulsewidth of the order of 20 ps are used [3]. For this reason, it is interesting to consider the case of τ_s much larger than the pulsewidth. With this assumption, the integral over time appearing in Eq. (1) can be calculated by approximating the exponential to 1. For simplicity,

we assume also $\eta = 1$ and $G \gg 1$. Eq. (1) has the exact solution

$$u(z,t) = A_0 \left[\text{sech}\left(\frac{t}{\tau}\right)\right]^{(1+i\beta)}, \tag{3}$$

where the parameters of Eq. (1) are determined by the following relations

$$0 = -(\Delta t - i\Delta\omega g'')(1+i\beta) - \frac{1-i\alpha}{2\ell}\frac{A_0^2\tau^2}{\tau_s P_s}, \tag{4}$$

$$0 = (-i\beta'' + g'')(-2+\beta^2-3i\beta) + 2i\delta r A_0^2\tau^2, \tag{5}$$

$$0 = (\Delta g + i\Delta\psi) + \frac{1-\beta^2+2i\beta}{2\tau^2}(-i\beta'' + g'') - \frac{1-i\alpha}{2\ell}\frac{A_0^2\tau}{\tau_s P_s}. \tag{6}$$

The relevant pulse parameters can be easily calculated from Eqs. (4) and (5). They are the frequency offset

$$\Delta\omega = -\frac{1}{2g''\ell}\frac{\alpha+\beta}{\beta^2+1}\frac{A_0^2\tau^2}{\tau_s P_s}, \tag{7}$$

the chirp parameter

$$\beta = \frac{3\beta''}{2g''} - \left[\left(\frac{3\beta}{2g''}\right)^2 + 2\right]^{1/2} \tag{8}$$

and the square of the area of the pulse

$$\mathcal{A}^2 = \tau^2 A_0^2 = -\frac{\beta''}{\delta r}\left[\left(1-\frac{\beta''}{2}\right) + \frac{3g''}{4\beta''}\beta\right]. \tag{9}$$

From Eq. (9), one sees right away that to get stable pulses negative β'' is required. The pulse energy, equal to

$$W = 2A_0^2\tau \tag{10}$$

is determined by Eq. (6). It is the solution of the following algebraic equation

$$\Delta g = -\left[(1-\beta^2)\frac{g''}{2} + \beta\beta''\right]\frac{W^2}{4\mathcal{A}^4} + \frac{1}{4\ell}\frac{W}{\tau_s P_s} = 0 \tag{11}$$

The excess gain Δg determines uniquely the pulse energy W. The frequency shift of the pulse, on the other hand, depends on the area of the pulses only, which in turn depends only on the fiber parameters. As anticipated, the frequency offset is independent of the pulse energy.

Assume now that the pulse $u_0(z, t+T)$ centered at time $t = -T$ is leading the pulse $u_1(z,t)$ centered at $t = 0$. The pulsewidth of both pulses is assumed much less than the carrier lifetime τ_s. Assume also that the two pulses are well separated, which implies $|u_1(z,t) + u_0(z,t+T)|^2 \approx |u(z,t)|^2 + |u_0(z,t+T)|^2$. Consider the evolution of the pulse centered at $t = 0$, $u_1(z,t)$. The time integral in Eq. (3) splits into two parts

$$\begin{aligned}\int_{-\infty}^{t}\frac{dt'}{\tau_s}\exp\left(-\frac{t-t'}{\tau_s}\right)\frac{|u(z,t')|^2}{P_s} &= \int_{-\infty}^{t}\frac{dt'}{\tau_s}\exp\left(-\frac{t-t'}{\tau_s}\right)\frac{|u_0(z,t'+T)|^2}{P_s} \\ &+ \int_{-\infty}^{t}\frac{dt'}{\tau_s}\exp\left(-\frac{t-t'}{\tau_s}\right)\frac{|u_1(z,t')|^2}{P_s},\end{aligned} \tag{12}$$

At $t \approx 0$, the first integral in Eq. (12) can be approximated as

$$\int_{-\infty}^{t} \frac{dt'}{\tau_s} \exp\left(-\frac{t-t'}{\tau_s}\right) \frac{|u_0(z,t'+T)|^2}{P_s} \approx \exp\left(-\frac{t+T}{\tau_s}\right) \frac{E_0}{\tau_s P_s} \approx \exp\left(-\frac{T}{\tau_s}\right) \frac{E_0}{\tau_s P_s}, \qquad (13)$$

where $E_0 = \int_{-\infty}^{\infty} dt' |u(z,t)|^2$ is the energy of the first pulse. Consequently, the case of two pulses can be reduced to the case of a single pulse with an excess gain

$$\Delta g' = \Delta g - \frac{1}{2\ell} \exp\left(-\frac{T}{\tau_s}\right) \frac{E_0}{\tau_s P_s}. \qquad (14)$$

The gain decrease will produce a decrease of the power of the pulse with respect to the single pulse case. The gain decrease does not prevent, however, a stable pulse propagation. As already pointed out, and mostly important, the decrease of power does not produce any frequency shift. The only problem connected with the use of filters might be the growing of a quasi continuous background of radiation close to the center of the filter peak. This effect might be eliminated by sliding the center frequency of the filters along propagation [5]. This would also reduce the effect of the large ASE noise of the semiconductor amplifiers, since the line becomes transparent only to pulses and opaque to the noise.

In conclusion, the use of filters allows the propagation of stable waveforms in a line of negative dispersion in which loss is compensated by semiconductor amplifiers. The filtering action exactly compensate for the spectral broadening induced by the saturation of the semiconductor amplifiers. The pulses are noticeably stable and robust against pattern effects.

Work carried out under an agreement between FUB and the Italian PT Administration.

References

[1] Ch. Holtman, P. A. Besse, T. Brenner, R. Dall'Ara, and H. Melchior, "Polarization insensitive bulk ridge-type semiconductor optical amplifiers at 1.3 μm wavelength," in *Optical amplifiers and their applications*, Yokohama, July 4-6, 1993, paper SuB2-1.

[2] L. F. Tiemeijer, P. J. A. Thijs, T. van Dongen, R. W. M. Slootweg, J. M. M. van der Heijden, J. J. M. Binsma, and M. P. C. M. Krijn, "Polarization insensitive multiple quantum well laser amplfiers for the 1300 nm window," Appl. Phys. Lett. **62**, 826–828 (1993).

[3] C. T. H. F. Liendenbaum, J. J. E. Reid, L. F. Tiemeijer, A. J. Boot, P. I. Kuindersma, I Gabitov, and A. Mattheus, "Experimental long haul 1300 nm soliton transmission on standard single mode fibers using quantum well laser amplifiers," Proceedings of the 20th Europen Conference on Optical Communication (ECOC '94), Sept. 25–29, Florence (1994), pp. 233–236.

[4] A. Mecozzi, J. D. Moores, H. A. Haus, and Y. Lai, "Soliton Transmission Control," Opt. Lett. **16**, 1841–1843 (1991); Y. Kodama and A. Hasegawa, "Generation of asymptotically stable optical solitons and suppression of the Gordon-Haus effect," Opt. Lett **17** 31–33 (1992).

[5] L. F. Mollenauer, J. P. Gordon, and S. G. Evangelides, "The sliding-frequency guiding filters, and improved form of soliton jitter control," Opt. lett. **17** 1575–1577 (1992).

9,000-km WDM Transmission of Three 2.5-Gbit/s Channels Covering a 5-nm Wavelength Range and Using No Pre-Emphasis

S.-H. Huang, X.Y. Zou, E. Park, and A.E. Willner

Room EEB 500, Dept. of Electrical Engineering - Systems
Univ. of Southern California
Los Angeles, California, USA 90089-2565
FAX: (213) 740-8729, shouhua@solar.usc.edu

INTRODUCTION

Error-free megameter transmission distances of a high-speed optical channel have been readily achieved by utilizing the Erbium-doped fiber amplifier (EDFA) to efficiently compensate for fiber attenuation losses with near-quantum-limited amplified-spontaneous-emission (ASE) noise.[1,2] This achievement of point-to-point ultra-long-distance optical transmission is quite valuable for both undersea and terrestrial communications. Furthermore, we can more efficiently utilize the available fiber bandwidth by simultaneously transmitting many independent channels, with each channel located on a different wavelength. Such wavelength-division-multiplexing (WDM) allows for a dramatic increase in the aggregate system transmission capacity. Due to the wide gain bandwidth (>THz) of the EDFA, many WDM channels can be simultaneously amplified and transmitted over long distances.[3,4,5,6] However, the EDFA only compensates for attenuation while other deleterious effects, such as dispersion and nonlinearities, are allowed to accumulate along the fiber link. The main challenge in transmitting several WDM channels is to achieve a delicate balance among the following critical issues: (i) placing the channels sufficiently close to the fiber's zero-dispersion-point in order to minimize intramodal dispersion, (ii) placing the channels sufficiently far from the fiber's zero-dispersion-point in order to minimize some nonlinear effects (i.e. four-wave mixing and cross-phase modulation),[7,8] and (iii) locating the channels in a region within the EDFA bandwidth which will provide adequate gain when cascading many amplifiers.[9,10,11] The bandwidth which can support the transmission of many WDM channels and which will effectively satisfy all the above constraints is severely limited.

Recently, work has been reported on the successful transmission of four 2.5-Gbit/s WDM channels through 9,000 km of dispersion-shifted fiber.[12] In that experiment, the four channels were placed on the 1.560-μm gain peak and covered only a 2.5-nm wavelength range. Moreover, since those channels were placed on the gain peak, channel pre-emphasis was required to compensate for the non-uniform EDFA gain. We report the simultaneous transmission of three 2.5-Gbit/s WDM channels through 9,000 km of dispersion-shifted fiber in which the channels were placed off the gain peak, avoiding the necessity for channel pre-emphasis. Furthermore, the wavelength range of the channels is 5 nm, which is two times larger than previously reported results. Although the larger 5-nm wavelength range of our experiment supports the simultaneous transmission of only three channels, we hope that this range will support the 9,000 km transmission of several more channels than just the three we demonstrate here.

EXPERIMENT

Figure 1 shows the experimental long-distance transmission system in which a recirculating fiber loop was used to replicate a linear long-distance link of arbitrary length as in Bergano, et al.[13] The general scheme is to: (i) fill the fiber loop with a pseudorandom stream of optical data bits, (ii) allow these bits to recirculate around the loop a finite number of times corresponding to some desired link distance, and (iii) remove these bits from the loop for bit-error-rate measurements. The details are as follows. A stream of bits was transmitted into the fiber loop until the loop was nearly filled with data. The input data stream was then terminated near the source, and the already-transmitted bits were allowed to propagate around the loop numerous times. After each revolution, light was partially and passively coupled out of the loop. Using

appropriate gating techniques, bit-error-rates were taken only on data bits which were output after propagating around the loop a total of 9,000 km. After the transmitted bits propagated the 9,000 km, the loop was emptied of bits by using an intra-loop acousto-optic modulator and refilled with a **new** data stream. The loop consisted of: (i) 3 EDFA's each having a small-signal gain of ~20 dB, (ii) 95 km of dispersion-shifted fiber (dispersion-zero ≈ 1.551 μm; loss ≈ 0.23 dB/km), (iii) a polarization controller, and (iv) an acousto-optic modulator gating switch. The data streams would propagate around the loop 95 times, replicating a 9,000 km link with 285 cascaded EDFA's. Appropriate electronic circuitry was used to gate the data into and out of the loop and to synchronize the bit-error-rate measurements. The three signal wavelengths were each modulated at 2.5 Gbit/s and were located at 1.5562, 1.5573, and 1.5615 μm covering a wavelength range of 5 nm. A polarization scrambler (i.e. phase modulator) was used before the loop input to partially negate any effects due to the slight polarization-dependence of the EDFA gain. The output of the loop included an EDFA preamplifier, a 0.6-nm angle-tuned optical filter, an optical attenuator, a 2.5-Gbit/s p-i-n receiver, and a high-speed clock-recovery circuit.

RESULTS

We have effectively balanced the criteria of low dispersion, minimal nonlinear effects, and high EDFA gain over a 5-nm wavelength range for 9,000 km transmission of three channels **without** requiring pre-emphasis to compensate for non-uniform EDFA gain. Figures 2a and 2b show the optical spectrum of the loop input and output, respectively, showing clearly the three WDM channels and a 1.560-μm peak in the ASE (i.e. gain) of the EDFA cascade. This newly-generated 1.560-μm gain peak occurs in long amplifier cascades due to the relative overlap of the emission and absorption cross-sections of Erbium.[10] The bit-error-rate curves for the three channels are shown in Fig. 3 in which the optical power was measured at the loop output. There is an ~ 3-dB differential in sensitivity among the three channels when achieving a 10^{-9} bit-error-rate over the 5-nm wavelength range. Furthermore, our results are achieved without any pre-emphasis (i.e. selective wavelength attenuation) at the transmitter. Pre-emphasis was unnecessary because our channels were **not** located on the 1.560-μm gain peak, resulting in relative gain uniformity; the channels were located on either side of the gain peak. This is in contrast to ref. [12] in which the channels were located on the nonuniform-gain peak, consequently requiring pre-emphasis to achieve a small signal-to-noise ratio differential among the channels.

Our reported large wavelength range is two times larger than previously-reported results.[12] This increased bandwidth range will hopefully accommodate several more channels than just the demonstrated three when transmitting optical signals over 9,000-km, which corresponds to transpacific distances.

SUMMARY

We have demonstrated near-error-free optical transmission of three 2.5-Gbit/s WDM channels through 9,000 km of dispersion-shifted fiber by using a recirculating loop. The wide wavelength range of the channels was 5 nm. These channels were transmitted off the 1560-nm peak, and no pre-emphasis of the channels was required.

ACKNOWLEDGMENTS

We thank the following individuals for their kind help: N.S. Bergano, N.K. Dutta, J.W. Sulhoff, and J.L. Zyskind. We also acknowledge the use of a loaned Panasonic DFB Laser Module as one of the signal sources.

REFERENCES

1. N.S. Bergano, C.R. Davidson, G.M. Homsey, D.J. Kalmus, P.R. Trischitta, J. Aspell, D.A. Gray, R.L. Maybach, S. Yamamoto, H. Taga, N. Edagawa, Y. Yoshida, Y. Horiuchi, T. Kawazawa, Y. Namihira, and S. Akiba, Topical Meeting on Optical Amplifiers '92, paper PD-11, Santa Fe, NM.

2. H. Taga, N. Edagawa, H. Tanaka, M. Suzuki, S. Yamamoto, H. Wakabayashi, N.S. Bergano, C.R. Davidson, G.M. Homsey, D.J. Kalmus, P.R. Trischitta, D.A. Gray, and R.L. Maybach, OFC '93, paper PD-1, San Jose.
3. H. Taga, N. Edagawa, S. Yamamoto, Y. Yoshida, Y. Horiuchi, T. Kawazawa, and H. Wakabayashi, OFC '93, paper PD4, San Jose, CA.; H. Taga, N. Edagawa, Y. Yoshida, S. Yamamoto, and H. Wakabayashi, Electron. Lett., vol. **29**, p. 485, 1993.
4. E.L. Goldstein, A.F. Elrefaie, N. Jackman, and S. Zaidi, OFC '93, paper TuJ3, San Jose, CA.
5. A.F. Elrefaie, E.L. Goldstein, S. Zaidi, and N. Jackman, Photonics Tech. Lett., **5**, p. 1026, '93.
6. K. Inoue, H. Toba, and K. Nosu, J. Lightwave Tech, vol. **9**, pp. 368-374, 1991.
7. A.R. Chraplyvy, J. of Lightwave Tech., vol. **8**, pp. 1548-1557, 1990.
8. A.R. Chraplyvy and R.W. Tkach, Photonics Technology Letters, vol. **5**, pp. 666-668, 1993.
9. J.P. Blondel, A. Pitel, and J.F. Marcerou, OFC '93, paper TuI3, San Jose, CA, Feb. 1993.
10. A.E. Willner and S.-M. Hwang, "Transmission of Many WDM Channels Through a Cascade of EDFA's in Long-Distance Link and Ring Networks," accepted for publication, J. of Lightwave Technology, Special Issue on Optical Amplifiers, vol. **13**, no. 5, May 1995; also OFC '94, paper WI2, San Jose, CA.
11. S.-M. Hwang and A.E. Willner, Photonics Technology Lett., vol. **5**, pp. 1190-1193, 1993.
12. N.S. Bergano and C.R. Davidson, Topical Meeting on Optical Amplifiers and Their Applications, paper PD7, Breckenridge, CO.
13. N.S. Bergano, J. Aspell, C.R. Davidson, P.R. Trischitta, B.M. Nyman, and F.W. Kerfoot, Topical Meeting on Optical Amplifiers and Their Applications '91, paper ThA5, Snowmass Village, CO.

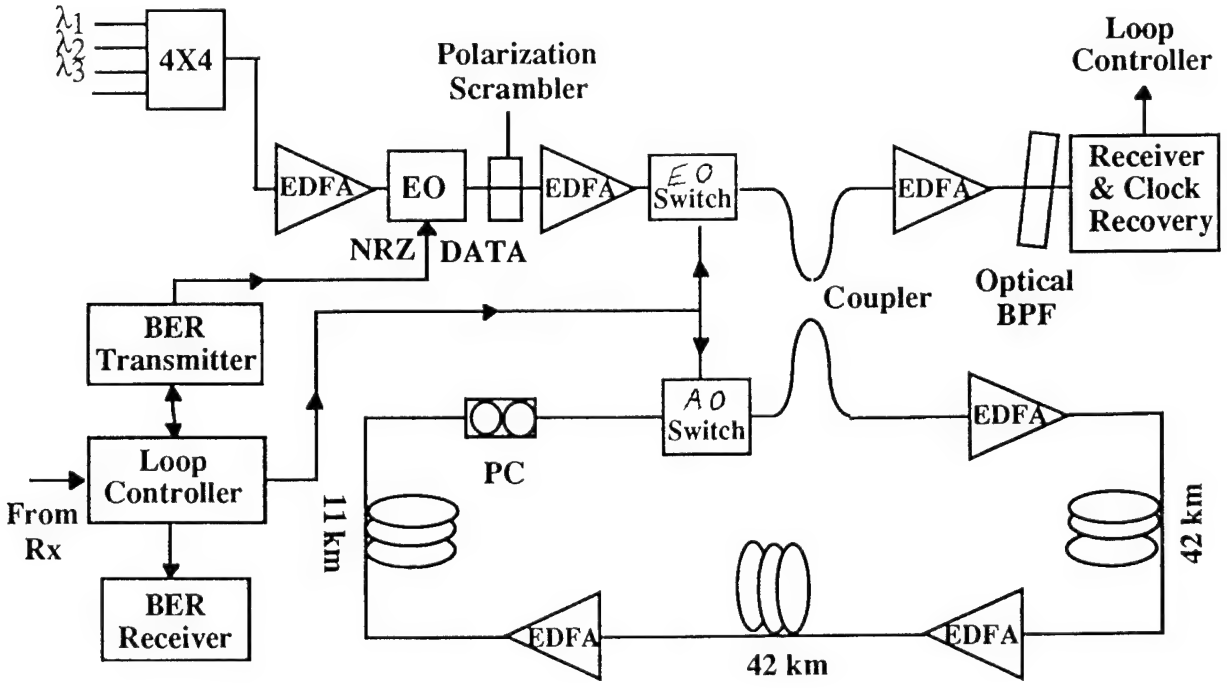

Figure 1. Experimental setup of the WDM recirculating loop. (PC = Fixed Polarization Controller; EO = Electro-Optic Modulator; AO = Acousto-Optic Modulator.)

(a) INPUT

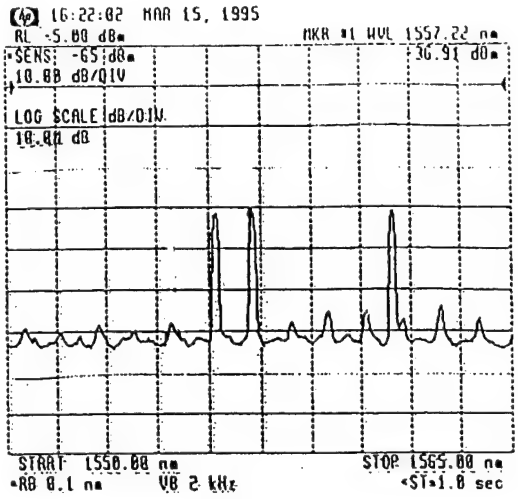

(b) OUTPUT

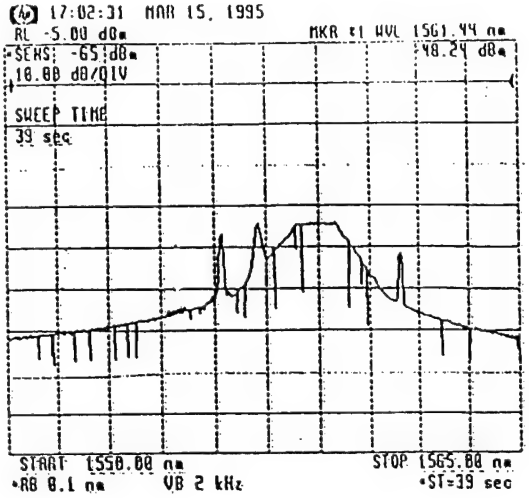

Figure 2. Optical spectrum of: (a) the input to the loop, and (b) the output of the recirculating loop after 9,000 km.

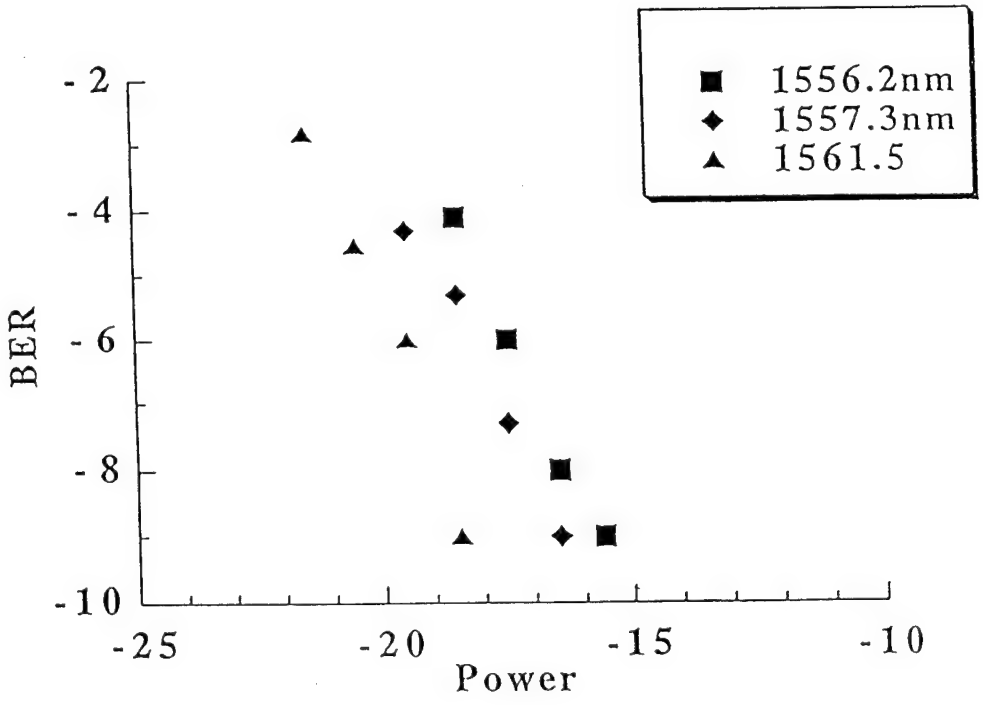

Figure 3. Bit-error-rate curves versus received optical power for the three WDM channels, with each channel propagating 9,000 km and being modulated at 2.5 Gbit/s.

Unregenerated single channel transmission at 10 Gbit/s over 300 km standard fiber

Bo Foged Jørgensen (bfj@emi.dtu.dk) and Rune J.S. Pedersen (rjp@emi.dtu.dk)

Center for Broadband Telecommunications
Electromagnetics Institute
Technical University of Denmark, Bldg. 348
DK - 2800 Lyngby, Denmark
Telephone: + 45 4288 1444, Fax: + 45 4593 1634

Introduction: 10 Gbit/s long distance transmission at 1.55 μm on standard single mode fibers (SSMF) has attracted a widespread interest because of the increasing need to upgrade existing transmission systems. Recently, unrepeatered transmission over 182 km [1] and 204 km [2], respectively, and unregenerated transmission over 253 km in a DST system with optical in-line amplifiers [3] have been reported. Here, we demonstrate experimentally for the first time unregenerated single channel 10 Gbit/s transmission at 1.55 μm over 300.4 km SSMF with two in-line amplifiers by employing pre-chirped ASK modulation.

Experimental set-up: The set-up is shown in Fig. 1. A 1547 nm DFB laser with a linewidth of 2 MHz is used as transmitter and the light is ASK modulated at 10 Gbit/s by a $LiNbO_3$ Mach-Zehnder Modulator. The rise time of the modulation signals is ~50 ps.

The signal is amplified to +11.7 dBm by a booster amplifier and transmitted over 300.4 km of SSMF with a total dispersion of 5050 ps/nm (i.e. 16.8 ps/nm/km). Stimulated Brillouin Scattering is suppressed by frequency dithering [4] at 10 kHz with an FM amplitude of ~1.8 GHz. In-line EDFA's are used after 65 km and

219.4 km. The gain/(noise figure) of the in-line amplifiers are 19 dB/(12 dB) and 26 dB/(5 dB), respectively. The loss of the fiber spans are 14.6 dB, 32.1 dB and 16.7 dB including connectors and splices. Fig. 2 shows the average power evolution.

The pin-receiver has a bandwidth of 4 GHz. The error counter is synchronized by the clock signal recovered from the received signal. The word length is 2^7-1 limited by the frequency response of the baseband receiver.

Results and discussion: Fig. 3 shows the BER curve after transmission for a chirp parameter [5] of ~0.2. The sensitivity is -11.7 dBm @ BER = 10^{-9}. The curve is slightly curved due to spontaneous emission from the two in-line amplifiers.

Fig. 4 shows the optical waveform evolution after 0 km (A), 65 km (B), 219.4 km (C) and 300.4 km (D). The extinction ratio which is chosen as low as 4 dB at the transmitter significantly improves as the optical signal propagates throughout the fiber. A pulse compression is seen to develop due to interaction of pre-chirp, Self-Phase Modulation and dispersion. The compression creates shoulders on edges of consecutive pulses of high intensity which gradually turn into a strong modulation of the signal. This effect is reduced by lowpass filtering in the receiver and do not impede operation of the system.

Conclusions: Unregenerated single channel transmission at 10 Gbit/s at 1.55 μm over the longest reported distance (300.4 km) of standard single mode fiber with a total dispersion of more than 5000 ps/nm has been demonstrated experimentally in a system with two optical in-line amplifiers.

References: [1] B. Wedding et al., Electron. Lett., Vol. 29, No. 4, 1993.
[2] B.F. Jørgensen, ECOC'94, Paper We.B3.3, 1994.
[3] B. Wedding et al., ECOC'93, Paper Tu.C4.3, 1993.
[4] A. Hirose et al., ECOC'90, Paper Mo.F3.6, 1990.
[5] A.H. Gnauck et al., Phot. Tech. Lett., Vol. 3, No. 10, 1991.

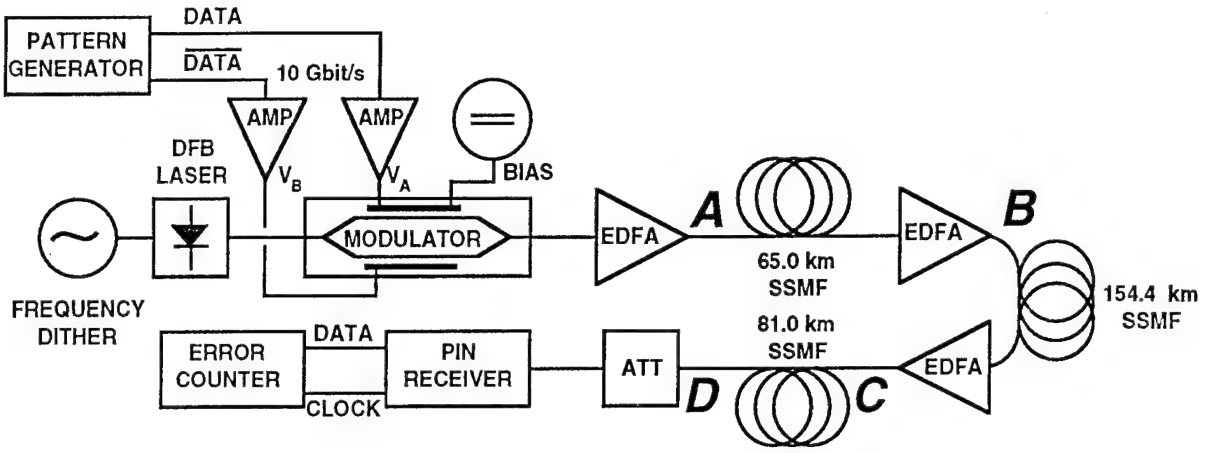

Fig. 1. 10 Gbit/s – 300.4 km experimental set-up.

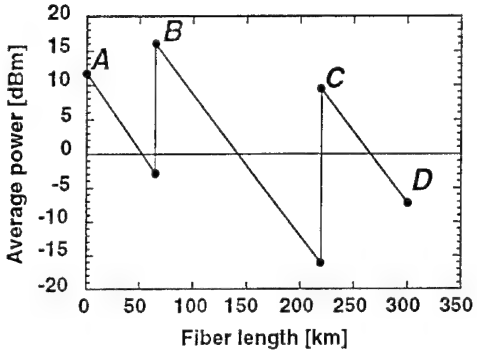

Fig. 2. Average power evolution.

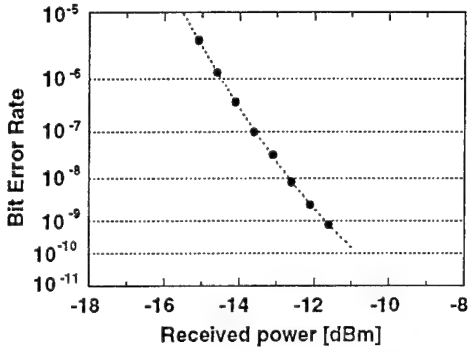

Fig. 3. BER curve after 300.4 km.

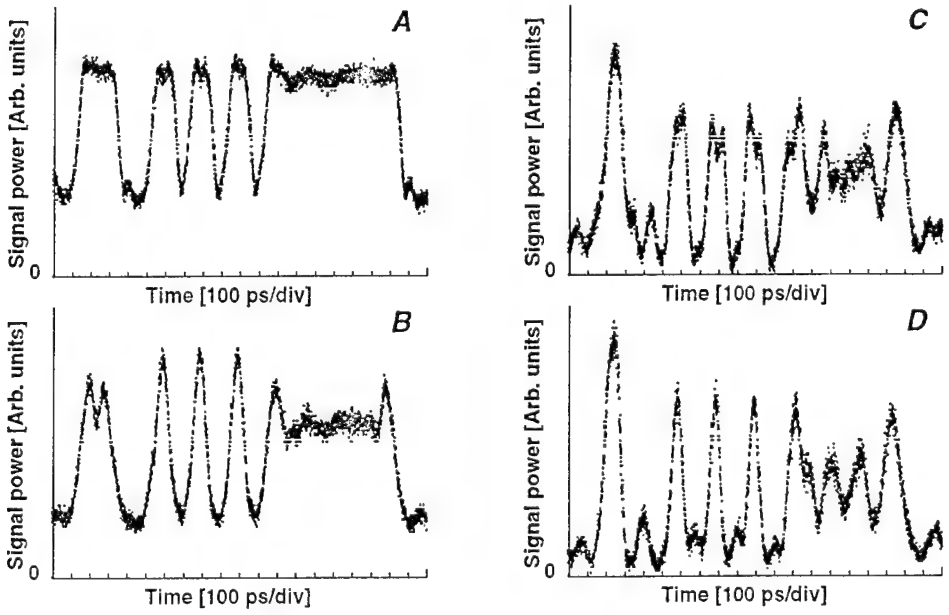

Fig. 4. Optical waveform evolution.
A) 0 km, B) 65 km, C) 219.4 km, D) 300.4 km.

Amplifier Characterization

ThE 16:15-17:30
Theatersaal

Douglas Baney, *Presider*
Hewlett Packard Laboratories, U.S.A.

Inhomogeneous Gain Saturation of Erbium-Doped Fiber Amplifiers

H. Chou and J. Stimple

Hewlett-Packard Company
1412 Fountaingrove Parkway
Santa Rosa, CA 95403, USA
Tel: (707)577-4547
Fax: (707)577-4951

Introduction

An important application of Erbium-doped fiber amplifiers is in future wavelength division multiplexed (WDM) communication systems. In such systems one needs to consider gain cross saturation, i.e., how a signal at one wavelength affects gains at other wavelengths. A contributing factor to gain cross saturation is the inhomogeneous broadening of the gain medium. In this paper we demonstrate a technique for characterizing the inhomogeneous nature of the small-signal gain spectrum in the presence of a saturating signal.

Inhomogeneous broadening of erbium in glass fiber has been examined by Desurvire et. al. [1], Tachibana et. al.[2] and Brocklesby[3]. In [2] the researchers used an edge-emitting LED (EELED) as the probe and lock-in amplifiers as the detector to separate the probe from the saturating signal. In this paper we used an EELED as the probe and time-domain extinction as the detection method[4]. For the amplifier we tested, we found the cross saturation effect to be on the order of 1 dB and the width of the spectral hole to be about 10 nm at room temperature.

Experiments

The experimental setup (Figure 1(a)) consisted of two saturating DFB lasers, one at 1543.3 nm and the other at 1555.8 nm. The probe source was an edge-emitting LED (EELED). These sources were combined by 3-dB fiber couplers at the input to the fiber amplifier under test. The output of the amplifier was detected with an optical spectrum analyzer (OSA) with fast detection electronics. For each displayed point on the OSA, the SYNC OUT triggers a 15-μs pulse from the output of the pulse generator, which shuts off the DFB lasers for that interval. Each data point was taken at 10 μs after the laser had been pulsed off. The pulse repetition rate was 1 kHz. Figure 1(b) shows the timing diagram.

The amplifier gain medium was Er-doped germanoaluminosilicate fiber. The exact composition and the Er doping level were unknown. Two 1480 nm lasers pumped the medium in both directions. A dichroic filter eliminated the pump at the output of the amplifier. Both the input and output had optical isolators.

In our experiments only one DFB laser was on at a time. For each saturating wavelength, three measurements were made: a) the EELED power spectrum; b) the amplifier output with both the EELED and the DFB laser on; and c) the amplifier output with only the DFB on. The data were processed as shown in Figure 2 to obtain the gain and noise figure spectra. The gain spectrum thus obtained is the amplifier's small-signal gain spectrum in the presence of a saturating signal.

The EELED spectral power density incident on the amplifier was approximately -38.6 dBm/nm and was flat to within 0.6 dB in the wavelength range of interest (1540 - 1560 nm). The DFB laser powers incident on the amplifier were -9.6 dBm at 1555.8 nm and -6 dBm at 1543.3 nm. We chose these powers so that the amplifier is saturated to the same degree independent of which DFB was on. We ensured the same degree of saturation by comparing the amplified spontaneous emission (ASE) from the amplifier for the two saturating conditions.

The repeatability of the measurement apparatus was characterized in two ways. In the first, the input polarization to the optical amplifier remained constant and the measurement was repeated 20 times. The gain spectrum was repeatable to within 0.03 dB (to three standard deviations.) In the second, we generated 20 different polarization states at the amplifier input. The gain spectrum was repeatable to within 0.3 dB (to three standard deviations.) Some of the latter was due to the polarization dependence of the amplifier itself.

Results

Figure 3(a) shows the small-signal gain spectra for the two saturating wavelengths, and Figure 3(b) shows their difference spectrum. As is clear from Figure 3(b), the gain of this amplifier saturates inhomogeneously. When the saturating signal is at 1543.3 nm, the amplifier's small-signal gain compressed by 0.8 dB more at that wavelength than when the saturating signal is at 1555.8 nm. The width of this spectral hole is approximately 10 nm. Thus for WDM spacing of a few nanometers or less, a saturating signal at one wavelength will affect the gains of adjacent wavelengths non-uniformly.

Conclusions

We have demonstrated a technique for characterizing the inhomogeneity of an Er amplifier's gain saturation. The results show that this inhomogeneity leads to spectral hole burning and therefore non-uniform gain compression of WDM channels adjacent to a saturating signal. However, for WDM applications, some inhomogeneous broadening in the gain medium may be desirable to avoid gain depletion of some channels due to a dominant signal.

Acknowledgment

The authors would like to thank Susan Sloan, Dennis Derickson and Patricia Beck for supplying the edge-emitting LED, and Tim Simmons, Andrew Harker and Bob Weissman for providing the amplifier used in these experiments.

References

1. E. Desurvire, J.W. Sulhoff, J.L. Zyskind, and J.R. Simpson, *IEEE Photonics Technology Lett.* **2** 653 (1990)
2. M. Tachibana, R.I. Laming, P.R. Morkel, and D.N. Payne, *Optics Letters* **16** 1499 (1991)
3. W.S. Brocklesby, *Annu. Rev. Mater. Sci.* **23** 193 (1993)
4. D.M Baney and J. Dupre, in *Proceedings for the European Conference on Optical Communication (ECOC)*, Paper WeP2.11, p. 509 (Berlin 1992)

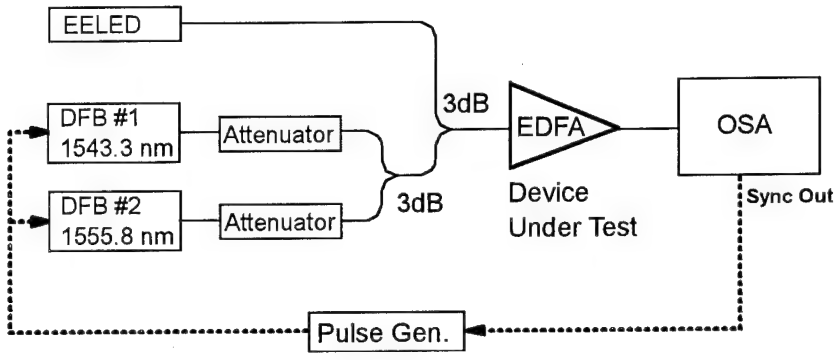

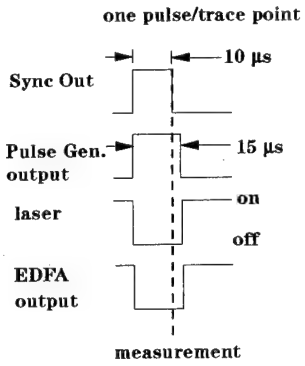

Figure 1(a) Experimental setup

Figure 1(b) Timing diagram

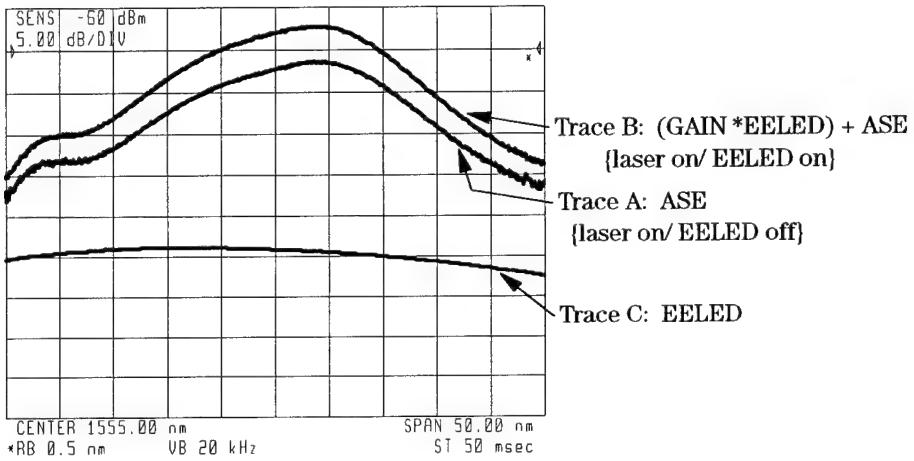

Figure 2(a) Three measurements for each saturating wavelength.

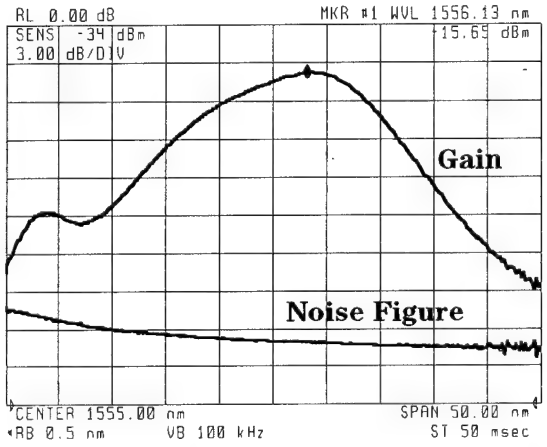

Gain = (Trace B - Trace A) / Trace C
= ((Gain * EELED) + ASE -ASE)/ EELED

G(dB) = 10 log Gain

Noise Figure = Trace A/ h*v*Gain*B
= ASE/h*v*G*B

NF (dB) = 10 log (Noise Figure)

Figure 2(b) Data processing steps for obtaining the gain and noise figure spectra.

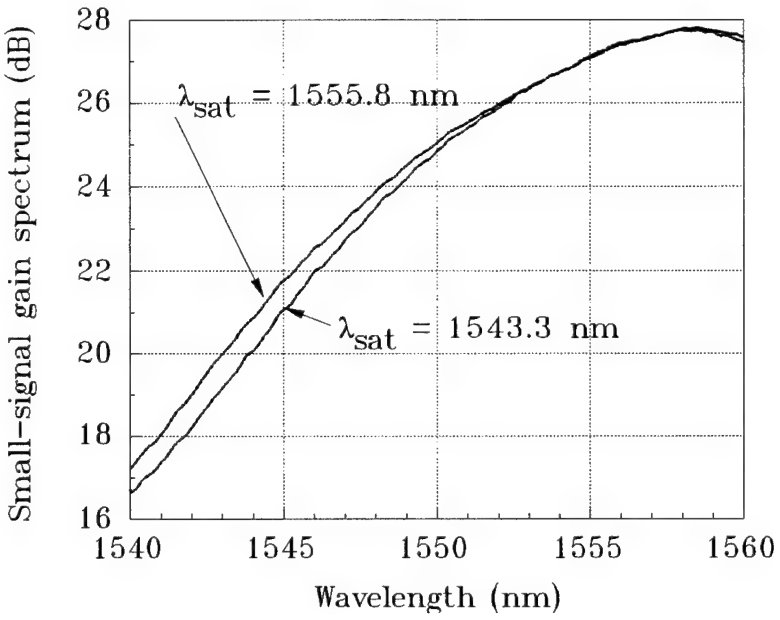

Figure 3(a) Small-signal gain spectra for two different saturating wavelengths. The amplifier was saturated to the same degree in the two cases.

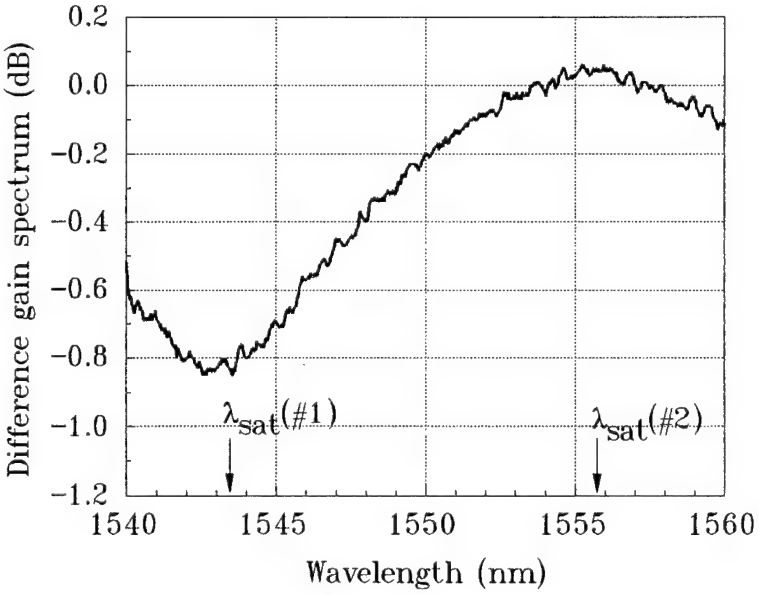

Figure 3(b) Difference between the two curves in Figure 3(a).

Noise Figure Increase of High Concentration Erbium-Doped Fiber Amplifiers Pumped by a 1.48-μm or 0.98-μm Laser Diode

Hiroji MASUDA and Kazuo AIDA

NTT Optical Network Systems Laboratories
1-2356 Take, Yokosuka, Kanagawa, 238-03 Japan
Phone. +81-468-59-5039, Fax. +81-468-59-5031

Introduction: 1.48-μm or 0.98-μm laser diode pumped erbium-doped fiber amplifiers (EDFAs) are very important in 1.5-μm optical transmission systems. Compact EDFAs having short EDFs can be constructed by using high erbium concentration EDFs. However, several studies have reported that the gain of high concentration EDFAs falls considerably as the erbium concentration increases [1] due to cooperative upconversion [2], [3], [4] and exited-state absorption at 1.48 μm [5]. Moreover, theoretical studies predict that the noise figure (NF) of the EDFAs increases with Er concentration [2], [3], [4]. Unfortunately, no experimental study on the NF increase has been reported to our knowledge. This study reports experimental results on the NF increase of EDFAs, which have erbium concentrations from 500 to 8,800 ppm and are pumped by a 1.48-μm or 0.98-μm laser diode. Comparing the experimental results with a theoretical model yields the origins of the measured NF increase.

Experiment and Discussion: EDFs having four different concentrations were tested. The EDFs are denoted by the concentrations as follows: EDF-a (500 ppm by weight), EDF-b (2,000 ppm), EDF-c (5,500 ppm), and EDF-d (8,800 ppm). Parameters of the EDFs are listed in Table 1. β is half the erbium pair ion ratio and was measured by the method of Ref. [6]. Erbium was doped into the core-center and erbium-doped area diameters were about half the core diameter. Aluminum concentrations were 1 to 5 %, germanium concentrations were 3 to 13 %, and mode field diameters were 4.3 to 5.1 μm for the four EDFs. Signal light was emitted by a DFB-LD, and signal wavelength was 1.552 μm. The EDFs were forward pumped by a 1.48-μm or 0.98-μm LD. To avoid the unfavorable NF variation due to pump wavelength variation, a wavelength stabilized 0.98-μm LD module (SEASTAR Optics Inc.) was used. Moreover, the wavelength of a Fabry-Perot type 1.48-μm LD was locked to 1.480 μm (FWHM = 5 nm) using the method of Ref. [7]. NF was measured by an optical method using an optical spectrum analyzer and a polarization beam spliter [8].

Figure 1 shows measured gain (EDF gain) as a function of an effective EDF length (L_{eff}) for 1.48-μm pumping (a) and 0.98-μm pumping (b). L_{eff} is defined for convenience to be the product of real EDF length and the absorption coefficient at 1.550 μm (α in Table 1). Launched signal power (P_{sin}) was -15 dBm, and launched pump power (P_{pin}) was 50 mW

for the two pump wavelengths. From Fig. 1, the maximum gain (G_{max}) can be derived. G_{max} decreases considerably with the concentration at both pump wavelengths.

EDF lengths for NF measurement were chosen so that the gain at P_{sin} = -30 dBm was about 20 dB. The lengths are listed in Table 1. Figure 2 shows the launched signal power dependence of NF and gain at P_{pin} = 50 mW. NF increases with concentration for the two pump wavelengths, and the difference between EDF-a and EDF-d is larger with 1.48-μm pumping. No difference in the profiles of the noise figure curves for the four EDFs is seen. Figure 3 shows launched pump power dependence of NF and gain at P_{sin} = -15 dBm. NF and gain approach their saturated values almost at the same pump power value for each EDF. For pump powers larger than about 20 mW, NF variation is less than about 0.5 dB. From Figs. 2 and 3, NFs of the EDFAs operating in typically practical condition are mainly limited by Er concentration, and the increase in pump power or gain results in only small decrease in NF.

The experimental results were compared the values determined using a theoretical model [5]. The model ("pair ion model") contains the effects of cooperative upconversion and exited-state absorption at 1.48 μm occurring in erbium pair ions. Figure 4 shows the maximum gain G_{max} (cf. Fig. 1) and NF as a function of the erbium pair ion ratio 2β at P_{pin} = 50 mW and P_{sin} = -15 dBm. The experimental values were derived from Figs. 1 and 2, and the theoretical values were calculated using the model equation of Ref. [5] and averaged fiber parameters of the four EDFs. The accuracy of the experimental gain and NF was about + - 0.2 dB. From Fig. 4(a), the experimental and theoretical gains coincide well except for the case of the 0.98-μm pumped EDF-d. On the other hand, from Fig. 4(b), the experimental and theoretical NFs coincide well only for the case of the 1.48-μm pumped EDF-a, -b, and -c and the 0.98-μm pumped EDF-a. However, a large part of the NF increase can be explained by the model.

Conclusion: NF increase in high concentration EDFAs pumped by a 1.48-μm or 0.98-μm LD was measured for the first time. NF increased from 3.2 dB at (erbium concentration of) 500 ppm to 4.2 dB at 8,800 ppm with 0.98-μm pumping, and from 4.5 dB at 500 ppm to 6.1 dB at 8,800 ppm with 1.48-μm pumping. The erbium pair ion model explained most of the measured NF increase.

References:

[1] R. I. Laming et al., *IEEE Photon. Techhnol. Lett.*, **3**, p. 253, 1991
[2] H. Masuda et al., *IEEE J. Lightwave Technol.*, **10**, p. 1789, 1992
[3] J. Nilsson et al.,*OAA,* MD19, p. 222, 1993
[4] J. L. Wagener et al., *Optics. Lett.*, **19**, p. 347, 1994
[5] H. Masuda et al.,*OAA,* ThB6, p. 86, 1994
[6] E. Delevaque et al., *IEEE Photon. Techhnol. Lett.*, **5**, p. 73, 1993
[7] H. Masuda et al., *Electron. Lett.*, **28**, p. 1855, 1992
[8] J. Aspell et al., *OFC,* ThA4, p. 189, 1992

Table 1 Parameters of Erbium-Doped Fibers

Symbol	Units	EDF-a	EDF-b	EDF-c	EDF-d
ρ	ppm	500	2,000	5,500	8,800
2β	%	4.6	8.4	11	27
α	dB / m	0.76	7.2	16.8	31.6
L(1.48 μm)	m	35.5	3.50	1.75	1.35
L(0.98 μm)	m	21.1	2.25	1.01	0.71

ρ: Erbium Concentration
2β: Er bium pair Ion Ratio
α: Absorption Coefficient at 1.550 μm

L(1.48 μm), L(0.98 μm): EDF Length in NF Measurement for 1.48-μm and 0.98-μm Pumping

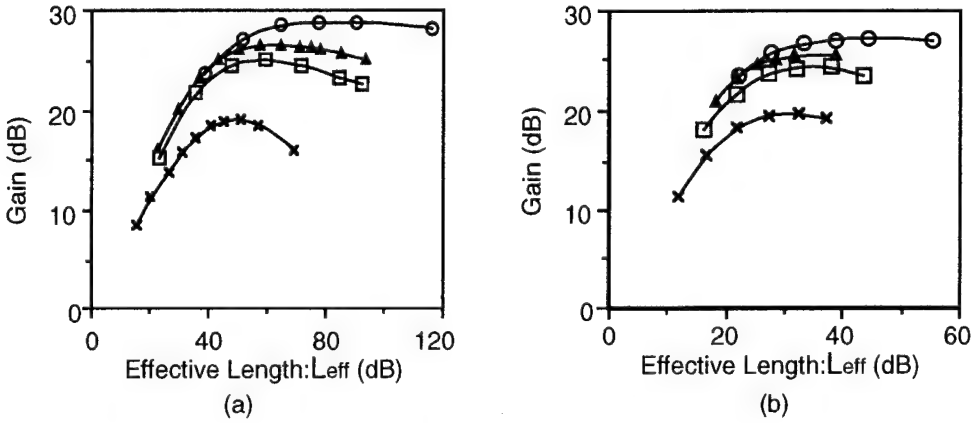

Fig. 1 Gain as a Function of the Effective EDF Length (L_{eff}).
(a) 1.48-μm, (b) 0.98-μm Pumping. ○ :EDF-a, ▲ :EDF-b, □ :EDF-c, × :EDF-d

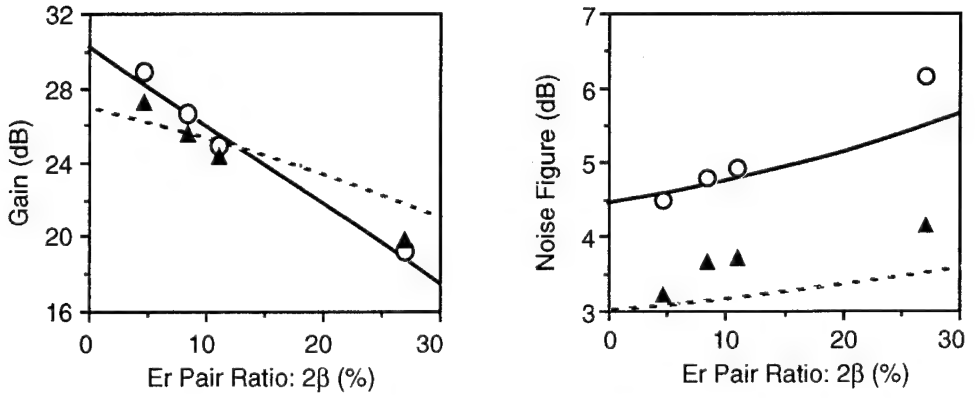

Fig. 4 Gain (a) and Noise Figure (b) as a Function of Erbium Ion Pair Ratio (2β).
○ (λ_p = 1.48 μm), ▲ (λ_p = 0.98 μm): Experiment
—— (λ_p = 1.48 μm), ····· (λ_p = 0.98 μm): Theory

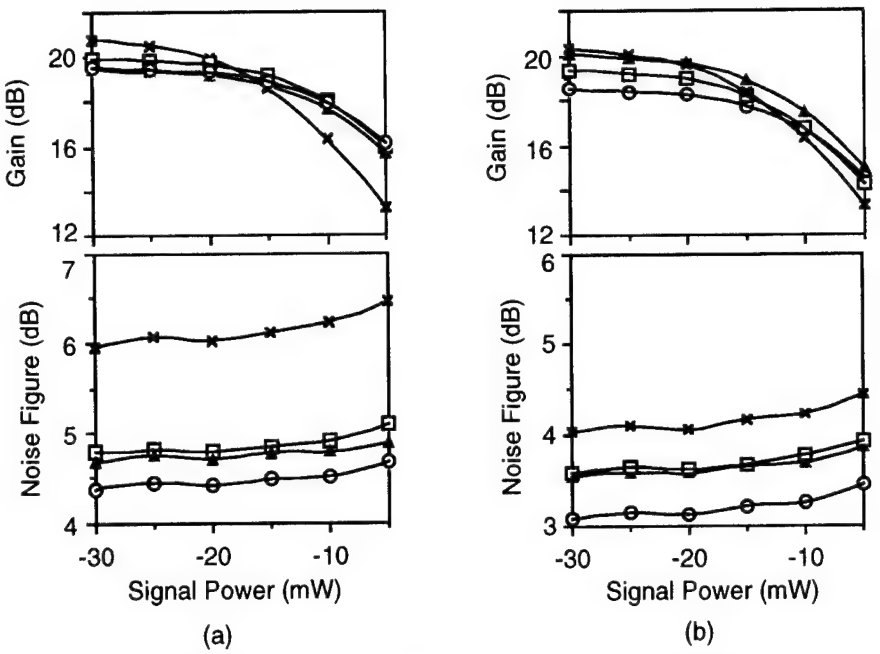

Fig. 2 Launched Signal Power Dependence of Noise Figure and Gain .
(a) 1.48-μm, (b) 0.98-μm Pumping. ○ :EDF-a, ▲ :EDF-b, □ :EDF-c, × :EDF-d

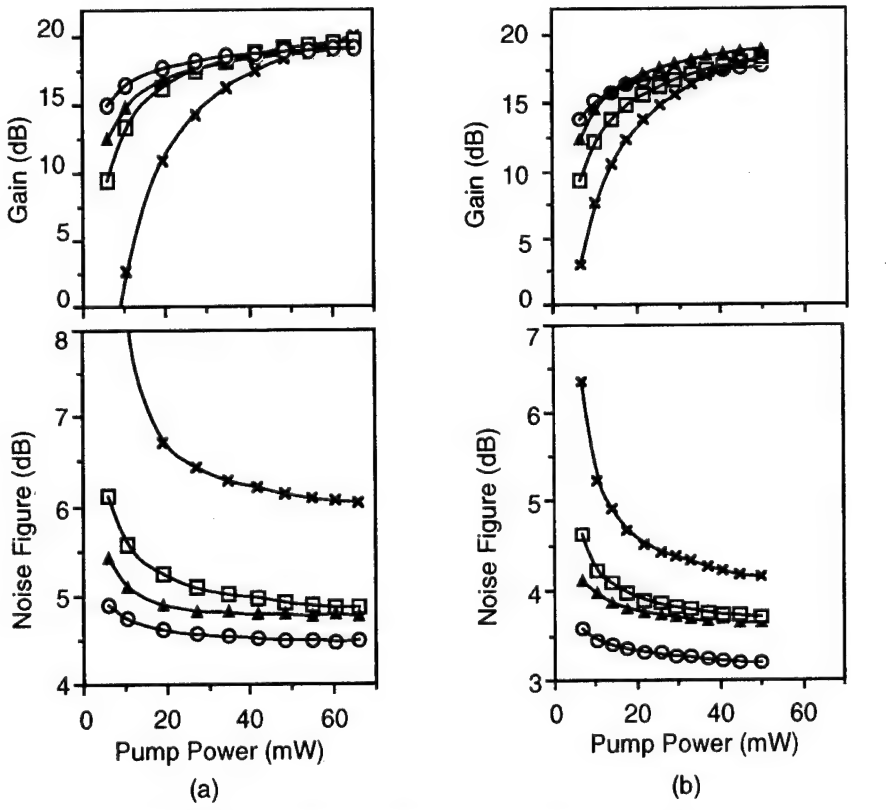

Fig. 3 Launched Pump Power Dependence of Noise Figure and Gain .
(a) 1.48-μm, (b) 0.98-μm Pumping. ○ :EDF-a, ▲ :EDF-b, □ :EDF-c, × :EDF-d

Nanosecond Kinetics of Upconversion Process in EDF and its Effect on EDFA Performance

P. Myslinski, J. Fraser, and J. Chrostowski
Institute for Information Technology, National Research Council
Ottawa, Ontario, Canada K1A 0R6
Tel: (631) 993-2524, Fax: (613) 952-0215

Abstract

The experimental study of the dynamics of erbium ion interactions in EDFA is presented. The lifetime of the excited ion pairs/clusters is determined to be about 50 ns, much shorter than currently assumed in the literature.

Introduction

Heavily doped silica fibres and waveguides are attractive for applications in fibre lasers and in integrated active waveguides [1–4]. For erbium doping, the limiting factors in increasing ion concentration are the effects of cooperative processes. Recently the physical mechanisms involved in cooperative processes have been studied by several techniques including microsecond time resolved spectroscopy [5], steady-state excited-state absorption [6], and power dependent fluorescence intensity [7,8]. Two different mechanisms have been distinguished: (i) homogenous upconversion associated with an interaction averaged over all ionic distances and (ii) inhomogeneous upconversion identified with interaction within ion pairs/clusters formed due to residual local charge compensation. The timescale related to homogenous interaction is millisecond, and for inhomogeneous is sub-microsecond [5]. This rapid cross-relaxation between fraction of ions that reside in clusters has been identified as the main cause of performance degradation of erbium-doped fibres (EDF) [9–15]. To date only the upper limit for the ion pair/cluster lifetime is known; it is estimated to be less than 7 μs [5]. Studies performed on the system level have been focused on experiments and theoretical modelling on pair/cluster induced nonsaturable absorption of EDF [9] and on the dependence of EDF performance on ion concentration, which leads to reduced quantum efficiency of EDF lasers [11,12] and amplifiers [13–15].

This paper presents an experimental study of the interaction dynamics of clustered erbium ions. From spectroscopic data, the relative number of pairs is determined and compared with the value inferred from the measured erbium-doped fibre amplifier (EDFA) performance. The full correspondence of the results obtained by these independent techniques is demonstrated. For the first time, the lifetime of the excited ion pair/cluster is determined experimentally. The measured value of about 50 ns is much shorter than currently assumed in the literature. The observed pair lifetime is concentration independent and varies only slightly (15%) for various fibres due to different co-dopants, which to a small degree modify interionic distances within the cluster.

Theory

The strong dependence of EDFA quantum efficiency, gain, and noise figure on the erbium ion concentration has been fully explained by the inhomogeneous upconversion process [13–15]. The upconversion process is a result of nonradiative energy transfer due to electric multipolar interactions and is illustrated in Fig. 1 [1]. It starts with two erbium ions in the excited state $^4I_{13/2}$. As an effect of the interaction one of the ions is nonradiatively transferred to the ground state ($^4I_{15/2}$) and another to the $^4I_{9/2}$ level, from which it rapidly (5 ns) relaxes to the $^4I_{11/2}$ state and then to the metastable level ($^4I_{13/2}$). In the dipole-dipole approximation the upconversion interaction rate is $W_p = 1/\tau_p = A/R^6$, where R is the

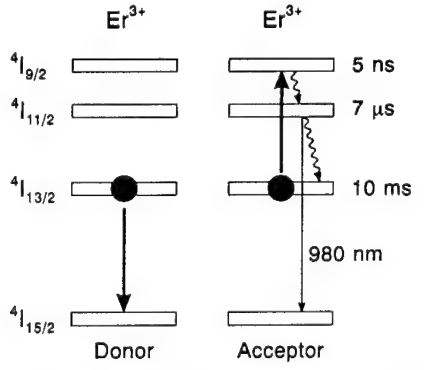

Figure 1. The energy level diagram of erbium ions with upconversion process indicated.

distance between two interacting ions, A is an interaction constant, and τ_p is the lifetime of the excited pair. In inhomogeneous upconversion model the process is limited to closely situated ions residing in clusters. When more than one ion is excited in the cluster, the excitation energy is rapidly transferred from one ion to another, and the rapid upconversion process continues until all but one ion in the cluster occupies the metastable excited state. As a result, fibres exhibit nonsaturable absorption that cannot be saturated even at extremely high light intensities. Experimentally observed relatively small values of nonsaturable absorption indicate that the description based on the smallest erbium ion clusters (i.e., pairs) is adequate for practical EDF.

Under the assumption that the pair lifetime τ_p is much shorter than the $^4I_{11/2}$ state lifetime (τ_{32} = 3 to 7 μs), it can be shown that the decay of 980 nm fluorescence (from the $^4I_{11/2}$ state) after the pulse excitation at 1530 nm is $I(t) = I(0)[\exp(-1/\tau_{32}) - \exp(-t/\tau_p)]$. The total number of photons emitted in the fast decaying 980 nm fluorescence is proportional to the total number of doubly excited pairs and is given by

$$n_{ph} \sim \int I(t)dt \sim \alpha^2 k N_{Tot} \qquad (1)$$

where N_{Tot} is the total number of absorbing ions, α is the probability of finding an ion in the excited state, and k is the relative number of pairs (i.e., the total number of ions residing in pairs is equal to $2kN_{Tot}$).

For theoretical modelling of EDFA performance the erbium ions are divided into two groups, single ions and clustered ions – situated in pairs [10, 15]. It is assumed that fraction $2k$ of the total ion population resides in pairs. Single ions are described by standard two-level rate equations including ASE [1], but excluding any higher order effects such as excited state absorption or homogenous upconversion. Paired ions are described by the two-state model, in which either none or one of the ions in the pair can be in its excited state [10].

Experimental and Discussion

Experiments are performed on aluminum co-doped fibres with concentrations from 8×10^{24} to 62×10^{24} m^{-3} (360 to 2800 molar ppm Er^{3+}). The fibre parameters are summarized in Table I. The experimental configuration for fluorescence decay measurements is shown in Fig. 2. The EDF are pumped at 1530 nm wavelength with 100 W peak power, 20 ns duration pulses emitted from Q-switched erbium-doped fibre laser [16]. Due to the very low radiative efficiency of the $^4I_{11/2}$ state, the 980 nm fluorescence is collected along the fibre. The part of the fluorescence guided in the fibre is filtered by WDM (980/1530 nm) and 980 nm interference filter, and detected by a silicon photon counting detector with 3 ns time gate. The signal is processed by OTDR (TDR30, PPC20, PDG20) systems from Opto-Electronics Inc. To reduce effects of reabsorption and stimulated emission the tested fibres are

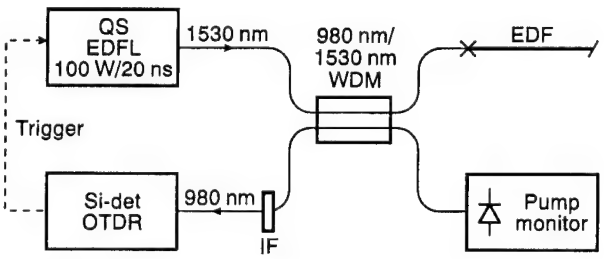

Figure 2. Experimental set up.

Table I. Parameters of the fibres tested.

Fibre number	Erbium ion concentr. N (10^{24}ions/m^3)	Fibre core radius a (μm)	Erbium ion confin. factor, b/a	Numerical aperture NA	Number of paired ions k inferred from: Fluorescence intensity (a.u.)	Number of paired ions k inferred from: EDFA performance (%)
1	8.3	1.5	0.70	0.24	1.1	0.4
2	20	1.8	0.50	0.20	1.3	0.7
3	27	2.1	0.35	0.18	2.2	1.4
4	36	1.8	1.00	0.19	6.8	5.0
5	50	1.3	1.00	0.29	7.4	6.5
6	62	2.4	0.50	0.15	10.6	12.0

short (e.g., 9 cm for fibre no. 6) and their lengths are selected such that small-signal absorptions at 980 nm are the same for all fibres.

Figure 3 presents the typical rise of 980 nm fluorescence intensity after pulse excitation. The rise times are similar for all tested fibres and range from 50 ns to 65 ns. The independence of the rise time of erbium ion concentration proves that the observed fluorescence originates from paired ions. Assuming that the paired ions are located at a distance equal to the erbium ion diameter of $R = 0.22$ nm, the interaction constant is estimated as $A = 2 \times 10^{-51}$ m^6/s. On the microsecond time scale, the fluorescence intensity decays with the time constant τ_{32} ranging from 3 μs to 7 μs and depending on the fibre. From the measured fluorescence decays and eq. (1) the relative number of paired ions k is determined. The total number of absorbing ions N_{Tot} and the probability of finding an ion in the excited state α are calculated from the geometry of the fibres and total number of absorbed pump photons. The relative fluorescence intensities are also corrected for small variations in the acceptance solid angle of the fibres. The value of the branching ratio between multiphonon and radiative deexcitation of the $^4I_{11/2}$ state is assumed to be the same for all fibres. The number of paired ions calculated from fluorescence decays using eq. (1) is presented in Table I.

Pieces of each tested fibre 10–20 times longer are used to build compact, 980 nm diode pumped, EDFAs for fibre performance measurements on the system level. Figure 4 shows typical experimental EDFA characteristics with theoretical predictions including ($k > 0$) and excluding ($k = 0$) pair effects. From fitting theoretical EDFA characteristics, the percentage of paired ions for each fibre is

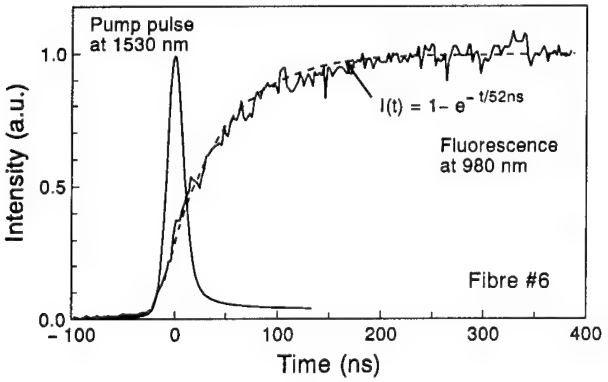

Figure 3. Intensity of 980 nm fluorescence induced by 20 ns/100 W pump pulse at 1530 nm.

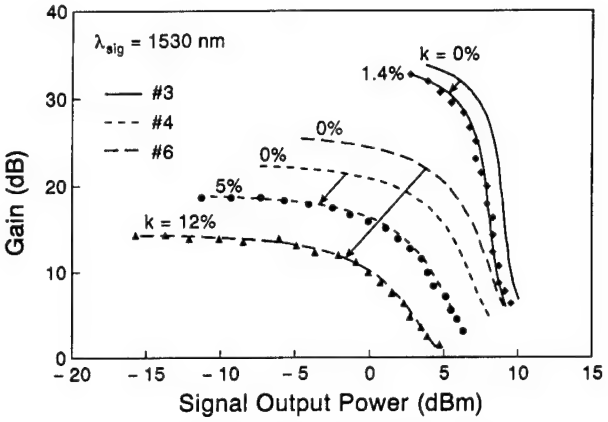

Figure 4. Experimental gain dependence (points) on the signal output power for EDFAs built with fibres #3, #4, and #6. Solid lines show theoretical predictions including ($k > 0$) and excluding ($k = 0$) pair effects.

determined and shown in Table I [15]. In addition, the transmission as a function of signal intensity presented in Fig. 5 is measured for fibre #6. The small-signal transmission of −16 dB is bleached to nonsaturable level of −2 dB. The typical s-shaped characteristics agree with the theoretical predictions for $k = 12\%$, the same relative number of pairs as obtained from modelling of the EDFA characteristics.

Figure 6 presents the concentration dependence of the relative number of pairs determined from the 980 nm fluorescence (eq. 1) and from the EDFA performance characteristics. The comparison shows a full correspondence of the results obtained by the two independent methods.

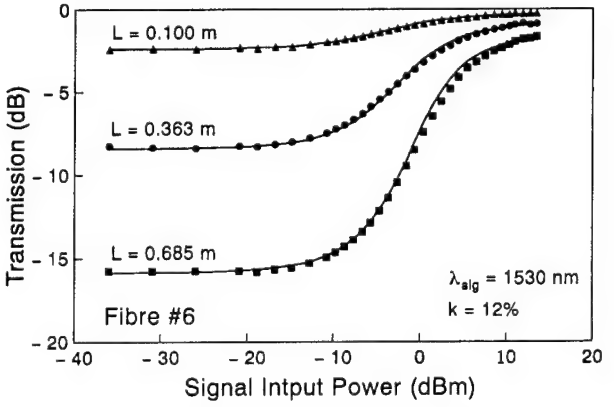

Figure 5. Saturated transmission characteristics for fibre #6 with high erbium ion concentration. The experimental points are measured for three different fibre lengths L. The solid lines show theoretical predictions based on the model for the relative pair number $k = 12\%$.

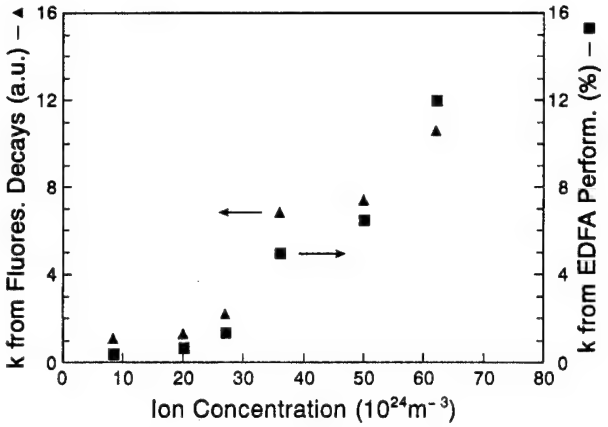

Figure 6. Experimental dependence of the relative number of pairs k inferred from EDFA performance (squares) and from 980 nm fluorescence intensity (triangles) for different fibres (Table I).

Summary

In conclusion, by analyzing the 980 nm fluorescence of EDF pumped by 1530 nm pulses, we have directly examined the dynamics of the upconversion process in erbium clusters. For the first time the erbium pair lifetime of about 50 ns is measured. Presented spectroscopic measurements and the experimental and theoretical data on the EDFA performance show that the inhomogeneous upconversion process dominates over the homogenous one and is the major mechanism degrading the performance of EDFAs. Experimental results show that, at high ion concentrations, many of the ions are paired. For presently available heavily doped fibres ($N > 50 \times 10^{24}$ m^{-3}) this indicates that under typical operating conditions of EDFA about 10% of the ions remain in the ground state. To develop highly doped waveguide devices, further research is required on improving erbium solubility in silica. Measurements of nanosecond time resolved 980 nm fluorescence presented in this work offer a convenient, OTDR based, diagnostic technique to characterize the level of erbium ion clustering.

Acknowledgments

The authors wish to thank Dr. H. Postolek from BNR Ottawa for kindly providing very high power 980 nm pump laser diodes and A. Dufour and R. Misner for expert electronic assistance.

References

[1] E. Desurvire, *Erbium-Doped Fiber Amplifiers, Principles and Applications*, Wiley, New York, 1993.

[2] G. Nykolak, M. Haner, P.C. Becker, J. Shmulovich, and Y.H. Wong, *IEEE Photon. Tech. Lett*, vol. 5, no. 10, p. 1185, 1993.

[3] M. Oguma, T. Kitagawa, K. Hattori, and M. Horiguci, *IEEE Photon. Technol. Lett.*, vol. 6, no. 5, p. 586, 1994.

[4] G. Nykolak, P.C. Becker, J. Shmulovich, Y.H. Wong, D.J. DiGiovanni, and A.J. Bruce, *IEEE Photon. Tech. Lett.*, vol. 5, no. 9, p. 1014, 1993.

[5] C.C. Ye, P.R. Morkel, E.R. Taylor, and D.N. Payne, *Proceedings of 19th European Conference on Optical Communication*, Sep. 12–16, TuC3.4, p. 73, 1993.

[6] S. Quimby, W.J. Miniscalco, and B. Thompson, *J. Appl. Phys.* vol. 76, no. 8, p. 4472, 1994.

[7] P. Blixt, J. Nilsson, B. Jaskorzynska, and J. Babonas, *Tech. Digest Series*, vol. 17, "Optical Amplifers and their applications," WE2, p. 63, 1992.

[8] P. Blixt, J. Nillsson, T. Carlnas, and B. Jaskorzynska, *IEEE Trans. Photon. Technol. Lett.*, vol. 3, no. 11, p. 996, 1991.

[9] E. Delevaque, T. Georges, M. Monerie, P. Lamouler, and J.-F. Bayon, *IEEE Photonics Technol. Lett.*, vol. 5, no. 1, p. 73, 1993.

[10] J. Nilsson, B. Jaskorzynska, and P. Blixt, *Optical Amplifiers and Their Applications Technical Digest.*, MD19-1, p. 222, 1993.

[11] J.L. Wagener, P.F. Wysocki, M.J.F. Digonnet, and H.J. Shaw, *Opt. Lett.* vol. 18, no. 23, p. 2014, 1993.

[12] P.F. Wysocki, J.L. Wagener, M.J.F. Digonnet, and H.J. Shaw, , SPIE vol.1789, *Fiber Laser Sources and Amplifiers IV,* p.66, 1992.

[13] H. Masuda, A. Takada, and K. Aida, *J. Lightwave Technol.*, vol. 10, no. 12, p. 1789, 1992.

[14] J.L. Wagner, P.F. Wysocki, M.J. Digonnet, and H.J. Shaw, *Opt. Lett.*, vol. 19, no. 5, p. 347, 1994.

[15] P. Myslinski, D. Nguyen, and J. Chrostowski, *WP3, Conference on Optical Fibre Amplifers*, San Diego, CA, Feb.–Mar., 1995.

[16] P. Myslinski, J.Chrostowski, J.A. Koningstein, and J.R. Simpson, *IEEE J. Quant. Electron.*, vol. 28, no. 1, p. 371, 1992.

Reliability of fluoride fibers for use in fiber amplifiers

Kazuo FUJIURA, Koichi HOSHINO, Terutoshi KANAMORI,
Yoshiki NISHIDA, Yasutake OHISHI and Shoichi SUDO
NTT Opto-electronics Laboratories
Tokai, Ibaraki, 319-11, Japan
Telephone: +81-292-87-7701, Facsimile: +81-292-87-7706
e-mail: fujiura@nttiba.ntt.jp

1. Introduction

The fiber amplifier is now established as a key component for practical optical transmission systems because of its excellent amplification characteristics.

With regard to fiber host materials, ZrF_4-based fluoride glasses now provide an important alternative to silica-based glasses for rare-earth doped fiber hosts. In particular, the Pr-doped fluoride fiber amplifier (PDFA) has emerged as the unique candidate for a practical amplifier in the 1.3-μm telecommunication window[1-4], and Er-doped fluoride fiber amplifier exhibits flat gain characteristics over a very wide wavelength range and is suitable for WDM applications[5, 6].

On the other hand, to date, little has yet been reported on reliability of fluoride fiber host, which is another key issue related to the practical application of fiber amplifiers, although many papers have been reported on optical performance.

Therefore, we summarize recent studies on the reliability and predicted lifetime of fluoride fiber for use in optical amplifiers.

2. Reliability of fluoride fiber for optical amplifiers

In order to demonstrate long-term reliability, optical devices must pass comprehensive reliability tests such as the Bellcore requirements[7]. In these test programs, exposure to damp heat (high temperature and high humidity) may be the most severe test for fluoride fiber. This is because fractures in fluoride fibers are mainly caused by crystals on their surface which may be formed by a reaction with environmental moisture[8-12]. In addition, the fibers are usually coiled around fiber bobbins in an amplifier module, and this configuration induces a bending strain on their outer surface. The stress on the fiber surface may accelerate crack growth and result in rapid failure. Therefore, the first step must be to clarify the acceptable environmental conditions under induced stress.

3. Fiber parameters related to reliability

3.1 Fiber strength

The maximum theoretical strength of fluoride fiber has been calculated to be 3.3 GPa or about 6% strain[13], which indicates the breaking stress of a flawless sample. As fluoride fibers may be degraded by surface crystallization, several types of preform surface treatment have been developed, such as polishing, chemical etching[10, 14], and surface fluorination using fluorine-containing gas[9, 15], and fluoride fiber with a strength of over 500 MPa has been fabricated[16, 17]. Figure 1 shows the Weibull distribution of tensile strength for recently developed fluoride fiber. The fiber diameter is 120 μm. The protective coating is UV-curable acrylate resin with a diameter of 260 μm. The mean strength of the fluoride fiber which we can fabricate is about 550 MPa (highest strength: 680 MPa) and Weibull distribution parameter m is 10 to 35[17]. These mechanical properties will be improved by improving the surface treatment and fiber drawing techniques.

3.2 Durability

In general, fluoride glasses are known to be susceptible to damage by moisture. The corrosion rate of ZBLAN is about five orders of magnitude higher than that of Pyrex[18]. However, this does not mean that fluoride glasses are hygroscopic. Figure 2 shows the strength degradation caused by zero-stress aging. This degradation is caused by H_2O, but large decreases in strength have not been observed at 80°C and 50%RH. It has been reported that no strength degradation could be observed over 2 years at 30°C and 40%RH[13].

Coating and overcladding have been investigated as way of protecting the surface against environmental moisture. Polymer coating using Teflon-FEP[19] and UV-curable acrylate[15-17], hermetic coating using carbon, oxide, nitride and fluoride[20, 21], and overcladding using phosphate[22-24] and chalcogenide glasses[25] have been applied to fibers and bulk glasses. In terms of fiber productivity and strength, only UV-curable acrylate is practically available at present. For practical applications, a hermetic coating or a polymer coating with low permeability is desirable, although this might be difficult to apply, but progress is now being made towards achieving this[13].

4. Lifetime predictions

4.1 General theory of lifetime prediction

It is important to be able to predict the lifetime of fluoride fibers subjected to a uniform long-term stress. Several theories are being discussed, and the power-law theory is so far the furthest developed[26, 27]. In this theory, crack growth velocity is assumed to be

$$da/dt = AK^n(t) \quad (1)$$

where K is a stress intensity factor, A is a material proportionality parameter, and n is a stress corrosion factor. Strength is distributed along the length of the practical fibers. This can be expressed by a Weibull survival distribution.

$$P(S, L) = exp\ [- (S/S_0)^m (L/L_0)] \quad (2)$$

Here, $P(S, L)$ is the cumulative survival probability of fiber length L up to inert strength S, and S_0 is the strength corresponding to a survival probability of e^{-1}, measured at a gauge length L_0.

The above equations are solved for a fiber crack in an active environment to derive a lifetime equation[28]. The parameters required for predicting the lifetime can be readily obtained by dynamic or static fatigue measurements.

4.1 Dynamic fatigue testing

For dynamic fatigue, the lifetime t_f is[28]

$$t_f(L, F, \sigma_a) = [\sigma_f^{n+1}(1)/(n+1)]\ [(L_0/L)F]^{(n+1)/m}\ \sigma_a^{-n} \quad (3)$$

Here, σ_a is applied stress, $\sigma_f(1)$ is the intercept of a failure stress vs. applied stress rate plot, and F is the allowable failure probability. In a dynamic fatigue test, about 20 fiber samples for each condition were submitted to tensile strength tests at a gauge length of 350 mm. The parameters were measured in a temperature range of 25 to 80°C and at a relative humidity of 0 to 70%.

Zero-stress aging is not taken into account in Eq.(3). The lifetime determined by zero-stress aging was estimated by fitting the results in Fig. 2 to an equation as follows[29],

$$\sigma_f = \sigma_{f0}/(1 + t/\tau)^p \quad (4)$$

Here, σ_{f0} is the measured strength at time $t = 0$. The lifetime can be calculated as the time at which σ_f is equal to the applied stress.

Figure 3 shows the predicted lifetime for fluoride fibers with various initial strengths at 80°C. In the prediction, it is assumed that the fibers are subjected to a stress of 36 MPa, which corresponds to a 10 cm-diameter fiber bobbin, and $F = 10^{-6}$. These results suggest that sufficient lifetime over 25 years can be guaranteed for fluoride fibers with initial strengths of 350 and 500 MPa in dry conditions and 80%RH at 80°C, respectively.

4.2 Static fatigue testing

In order to confirm the above prediction, a static fatigue test was carried out for lifetime prediction. An equation has been prepared which combines zero-stress aging and static fatigue[30].

$$d(\sigma/\sigma_i)/dt = x/\tau(\sigma/\sigma_i)^{(x-1)/x} - 1/[B\sigma_i^{n-2}(n-2)]\ \sigma_a{}^n\ (\sigma/\sigma_i)^{3-n} \quad (5)$$

Here, σ_i is the initial strength, B is a constant, and $x=(n+1)/(n-2)p$. The differential equation was solved numerically. The results measured at 80°C in a relative humidity of 50% are shown in Fig. 4. These results are comparable to the prediction by the dynamic fatigue test.

Therefore, it is confirmed that these fluoride fibers for use in optical fiber amplifiers offer long-term reliability under practical conditions.

5. Conclusion

We have summarized recent studies on the reliability of fluoride fibers and lifetime prediction under practical conditions. A fluoride fiber with a high strength of over 500 MPa can be fabricated and lifetime predictions for this fiber have shown that it offers long-term reliability for use in a practical amplifier. We hope that highly reliable fluoride fibers will accelerate the use of fluoride fiber hosts in fiber amplifiers.

Acknowledgments

The authors wish to thank H. Hiratsuka for his encouragement, and also thank all the members of our laboratory for their contributions.

References

1) Y. Ohishi, T. Kanamori, T. Kitagawa, S. Takahashi, E. Snitzer and G. H. Sigel, Jr., in Proc. OFC'91, Washington DC, paper PD2, 1991.
2) Y. Durtste, M. Monerie, J. Y. Allain and H. Poignant, Electron. Lett. 27(1991) 626.
3) S. F. Carter, D. Szebesta, S. T. Davey, R. Wyatt, M. C. Brierly and P. W. France, Electron. Lett. 27(1991) 628.
4) M. Yamada and M. Shimizu, in Proc. OAA'94, Breckenridge, paper WC1, 1994.
5) J. M. Marcerou, S. Artigaud, J. Hervo and F. Fevrier, in Tech. Dig. ECOC'92, Berlin, paperMo A2.3.
6) D. Bayart, B. Clesca, L. Hammon and J. L. Beylat, IEEE Photon. Technol. Lett. 6(1994) 613.
7) Bellcore, TA-NWT-001209 and TA-NWT-001221.
8) G. Orcel and D. Biswas, J. Am. Ceram. Soc. 74(1991)1373.
9) P. H. Klein, P. C. Pureza, W. I. Roberts and I. D. Aggarwal, Mater. Sci, Forum 32-33(1988)571.
10) H. W. Scheider, A. Schoberth, A. Staudt and C. Gerndt, Electron. Lett. 22(1986)949.
11) J. Colaizzi and M. J. Matthewson, J. Lightwave Technol. 12(1994)1317.
12) S. Sakaguchi, Y. Terunuma, Y. Ohishi and T. Kanamori, J. Mater. Sci. Lett. 6(1987)1063.
13) S. F. Carter, in Fluoride Glass Optical Fibers, P. W. France, ed London, U. K. :Blachie, 1990, PP.219.
14) S. Sakaguchi, Y. Hibino, Y. Ohishi, and S. Takahashi, J. Mater. Sci. Lett. 6(1987)1440.
15) H. W. Schneider, Mater. Sci. Forum 32-33(1988)561.
16) H. Poignant, J. Le Mellot, A. Leve, P. Le Cabec and D. Riviere, J. Non-Cryst. Solids,161(1993)192.
17) K. Fujiura, Y. Nishida, T. Kanamori, Y. Terunuma, K. Nakagawa, K. Hoshino, Y. Ohishi and S. Sudo, to be submitted.
18) C. T. Moynihan, S. R. Lochr, Mater. Sci. Forum 32-33(1988)243.
19) S. Mitachi, S. Shibata T. Manabe, Electron. Lett. 17(1981)128.
20) P. C. Schultz, L. J. B. Vacha, C. T. Moynihan, B. B. Harbison, K. Cadien and R. Mossadegh, Mater. Sci. Forum 19-20(1987)343.

21) J. J. McNally, G. A. Al-Jumaily, J. R. Maneil and B. Bendow, Appl. Opt. 25(1986)1973.
22) Y. Ohishi, K. Fujiura and S. Takahashi, Mater. Res. Soc. Symp. Proc. 172(1990)77.
23) G. Orcel and D. Biswas, J. Am. Ceram. Soc. 74(1991)1373.
24) L. J. B. Vacha, P. C. Schultz, C. T. Moynihan and S. N. Crichton, Mater. Sci. Forum 19-20(1987)419.
25) Y. Mimura, H. Tokiwa, T. Nakai and O. Shinbori, ibid. 387.
26) A. G. Evans and S. M. Wiederhorn, Int. J. Frac. 10(1974)379.
27) R. J. Charles, J. Appl. Phys. 29(1958)1657.
28) F. P. Kapron and H. H. Yuce, Opt. Eng. 30(1991)700.
29) P. W. France, W. J. Duncan, D. J. Smith and K. J. Beales, J. Mater. Sci. 18(1983)785.
30) P. Haslov, K. B. Jensen and N. H. Skovgaad, J. Am. Ceram. Soc. 77(1994)1531.

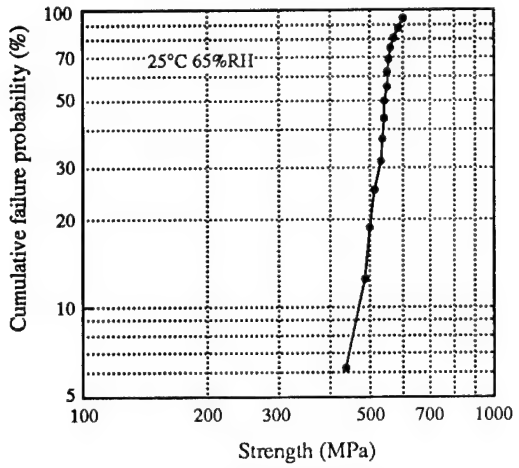

Fig. 1 Weibull distribution plot of the fluoride fiber.

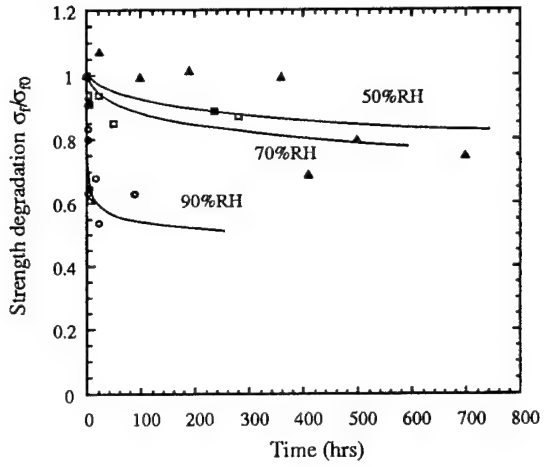

Fig. 2 Strength degradation at 80°C.

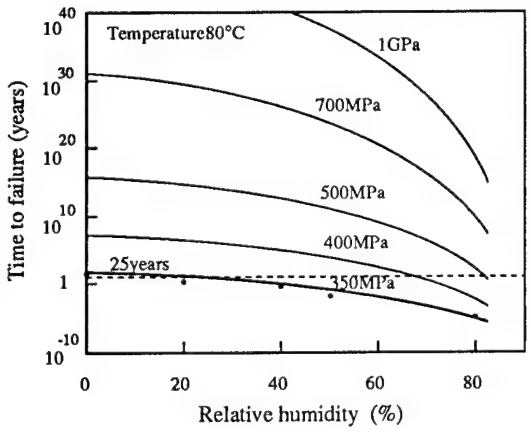

Fig.3 Predicted lifetime of fluoride fibers with various initial strengths at 80°C by dynamic fatigue test; bobbin diameter: 10 cm.

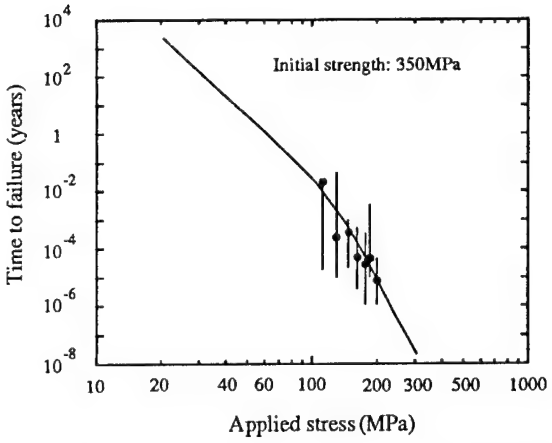

Fig.4 Predicted lifetime of fluoride fibers at 80°C and 50%RH by static fatigue test.

Semiconductor Devices and Functional Circuits

FA 9:00-10:30
Theatersaal

Francois Brillouet, *Presider*
Alcatel Alsthom Recherche, France

New developments in OEIC's

U. Koren, AT&T Bell Laboratories, Holmdel N.J. 07733, U.S.A.
Tel 908 949 3056, Fax 908 949 8988

Semiconductor optical amplifiers can be used as elements in opto-electronic integrated circuits (OEIC's) where active and passive optical components are integrated on a single semiconductor chip. There are several different roles for optical amplifiers in OEIC's. Specifically, integrated optical amplifiers have been used as power boosters, to compensate for optical coupling and propagation losses in the OEIC, but also in utterly different roles as switching elements in complex optical switches, or as non-linear elements which can provide a convenient medium for frequency conversion.

To demonstrate the use of an amplifier as a power booster, consider a WDM transmitter where an array of lasers with different wavelengths are combined using a passive waveguide combiner and then feeding the different inputs into a single optical amplifier [1-3]. In this application the amplifier is operating at high optical saturation and therefore can cause errors with WDM digital signals due to inter-symbol interference (ISI). One can however use the array as a wavelength selectable source, operating only one laser at a time, in which case error free operation and low chirp can be obtained [4]. In a similar configuration, ISI can be eliminated by injecting a selectable CW input from the array into the amplifier, which is then followed by an electroabsorption modulator at the output of the amplifier. Such devices are very desirable for high bit rate - long distance WDM transmission systems. Simultaneous direct modulation of multi-wavelength laser arrays with optical amplifiers is also useful for fiber to the loop (FTTL) applications, which may employ WDM architectures [5,6]. Another development that may be significant for the introduction of semiconductor optical amplifiers to FTTL applications is the use of waveguide tapers [7] to improve fiber coupling efficiency, and to reduce coupling tolerances so that packaging of these devices will eventually become an easier and less costly task.

REFERENCES

1. U. Koren et al, Appl. Phys. Lett. 54, 2056, (1989).
2. C.E. Zah et al, Electronics Lett. 28, 2361, (1992).
3. M.G. Young et al, Photonics Technology Lett. 5, 908, (1993).
4. G. Raybon et al, Electronics Lett. 29, 1295, (1993).
5. N.J. Frigo et al, Photonics Technology Lett. 6, 1365, (1994).
6. M. Zirngibl et al, Electronics Lett. 30, 1484, (1994).
7. P. Doussiere et al, Photonic Technology Lett. 170, (1994).

Dynamic effects in integrated 4×4 InGaAsP/InP semiconductor optical gate amplifier switch matrices

Lars Gillner*, Eilert Berglind, Claus Popp Larsen*†, Erland Almström††****

*Ericsson Components AB, S-164 81 Stockholm, Sweden, **Royal Institute of Technology, S-164 40 Kista, Sweden

†L. M. Ericsson A/S, Denmark and Techn. Univ. of Denmark, ††Ellemtel Utvecklings-AB, S-125 25 Älvsjö, Sweden

Abstract: **Integrated 4×4 InP amplifier gate switch arrays are analysed with respect to dynamic gain saturation and residual reflections within the chip. Comparison with measurements is made.**

Introduction

Optical switches with low losses are anticipated to be key components in future transparent optical networks[1]. Integrated 4×4 InGaAsP/InP amplifier gate switch matrices with low losses or even net gain are promising candidates for this task[2]. These devices accomplish ~0 dB insertion loss by having semiconductor optical amplifiers (SOA's) integrated with the passive waveguides. The disadvantages as compared to purely passive optical switches are that the amplifier sections apart from amplifying an optical signal also add optical noise — amplified spontaneous emission (ASE) — and that the active semiconductor material has dynamic processes with lifetimes in the order of nanoseconds. The latter property implies that for a digitally intensity modulated bit stream incident on the device, a bit can affect the gain of the following bits — intersymbol interference.

The purpose of this paper is to study these phenomena with a computer model for InP switch matrices. ASE mainly restricts the performance at low optical input powers to the switch and degradation of the extinction ratio and intersymbol interference restrict the performance at high input powers. Reflections within the switch matrix and at the chip boundaries may degrade the performance of the device.

In a direct detection receiver, there is an electrical low-pass filter to reduce the electrical noise. In earlier time domain analyses of gain saturation in SOA's for digital communication systems including the electrical filtering[3][4], the optical noise has been neglected and only receiver noise has been included[3], or the optically induced noise has been given one fixed value for each bit slot[4], and reflections from the SOA facets have not been included.

Numerical model

The block diagram of the simulation model is illustrated in Fig. (1a). In Fig. (1b), the detailed model of the InP switch matrix shows where the internal reflections take place. The losses and lengths for the various L's and ℓ's as well as other relevant data are given in Table 1. The multiple reflections and filtering of the signal and ASE within the switch are accounted for with the model outlined in Ref. [5], which is based on transfer matrices, treating the optical signal and ASE as amplitudes rather than intensities. The filter in front of the receiver is a three-stage double half-wave interference filter with 1 nm bandwidth.

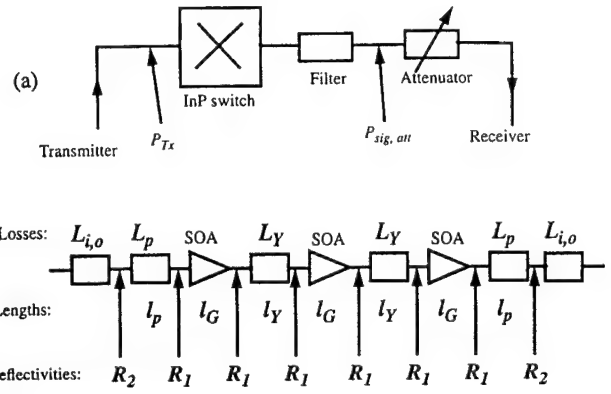

Figure 1: (a) Block diagram representation of the components involved in the BER calculation. P_{Tx} and $P_{\mathrm{sig,att}}$ are the average transmitted power in front of the switch and in front of the attenuator.
(b) Detailed model of InP switch matrix. R_1 and R_2 are the intensity reflection coefficients between active and passive waveguides and at the chip boundaries, respectively. The losses and lengths for the various L's and ℓ's are given in Table 1.

For each SOA, the rate equation for the electron density, N, is given by[6]

$$\frac{dN}{dt} = \frac{I}{qV} - R(N) - S_{\mathrm{sig}}, \tag{1}$$

where I is the pump current, q is the electron charge, V is the volume of the active region, $R(N)$ is the electron spontaneous recombination rate, and S_{sig} is the recombination due to the optical input signal. The saturation caused by ASE was neglected, as it only incurred a small correction. This is a one-section model with the electron

$B_R = 2.5$ Gb/s	Bit rate
$r = 10$ dB	Transmitter exinction ratio
BER $= 10^{-9}$	Bit error rate
$\ell_G = 500$ μm	SOA active region length
$L_{i,o} = -5$ dB	switch input or output coupling loss
$L_p = -1.5$ dB	switch input or output waveguide loss
$\ell_p = 500$ μm	switch input or output waveguide length
$L_Y = -10$ dB	switch Y branch splitting loss
$\ell_Y = 2$ mm	switch Y branch length
$R_1 = 10^{-3}$	active-passive waveguide reflection coefficient
$R_2 = 10^{-2}$	chip facet reflection coefficient
$dn/dN = -1.4 \cdot 10^{-26}$ m^3	Refractive index shift coefficient

Table 1: Estimated parameter values (default values) for the numerical simulations.

density averaged over the length of the SOA. This means that the transit time over the SOA (and the switch matrix) is neglected. The single-pass phase, φ_s, through an SOA is calculated as

$$\varphi_s = -k\ell_G = -\frac{2\pi\ell_G}{\lambda_{in}}\left[n + \frac{dn}{dN}(N - N_{th})\right]. \quad (2)$$

Here, k is the wave number, ℓ_G is the length of the active region, λ_{in} is the wavelength of the input signal, n is the effective real refractive index, and dn/dN is the first coefficient in the Taylor expansion of n. N_{th} is the electron density at the original lasing threshold, which was arbitrarily chosen as the reference point for the refractive index. The remaining equations for the SOA's can be found in Ref. [6]

The transmitter optical signal power incident on the InP switch matrix is assumed to be purely intensity modulated with transmitter extinction ratio $r = 10$ dB. The bit error rate (BER) is calculated with a 32 bit ideal square-wave sequence as input to the InP switch matrix. For each switch operation point, the decision threshold level, D, is set to minimise the BER, which simulates measurement with a BER analyser.

$$\mathrm{BER} = \min_D \left(\frac{1}{N_b\sqrt{2\pi}} \sum_{i=1}^{N_b} \frac{\exp\left(-{Q_i}^2/2\right)}{Q_i}\right), \quad (3)$$

$$Q_i = \begin{cases} \dfrac{\sqrt{P_{\mathrm{s,mark},i}} - D}{\sqrt{P_{\mathrm{n,mark},i}}} & \text{for a "mark",} \\ \dfrac{D - \sqrt{P_{\mathrm{s,space},i}}}{\sqrt{P_{\mathrm{n,space},i}}} & \text{for a "space",} \end{cases} \quad (4)$$

where $N_b = 32$ (number of bits). $P_{\mathrm{s},i}$ and $P_{\mathrm{n},i}$ — for a "mark" or a "space" — are the electrical total signal (signal and ASE) and noise powers per unit load resistance after a unit quantum efficiency detector. They can be written as[7]

$$P_{\mathrm{s},i} = \left\{\frac{q}{h\nu_0 L_{\mathrm{att}}}\left(P_{\mathrm{sig,att},i} + \int_{B_o} R_{\mathrm{ASE,att},i}(\nu)\, d\nu\right)\right\}^2, \quad (5)$$

$$P_{\mathrm{n},i} = q^2 2B_e\left\{\left(\frac{1}{h\nu_0 L_{\mathrm{att}}}\right)^2\left[2P_{\mathrm{sig,att},i}\frac{R_{\mathrm{ASE,att},i}(\nu_0)}{m_t} + \int_{B_o}\left[R_{\mathrm{ASE,att},i}(\nu)\right]^2\frac{d\nu}{m_t}\right] + \frac{1}{h\nu_0 L_{\mathrm{att}}}\left[P_{\mathrm{sig,att},i} + \int_{B_o} R_{\mathrm{ASE,att},i}(\nu)\, d\nu\right]\right\} + {j_c}^2 B_e, \quad (6)$$

where h is Planck's constant, ν_0 is the optical carrier frequency, $B_e = 0.7 \cdot B_R$ is the noise-equivalent bandwidth of the electrical filter (B_R is the bit rate), $m_t = 2$ is the number of polarisations and $j_c = 10$ pA/$\sqrt{\mathrm{Hz}}$ is the equivalent receiver noise. B_o is the optical bandwidth of the ASE and $B_e \ll B_o$ has been assumed. $P_{\mathrm{sig,att},i}$ and $R_{\mathrm{ASE,att},i}$ are the optical signal power and the optical spectral density of the ASE (in both polarisations), respectively, at the position between the filter and the variable attenuator in Fig. (1a). The five noise terms in Eq. (6) are usually referred to as signal-ASE beat noise, ASE-ASE beat noise, signal shot noise, ASE shot noise, and receiver noise, respectively.

To obtain P_{s} and P_{n} as functions of time, we replace P_{sig} by $P_{\mathrm{sig}}(t)$. Furthermore, $R_{\mathrm{ASE}}(\nu)$ is replaced by $R_{\mathrm{ASE}}(\nu;t) = \rho_{\mathrm{ASE},\nu_0}(t)H_{\mathrm{ASE}}(\nu)$, where $\rho_{\mathrm{ASE},\nu_0}(t)$ is the instantaneous peak of the ASE spectral density (at ν_0) and all spectral information is in $H_{\mathrm{ASE}}(\nu)$, which is normalised according to $\max[H_{\mathrm{ASE}}(\nu)] = 1$. Its spectral shape is the *optically* filtered or unfiltered gain curve of the optical amplifier or amplifiers, meaning that homogeneous gain saturation is assumed (the intra-band processes are assumed to be much faster than the length of a bit slot).

In general, the output $y(t)$ of a linear system with impulse response $h(t)$ subject to an input $x(t)$ is given by the convolution

$$y(t) = \int_{-\infty}^{+\infty} x(\tau)h(t-\tau)\, d\tau. \quad (7)$$

Here, $h(t)$ is the impulse response of the receiver *electrical* filter and $x(t)$ is the time-dependent version of P_{s}, which in the numerical analysis will be treated as a sampled variable. The time response of each SOA is calculated from Eq. (1) with a time step of $T/32$, where T is the bit slot. The sampling instant is chosen as the one with the largest eye opening over the bit slot. The average received signal power at the detector is obtained from all the sampled values of the electrically filtered $P_{\mathrm{s}}(t)$ in the bit sequence.

The BER calculation after the electrical filter is based on the assumptions that the optically induced noise has a

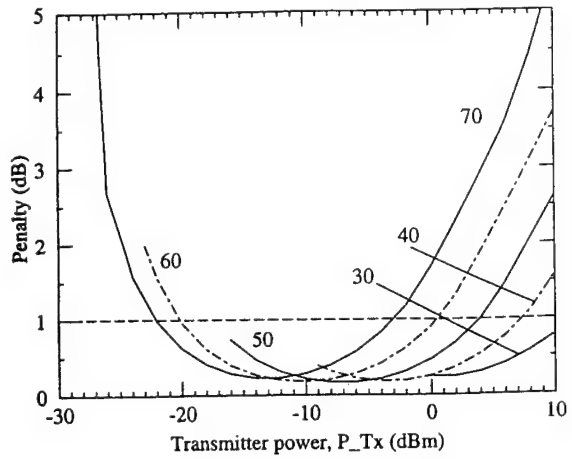

Figure 2: Calculated power penalty at BER = 10^{-9} as function of average transmitter power with pump current I to each SOA in mA as parameter. $R_1 = R_2 = 0$. The dashed line shows the dynamic range.

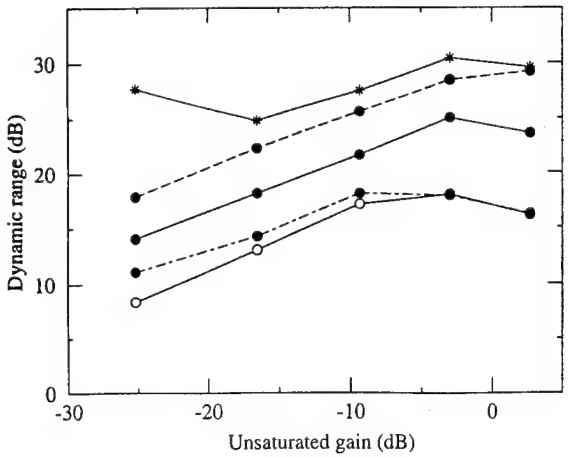

Figure 3: Calculated dynamic range of transmitter power (power penalty $\leq$ 1 dB at BER = 10^{-9}) as function of unsaturated switch gain. $R_1 = R_2 = 0$.
Dashed line: $B_R = 622$ Mb/s.
Solid lines: $B_R = 2.5$ Gb/s.
Dash-dotted line: $B_R = 10$ Gb/s.
White circles: $r = 5$ dB.
Black circles: $r = 10$ dB.
Stars: $r = 15$ dB.

δ-function correlation relative to the modulation time constants and that the impulse response of the electrical filter is rectangular. The two time-dependent terms in Eq. (5), $P_{\text{sig}}(t)$ and $\rho_{\text{ASE},\nu_0}(t)$, are electrically filtered individually numerically in the time domain and added subsequently to give the two contributions, $P'_{\text{sig}}(t)$ and $\rho'_{\text{ASE},\nu_0}(t)$ to the filtered version of Eq. (5).

Eq. (6) can then be expressed in different combinations of these two terms. The signal shot noise and ASE shot noise will be available directly. The ASE-ASE beat noise is proportional to

$$[\rho'_{\text{ASE},\nu_0}(t)]^2 \int_{B_o} [H_{\text{ASE}}(\nu)]^2 \, \frac{d\nu}{m_t}.$$

The signal-ASE beat noise is proportional to $P'_{\text{sig}}(t) \cdot \rho'_{\text{ASE},\nu_0}(t)$. Thus, all necessary noise variances are calculated from Eq. (7) by filtering $P_{\text{sig}}(t)$ and $\rho_{\text{ASE},\nu_0}(t)$ one at a time. The receiver noise is assumed to be time-independent.

Another question is how to numerically calculate the convolution (7) efficiently. The most straightforward method is either to perform the convolution directly or to Fourier transform the signal, multiply by the filter transfer function, and inverse Fourier transform to the time domain. A more time-saving method is to use the z transform. As the optical signal in a numerical treatment is sampled, it can be directly multiplied with the filter's digital transfer function [the z transform of the sampled version of $h(t)$]. Here, we use a sampled fourth order Bessel filter.

Results

Fig. (2) shows the calculated power penalty as function of average transmitter power P_{Tx} for a reflection-free switch matrix. The power penalty is defined as the difference in received power at BER = 10^{-9} between a particular switch operation point and the sensitivity of transmitter and receiver connected back to back. The penalty for low input powers is caused by excessive ASE accumulation (too much ASE reaches the detector as compared to signal power), whereas the penalty for high input powers is caused by degradation of the extinction ratio due to gain saturation (i.e., the dynamic variation in input power from the bit sequence gives variation within each bit slot in the signal power received by the detector). Lowering the pump current to each SOA reduces the penalty at high input powers, because then the onset of gain saturation is translated to greater input powers. On the other hand, then the device introduces more losses into the system, implying that the lower limit on transmitter power increases. Looking at the curve with $I = 30$ mA as an example, for input powers lower than 0 dBm, the requirement of BER = 10^{-9} cannot be fulfilled, because the signal power reaching the detector is too low.

The input power range, within which the switch matrix introduces a power penalty less than, e.g., 1 dB (the dashed line) is defined as the dynamic range. The optimum input power, giving the lowest power penalty, is lower for higher pump currents. The explanation is the same as above, viz., that higher pump current (higher gain) implies gain saturation at lower input powers.

The dynamic range as function of switch matrix unsaturated gain is shown in Fig. (3). The dynamic range is larger for low data rates and high transmitter extinction ratios. For each case, there is an optimum in unsaturated switch gain between -10 and $+5$ dB, where the dynamic

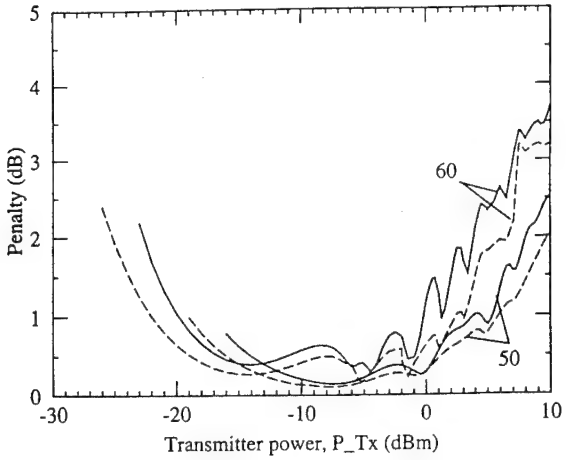

Figure 4: Calculated power penalty as function of average transmitter power with pump current to each SOA in mA as parameter.
Solid lines: $B_R = 2.5$ Gb/s.
Dashed lines: $B_R = 622$ Mb/s.

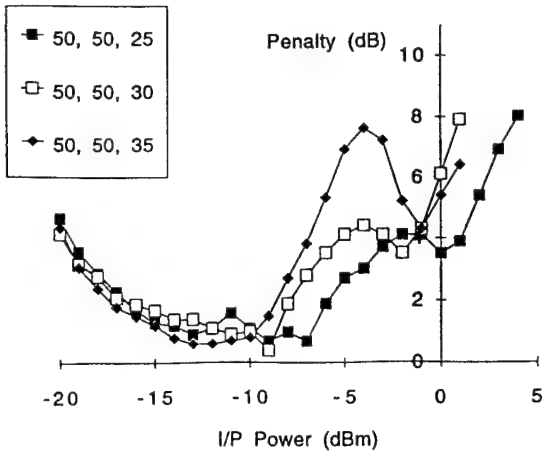

Figure 5: Measured power penalty at 2.5 Gb/s as function of average transmitter power with pump currents to the three SOA's in mA as parameters.

range is maximum. The optimum gain is more or less independent of extinction ratio, cf. the solid lines. On the other hand, the optimum gain is lower for high bit rates, cf. the black circles. This is due to the fact that at higher bit rates, the device has to be operated at higher input powers, where the performance is enhanced at lower pump current (gain). The local maximum around -25 dB gain for 2.5 Gb/s and $r = 15$ dB cannot be used because of the extremely large transmitter power required (> 20 dBm). Note that with our assumptions, the receiver sensitivities are different for the five curves, as the baseline sensitivity depends on transmitter extinction ratio and bit rate.

When finite values of the reflections within the switch matrix and the derivative of refractive index with respect to electron density in the SOA's are included (Table 1), the situation becomes more complicated, see Fig. (4). For $I = 60$ mA, some of the peaks in the penalty curves are more pronounced at the higher bit rate (solid) than at the lower bit rate (dashed), which indicates intersymbol interference. This means that upgrading a low bit rate system with an InP switch to higher bit rates may impose problems within the operating region allowed by the low bit rate dynamic range, if residual reflections are present.

Fig. (5) shows the measured power penalty. As the pump current to the last SOA is increased, the penalty peak at -5 dBm increases. The simulations indicate that this behaviour could be caused by residual reflections in this particular switch matrix. Due to parameter uncertainties, quantitative comparison is difficult to perform and the values of the pump currents in the simulations and measurements cannot be directly compared. However, it should be noted that satisfactory penalty curves without peaks have been measured[8].

Conclusions

Dynamic effects in InP switch matrices due to internal dynamics in the amplifier gates have been examined with a computer model. The optimum operating range in terms of input power and internal gain and its dependence on bit rate and transmitter extinction ratio have been identified. It has been shown that reflections, both within the chip and at the chip facets, may degrade the performance. The simulation results are in qualitative agreement with measurements.

Acknowledgments

The authors thank M. Gustavsson and A. Djupsjöbacka of Ericsson for useful discussions. This work was partly supported by the RACE II project MWTN (R2028).

References

[1] G. R. Hill et al., *IEEE J. Lightwave Technol.*, vol. 11, no. 5/6, pp. 667–679, May/June 1993.

[2] M. Gustavsson et al., *Electron. Lett.*, vol. 28, no. 24, pp. 2223–2225, 19th November 1992.

[3] A. A. M. Saleh, I. M. I. Habbab, *IEEE Trans. Commun.*, vol. 38, no. 6, pp. 839–846, June 1990.

[4] M. Le Ligne, S. Mottet, *IEEE J. Lightwave Technol.*, vol. 10, no. 8, pp. 1071–1077, August 1992.

[5] E. Berglind, L. Gillner, *Third topical meeting on Optical Amplifiers and their Applications*, paper ThC6, Santa Fe, NM, USA, June 1992.

[6] L. Gillner: *IEE Proc. J*, vol. 140, no. 5, pp. 309–315, October 1993.

[7] E. Berglind, L. Gillner, *IEEE J. Quantum Electron.*, vol. 30, no. 3, pp. 846–853, March 1994.

[8] C. P. Larsen et al., *Photonics in Switching*, paper PThD3, Salt Lake City, UT, USA, March 1995.

Polarization Resolved, Complete Noise Characterization of Bulk Ridge-Waveguide Semiconductor Optical Amplifiers

Ch.Holtmann, P.A.Besse[1] and H.Melchior

Institute of Quantum Electronics, Swiss Federal Institute of Technology
CH-8093 Zürich, Switzerland

1. Introduction

Semiconductor optical amplifiers (SOAs) at 1.3µm wavelength, with polarization insensitive gain over the entire current and wavelength range, and with tilted and antireflection coated facets for low reflectivities, are attractive for transparent switching- and optical communication systems. Moreover, the noise performance of SOAs is one of the key parameters influencing their effectiveness in telecommunications networks and systems.

The noise characteristics has been studied in detail. T. Saitoh et al. [1] gave the photon number fluctuation at the amplifier output, including the amplified signal shot noise, spontaneous emission shot noise, signal-spontaneous beat noise, spontaneous-spontaneous beat noise and signal excess noise. However, their description excluded the input coupling losses, which are practically unavoidable. J.-C. Simon et al. [2] proposed to define a realistic "users's" noise figure, taking such input coupling losses into account.

The polarization sensitivity of optical amplifiers, another important issue for a realistic description of the amplifier noise figure, is usually omitted. For fiber amplifiers, there is no need for accounting for polarization imbalances, because they intrinsically have a polarization insensitive gain. Semiconductor optical amplifiers, however, rarely show a gain polarization sensitivity below 1dB over the entire current and wavelength range. A realistic description of the noise figure, has to consider the imbalance of TE and TM amplified spontaneous emission powers, especially if the SOA is operating in the spontaneous-spontaneous beat noise limit.

In this paper we present results of polarization resolved, complete noise figure measurements on 10°-tilted, antireflection coated SOAs. The results are discussed using a realistic noise figure model for pigtailed optical amplifiers, taking input coupling losses as well as polarization imbalances into account. A systems engineer is enabled to get a realistic noise figure for any input power, at any signal wavelength and for any optical filter used in his system.

2. Theory

The semiconductor optical amplifier noise model we present is based on [1], [2] and [3]. We converted it into a form, that enables a convenient noise characterization of pigtailed SOAs and we introduced terms, accounting for the unequal TE and TM characteristics of the SOA, that influence the spontaneous-spontaneous beat noise and spontaneous emission shot noise contributions of the total noise figure.

The total noise figure is the algebraic sum of the signal-spontaneous beat noise, amplified signal shot noise, spontaneous-spontaneous beat noise and spontaneous emission shot noise contributions, that we show to be of the form:

$$NF_{sig-sp} = \frac{2}{h\nu} \cdot \frac{1}{G_{ff}} \cdot \left[\frac{P_{sp}^{I}}{(c \cdot \delta\lambda)/\lambda^2} \right] \qquad (1)$$

$$NF_{sig,shot} = \frac{1}{G_{ff}} \qquad (2)$$

[1] *Now with the Swiss Federal Institute of Technology, Lausanne, Switzerland*

$$NF_{sp-sp} = \frac{1}{P_{in}} \cdot \frac{1}{G_{ff}^2} \cdot \int_{ASE-band} A(\lambda)\, d\lambda \qquad (3)$$

$$NF_{sp,shot} = \frac{1}{P_{in}} \cdot \frac{1}{G_{ff}^2} \cdot \int_{ASE-band} B(\lambda)\, d\lambda \qquad (4)$$

where G_{ff} is the fiber-to-fiber gain at the signal wavelength λ_{sig} including the losses of an optical filter with equivalent filter bandwidth $\Delta\lambda$, that eventually would be used in a system. $h\upsilon$ is the signal photon energy, P^I_{sp} the spontaneous emission power having the same polarization as the input signal and emitted in the wavelength interval $\delta\lambda$ and P_{in} the input signal power.
$A(\lambda)$ and $B(\lambda)$ are the normalized spontaneous-spontaneous beat noise and the normalized spontaneous emission shot noise, respectively. They are given by

$$A(\lambda) = \frac{c}{\lambda^2} \cdot \left(1 + r^2\right) \cdot \frac{1}{h\nu} \cdot T_{opt}^2 \cdot \left[\frac{P^I_{sp}}{(c \cdot \delta\lambda)/\lambda^2}\right]^2 \qquad (5)$$

$$B(\lambda) = \frac{c}{\lambda^2} \cdot (1 + r) \cdot T_{opt} \cdot \left[\frac{P^I_{sp}}{(c \cdot \delta\lambda)/\lambda^2}\right] \qquad (6)$$

T_{opt} is the intensity transmission of the polarization independent optical filter of bandwidth $\Delta\lambda$ normalized to unity at the signal wavelength λ_{sig}. The expression in brackets corresponds to the spectral density of the spontaneous emission power, P^I_{sp}, having the same polarization as the input signal.
The term, that accounts for the imbalance of TE and TM characteristics, is $(1+r^2)$ and $(1+r)$ in (5) and (6), respectively. r is defined as the ratio of the spontaneous emission power having the same polarization as the input signal P^I_{sp} and the spontaneous emission power with the other polarization P^{II}_{sp}: $r = P^I_{sp}/P^{II}_{sp}$. r appears squared in (5), because $A(\lambda)$ is proportional to $(P^I_{sp})^2$. In equation (1) the term P^I_{sp} appears, because the signal only beats with the spontaneous emission of the same polarization.
The analysis presented above applies to travelling-wave amplifiers and shot noise limited sources, temperature effects are not included.

3. Experimental Results and Discussion

Figure 1 shows the measurement set-up used for the complete polarization resolved gain and noise figure characterization of pigtailed SOAs. The external cavity laser that is tunable over the whole gain spectrum generates the input signal. The polarization of the input signal at (B) is adjusted with a polarization controller and the input power is monitored at (A) with $P_{in} = \alpha \bullet P_1$. The fiber-to-fiber gain is measured with photodiodes at (A) and (D). It is given by

$$G_{ff} = \frac{P_{out}}{P_{in}} = \frac{P_{out,sig} - P_{out,sp}}{P_{in}} = \frac{1/\beta \cdot (P_{2,sig} - P_{2,sp})}{\alpha \cdot P_1} \qquad (8)$$

P_{in} and P_{out} are the input signal power and the amplified signal power, respectively, the indices *sig* and *sp* indicate, that the corresponding power is measured without or with the input signal, respectively, and $\beta = P_2/P_{out}$ accounts for the losses between (C) and (D). The spontaneous emission power at (C) with the same polarization as the input signal, P^I_{sp}, is measured as $P^I_{2,sp}$ with an optical spectrum analyzer at (D) using the relation $P^I_{sp} = P^I_{2,sp}/\beta$. The optical bandwidth of the spectrum analyzer is chosen to be $\delta\nu = (c \cdot \delta\lambda)/\lambda^2$ as in equation (1), (5) and (6).
The optical amplifier we used for the experiment was a polarization insensitive bulk active layer, ridge-waveguide SOA with 10°-tilted waveguides and antireflection coated facets operating at 1.3µm wavelength. The polarization independent fiber-to-fiber gain was as high as 23dB at 200mA driving current with a spec-

tral ripple below 0.1dB, corresponding to a facet reflectivity below $5 \cdot 10^{-6}$. With such SOA structures we realized very low polarization sensitivities as a function of driving current as well as a function of wavelength [4].

The measurements were performed at 20°C and under cw-operation. The four curves in figure 2 and figure 3 represent the basic noise characteristics of the pigtailed SOA. Out of that data, the total noise figure, which is the algebraic sum of the contributions (1) to (4), can be derived for any input signal power at any input signal wavelength and for any bandpass filter with bandwidth $\Delta\lambda$. Figure 2 shows the signal-spontaneous beat noise and the amplified signal shot noise as a function of wavelength for an amplifier current of 200mA. The amplified signal shot noise contribution is of minor influence on the total noise figure. It equals the reciprocal of the fiber-to-fiber gain. That means that the fiber-to-fiber gain spectrum can directly be read out of figure 2.

Figure 3 shows the normalized spontaneous-spontaneous beat noise and the normalized spontaneous emission shot noise. The effective spontaneous-spontaneous beat noise and spontaneous emission shot noise can be obtained out of the curves $A(\lambda)$ and $B(\lambda)$, respectively. They only have to be integrated over the filter bandwidth $\Delta\lambda$ at the input signal wavelength λ_{sig}, and divided by the input power and the square of the fiber-to-fiber gain, as shown in equation (3) and (4).

A perfectly polarization insensitive SOA has an r that equals unity, whereas a fully polarization sensitive SOA has a r-factor that goes to zero. The r-factor of our SOA is 0.95, indicating the very good polarization independency of our bulk ridge-waveguide semiconductor optical amplifiers.

Figure 4 shows the total noise figure of the SOA for an application in a system at 1.31μm wavelength, corresponding to the gain peak, as a function of the signal input power for various optical filter bandwidths $\Delta\lambda$. The total noise figure difference when using a filter with bandwidth of 0.1nm compared to a filter with bandwidth of 1nm is only slightly more than 1dB at an input signal power of -30dBm. It is obvious that the use of an optical bandpass filter after the SOA, filtering out the amplified spontaneous emission, is strongly necessary to improve the systems performance, especially for low signal input powers. Figure 5 shows the individual noise contributions to the total noise figure as a function of input power and for different filter bandwidths. It can be seen that using no bandpass filter in the system, the total noise figure is limited by the spontaneous-spontaneous beat noise up to signal input powers of about -22dBm. To be signal-spontaneous beat noise limited, a 1nm bandpass filter has to be used and the input power must be larger than about -39dBm. Increasing the input power level would decrease the required filter bandwidth, needed to be signal-spontaneous beat noise limited.

4. Conclusions

A model for a realistic noise figure of pigtailed SOAs, taking into account imbalances in TE and TM characteristics, has been presented. We experimentally characterized our 10°-tilted and AR-coated bulk ridge-waveguide semiconductor optical amplifiers. The polarization independency of our devices, with 23dB fiber-to-fiber gain at 200mA driving current, a spectral ripple less than 0.1dB, a facet reflectivity below $5 \cdot 10^{-6}$ and a ratio of TE to TM spontaneous emission of 0.95, has been confirmed.

The measured noise contributions, corresponding to our model, enables a systems engineer to get a realistic noise figure for any input power, at any signal wavelength and for any optical filter used in his system.

Acknowledgments

This work was partly supported by the Swiss Federal Office for Education and Science, Berne.

References

[1] T. Saitoh et al., IEEE J. Quantum Electron., 1987, QE-23, pp. 1010-1020
[2] J.-C. Simon et al., Electron. Lett., 1989, 25, pp. 434-435
[3] Ch. Hentschel et al., Proc. OAA'94, Breckenridge CO, USA, FB-5, pp. 136-138, 1994
[4] Ch. Holtmann et al., Proc. OAA'93, Yokohama, Japan, SuB2, pp. 8-11, 1993

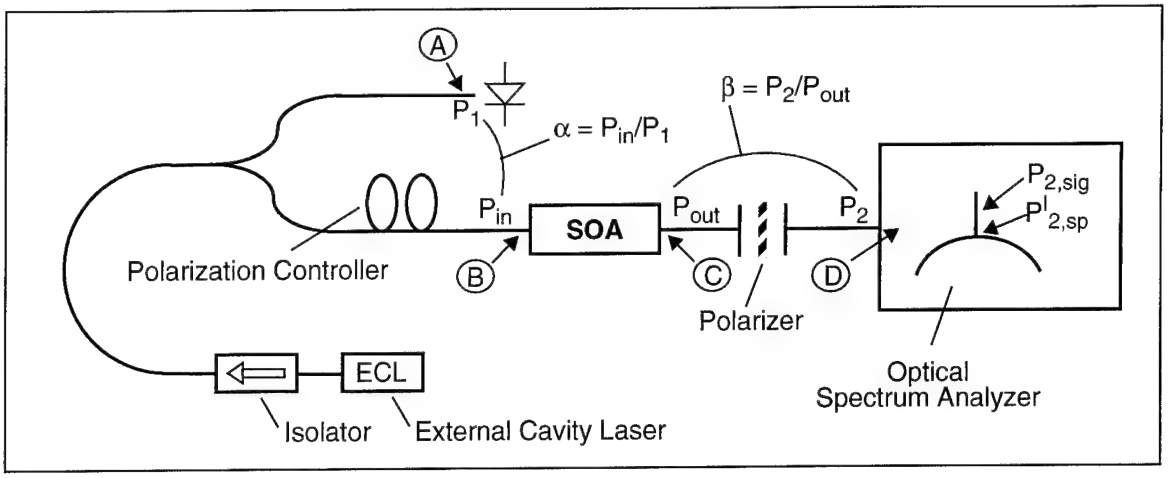

Fig. 1: Experimental set-up for complete polarization resolved gain and noise characterization of pigtailed SOAs (ETHZ).

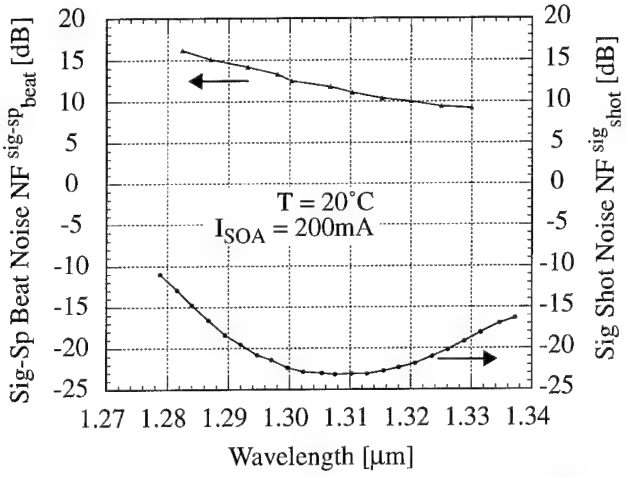

Fig. 2: Signal-spontaneous beat noise and amplified signal shot noise contributions (ETHZ).

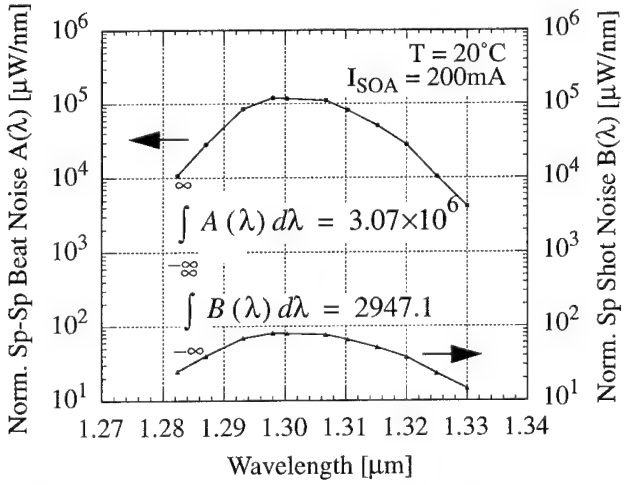

Fig. 3: Normalized spontaneous-spontaneous beat noise and normalized amplified spontaneous shot noise (ETHZ).

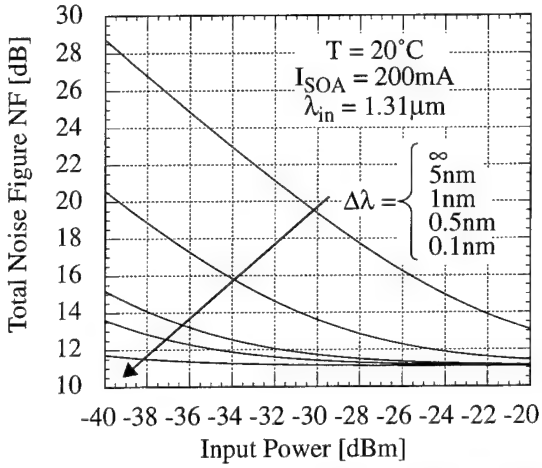

Fig. 4: Total noise figure for different filter bandwidths Δλ (ETHZ).

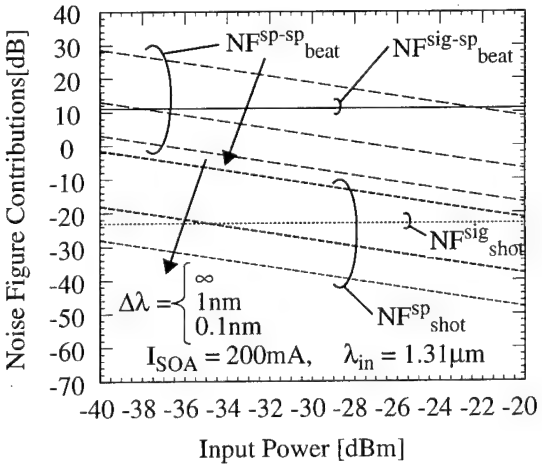

Fig. 5: Total noise figure contributions for different filter bandwidths Δλ (ETHZ).

Polarization independent 1550 nm semiconductor optical amplifier packaged module with 29 dB fiber to fiber gain.

P.Doussiere, F. Pommerau, D. Leclerc, R. Ngo, M.Goix, T. Fillion P. Bousselet

ALCATEL ALSTHOM RECHERCHE Route de Nozay, 91460 Marcoussis, France
and G. Laube
ALCATEL-SEL Reserch center,Optoelectronic Components Division, ZFZ/WO, Lorenzstr. 10, D-70435 STUGTTGART, Germany.

INTRODUCTION

Recent progress in 1550 nm semiconductor optical amplifier (SOA) [1] in addition to attractive results obtained in preamplifier application [2] have retain much attention. Besides, the ability of (SOA) to provide strong non-linear effects such as four wave mixing,cross gain and cross phase modulation for relatively low optical intensity has enlarged their field of applications. Optical time division multiplexed (OTDM) communication systems using SOA based nonlinear optical loop mirror (NOLM) [3], phase conjugation for in-line chromatic dispersion compensation [4] and fast signal processing [5] are extensively studied and show that an increasing demand exists for solitary SOA module. For most of applications polarization independence is generally required as well as a high coupling efficiency to external fiber. In this view, we report on a semiconductor amplifier module operating at 1550 nm and giving very high fiber to fiber gain as well as a low polarization dependence and a very low spectral gain ripple.

DEVICE STRUCTURE AND FABRICATION

The structure of the device is shown on figure 1 and is almost similar to previous work reported in [1. It is based on a square shaped active waveguide made of bulk material with lateraly tapered regions. Compared to previous work, this new structure includes 7° tilted configuration for a more efficient suppression of residual facet reflectivity, and an increased length of the tapered regions for improved coupling efficiency. The combination of a square active waveguide, in the central section, with 100 µm tip like tapered regions at both ends allow to insure a low polarization dependence of the gain together with a reduced far-field divergence (20° x 20°). The mode size expansion wich occures in the tapered regions results in a much improved coupling efficiency to the external lensed fiber compared to an untapered structure. Internal gain obtained on such structure exceeds easily 30 dB and requires very low residual facet reflectivity close to 10^{-5} for a complete suppression of the spectral gain ripple. For this, 7° tilted buried facets combined with TiO2 / SiO2 two layers coating have been recognised to be a very efficient configuration. Total length of the device including windows and tapered regions is 800 µm.

In contrast to quantum well structures, bulk based amplifier structures have large modal confinement factor (> 0,5) wich favours a strong interaction beetween photons and carriers providing quick nonlinear effects with optical intensity.

Device fabrication includes first molecular beam epitaxy growth and contact lithography. Compared to previous report [1], the recent introduction of an oxyde film underetching combined with RIE for the mesa definition has enabled us to greatly improved the homogeneity of the process. Even 2" feasabilty has been demonstrated. Single higly doped InP regrowth performed with MOVPE technique allows to bury the structure whereas a deep proton implantation is carried out for lateral current confinement.

Once soldered P side down on tilted embasis (figure 2) for refraction compensation, the device is packaged using laser YAG welding technique for better mechanical reliability. A peltier cooler is inserted beetween the device submount and the "Butterfly" package (figure 3).

Special lensed fiber with low sperical aberration and long working distance are used for both achievement of high coupling efficiency and very low residual optical feed-back. Coupling losses as low as 2 dB per facet are currently obtained together with -50 dB residual feed-back .

MODULE CHARACTERISTICS.

Fiber to fiber gain characteristic versus amplified output power is shown on figure (4) for 150 mA an 200 mA driving current. A record 29 dB fiber to fiber gain is obtained for -30 dBm input power and 200 mA at 1540 nm. The 3 dB saturation output power is close to 10 dBm in the fiber at 200 mA whereas the maximum absolute output power in the fiber is 11dB for the same current value. Saturation output power in bulk material based amplifier structure is known to be lower than for quantum well based structures. However the present work shows that a relatively high saturation output power can be achieved in bulk structures. Polarization sensitivity is lower than 0.5 dB. Amplified spontaneous emission spectrum measured at 100 mA shows 30 nm 3dB bandwidth and spectral ripple lower than 0.5 dB. This last value corresponds to a residual facet reflectivity as low as 10^{-5}. Noise factor measurement indicates a Nsp/C1 value of 6,8 dB for 200 mA and -20 dBm input power.

CONCLUSION.

In conclusion, packaged module semiconductor optical amplifier operating at 1550 nm has been fabricated with 29 dB fiber to fiber gain, 0.5 dB polarization sensitivity and less than 0.5 dB spectral gain ripple. Owing to its good characteristics, this kind of module can be used in preamplification or in-line amplification as well as for nonlinear effects based applications.

REFERENCES.

[1] P. Doussiere, P. Garabedian, C. Graver, D. Bonnevie, T. Fillion, E. Derouin, M. Monnot, J.G. provost, D. Leclerc and M. Klenk "1.55 µm polarisation independent semiconductor optical amplifier with 25 dB fiber to fiber gain" IEEE Photon. Technol. Lett. Vol. 6, pp 170-172, February 1994.

[2] T. Durhuus, B. Mikkelsen, C. Joergensen, K.E. Stubkjaer, P. Doussiere, P. Garabedian and D.Leclerc "High performance semiconductor optical preamplifier"5th Topical meeting Optical Amplifiers and Their applications, june 1994, Breckenridge.

[3] M. Eiselt, W. Pieper and H.G. Weber "All-optical high speed demultiplexing with a semiconductor laser amplifier in a loop mirror configuration" Electron. Lett. Vol. 29, pp 1167 - 1168, June 1993.

[4] M.C. Ta tham, G. Sherlock and L.D. Westbrook " " Electron. lett. Vol. 29, pp , October 93.

[5] N. Storkfelt, K.B. Jakobsen, M. Vaa, K.S. Jepsen, J.C.T. Nielsen, K.E. Stubkjaer, P. Doussiere, P. Garabédian, C. Graver and D. Leclerc. "High speed all optical time-division demultiplexing using semiconductor optical amplifier"5th Topical meeting Optical Amplifier and their Applications, june 1994, Breckenridge.

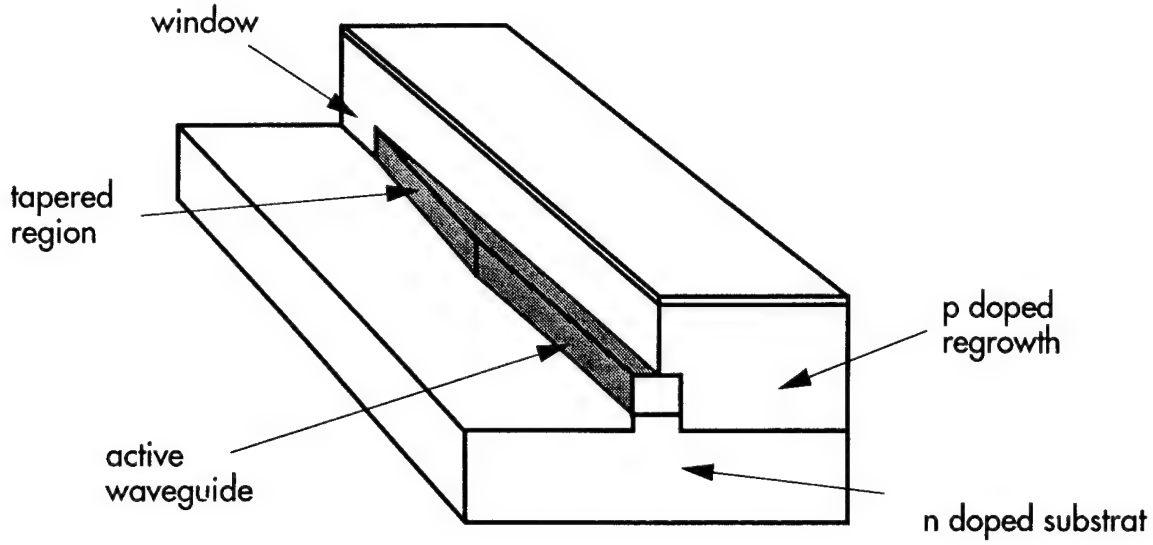

Figure 1: Schematic view of tapered amplifier structure

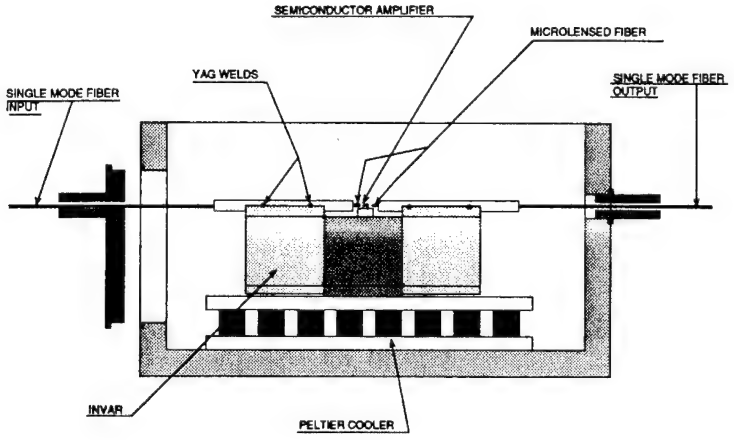

Figure 2 : inner view of amplifier module

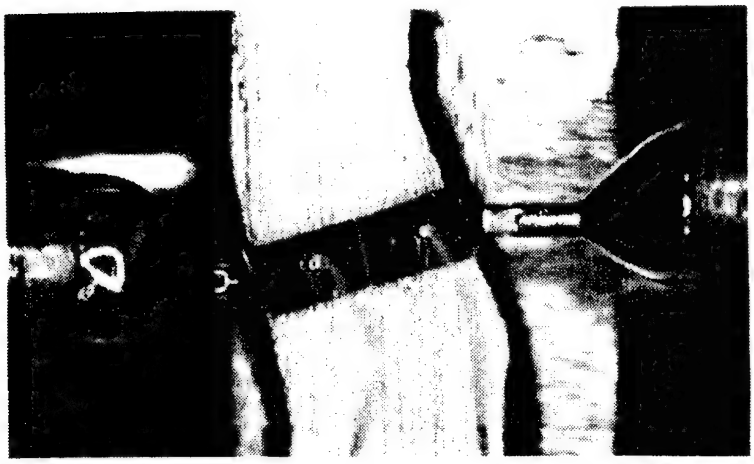

Figure 3 : Overview of pigtailed device

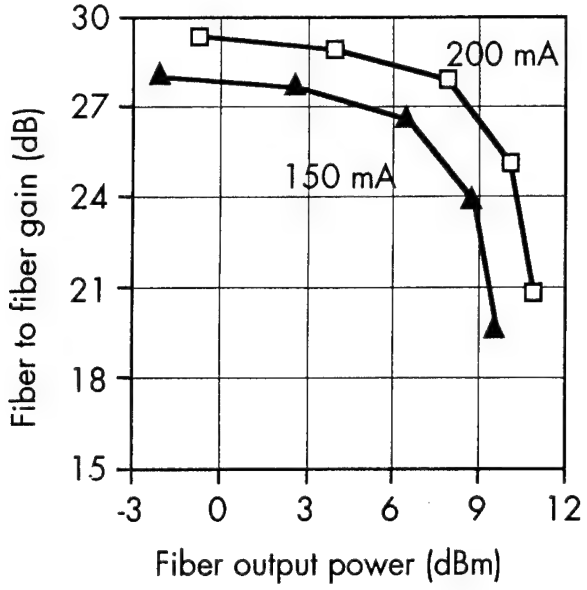

Figure 4 : Gain saturation curve of amplifier module for 150 and 200 mA driving current

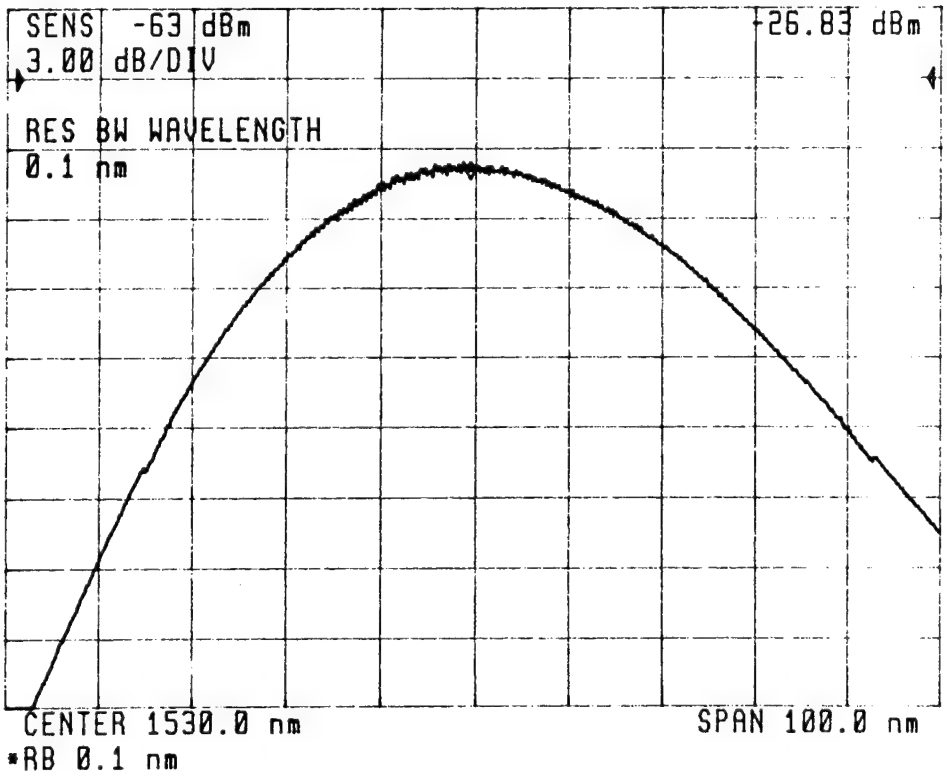

Figure 5 : Amplified Spontaneous emission spectrum of packaged module fo 100 mA

Performance of Cascaded 1300 nm QW Laser Amplifiers in 10 Gbit/s Long Haul NRZ Transmission

Jean G.L. Jennen
Eindhoven University of Technology, Den Dolech 2, 5612 AZ Eindhoven, The Netherlands
Luuk F. Tiemeijer
Philips Optoelectronics Centre, Prof. Holstlaan 4, 5656 AA Eindhoven, The Netherlands
Coen T.H.F. Liedenbaum, John J.E. Reid
Philips Optoelectronics Centre, Prof. Holstlaan 4, 5656 AA Eindhoven, The Netherlands
Hugo de Waardt
PTT Research, Postbox 421, 2260 AK Leidschendam, The Netherlands

Introduction

At present more than 55 million kilometers of the standard type single mode fibre (SMF) have been installed. Showing zero dispersion at a wavelength of about 1310 nm, SMF offers great potential when the bitrate $\times$ distance product is considered, if it were not for the attenuation of the fibre. Therefore, design of very high speed digital transmission systems in the 1300 nm region is very attractive. Recently significant progress has been achieved in the development of Quantum Well Laser Amplifiers (QWLAs) with the use of suitably strained Quantum Well materials [1, 2]. Although a few promising results have been published using these amplifiers [3, 4], especially a 10 Gbit/s transmission over 200 km, representing a record NRZ transmission capacity using Semiconductor Laser Amplifiers (SLAs), the study on the performance of cascaded QWLAs in high bitrate long haul transmission systems is far from completed yet.

In this paper we present a numerical model for a transmission system of cascaded QWLAs and focus on 10 Gbit/s NRZ optical transmission. The 10 Gbit/s system has been simulated with the implementation of our QWLA model and the acquired simulation data show good agreement when compared to experimental observations.

System model

The transmission system consists of four different components, namely QWLAs, fibres, a transmitter and a receiver. Therefore, four models are needed for a theoretical description of this system.

QWLA model To formulate a model for QWLAs we have started with the rate equations presented in [5]. After elimination of z by integration over the amplifier length L and introduction of wavelength dependency we arrive at the following reduced rate equations, namely

$$P_{out}(\tau,\lambda) = P_{in}(\tau,\lambda)e^{h(\tau,\lambda)} + h\frac{c^2}{\lambda^3}\frac{NF}{2}e^{h(\tau,\lambda)}\mathrm{d}\lambda \text{ with } h(\tau,\lambda) = \int_0^L g(z,\tau,\lambda)\mathrm{d}z\,, \tag{1}$$

$$\varphi_o ut(\tau,\lambda) = \varphi_{in}(\tau,\lambda) - \frac{1}{2}\alpha_H h(\tau,\lambda) \quad \text{and} \tag{2}$$

$$\frac{\partial h(\tau,\lambda)}{\partial \tau} = -\frac{h(\tau,\lambda) - g_0(\lambda)L}{\tau_c} - \frac{\sum_{\lambda_i}\frac{\lambda_i}{\lambda}P_{in}(\tau,\lambda_i)/P_{sat}(\lambda)}{\tau_c}\left(e^{h(\tau,\lambda)} - 1\right)\,, \tag{3}$$

where τ_c is the carrier lifetime, $P_{sat}(\lambda)$ represents the 1/e saturation output power, $g_0(\lambda)L$ stands for the small signal amplifier gain, $h(\tau, \lambda)$ is the time dependent amplifier gain, α_H is the linewidth enhancement factor, dλ represents the wavelength discretisation stepsize, h is the Planck constant, c stands for the velocity of light, NF is the fibre coupled noise figure, and $P_{in}(\tau, \lambda_i)$ represents the total input power to each amplifier, i.e. the sum of input signal power and ASE originating from the previous amplifiers, and near zero facet reflectivity is assumed. In order to solve these equations numerically measured or estimated values for small signal gain, peak wavelength, saturation output power, optical bandwidth, noise figure, and carrier lifetime have to be provided. For the gain we assume a Gaussian shaped spectrum. Using *Euler forward iteration* and an appropriate stepsize we have numerically solved Equation 3. Residual polarisation sensitivity can be taken into account by solving the Rate Equations 1, 2 and 3 applying different parameter sets for TE and TM gain respectively, assuming all gains are saturated equally by TE and TM intensities.

Fibre model Attenuation, dispersion and self-phase modulation have been accounted for in our fibre model. The waveguide propagation through the fibre is calculated by solving the *NonLinear Schrödinger Equation* (NLSE) [6].

Transmitter model We used a $2^7 - 1$ PRBS data pattern which was converted into a 10 Gbit/s laser signal. In our model a simplified laser pulse has been used. This pulse lacks a relaxation oscillation, but shows an extinction ratio and slopes equal to the experimentally observed values of our laser module.

Receiver model For the photodiode a quantum efficiency of 0.8 is assumed. The thermal noise is adjusted, so that the receiver has a sensitivity of -13.7 dBm at 10 Gbit/s and a BER of 10^{-9}. In order to calculate the BER we assume Gaussian probability density functions for all noise sources and determine their variances according to [7]. The BER is then obtained by averaging the error probabilities of all $2^7 - 1$ consecutive bits.

10 Gbit/s NRZ transmission experiment

The model described in the preceding section can be used to simulate several applications of QWLAs. In this paper we confine ourselves to the 10 Gbit/s NRZ system as shown in Figure 1.

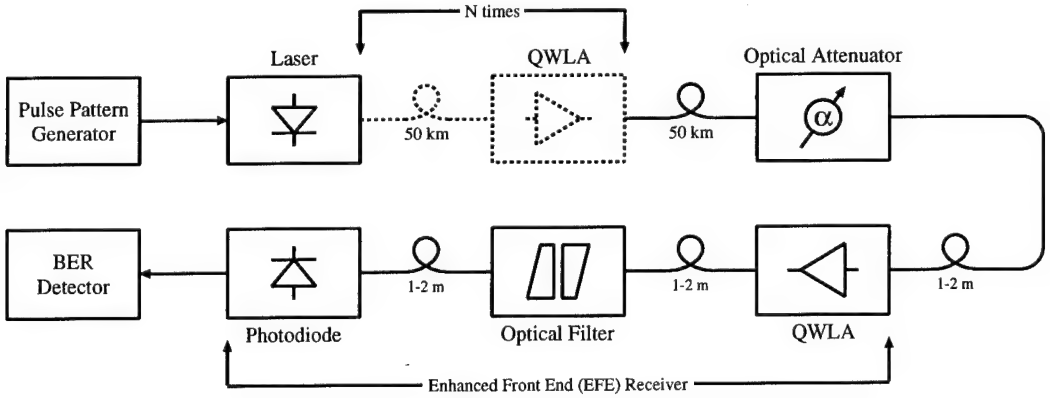

Figure 1: 10 Gbit/s NRZ optical transmission system set up.

In the transmission experiments [4] a DFB laserdiode module is used which is directly NRZ modulated with a 10 Gbit/s, $2^7 - 1$ PRBS data pattern. The transmission link consists of N 1310 nm QWLAs [2] and N+1 segments containing 50 km of optical fibre. The receiver comprises a 50 Ω optical front end followed by an AC-coupled broadband electrical amplifier and has a total electrical bandwidth of 10.2 GHz. This combination yields a sensitivity of -13.7 dBm at 10 Gbit/s. In order to boost the receiver sensitivity a single QWLA is used as an optical preamplifier. Between the preamplifier and the photodectector an optical band pass filter (2 nm bandwidth, 2 dB insertion loss) has been placed in order to reduce the spontaneous emission beat noise generated by the amplifier cascade. To acquire a more profound insight in the system performance

as a function of the number of cascaded QWLAs (N) or equivalent distance we have determined several bit error ratio curves for N upto 3 representing 10 Gbit/s transmission over 200 km [4].

Figure 2 shows the bit error ratio curves for N=0 (50 km), N=1 (100 km), and N=3 (200 km). In order to demonstrate the improvement in receiver sensitivity of the Enhanced Front End (EFE) Receiver when compared to the standard 50 Ω optical front end the corresponding BER curve has been inserted. An increased receiver sensitivity of approximately -27.3 dB is observed. Furthermore, it would appear that no dispersion penalty ($D \approx 0.6$ ps/(nm.km)) is found after 50 km of fibre when compared to a back-to-back measurement.

Simulation results

Simulations of the 10 Gbit/s NRZ system yield the BER curves presented in Figure 3. For the QWLAs a gain peak wavelength of 1305 nm, equal to the zero dispersion wavelength of the fibre, a bandwidth of 60 nm, and a gain of 22.5 dB at the signal wavelength of 1311 nm, almost equal to the loss of the 50 km fibre span were assumed, together with an estimated fibre noise figure of 9 dB, a P_{sat3dB} of 10 dBm, a τ_c of 200 ps, and an estimated linewidth enhancement factor α_H of 5.

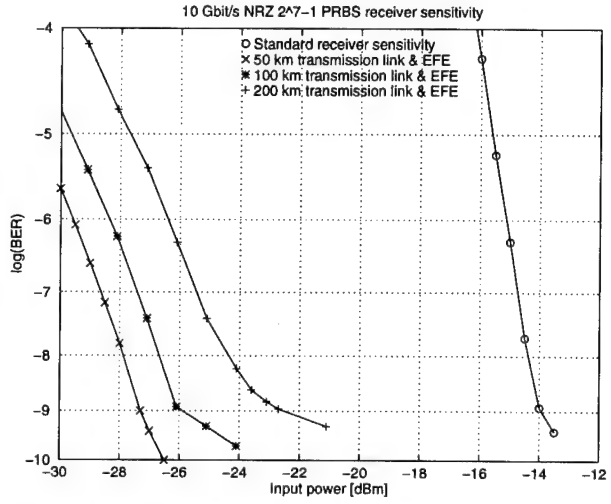

Figure 2: Measured bit error ratio curves [4], input extinction ratio is 6.

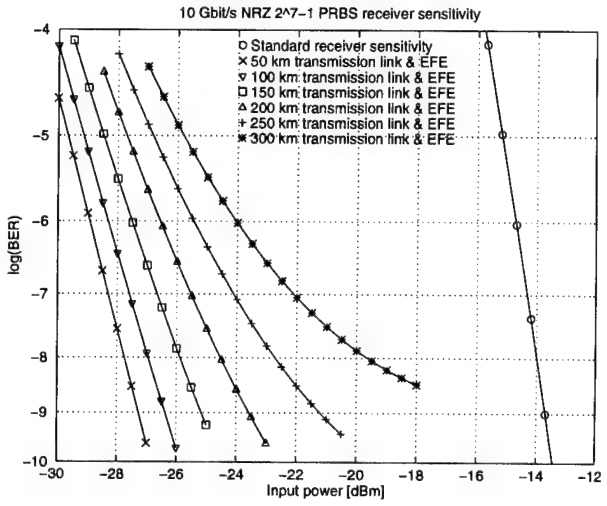

Figure 3: Simulated bit error ratio curves when using an input extinction ratio of 6.

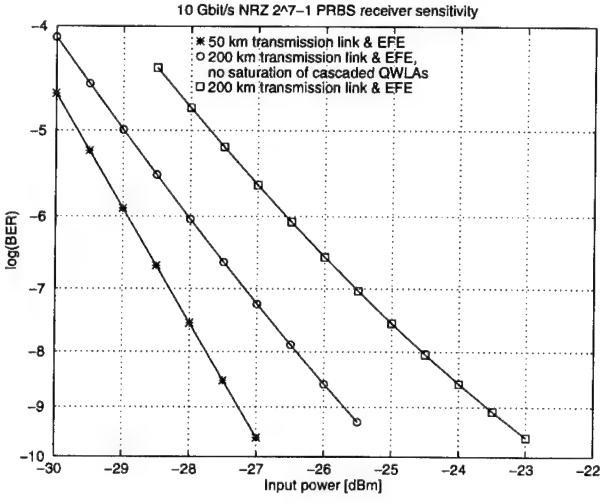

Figure 4: Determination of penalty origins when using an input extinction ratio of 6.

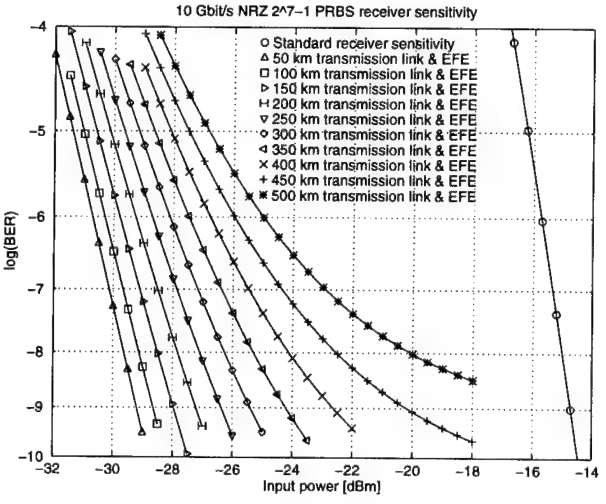

Figure 5: Simulated bit error ratio curves when using an input extinction ratio of 20.

When comparing the measurements of [4] to the simulation results we observe a good agreement between the 200 km and standard receiver BER curves. However, the measured 200 km BER curve shows a floor just below 10^{-9}. This is probably due to timing jitter, because the clock signal for the BER detector was derived from the pulse pattern generator. Back-to-back measurements do not reveal this floor. The experimentally determined penalties are comparable to the theoretical ones. Due to the simplified laser pulse used in the simulations small differences between measurements and simulations can be expected.

To determine the origin of the observed penalties at a BER of 10^{-9} some additional simulations have been performed. The results are summarized in Figure 4. This figure shows that the penalties can be divided into two contributions. Firstly, about 1.5 dB is accounted for by the accumulated ASE of the cascaded QWLAs. The remaining 2 dB is caused by extinction ratio degradation due to saturation of the QWLAs. Penalties caused by dispersion seem to be absent, as all simulations whether or not including the fibre dispersion yield identical BER curves for the 200 km transmission link.

When a BER of 10^{-9} is required the maximum transmission length amounts to 250 km. This distance limitation occurs because of accumulation of ASE along the link and eye closure due to gain saturation, thus reducing the signal to noise ratio and increasing the BER. Improvement of the maximum distance can be achieved by enlarging the extinction ratio as illustrated in Figure 5 or by using an optical filter with a smaller bandwidth.

Conclusions

The feasibility of 10 Gbit/s NRZ optical transmission over 200 km of fibre using QWLA repeaters has been investigated with simulations using realistic QWLA parameters. The main factors limiting the maximum link length are extinction ratio degradation and accumulated ASE. Furthermore, simulations reveal that for a BER of 10^{-9} and for a $2^7 - 1$ PRBS the maximum transmission link length of 250 km can be extended to 450 km when the extinction ratio of the input signal is increased from 6 to 20.

Acknowledgement

The authors would like to express their gratitude to A.J. Boot - PTT Research, Leidschendam, The Netherlands - for useful discussions on the subject and for providing us with an adequate fibre model.

References

[1] L.F. Tiemeijer, et al., "Polarization Insensitive Multiple Quantum Well Laser Amplifiers for the 1300 nm Window," *Applied Physics Letters*, vol. 8, pp. 826–828, February 1993.

[2] L.F. Tiemeijer, et al., "27 dB Gain Unidirectional 1300 nm Polarization-Insensitive Multiple Quantum Well Laser Amplifier Module," *IEEE Photonics Technology Letters*, vol. 6, no. 12, pp. 1430–1432, December 1994.

[3] J.J.E. Reid, et al., "Realisation of 20 Gbit/s Long Haul Soliton Transmission at 1300 nm on Standard Single Mode Optical Fibre," in *Proceedings 20th European Conference on Optical Communication / Post-deadline Papers*, pp. 61–64, September 1994.

[4] C.T.H.F. Liedenbaum, et al., "10 Gbit/s NRZ Transmission over 200 km at 1300 nm using Quantum Well Laser Amplifier Modules," *submitted to IEEE Electronics Letters.*

[5] G.P. Agrawal and N.A. Olsson, "Amplification and Compression of Weak Picosecond Optical Pulses by using Semiconductor-Laser Amplifiers," *Optics Letters*, vol. 14, no. 10, pp. 500–502, May 1989.

[6] G.P. Agrawal, *Nonlinear Fiber Optics.* Academic Press, Inc., 1989. ISBN 0-12-045140-9.

[7] N.A. Olsson, "Lightwave Systems with Optical Amplifiers," *IEEE Journal of Lightwave Technology*, vol. 7, no. 7, pp. 1071–1082, July 1989.

Friday, June 16, 1995

High-Rate and Short Pulse Systems

FB 11:00-12:30
Theatersaal

Neal Bergano, *Presider*
AT&T Bell Laboratories, U.S.A.

Soliton transmission with sliding-frequency guiding filters: progress toward 100 Gbit/s over transoceanic distances.

P. V. Mamyshev and L. F. Mollenauer

Rms 4C-310 and 4C-306
AT&T Bell Laboratories
101 Crawfords Corner Road
Holmdel, NJ 07733
USA
Tel. (908) 949 8924 and (908) 949 6766, FAX (908) 949 5784

The sliding-frequency guiding filters dramatically reduce timing and amplitude jitter in long-distance soliton data transmission [1,2]. They also reduce the soliton pair interaction, so the soliton pulses can be packed closer together. The sliding filters effectively remove dispersive wave radiation from imperfect input pulses, which permits the soliton data transmission using even NRZ sources [3]. The technique of sliding-frequency guiding filters has enabled extremely robust, error-free soliton data transmission at single channel rates of 10 to 20 Gbit/s, over distances often approaching the circumference of the earth [2,4]. Guiding-frequency filters provide additional benefits when used in WDM systems. One of these benefits is the equalization of relative signal amplitudes of WDM channels. Depending on the soliton energy, solitons experience different loss when pass through the guiding filters: the higher the soliton energy the higher the loss. As a result, the guiding filters equalize relative signal amplitudes of WDM channels, automatically compensating for the unflatness of the amplifiers' gain spectrum. We demonstrate this effect of WDM channel energy self-equalization in soliton transmission experiments with sliding-frequency filters. Filters can also reduce or eliminate residual defects of WDM. Soliton transmission using frequency guiding filters has enabled 40 Gbit/s, in the form of an 8×5 Gbit/s WDM transmission over 9600 km [5]. One would

like to extend the filtered soliton transmission to many WDM channels at 10 Gbit/s each. Increased bit rate per channel leads to the increased number of soliton collisions. Increased bit rate per channel also requires shorter pulses, which as a rule increases the residual effects from each soliton collision. At the same time, the allowable timing jitter for error-free propagation at higher bit rate per channel is less. All these factors require a very careful design of multi-channel WDM system with 10 Gbit/s per channel, taking into account many different factors. In particular, we will discuss the following points which were recently discovered in our experiments and theoretical analysis.

1. Depolarization of the WDM channels. The relative state of polarization of interfering channels changes with propagation due to the effect of polarization mode dispersion (PMD). Depending on the relative polarizations of the colliding soliton pulses, the state of polarization of the pulses after the collision could change. Each pulse experiences a different number of collisions, depending on the data pattern in the interfering WDM channel. This effect leads to the depolarization of each WDM channel (different pulses are scattered into different states of polarization). The depolarization leads (through the effect of polarization mode dispersion) to additional jitter of the soliton arrival times. Note that in many cases the depolarization effect can also make impossible the combination of WDM with polarization multiplexing.

2. In the case of a broadband soliton transmission (i. e. without guiding filters), the residual effect caused by cross-phase modulation during the soliton collision is a temporal shift of the solitons. This effect increases the jitter of the soliton arrival times, once again, because different pulses can experience different numbers of collisions [6].

Guiding frequency filters with the ideal Gaussian shape can greatly reduce or eliminate this residual effect of WDM soliton collisions. Practical filters, however, have transmission shapes which are different from the ideal Gaussian shape. We will discuss the effect of the filter shape on the efficiency of the suppression of the jitter caused by the WDM soliton collisions.

3. Another important question is the dispersion properties of the filter. During the collisions the soliton mean frequency deviates from its equilibrium value. If the transition time through the filter depends on the frequency detuning of the soliton carrier frequency with respect to the transmission peak of the filter, this effect will introduce an additional timing jitter.

4. It is well-known from soliton theory that in a lossless fiber the four-wave mixing product generated during the soliton collision totally disappears at the end of the collision. In systems with lumped amplification, however, the periodicity of the amplification can compensate for the phase mismatch of the four-wave mixing process. This leads to quasi-phase-matching of the process and to growth of four-wave mixing components, which can result in additional timing and amplitude jitter. We will discuss how to eliminate this undesirable effect by an appropriate choice of system parameters (WDM channel spacing, fiber dispersion, amplifier spacing) and/or by using different dispersion maps.

REFERENCES

[1] L. F. Mollenauer, J. P. Gordon, and S. G. Evangelides, "The sliding-frequency guiding filter: an improved form of soliton jitter control," *Opt. Lett.* **17**, 1575 (1992)

[2] L. F. Mollenauer, P. V. Mamyshev, and M. J. Neubelt, "Measurement of timing jitter in soliton transmission at 10 Gbits/s and achievement of 375 Gbits/s-Mm, error-free, at 12.5 and 15 Gbits/s", *Opt. Lett.* **19**, 704 (1994)

[3] P. V. Mamyshev and L. F. Mollenauer, "NRZ-to-soliton data transmission by a filtered transmission line", *Optical Fiber Communication conference OFC-95,* San Diego 1995, Paper FB-2, pp. 302-303.

[4] P. V. Mamyshev and L. F. Mollenauer, "Stability of soliton propagation with sliding frequency guiding filters", *Opt. Lett.* **19**, 2083 (1994).

[5] B. M. Nyman, S. G. Evangelides, G. T. Harvey, L. F. Mollenauer, P. V. Mamyshev, M. L. Saylors, S. K. Korotky, U. Koren, V. Mizrahi, T. A. Strasser, J. J. Veselka, J. D. Evankov, A. Lucero, J. Nagel, J. Sulhoff, J. Zyskind, P. C. Corbett, M. A. Mills, and G. A. Furguson, "Soliton WDM transmission of 8 × 2.5 Gbit/s, error free over 10 Mm",
Optical Fiber Communication conference OFC-95, San Diego 1995, Postdeadline paper PD-21.

[6] L. F. Mollenauer, S. G. Evangelides, and J. P. Gordon, "Wavelength division multiplexing with solitons in ultra-long distance transmission using lumped amplifiers", *J. Light. Techn.,* **9**, 362 (1991).

Soliton Transmission at High Bit Rates through Distributed Erbium-doped Fibres

Christian Lester, *Kent Bertilsson, Karsten Rottwitt,
*Peter A. Andrekson, **Mark A. Newhouse and **A.J. Antos

Center for Broadband Telecommunications, Electromagnetics Institute,
Technical University of Denmark, DK-2800 Lyngby, Denmark.
Telephone: + 45 42 88 14 44; Fax: + 45 45 93 16 34
*Department of Optoelectronics and Electrical Measurements,
Chalmers University of Technology, 412 96 Göteborg, Sweden.
**Corning Inc., Technology Group, Corning, New York 14381, USA.

Introduction:

In ultra-long transmission systems, the combined effects of fibre-dispersion and optical Kerr effect, can be used to transmit soliton pulses well beyond the dispersion limit [1]. To overcome fiber loss in an all-optical soliton link, both lumped and distributed amplification have been used. Excursions in the signal power reduce the stability of the soliton. To sustain stable soliton propagation in a system with lumped amplifiers, the spacing between the amplifiers, Z_a, has to be much shorter than the soliton period, Z_0, i.e. $Z_a/Z_0 << 1$ [2]. Z_0 is inversely proportional to the square of the bit rate and thus to satisfy the stability criterion at high bit rates, relatively small amplifier spacing will be required. When using distributed amplification, the signal power still varies with the periodicity of the pump separation. Nevertheless, the excursions will be smaller than for lumped amplifiers and numerical modelling [3] predicts that the above mentioned criterion is relaxed by as much as an order of magnitude, i.e. $Z_a/Z_0 < 1$, where now Z_a represents the pump separation. The exact stability criterion will be a function of the magnitude of the signal power excursions along the link. In addition to this, it has been predicted that stable soliton propagation can also be achieved when $Z_a/Z_0 >> 1$ [3], when using distributed amplification. Distributed amplification may be realized through the use of the Raman effect [4] or distributed erbium-doped fibres (d-EDF's) [5]. Here we present an experimental characterization of the transmission of solitons over 90 km using d-EDF's. We characterize the performance of the d-EDF according to the relation Z_a/Z_0 and the magnitude of the signal excursion along the d-EDF, and verify experimentally that stable soliton transmission also is achievable when $Z_a/Z_0 > 1$.

Theory:

To study the stability of a transmission line using distributed amplification in more detail, we have solved the nonlinear Schrödinger equation numerically, where the signal has a sinusoidal power

variation between two pump power stations. Since we evaluate the soliton pulses after approximately 90 km of transmission, system noise accumulation is negligible [5]. To evaluate the quality of the output pulses we calculate the root-mean-square (RMS) width of the pulses in the time domain ,τ_{RMS}, and in the frequency domain, ω_{RMS}. For a transform limited soliton, the time-bandwidth-product (TBP) $\tau_{RMS} \cdot \omega_{RMS} = \pi/6 \approx 0.52$; if the TBP exceeds $\pi/6$, the soliton is deformed.

Experimental setup:

The experimental setup for the transmission experiments is shown in Fig. 1. The pulses are generated in an external cavity mode-locked semiconductor laser, with a repetition rate of 3.6 GHz. The pulses were compressed in a 2.5 km dispersion shifted fibre, with a zero dispersion wavelength at 1560 nm. The length of the pulse compressing fibre is optimized to achieve the shortest pulses possible. The pulses were amplified in a 1480 nm backward pumped erbium-doped fibre amplifier, which was protected against external reflections by optical isolators at the input and the output end of the amplifier.

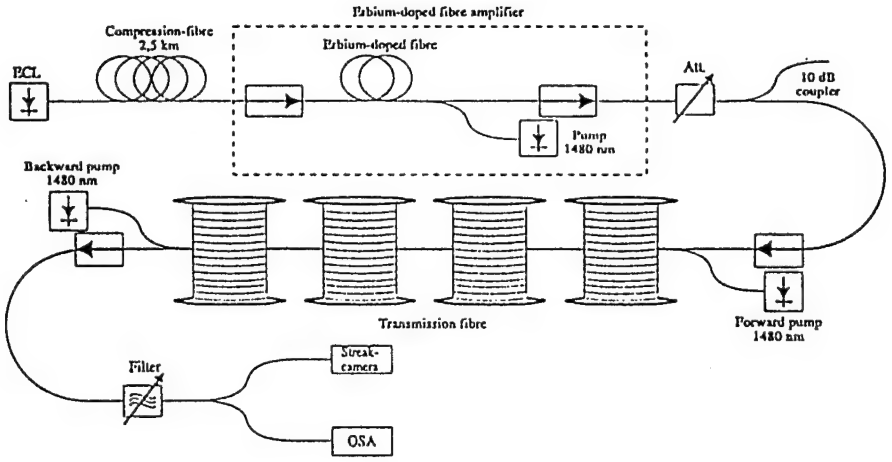

Fig 1: Experimental setup for characterizing soliton transmission on d-EDF's.

The fibre amplifier was operated in the saturated regime to obtain a more stable pulse output power. Before the pulses are coupled into the transmission fibre, their power levels are adjusted by a variable attenuator to obtain a first order soliton at the beginning of the transmission line. The d-EDF was pumped bidirectionally by two 1480 nm semiconductor lasers. To protect the transmission fibre from external reflections, optical isolators were inserted at the input and the output ends of the d-EDF. The pump power was adjusted until the power in the soliton was unaltered at the output end of the transmission line. The input and the output pulses were measured with a synchroscan streak camera (Hamamatsu C1587) with approximately $\pm$ 0.5 ps accuracy and an optical spectrum analyzer (OSA). When necessary, an optical filter was inserted to attenuate the amplified spontaneous emission from the d-EDF.

Results of soliton propagation on d-EDF's:

The assembled transmission line consists of two d-EDFs surrounding a 29.3 km dispersion-shifted single-mode undoped fiber. With this configuration we transmitted solitons over a distance of 90.2 km (Z_a). Initially, we transmitted solitons having a 9.0 ps Full-Width-Half-Maximum pulse width (T_{FWHM}) and the corresponding soliton period (Z_0) was 200.9 km, the ratio, Z_a/Z_0, for this configuration was 0.45. The time average signal power was - 9.4 dBm, and from OTDR measurements we estimate the signal excursions to be approximately 10 dB at this signal power level. The output soliton in the time domain and the spectrum is shown in Fig. 2. The TBP for the input and the output pulse was 0.63 and 0.71, respectively. The T_{FWHM} of the output soliton remained unchanged within the accuracy of the measurement, and we conclude that the interaction between the Kerr effect and the dispersion of the fibre has kept the pulse nearly unchanged over the 90.2 km..

Fig 2: Output pulse after 90.2 km transmission on d-EDF. Fig. 2a displays the pulse in the time domain, and 2b shows the optical spectrum. The power is normalized with respect to the peak power.

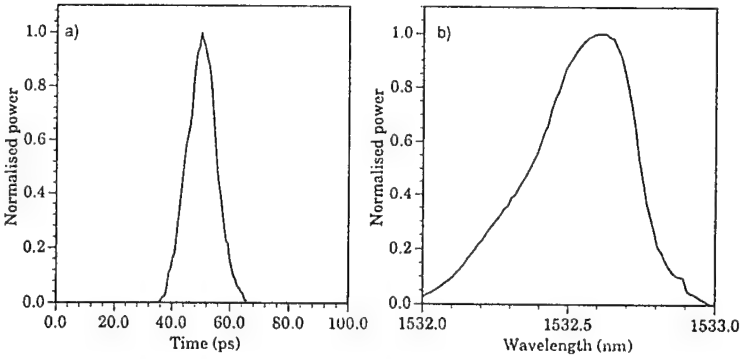

To study the soliton behaviour when $Z_a/Z_0 > 1$, the pulse width, and signal wavelength was then changed to reduce the soliton period. By doing this, the average signal power also had to be adjusted accordingly; the lower Z_0 the higher signal power. At the lowest Z_0=11.3 km, the signal power was 2.1 dBm. From numerical calculations on the d-EDF we expect the signal power excursions to reduce with increasing signal power. Due to the 29.3 km dispersion-shifted single-mode undoped fiber, having a 0.26 dB/km attenuation, the lowest signal power excursions are expected to be close to 7.6 dB. In Fig. 3 we compare the measured TBP (marked by the dots) with results from numerical calculations of soliton propagation, for various signal excursions (± 3.5 dB, ± 4 dB or ± 5 dB) as a function of Z_a/Z_0. In the calculations, we have in agreement with OTDR measurements, assumed that the signal power vary nearly sinusoidally. The measured data in Fig. 3 is not completely consistent with any one of the calculated curves. However, this could not be expected, as the mean signal power of a first order soliton, as mentioned above, will increase with decreasing Z_0, and hence, the measured TBPs will not follow one of the calculated curves. In Fig. 3 the TBP will shift between the three curves, for low Z_a/Z_0, the TBP will nearly follow the curve ± 5B, passing ± 4 dB for medium values of Z_a/Z_0 and ending close to ± 3.5 dB for large Z_a/Z_0 .

From the figure we conclude that stable transmission of solitons over 90.2 km is achievable for Z_a/Z_0

< 0.50. Increasing Z_a/Z_0, the TBP is first increased; but with further increases, the TBP actually decreases. It was not possible to increase the relation Z_a/Z_0 above 7.97 in the measurements, because an input pulse width (T_{FWHM}) less than 6.8 ps could not be achieved.

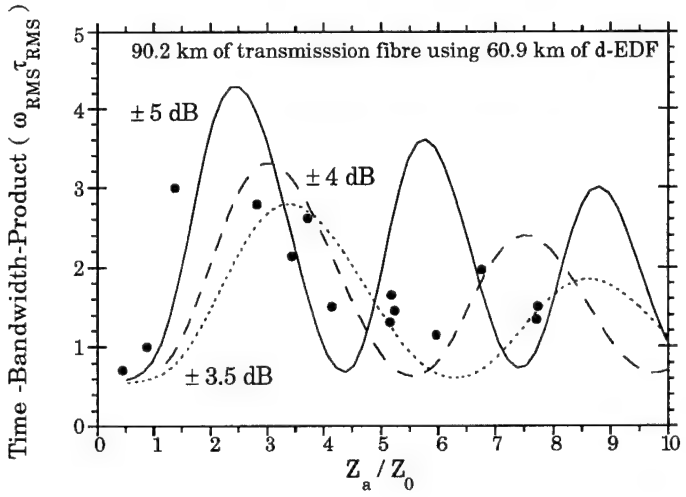

Fig 3: The TBP of the output soliton after 90.2 km transmission as a function of the fraction Z_a/Z_0. Dots are measured values, and the curves are calculated. The amplitude of the sinusoidal signal variation in the numerical calculations was ± 3.5 dB (dotted curve), ± 4 dB (dashed curve).or ± 5 dB (solid curve).

Conclusion:

In the experiments, we have succeeded in transmitting 9.0 ps solitons through a 90.2 km long transmission fiber, without any in-line components, using distributed erbium doped fiber, (Z_a/Z_0 = 0.45). If the bit period is chosen to be 5 times the pulse width in order to avoid interaction between neighbouring solitons, this corresponds to a bit rate of 22 Gbit/s. In agreement with theoretical predictions, our experiments demonstrated that the stability of transmitted solitons can be improved by increasing the ratio of the length of the distributed erbium-doped fiber relative to the soliton period, Z_a/Z_0 greater than 1, assuming that the maximum signal power excursions are kept below a few dB's.

References:

[1] A. Hasegawa and F. Tappert, Appl. Phys. Lett., vol. 23, pp. 142-144, 1973.

[2] L.F. Mollenauer, S.T. Evangelides and H.A. Haus, J. Lightwave Technol, vol. 9, pp. 194-197, 1991.

[3] K. Rottwitt, P. Varming, C. Lester, J.H. Povlsen and J. Elgin, Conf: "Nonlinear Guided Waves and Their Applications", Dana Point, USA, 23-25 Feb. 1995, Paper NFA5, 1995.

[4] A. Hasegawa, Optics Letters, vol. 8, pp. 650-652, 1982.

[5] K. Rottwitt, J.H. Povlsen and A. Bjarklev, J. Lightwave Technol, vol. 11, pp. 2105-2115, 1993.

Optical Filtering Technique for Suppressing Nonlinear Pulse Distortion caused by Long Transmission Distance

Ken-ichi Suzuki, Katsumi Iwatsuki, and Shigendo Nishi
NTT Optical Network Systems Laboratories
1-2356 Take, Yokosuka, Kanagawa, Japan 238-03

Introduction; The optical pulses of around a few pico-seconds required for an ultra-high speed transmission are extremely distorted by the higher order dispersion in the transmission line. Especially in non-repeated transmission, high bit rates require the high fiber-input power to achieve a sufficient signal to noise ratio, thus leading to pulse degradation due to the combination effect of fiber nonlinerity and fiber dispersion. This paper demonstrate a new approach to overcome this pulse distortion with the use of optical filtering. The transmitted pulses generate dispersive waves at the trailing edge which is shifted by fiber nonlinearity into the normal dispersion region, while the main part of pulse spectrum moves to the anomalous dispersion region[1]. Therefore, optical filtering can remove the pulse distortion at the trailing edge[2]. This technique is experimentally confirmed by ultra-short pulse long-distance transmission.

Experimental setup; The experimental setup is shown in Fig. 1. The transmitter was constructed of a gain-switched distributed-feedback laser-diode (GS-DFB-LD) with a 10 GHz repetition rate. These pulses were compressed and shaped with a normal dispersion fiber and a spectral filter. The pulse train was encoded by a Ti:$LiNbO_3$ intensity modulator (LN mod.) driven by a pulse pattern generator (PPG) at 10 Gbit/s (PRBS 2^{23}-1). The encoded pulses are adiabatically compressed with a 2 km dispersion decreasing fiber (DDF). The adiabatically compressed pulses were optically multiplexed with a four stage Mach-Zehnder interferometer type multiplexer fabricated with a Planer Lightwave Circuit (PLC) technology[3], to achieve a 160 Gbit/s single polarized pulse stream. To attain transform-limited pulses and also to make the central pulse wavelength approach the zero dispersion wavelength of the transmission fiber, we employed a 3 nm optical bandpass filter (OBPF1). The attained pulse width and central wavelength were 2 ps and 1552.5nm, respectively.

The pulse stream was injected into a 75 km dispersion shifted fiber (DSF). The zero dispersion wavelength of the DSF was 1553 nm. The dispersion slope was ~0.07 ps/km/nm^2, which corresponds to the higher order dispersion length L_D' of 12.7 km.

The receiver consisted of a timing recovery circuit, an optical demultiplexer, and a 10 Gbit/s optical receiver (OR) following an Er-doped fiber pre-amplifier. The 10 GHz component was

electrically extracted from the 160 Gbit/s multiplexed signal as a clock and provided to a control pulse source for the demultiplexer. The 160 Gbit/s transmitted signal was demultiplexed to 10 Gbit/s with a nonlinear optical loop mirror, which included a traveling wave semiconductor laser amplifier(TW-SLA NOLM) so called TOAD[4], gated with the ~1 ps control pulse[5]. The demultiplexed pulse stream was received with the OR, and the bit error rate(BER) was measured by an error detector (ED).

Experimental results and discussions; Figure 2 shows the wavelength shift of transmitted pulses as a function of averaged power input into the 75 km DSF. The wavelength shift, which casused by the combination of fiber nonlinearity and higher order dispersion, was defined as the wavelength difference between the spectral peak wavelength in the anomalous dispersion region of transmitted pulses and the central wavelength of the initial pulses. The insets in Fig.2 show the spectra of transmitted pulses for each input power. The wavelength shift increased with the input power as shown in Fig.2.

Figure 3 (a) shows the spectrum and streak image of initial pulses. Figures 3 (b) and (c) show the spectra and streak images without and with a 3 nm optical bandpass filter(OBPF2) after transmission. The input power P_{in} to the DSF was 15 dBm, which corresponds to the wavelength shift of around 1.5 nm. The value of P_{in} was experimentally determined to achieve the minimum pulse width of transmitted pulses(2.5 ps) after spectral filtering. When P_{in} was lower than 15 dBm, the spectrum of optical pulses was located in the zero dispersion region due to the small wavelength shift, thus leading to pulse broadening with higher order dispersion. On the other hand, the large wavelength shift at high P_{in} also caused pulse broadening due to anomalous dispersion. As shown in Fig. 3(b), the streak image was degraded by the dispersive wave around the pulse edges in the normal dispersion region, as compared with Fig. 3 (a). As shown in Fig. 3 (c), the temporal waveform was improved by eliminating the optical spectrum in the normal dispersion region, thus suppressing the dispersive wave.

We investigated the BER performance by varying the central wavelength of OBPF2 to confirm the validity of this filtering technique. Figure 4 shows the BER as a function of the central wavelength of OBPF2 at the received power of -23.5 dBm. The input power to the optical demultiplexer was 0 dBm. At wavelengths less than 1554 nm, the BER degraded due to the dispersive wave at the trailing edge of optical pulses. Around the 1554 nm, the BER was improved because of dispersive wave suppression. Figure 5 shows the bit error rate as a function of averaged

received power to the OR at the optimum wavelength of 1554 nm. The closed and open circles correspond to the BER before and after transmission. The insets in Fig. 5 show the eye patterns before and after transmission. Good eye openings were obtained after transmission.

Conclusion; We have demonstrated an optical filtering technique to suppress the pulse distortion generated over long transmission distances. That the dispersive wave at the pulse trailing edge could be removed with this technique, was successfully confirmed by 2 ps pulse transmission over 75 km. Our approach could also realize ultra-fast long-span in-line optical amplifier transmissions.

Acknowledgment; The authors would like to thank Dr. T. Miki, Dr. I. Kobayashi and Dr. M. Saruwatari for their encouragement. They also express their thanks to Mr. S. Kitoh for providing the optical multiplexer.

References

[1]P. K. A. Wai, C. R. Menyuk, H. H. Chen, and Y. C. Lee, "Soliton at the zero-group-dispersion wavelength of a single-mode fiber", Opt. Lett., vol. 12, no. 8, pp. 628-630, 1987.
[2]K. Suzuki, K. Iwatsuki, S. Nishi, and M. Saruwatari, " 160 Gb/s single polarized ultra-short pulses transmission over 62 km wiht fiber nonlinearity near zero dispersion wavelength.", OAA'94 Postdeadline papers, PD8, 1994.
[3]M. Kawachi and K.Jinguji, " Planar Lightwave circuits for optical signal processing.", OFC'94 Technical Digest, FB7, pp.281-282,1994.
[4]J. P. Sokoloff, P. R. Prucnal, I. Glesk, and M. Kane, "A terahertz optical asymmetric demultiplexer(TOAD)", IEEE Photon. Technol. Lett., vol. 5, no. 7, pp. 787-790, 1993.
[5]K. Suzuki, K. Iwatsuki, S. Nishi, and M. Saruwatari, "Error-free demultiplexing of 160 Gbit/s pulse signal using optical loop mirror including semiconductor laser amplifier", Electron. Lett., vol. 30, no.18, pp.1501-1502, 1994.

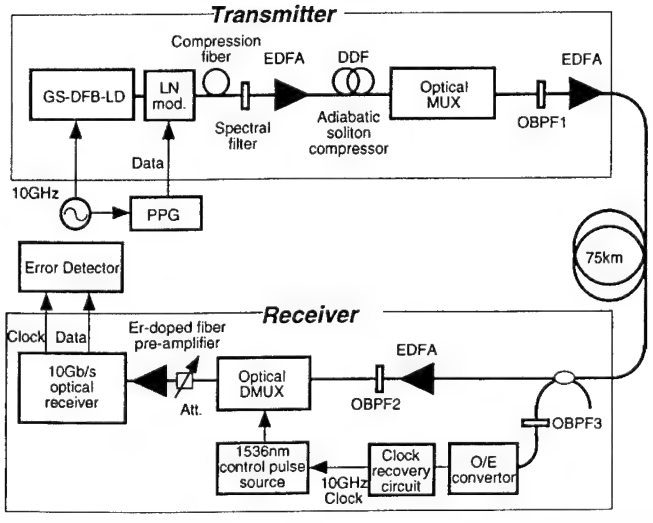

Fig.1 Experimental setup.

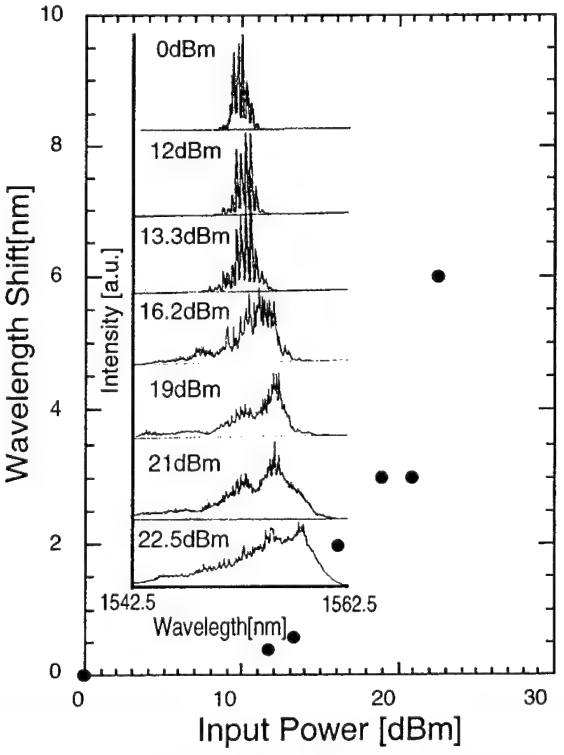

Fig.2 Wavelength shift as a function of input power to the DSF.

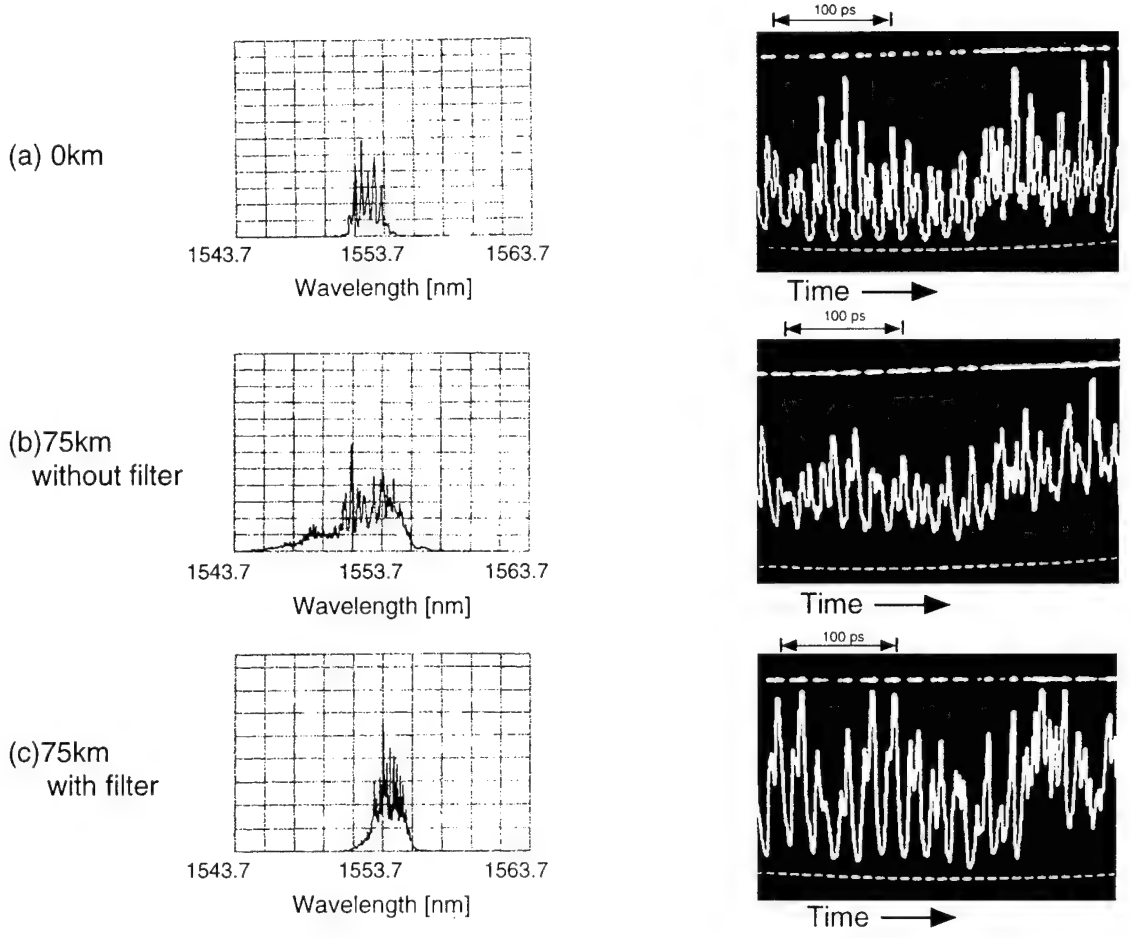

Fig.3 Spectra and temporal waveforms before and after transmission

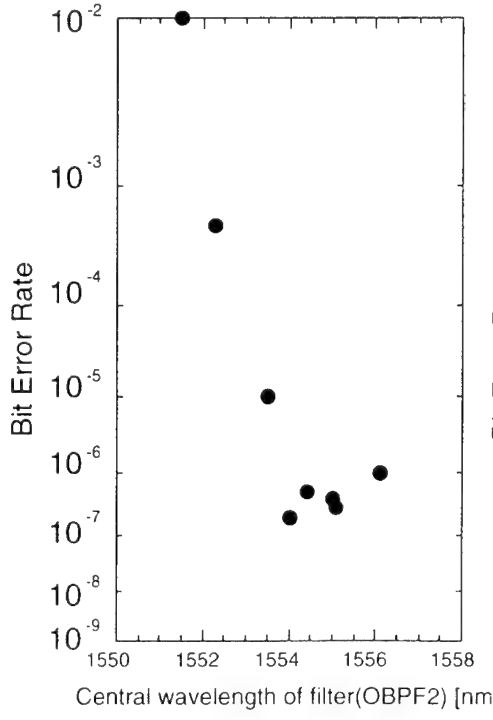

Fig.4 Bit error rate as a function of central wavelength of filter(OBPF2).

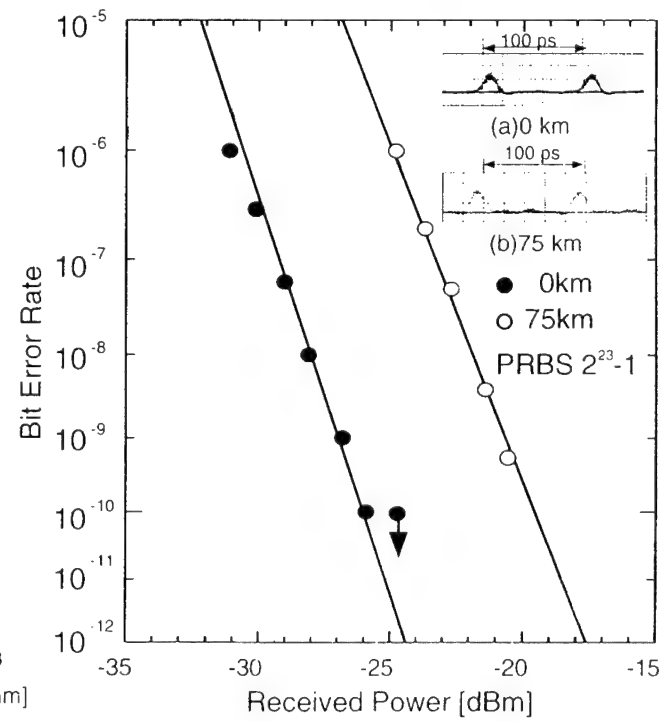

Fig.5 Bit error rate as a functon of avraged raceived power

10Gbit/s signal transmission in a 1600 km line employing distributed erbium-doped fiber to suppress the nonlinear effect

H. Kawakami and T. Kataoka,
NTT Optical Network Systems Laboratories
Y-808, 1-2356 Take, Yokosuka, Kanagawa, 238-03 Japan
Telephone +81-468-59-8554
Facsimile +81-468-59-3396

Introduction

Long span transmission system employing in-line amplifiers is limited by the combined effect of chromatic dispersion and fiber nonlinearity[1, 2]

Distributed erbium-doped fiber line can decrease the highest level without decreasing the lowest level in the system. Thus it is very attractive for in-line amplifier transmission systems with long repeater span.

In this paper, we propose a new system configuration using distributed erbium doped fiber (dEDF) for 50% of the transmission line. By using the dEDF in the transmission line, the repeater span can be expanded to 80km with few spectrum broadening due to fiber nonlinearity. Propagation of a data stream at a 10 Gbit/s are demonstrated over 1600 km in a recirculating loop experiment. It is confirmed that the signal degradation is smaller in the proposed system than in the conventional in-line amplifier system.

Conception of hybrid in-line amplifier system

The hybrid in-line amplifier system proposed in this paper, consists of a lumped optical amplifier, dEDFs, and dispersion shift fiber(DSF) (Fig. 1, line B). Two dEDFs are used at both ends of each transmission span; a DSF is set between the dEDFs. The dEDFs are pumped from both ends of the span. Because the total loss is decreased by the gain of dEDF, the highest level is decreased without decreasing the lowest level in the system, compared to the conventional in-line amplifier system. (Fig. 1 , line A).

Order estimations of the GVD limit and the SPM+GVD limit are shown in Fig. 1 [2]. We assume dispersion is -0.5 ps/nm/km. Signal rate is 10 Gbit/s, and launched power into the lumped amplifier P_{in} is -10 dBm. Though conventional in-line amplifier system (line A)

and hybrid in-line amplifier system (line B) have same GVD limitation, SPM+GVD limit for hybrid in-line amplifier system (line B) is relaxed, because of the decrement of fiber launched power. The solid dot corresponds to the experimental setup mentioned below.

Experiment

The experimental setup is shown in Fig. 2. The light source is a DBR LD frequency modulated for suppressing stimulated Brillouin scattering [3]. Wavelengths were varied (1.551 - 1.553 μm) to change the total dispersion value of the transmission fiber. The intensity modulated signal (10Gbit/s, PRBS23 stages) was output by an LN intensity modulator; the α parameter of its was set to be positive.

For line A, we inserted a 80 km DSF into the loop. For line B, we inserted 23.8 km dEDF, 15.9 km dEDF, and 39.4 km DSF into the loop (Fig. 2). Forward and reverse pump powers at the ends of the dEDFs are 83mW and 79mW, respectively. The gains of dEDFs are -6.2dB and -0.4 dB, respectively (include the loss of WDM and BPF). The signal powers in the loop are shown in Fig. 2 for both lines. Lowest power of line A and line B are the same. NF of line B is larger than NF of line A, because line B has 2 more optical amplifiers; i. e, dEDFs.

The dispersion values of the DSF were ordered to place negative dispersion fiber at the OS side and positive dispersion fiber at the OR side. This arrangement suppresses spectrum broadening [4]. Overall DSF dispersion at 1.5520 μm is -0.01 ps/nm/km, the slope of dispersion is +0.07 ps/nm/nm/km.

The dispersion values of the dEDFs and DSF used in line B were not optimized. Overall dispersion at 1.5520 μm is 0.00 ps/nm/km, the slope of dispersion is +0.07 ps/nm/nm/km.

Result and discussion

The signal spectra after 1600km transmission (20 circuits) are shown in Fig. 3 for both setups. At +100 ps/nm, the spectrum width (20 dB down) of line A is broadened by about 6 times, compared with spectrm width after 80 km (1 circuit) transmission (0.3nm), despite its optimized dispersion arrangement. In the anomalous dispersion region, spectrum broadening is large. At the region from +100 ps/nm, to -100 ps/nm, the spectrum width of line B is broadened by less than 2 times, compared with spectrm width after 80 km transmission (0.3nm). Suppression of spectrum broadening due to the decrease in signal power was confirmed.

The bit error rate after 1600km (20 circuits) in the anomalous dispersion region is shown in Fig. 4. Line A (at +42.0 ps/nm) has an error floor at the error rate of 10^{-9}. Nonlinear effects degrade the

signal. Line B (at +46.0 ps/nm) has no error floor, despite its larger NF.

Conclusion

We propose a hybrid in-line amplifier system consisting of lumped amplifier and dEDF to relax the SPM+GVD limit. 10 Gbit/s signal transmission was demonstrated successfully to 1600km with 80km in-line amplifier spacing in a recirculating loop. We observed the spectrum width and confirmed the suppression of nonlinear effects.

Acknowledgment

We would like to thank Y. Miyamoto, H. Tsuda H. Masuda and Y. Fukada of NTT Optical Network System Laboratories, for their useful discussion. We would like to thank K. Hagimoto of NTT Optical Network System Laboratories, for his advice.

Reference

[1] D. J. Malyon et al., Electron. lett., 27, pp120-121 (1991).
[2] A. Naka and S.Saito, Electron. lett., 28, pp 2221-2222 (1992).
[3] Y. Aokiet al., Technical report of IEICE, 91, pp75-80 (1991).
[4] N. Henmi et al., J. Lightwave Technol., 11, pp1615-1621 (1993).

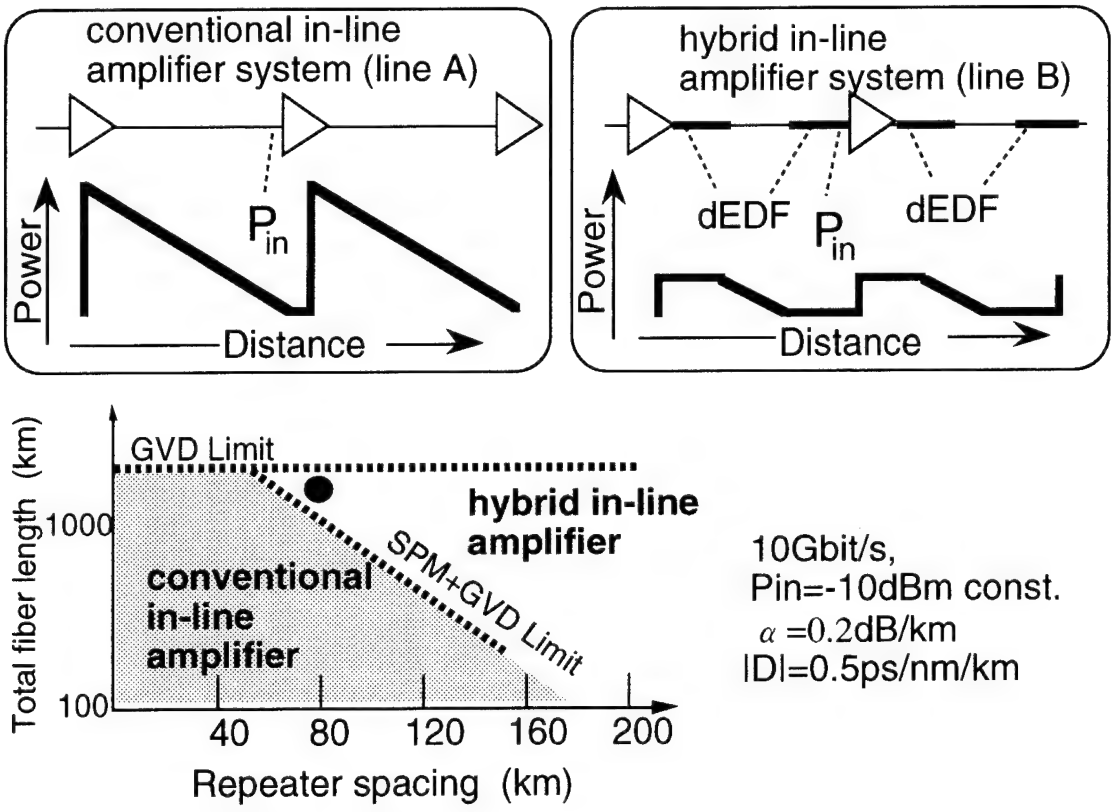

Fig. 1 Concept of hybrid in-line amplifier system

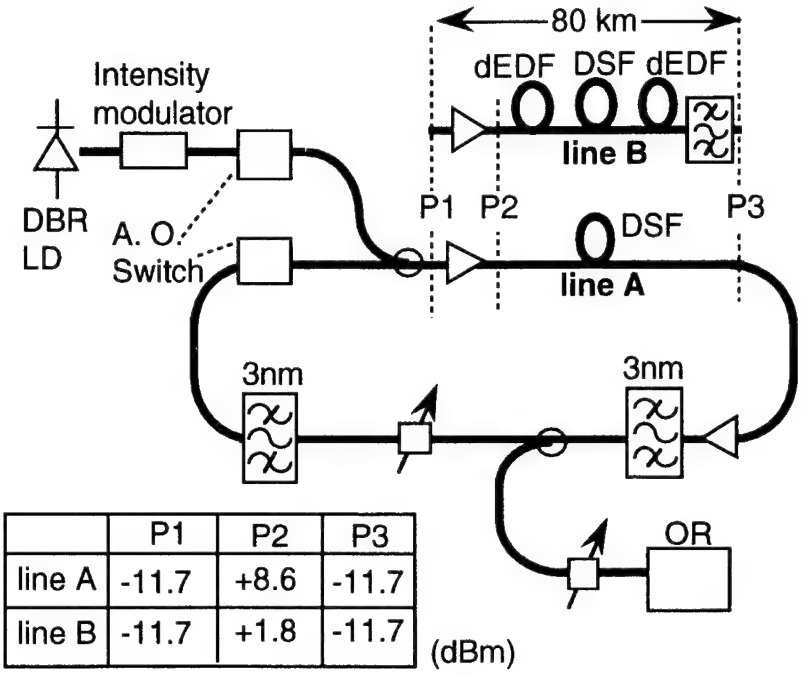

	P1	P2	P3
line A	-11.7	+8.6	-11.7
line B	-11.7	+1.8	-11.7

(dBm)

Fig. 2 Experimental setup

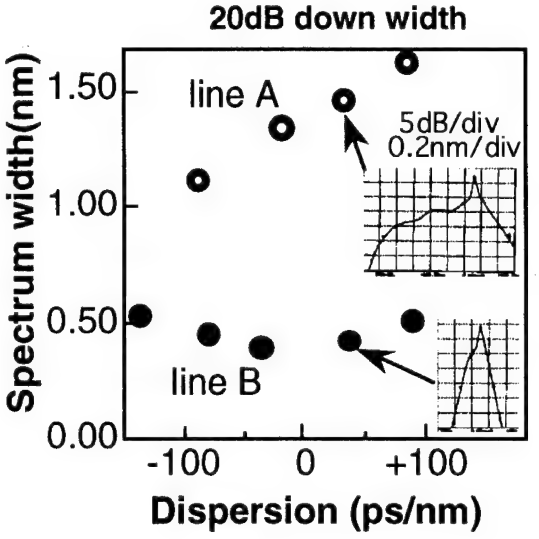

Fig. 3 Spectrum broadening after 1600 km transmission

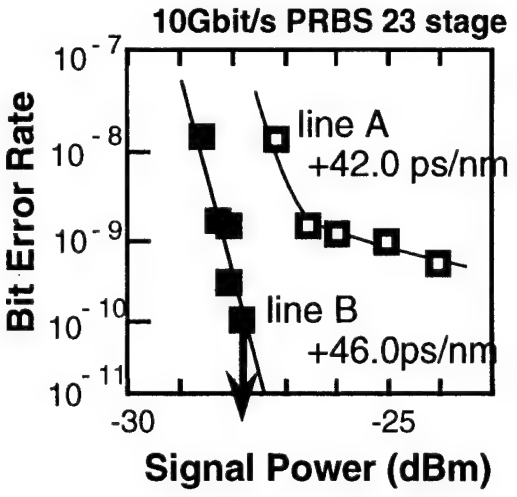

Fig. 4 Bit error rate after 1600 km transmission

Long-haul Transmission using Actual Optical Amplifier Submarine Cable Systems

Toshio Kawazawa, Koji Goto, Tomohiro Otani, Haruo Abe,
Masando Tanaka, Hitoshi Yamamoto and Hiroharu Wakabayashi

KDD Submarine Cable Systems Department
2-3-2 Nishi-shinjuku, Shinjuku-ku, Tokyo, 163-03, Japan

TEL: +81-3-3347-7362
FAX: +81-3-3347-5287

Introduction Transmission performance of an optical amplifier repeater system has been intensively investigated and confirmed through long-haul testbed experiments[1]-[2]. Now, several optical amplifier communication systems are under installation all over the world. We have conducted the research and the development of optical amplifier technologies to implement optical amplifier submarine cable systems[3]-[4], and the developed system is named OS-A system. This OS-A system has four sub-systems at maximum and each sub-system transmits 5.3 Gbit/s signal . Development of OS-A system has been successfully conducted and the system is to be applied to TPC-5 Cable Network (TPC-5CN).

In this paper, we report the signal transmission capability beyond the design target in two actual systems for the purpose of confirming that the system implementation has been successful with the minimum design offset in manufacturing. One system is Type-A designed as 1,000km cable system with 85km repeater spacing and the other is Type-B designed as 3,000km cable system with 60km repeater spacing. We have successfully achieved the 5.3Gbit/s signal transmission over 4,000km for Type-A and 11,300km for Type-B.

OS-A Systems Table 1 shows the major design parameters of OS-A systems. The repeater uses Er-doped fiber amplifier and the optical submarine cable mainly consists of dispersion shifted fibers (zero dispersion wavelength λ_0 = 1.55μm) and conventional optical fibers (λ_0 = 1.3μm) for compensation in system chromatic dispersion. By means of such dispersion management, we have well suppressed the effect of fiber non linearity associated with fiber chromatic dispersion. In both systems, the nominal signal wavelength is 1558.5nm, and the repeater gain peak and optical submarine cable zero dispersion is designed at 1558.5nm under sea environment.

Experiments and Results Two fiber pairs in both types are connected as shown in Fig. 1 to investigate the transmission performance beyond the design target. The optical attenuators are inserted between each sub-system to adjust the repeater input power to the nominal level.

To evaluate the transmission quality, the BER and Q performance were investigated. The 2^{23}-1 pseudo random NRZ optical signal was used and the value of Q is measured by an error detector[5]. We have confirmed the error-free signal transmission to the distance which is the longest that we can make a configuration of in each type, and obtained the Q^2 value of 19.2dB (corresponding to BER=2.7×10^{-20}) at 4,000km with 85km spacing (type-A) and 16.4dB (BER=2.1×10^{-11}) at 11,300km with 60km spacing(Type-B). Fig. 2 (a) shows an example of the measured data at at the maximum distance in Type-B for the logarithm of the BER versus the decision threshold in the decision circuit of the error detector. From this figure, the value of Q^2 is calculated to be 16.4dB. Since this evaluation was done in the room temperature, λ_0 (zero dispersion wavelength) didn't match to the system gain peak, which may cause some penalty. To investigate the stability of the value of Q at the maximum distance, the value of Q^2 was continually measured. As shown in Fig. 2 (b) for the Type-A, we have achieved the error-free signal transmission for about one hour and the standard deviation of measured Q^2 was 0.06 dB which was almost a measurement error. These results of the high performance shows that we could manage to suppress the various system impairments possibly caused by manufacturing offsets from the design centers.

Next Figure 3 shows the C/N (Carrier to Noise ratio) characteristic which is one of important parameters to evaluate system performance, defined here as the ratio of signal power to ASE power with 0.5nm bandwidth in each type. In this measurement, the depolarized CW (Continuous Wave) light source at 1558.5nm and the optical spectrum analyzer were used. The noise level at the signal wavelength is estimated from the fitting curve of accumulated ASE level. Solid and dotted lines show calculated value based on the linear model, which does not include fiber non linearity, PHB (Polarization hole burning) , and saturation effect of EDF, but does take into account of the measured repeater gain, the repeater noise figure and the fiber loss. The measurement results well agree with the calculated curve. The difference between measured data and calculated data is large as the repeater number increase. Degradation due to PHB of repeaters was confirmed by 3dB at 11,300 km with a polarization scrambler.

FWHM (Full Width Half Maximum) of accumulated ASE was measured to confirm the self-filtering effect in concatenated repeaters[6]-[7]. The optical resolution bandwidth of an optical spectrum analyzer was 0.1nm. As seen in Fig. 4, the accumulated ASE FWHM is obviously getting narrower according to the repeater's number. For example, after the 11,300km transmission, the ASE FWHM is as narrow as about 1.7nm due to self-filtering effect of concatenated repeaters, and the data coincides to the logarithm curve well.

The PMD is measured by Jones Matrix of wavelength scanning method[8] . These systems states of polarization were stable during the scanning wavelength with tunable laser for one PMD measurement. The measured PMD of these system was very small and well fitted to the

theoretical curve based on the square-root length rule, as shown in [9] , whose coefficient is 0.08 $ps/\sqrt{km}$. Some data points were scattered around this curve because they depend on the modal birefringence axes of optical fibers at the many splicing points.

Conclusion We have successfully achieved the 5.3 Gbit/s optical signal transmission without any bit errors over 4,000km with 85 km optical amplifier repeater spacing and 11,300km with 60km spacing, which were far beyond the design target distance in the actual submarine cables and repeaters. Such performance are attributed to the well controlled manufacturing, design, and development of the OS-A system.

Reference

[1] N. S. Bergano, et al, "9,000km, 5Gbit/s NRZ transmission experiment using 274 Erbium-doped fiber amplifiers", OAA '92, PD 11, pp.48-51, 1992.

[2] H. Taga, et al, "10Gbit/s, 9,000km IM-DD Transmission experiments using 274 Er-doped fiber amplifier repeaters", OFC '93, PD1-1, pp.9-12, 1993.

[3] S. Akiba, et al, "Recent progress of transoceanic optical amplifier transmission system", ECOC '92, pp.719-726, 1992.

[4] H. Wakabayashi, et al, "OS-A Optical amplifier submarine cable system", Suboptic '93, pp155-160, 1993.

[5] N. S. Bergano, et al, "Margin measurements in optical amplifier systems", IEEE Photon. Technol., Lett., pp.304-306, 1993.

[6] C. R. Giles, et all, "Propagation of signal and noise in concatenated Erbium-Doped fiber optical amplifiers", IEEE J. Lightwave Technol., pp.147-154, 1991.

[7] B. M. Desthieux, et all, "Theoretical and experimental study of self-filtering effect in concatenated erbium-doped fiber amplifiers", IEEE J. Lightwave Technol., pp.1405-1411, 1994.

[8] B. L. Hefner, "Automated measurement of polarization mode dispersion using Jones matrix eigen analysys", IEEE Photonics Technol. Lett., 1992, pp.1066-1069.

[9] Y. Namihira, et all, "PMD reduction of optical fiber cables for transoceanic optical amplifier submarine cable systems", IWCS '93, pp.655-664, 1993.

Item	unit	Short-haul (Type-A)	Middle-haul (Type-B)
System Length	km	1,000	3,000
Repeater Spacing	km	85	60
Signal wavelength	nm	1558.5	1558.5
Transmission bit rate	Gbit/s	5.3	5.3
System Fiber paires		2	2
Fiber Transmission Loss	dB/km	0.21	0.21
Repeater Output Level	dBm	+4	+4
Repeater Input Level	dBm	-14.5	-9
Repeater Gain	dB	18.5	13
Repeater Noise Figure	dB	less than 6	less than 6

Table 1 OS-A system Major design parameters

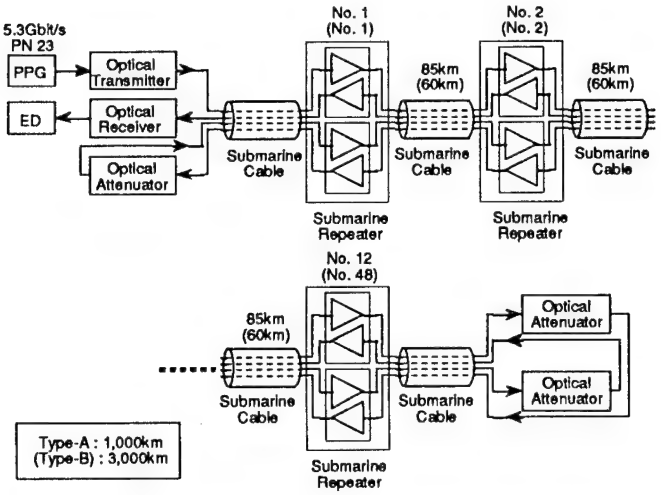

Fig. 1 Schematic of measurement setup and system configuration.

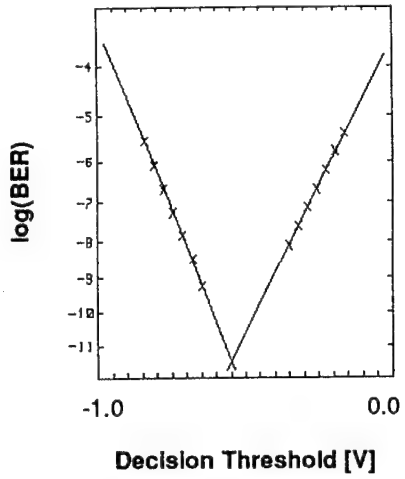

(a) BER versus the decision threshold at 11,300km for Type-B.

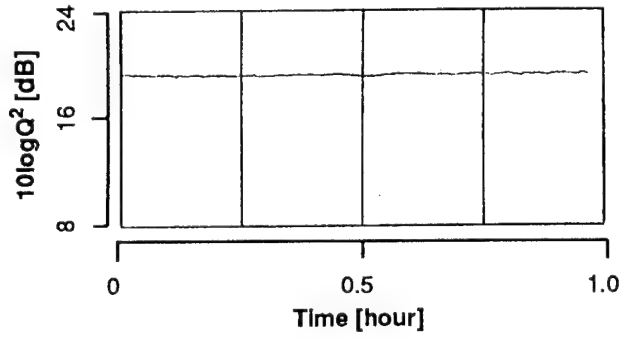

(b) The stability of measured Q at 4,000km for Type-A.

Fig. 2 The example of Q factor measurement.

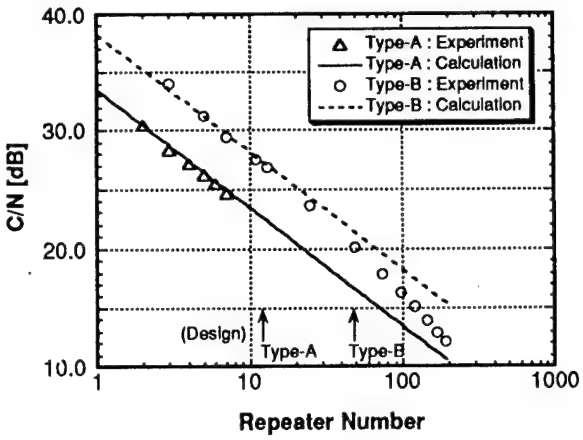

Fig. 3 Carrier to noise ratio dependence on the number of optical submarine repeaters.

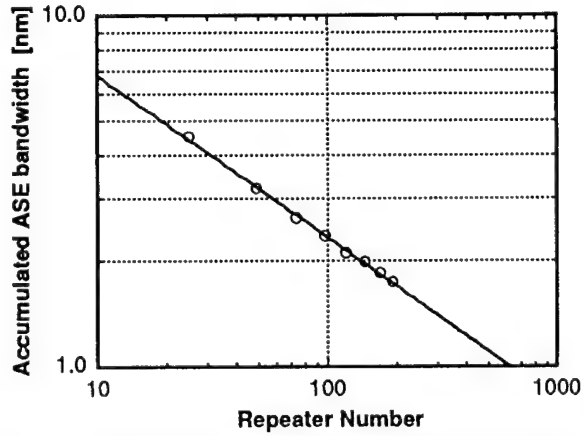

Fig. 4 Accumulated ASE bandwidth dependence on the number of optical submarine repeaters for Type-B.

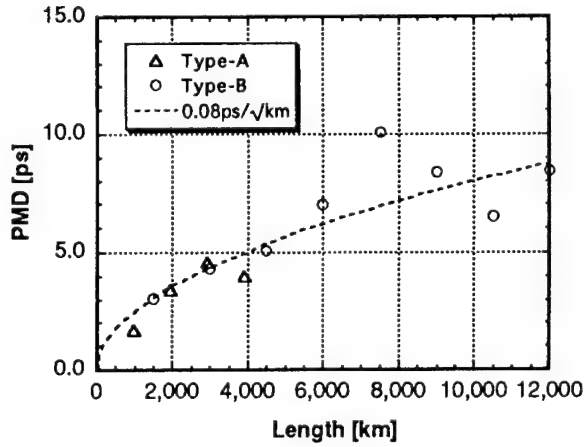

Fig. 5 PMD dependence on system fiber length.

Friday, June 16, 1995

Amplifier Performance and Characteristics

FC 14:00-15:30
Theatersaal

Michael N. Zervas, *Presider*
Southampton University, U.K.

A low-cost intrinsically low-distortion EDFA design for AM-CATV applications with a wide input power and wavelength range

F.W. Willems, J.C. van der Plaats
AT&T Network Systems Nederland B.V.
P.O. Box 18, 1270 AA Huizen, The Netherlands

D.J. DiGiovanni, M.J. Andrejco, P. Wysocki and J. Aspell
AT&T Bell Laboratories
600 Mountain Avenue, P.O. Box 636, Murray Hill, NJ 07974, USA

Abstract We present a 980 nm pumped low-cost EDFA design for AM-CATV applications with intrinsic low distortion and noise-figure over a wide input power and wavelength range by using an optimized Erbium Doped Fibre.

1 Introduction

An EDFA for analogue applications differs from its "digital" counterpart in that care must be taken to reduce its inversion locked gain-slope which causes second order distortion in systems employing directly modulated 1.5 μm DFB lasers [1]. Several approaches have been reported to tackle the problem, however they require an increase in the number of components compared to a standard EDFA, or tuning to a specific wavelength and input power [2, 3]. An EDFA design has been reported which has none of these disadvantages[4], but works in a limited wavelength and input power range. In this paper we will report on the design of an EDFA for analogue applications using an Erbium doped fiber that requires no tuning, enables the use of the smallest number of components possible and still fulfills the stringent requirements for operation in current lightwave AM-CATV systems over a very wide input power and wavelength range. In addition it is shown that the gain-slope can be approximated well by the ASE-slope, which enables low-cost characterization of the distortion caused by an EDFA.

2 Theoretical background

The CSO (Composite Second Order) distortion caused by the interaction of laser chirp and gain-slope of an EDFA is given by the product of the number of distortion products that generate second order distortions, N_{CSO} (determined by frequency channel allocation for a particular CATV system), and harmonic distortion from one of those products. We found, using Giles modeling [5], that the total second order harmonic distortion caused by gain-slope is given by

$$CSO_{gsl,edfa} = N_{CSO} \cdot \left(\frac{1}{2}\beta L\left[\frac{\partial\alpha(\nu)}{\partial\nu}(\overline{\bar{n}_2(z)} - 1) + \frac{\partial g^*(\nu)}{\partial\nu}\overline{\bar{n}_2(z)}\right]\right)^2 \quad (1)$$

with β the laser chirp in Hz/mA, L the fibre length, α the absorption in Np/m, ν the optical frequency, g^* the stimulated emission in Np/m and $\overline{\bar{n}_2(z)}$ the averaged (time and location z) Erbium ion inversion level. This equation tells us that the distortion can be minimized by three parameters: the Erbium doped fiber length, the average inversion, and the emission and absorption profiles. These parameters also determine the noise figure and output power, and therefore a balance must be found between them to make the EDFA fulfill the specification. Note that the harmonic distortion vanishes if we zero the term between square brackets in eq.1, i.e. if

$$\frac{\partial g^*(\nu)}{\partial\nu} = \left(\frac{1}{\overline{\bar{n}_2(z)}} - 1\right)\frac{\partial\alpha(\nu)}{\partial\nu} \quad (2)$$

In practice this implies that in the signal wavelength range the emission and absorption slope

must be proportional. E.g. with $\overline{\bar{n}_2(z)} \approx 0.8$, this proportionality constant is around 0.25, which is the case for wavelengths between 1540 and 1560 nm, using the fiber discussed here (see figure 1). We can rewrite equation 1 to translate

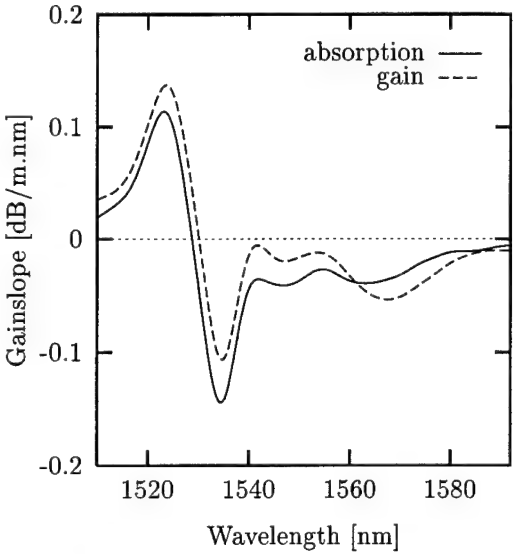

Figure 1: Measured derivatives of emission and absorption spectra

it into system-relevant parameters:

$$CSO_{gsl,edfa} = N_{CSO} \cdot \left(\frac{\ln 10}{20} \frac{\lambda^2}{c} \eta_{FM} m I_o \frac{dG}{d\lambda} \right)^2 \quad (3)$$

with η_{FM} the laser chirp in Hz/mA, m the modulation index per channel, I_o the bias minus threshold current in mA, and $\frac{dG}{d\lambda}$ the gain-slope of the EDFA in dB/m.

3 Specification and results

The system related device specifications can be found in table 1. The parameter of interest is the inversion locked gain-slope which should stay below 0.16 dB/nm to enable the EDFA to work well in one of the most demanding frequency plans, the 42 channel NTSC allocation, with broad input power ranges. Negative values of the gain slope help to reduce the intrinsic second order distortion of most transmitter lasers since the amplitude and wavelength modulation are in phase, respectively π radians out of phase with

Signal wavelength	1540 - 1560nm
Input power range	-3 - +7 dBm
Min output power	12.0 dBm
Max Noise figure	5.5 dB
Max Laser chirp	90 MHz/mA
Modulation index/ch	0.05
Max mod. current	30 mA
Max CSO count	124
Max EDFA CSO	-73 dBc
gain-slope range	**-0.4 ... 0.16 dB/nm**

Table 1: System specification

the current modulation and can therefore be tolerated [6] if the EDFA induced distortion power stays below that of the laser. Since typical intrinsic second order distortion will be around -65 dBc, we require that the gain slope stays above -0.40 dB/nm.

We propose a simple EDFA configuration as shown in figure 2 using 55 mW from a single 980 nm pump and a very efficient Erbium Doped Fibre of which the derivatives of the measured emission and absorption profiles are shown in figure 1. Modeling shows that the output power

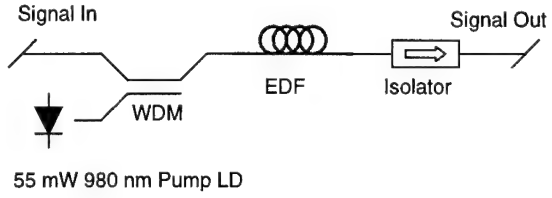

Figure 2: Proposed configuration for an analogue EDFA

and noise figure specifications are satisfied (see figure 3) as well as the gain-slope specification between 1540 and 1560 nm. We could not see any degradation of the CSO of -65 dBc, when the EDFA was inserted in an analog CATV system at the available wavelength of 1555 nm. (see figure 4).

4 Measurement Method

We have verified the modeling for -3 dBm input power. The gain-slope under saturated and inversion locked conditions can be approximated

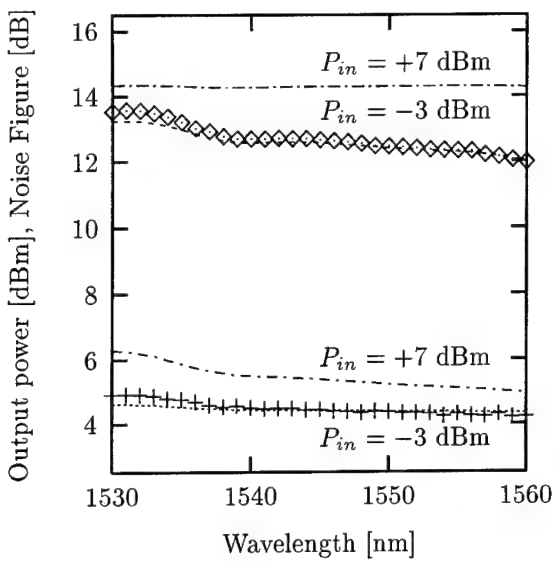

Figure 3: Output power and noise figure as function of wavelength with signal input power as parameter. Diamonds and plus signs represent measured data

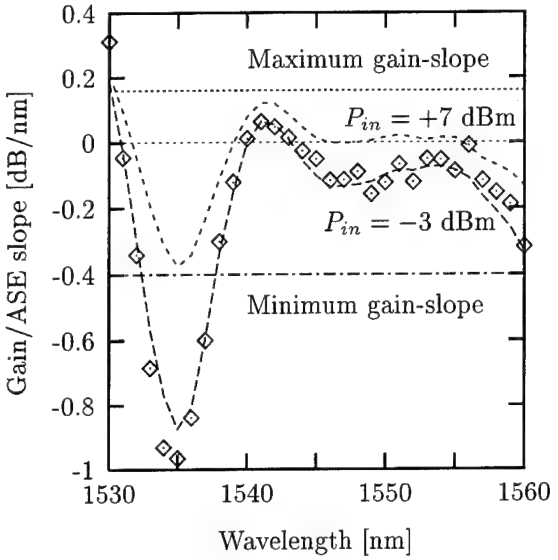

Figure 4: Gain/ASE-slope in dB/nm as function of signal wavelength with signal input power as parameter. Diamonds represent measured data.

by the ASE-slope, which can be measured by using the equipment for the noise figure determination using the well known polarization nulling technique. The validity of the approximation can be made clear by the following argument: the ASE power in Watts is given by $p_{ASE} = 2n_{sp}(g-1)h\nu B_o$, with n_{sp} the average Erbium inversion factor, g the gain in linear units and B_o the optical bandwidth. We find for the gains above 10 dB to a very good approximation that, in dB/nm, $\frac{dP_{ASE}(\lambda)}{d\lambda} \approx \frac{dG(\lambda)}{d\lambda}$ i.e. the gain-slope equals the ASE slope. Giles modeling has verified this simple treatment.

Figure 5 shows the setup to measure the ASE slope. It contains a Tunable External Cavity Laser (TECL) that emits a polarized signal with a linewidth around 50 kHz. After the device under test, an EDFA, we have positioned an isolator to avoid reflections to enter the EDFA. With a polarization controller, the polarization input state to the polarizer is adjusted. Thus it is possible to view on the Optical Spectrum Analyzer (OSA), the (amplified) signal, and/or half of the randomly polarized ASE from the EDFA, depending on the position of the polarization controller. A computer controls both the TECL and the OSA. In fact this is the setup for measuring the noise figure with the polarization nulling technique. Figure 6 shows that over a wide input power and wavelength range, the ASE-slope measurement corresponds with Giles modeling of both the Gain and ASE-slope.

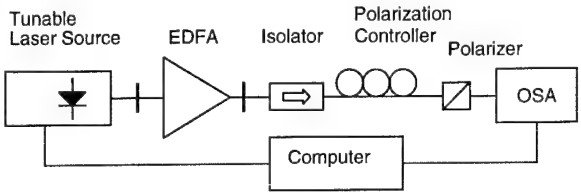

Figure 5: Experimental setup to measure the ASE-slope

5 Conclusions

We have demonstrated that it is possible to design a simple, low-cost EDFA that fulfills the stringent requirements for AM-CATV systems employing currently available directly modulated DFB laser diodes.The EDFA has intrinsically a low second order distortion over a very wide input power and wavelength range and still does not use wavelength flattening components or compensation elements that need tuning, but instead uses an Erbium doped fiber with optimized emission and absorption profiles. In ad-

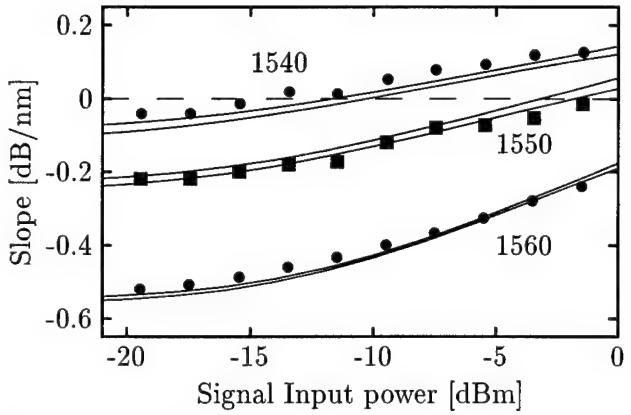

Figure 6: ASE-slope corresponds to gain-slope for a range of input powers and wavelengths. Three pairs of solid lines are from Giles simulations of ASE-slope (upper line) and gain-slope.

dition we described a low-cost method to characterize the gain-slope of an EDFA, based on measuring the ASE-slope under inversion locked conditions.

6 Acknowledgments

This work was partly supported by the Commission of the European Union under the RACE II program, project R2062, "COMFORT".

References

[1] S. L. Hansen, P. Thorsen, K. Dybdal, and S. B. Andreasen, "Gain tilt of Erbium-doped fiber amplifiers due to signal-induced inversion locking," *IEEE Photonics Technology Letters*, vol. 4, pp. 409–411, Apr. 1993.

[2] M. Shigematsu, H. Go, M. Kakui, and M. Nishimura, "Distortion-free optical fiber amplifier for analog transmission based on hybrid Erbium doped fiber configuration," in *Optical amplifiers and their applications, OAA'94, Breckenridge*, pp. 162–164, Aug. 1994. Paper FD2.

[3] H. Nakamura, S. Ichino, H. Hayakawa, and H. Ogoshi, "CSO distortion suppression by gain spectrum control of cascaded EDFAs," in *Optical amplifiers and their applications, OAA'94, Breckenridge*, pp. 127–129, Aug. 1994. Paper FB2.

[4] D. Lipka and D. Werner, "Design of erbium doped fibre amplifiers with minimised gain tilt for CATV transmission systems," *IEE Electronics Letters*, vol. 30, pp. 1940–1941, Nov. 1994.

[5] C. R. Giles and E. Desurvire, "Modeling Erbium-Doped Fibre Amplfiers," *IEEE Journal of Lightwave Technology*, vol. 9, pp. 271–283, Feb. 1991.

[6] J. Ohya, H. Sato, and T. Fujita, "Cancellation of Second-order distortion of directly modulated laser in Erbium-doped fiber," *IEEE Photonics Technology Letters*, vol. 4, pp. 414–416, Apr. 1993.

AC Gain Tilt Variations With Gain Compression In Erbium Doped Fiber Amplifiers

J. Nilsson, S. J. Kim, S. H. Lee, and W. H. Choe

Opto-Device Lab, Samsung Advanced Institute of Technology, P. O. Box 111, Suwon, Korea 440-600
Phone +82 331 280 9328, Fax +82 331 280 9349, E-mail nilsson@saitgw.sait.samsung.co.kr

Introduction

Recently, the use of erbium-doped fiber amplifiers (EDFAs) in amplitude modulated (AM) sub-carrier multiplexed (SCM) CATV networks has attracted considerable attention [1], [2], [3], [4], [5]. For AM SCM signals, AC gain tilt in the EDFAs leads to signal degradation through composite second order (CSO) nonlinear distortion [5], [6], [7], [8], [9], [10]. Therefore, the AC gain tilt needs to be controlled.

In this paper, we present measurements on how the AC gain tilt changes when the gain is changed, and compare the results to theory. Theoretically, the AC gain tilt change can be evaluated from a knowledge of the absorption spectrum of the fiber only, under the important assumption that the gain is homogeneously broadened. We verify the validity of the expression experimentally, for gain variations induced by a pump power reduction, gain saturation, and cross-saturation, although discrepancies that may be caused by spectral holeburning appear to be present at some wavelengths. We also verify that the result is independent of fiber length. The results are relevant for the design of EDFAs for AM SCM CATV networks. They can be used for predicting how much the signal powers in the network can deviate from intended ones before the gain tilt becomes too large. The amount of deviation depends on the signal wavelength. Thus, some signal wavelengths will be less suitable than others, from this point of view.

CSO distortions result from a combination of transmission laser chirp and AC gain tilt. For AM TV, CSO should not exceed -60 dBc (cf. e.g. [3]). This leads to the requirement that the AC gain tilt should typically not exceed 0.2 dB/nm [10] for a chirped laser linewidth of 10 GHz, although the maximum allowable AC gain tilt is inversely proportional to the chirp [5], [6], [7], [9], [10].

Theoretical

Let T_{AC} be the AC gain tilt in an EDFA, defined by

$$T_{AC}(n_2,\lambda) \equiv \frac{\partial G(n_2,\lambda)}{\partial \lambda} \tag{1},$$

where $G(n_2, \lambda)$ is the gain in dB at a given wavelength λ and with an average fraction n_2 of the Er^{3+}-ions in the metastable state. Only the metastable state $^4I_{13/2}$ and the ground state $^4I_{15/2}$ are assumed to be populated. Note that n_2 is constant when T_{AC} is evaluated [9], [10]. If the gain is homogeneously broadened, it can be shown [11] that the derivative of the AC gain tilt at a wavelength λ with respect to the gain at the same wavelength is given by:

$$\beta(\lambda) \equiv \frac{dT_{AC}(n_2,\lambda)}{dG} = \frac{\frac{dg(\lambda)}{d\lambda} + \frac{d\alpha(\lambda)}{d\lambda}}{g(\lambda)+\alpha(\lambda)} \tag{2},$$

where $\alpha(\lambda)$ is the absorption spectrum of the erbium doped fiber (EDF), and $g(\lambda)$ is the gain of the EDF at complete inversion, i.e., for $n_2 = 1$. Both $\alpha(\lambda)$ and $g(\lambda)$ are in dB/m. Furthermore, $\alpha(\lambda)$ and $g(\lambda)$ can either both exclude or include background losses such as scattering [11]. Equation 2 is only valid if the gain change dG is caused exclusively by a change of the average excited state population n_2.

Equation 2 can be interpreted as follows: If the gain compression caused by a signal at a wavelength λ decreases by 1 dB (i.e., the gain increases by 1 dB), the AC gain tilt at this wavelength will change by β dB/nm, if the wavelengths in Eq. 2 are measured in nanometers. Thus, Eq. 2 is an expression for how the gain tilt changes as the gain is varied. We will call β the normalized AC gain tilt change. Since the right hand member of Eq. 2 is a constant which only depends on the intrinsic properties of the transverse cross-section of the EDF, also β will be independent of between which values the gain changes as well as of the fiber length. In addition, it does not matter how the gain is changed, as long as it is caused only by a change of the population inversion of the Er^{3+}-ions n_2.

The following expression by McCumber [12], verified for EDFAs in [13] can be used to approximately calculate $g(\lambda)$ if $\alpha(\lambda)$ is known:

$$g(\lambda) = \alpha(\lambda)\exp\left[\frac{hc/\lambda_c - hc/\lambda}{kT}\right] \tag{3},$$

where h is Planck's constant, c is the speed of light, k is Boltzmann's constant, T is the temperature, and λ_c is a cross-over wavelength, where the sizes of the gain at complete inversion and absorption are equal. Equation 3 is normally given as a relation between the cross-sections for absorption and stimulated emission, but is equally valid for $\alpha(\lambda)$ and $g(\lambda)$. However, in this case, the used spectra $\alpha(\lambda)$ and $g(\lambda)$ must exclude the background losses. With Eq. 3 in Eq. 2, we get the following expression for the normalized AC gain tilt change:

$$\beta(\lambda) \equiv \frac{dT_{AC}(n_2,\lambda)}{dG} = \frac{\frac{d\alpha(\lambda)}{d\lambda}}{\alpha(\lambda)} + \frac{hc}{\lambda^2 kT\left(1+\exp\left[-\frac{hc/\lambda_c - hc/\lambda}{kT}\right]\right)} \qquad (4).$$

The evaluation of Eq. 4 requires only knowledge of the shape of the Er^{3+}-induced absorption, which is one of the most basic characteristic of an EDF. It is independent of any possible wavelength-dependent linear (i.e., power independent) filtering and background loss. It is also valid for a cascade of EDFAs, provided the EDFAs are made from EDFs with the same properties, and the gain variation and tilt change are measured from the input of the first EDFA to the output of the last one. The assumptions of Eq. 4 are that Eq. 3 is valid, and that the gain is homogeneously broadened. The first of these assumptions can be relaxed if Eq. 2 is used instead of Eq. 4.

Experimental

In order to determine whether Eq. 4 is valid, the gain of an EDFA was measured under various conditions. Then, $\beta(\lambda)$ was calculated with Eq. 4, both according to its definition and to the derived expression. The EDF was a standard Er^{3+}:Al^{3+}:Ge^{4+}:silica glass fiber, fabricated with the solution doping method. Its Al^{3+}-content was high, and its Ge^{4+}-content low. The EDFA was pumped by a laser diode at 980 nm. The gain was measured with a standard method, namely, with the help of a modulated probe laser and a lock-in amplifier. It is important that the light beam used for the measurement of the gain is small, so that it does not affect the population inversion. From the gain measurements, the gain tilt was evaluated according to Eq. 1. Subsequently, the gain tilt change dT_{AC} and the gain change dG were calculated, so that β could be evaluated according to its definition. Furthermore, the absorption spectrum of the fiber was measured, and used for the evaluation of β according to the rightmost member of Eq. 4.

Figure 1 shows β as the pump power was changed. The fiber length was 22 m. Furthermore, β calculated from the absorption spectrum is also shown. Two conclusions can be drawn from Fig. 1: Firstly, β is independent of the pump power (i.e., the value of the gain or n_2), since three curves with different pump powers involved coincide. Secondly, those three curves also coincide with the one calculated from the absorption spectrum. Hence, Eq. 4 is valid in this case. Moreover, the value of β (evaluated from $\alpha(\lambda)$) is between -0.01 dB/nm/dB and -0.04 dB/nm/dB in the wavelength range 1545 nm to 1565 nm, normally considered for AM CATV. At 1545 nm, β = -0.009 dB/nm/dB, at 1555 nm, β = -0.015 dB/nm/dB, and at 1565 nm, β = -0.044 dB/nm/dB. Thus, for a wavelength of 1565 nm, a gain change of 5 dB is sufficient for changing the AC gain tilt from zero to a value where CSO becomes unacceptable. This limits the use of gain saturation for automatic power control in AM CATV systems. On the other hand, at 1545 nm, the gain can change by 20 dB while the gain tilt remains below 0.2 dB/nm, if T_{AC} = 0 initially.

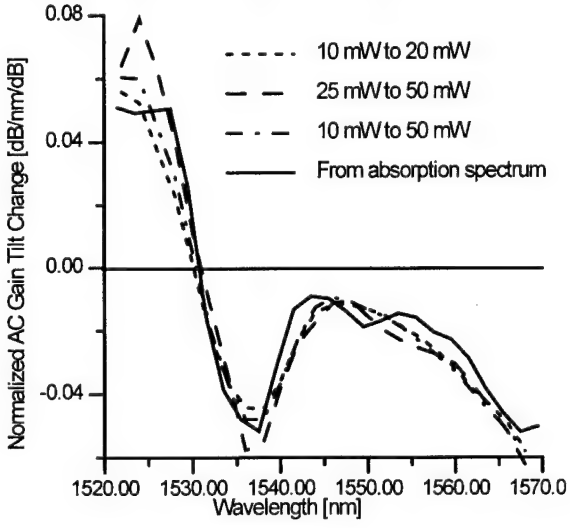

Fig. 1. Normalized AC gain tilt change vs. wavelength, calculated from the absorption spectrum (solid line), and measured as the pump power changes. Short dash: Measured β as the pump power is changed from 10 mW to 20 mW. Long dash: Measured β as the pump power is changed from 25 mW to 50 mW. Chain dash: Measured β as the pump power is changed from 10 mW to 50 mW.

To further test the validity of Eq. 4, β was also measured for different fiber lengths. The result is depicted in Fig. 2, again together with the curve calculated from the absorption spectrum. Also in this case, good agreement is obtained. From the curves in Figs. 1 and 2, we can conclude that Eq. 4 is valid for a wide variety of pump powers, pump and EDF lengths, when the gain and gain tilt change are brought about by a pump power variation.

EDFs at room temperature are partially inhomogeneously broadened, and some spectral hole burning effects have been reported [14]. Spectral hole burning can invalidate Eqs. 2 and 4, since the gain will change in a non-uniform way. The amount of homogeneous and inhomogeneous broadening is different for different EDFs, since it depends on the host glass composition [15]. In an inhomogeneously broadened system, the population inversion is wavelength-dependent. The effect of this should be most noticeable if a strong beam resonant with the transition between the ground and metastable state is launched into the fiber, e.g. a pump at 1.48 μm or a strong saturating signal. This is especially relevant for AM CATV systems, since any used EDFAs will operate in saturation. Therefore, we investigated the validity of Eq. 4 when the gain was compressed by a strong saturating signal, first at 1532 nm and then at 1550 nm. See Fig. 3. The agreement between β measured under different conditions, or calculated in different ways, is worse than in Figs. 1 and 2, especially for wavelengths shorter than 1530 nm, and the validity of Eq. 4 can be questioned. To further investigate this point, we made more careful measurements of the gain tilt changes near a saturating signal. The results are summarized in Table 1.

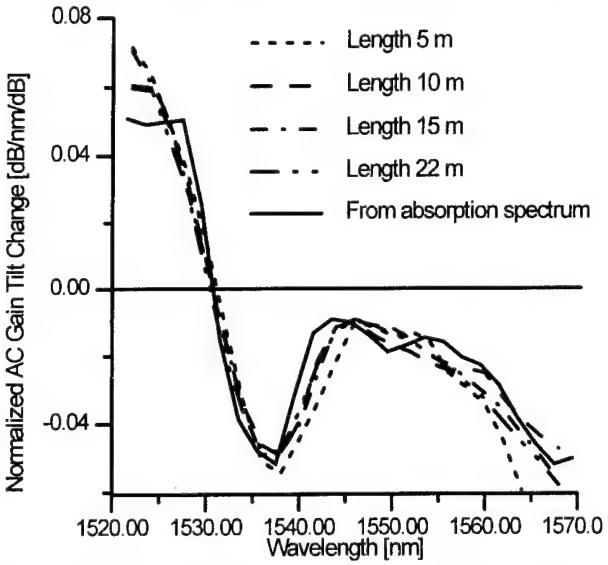

Fig. 2. Normalized AC gain tilt change vs. wavelength for different fiber lengths, calculated from the absorption spectrum (solid line), and measured as the pump power changes for four different fiber lengths (dashed lines).

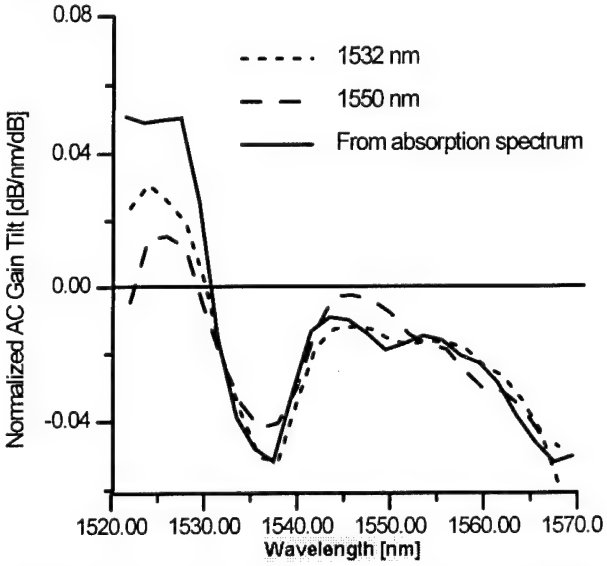

Fig. 3. Normalized AC gain tilt change vs. wavelength, calculated from the absorption spectrum (solid line), and measured as the gain compression, caused by a saturating signal at different wavelengths, changes. Short dash: Measured β for a compressing signal at 1532 nm. Long dash: Measured β for a compressing signal at 1550 nm.

Row	Wavelength [nm]	1529.2	1550.4	1560.4
1	β from absorption spectrum [dB/nm/dB]	0.031	-0.019	-0.025
2	β from a change of pump power [dB/nm/dB]	0.025	-0.015	-0.033
3	β from a change of signal power [dB/nm/dB]	0.016	-0.016	-0.031
4	β from a change of signal power [dB/nm/dB]	0.010	-	-0.031
5	β from cross saturation [dB/nm/dB]	-	-	-0.032

Table 1. Normalized AC gain tilt change β at three different wavelengths. Row 1: β calculated from absorption spectrum. Row 2: β measured by varying the pump power. Rows 3 and 4: β measured for gain compression induced by a strong signal at 1529.2 nm, 1550.4 nm, and 1560.4 nm, respectively. Two different measurements were made. Row 5: β measured for gain compression induced by a strong signal at 1550.4 nm (cross-saturation).

From Figs. 1-3 and Table 1, it is clear that Eq. 4 seems more accurate in the range 1535 nm to 1560 nm than in the range 1520 nm to 1530 nm. We cannot explain why this is the case. Furthermore, also repeatability was worse in the shorter wavelength range. Table 1 can be summarized as follows: At 1529.2 nm, Eq. 4 does not describe measured results in a meaningful way. Furthermore, the measured β was different depending on how the gain was varied, although the uncertainties in the measurements are large. At 1550.4 nm, Eq. 4 describes β well, both for signal-induced and pump-induced gain changes. The same is true at 1560.4 nm, and even for cross-saturation-induced gain variations. Furthermore repeatability is good at 1560.4 nm. An analysis of wavelengths close to 1560.4 nm (not included in Table 1) shows the repeatability to be ca. 0.003 dB/nm/dB.

Conclusions

We have measured how the AC gain tilt changes with the degree of gain compression in EDFAs, and compared it to model calculations for a homogeneously broadened gain. Theoretically, for a homogeneously broadened gain, this change can be evaluated from a knowledge of the absorption spectrum of the fiber only. Experimentally, we found that the theoretical expression seems valid in some wavelength ranges, but not in others. The expression was analyzed for gain changes caused by a pump power reduction, gain saturation, and cross-saturation. The result was independent of fiber length. From the point of view of gain tilt change, for AM CATV networks and links, an operating wavelength of 1545 nm appears more suitable than other possible ones, e.g. 1555 nm or especially 1565 nm. However, this will be different for EDFs of different compositions.

References

1. Jan Lipson, L. Chainulu Uphadhyayula, Sun-Yuan Huang, Charles B. Roxlo, E. J. Flynn, Paul M. Nitzshe, Carl J. McGrath, Gerald L. Fenderson, and Mark S. Schaefer, "High-fidelity lightwave transmission of multiple AM-VSB NTSC signals", IEEE Trans. Microwave Theory Tech. **38**, 483-493 (1990)
2. Kiyoshi Nakagawa, Shigendo Nishi, Kazuo Aida, and Etsugo Yoneda, "Trunk and distribution network application of erbium-doped fiber amplifier", J. Lightwave Technol. **9**, 198-208 (1991)
3. P. M. Gabla, C. Bastide, Y. Cretin, P. Bousselet, A. Pitel, J. P. Blondel, "45-dB power budget in a 30-channel AM-VSB distribution system with 3 cascaded erbium-doped fiber amplifiers", IEEE Photonics Technol. Lett. **4**, 510-512 (1992)
4. H. Ibrahim, D. Ronarch, L. Pophillat, A. Madani, J. Moalic, M. Guibert, J. Leroch, P. Jaffre, "Comparison between erbium-doped fluoride and silica fiber amplifiers in an AM-CATV transmission system", IEEE Photonics Technol. Lett. **5**, 540-543 (1993)
5. D. Lipka and D. Werner, "Design of erbium doped fibre amplifiers with minimised gain tilt for CATV transmission systems", Electron. Lett. **30**, 1940-1941 (1994)
6. C. Y. Kuo and E. E. Bergmann, "Erbium-doped fiber amplifier second-order distortion in analog links and electronic compensation", IEEE Photonics Technol. Lett. **3**, 829-831 (1991)
7. K. Kikushima and H. Yoshinaga, "Distortion due to gain tilt of erbium-doped fiber amplifiers", IEEE Photonics Technol. Lett. **3**, 945-947 (1991)
8. J. Ohya, H. Sato, T. Fujita "Second-order distortion generated by amplification of intensity-modulated signals with chirping in erbium-doped fiber", IEEE Photonics Technol. Lett. **4**, 1000-1002 (1992)
9. S. L. Hansen, P. Thorsen, K. Dybdal, S. B. Andreasen, "Gain tilt of erbium-doped fiber amplifiers due to signal-induced inversion locking", IEEE Photonics Technol. Lett. **5**, 409-411 (1993)
10. Koji Kikushima, "AC and DC gain tilt of erbium-doped fiber amplifiers", J. Lightwave Technol. **12**, 463-470 (1994)
11. J. Nilsson et al., to be submitted for publication.
12. D. E. McCumber, "Theory of phonon-terminated optical masers", Phys. Rev. **134A**, 299-306 (1964)
13. W. J. Miniscalco, and R. S. Quimby, "General procedure for the analysis of Er^{3+} cross sections", Opt. Lett. **16**, 258-260 (1991)
14. M. Tachibana, R. I. Laming, P. R. Morkel, D. N. Payne, "Gain cross saturation and spectral hole burning in wideband erbium-doped fiber amplifiers", Opt. Lett. **16**, 1499-1501 (1991)
15. William J. Miniscalco, "Optical and electronic properties of rare earth ions in glasses", in *Rare earth doped fiber lasers and amplifiers*, ed. Michel J. F. Digonnet (New York, Basel, Hong Kong: Marcel Dekker 1993).

Novel configuration for low-noise and wide-dynamic-range Er-doped fiber amplifier for WDM systems

Y. Sugaya, S. Kinoshita, and T. Chikama

Fujitsu Laboratories Ltd.
1015 Kamikodanaka, Nakahara-ku, Kawasaki 211, Japan
Tel.: +81-44-754-2643; Fax : +81-44-754-2640

1. Introduction

Recently, wavelength division multiplexed (WDM) optical transmission systems have become more attractive for use in multi-media networking systems. In a WDM system, Er-doped fiber amplifiers (EDFAs) are expected to play an important role as multi-wavelength amplifier repeaters. The broadening of gain bandwidth and the maintaining of gain flatness are issues which have been discussed [1-3]. The effectiveness of an aluminosilicate EDF and an automatic gain control (AGC) scheme have been reported for the requirements mentioned above [4-7]. However, there are still some vital requirements for practical EDFA repeaters as follows. The output power level of each channel should be kept in a range determined by ASE accumulation and nonlinear effects such as self-phase modulation (SPM) and four wave mixing (FWM). The noise figure must be kept low. An efficient conversion of pump power to signal power is desired, because the allowable pump power for an EDFA repeater is limited when employing the above-mentioned AGC scheme. Another requirement is a wide input power dynamic range.

2. Proposed configuration of EDFA for WDM systems

We propose a two-stage novel configuration for an EDFA repeater designed for WDM systems as shown in Fig. 1. The isolator, 1530 nm rejection optical filter and variable attenuator are located between the two stages to achieve the requirements mentioned in the introduction. It also includes a high alumina co-doped EDF and an AGC to control gain flatness. We experimentally investigated this new configuration with a 4-channel signal and found that it performed as expected.

2.1 Broad flat gain and output level control

EDFA repeaters designed for WDM systems should have a broad flat-gain area and their output level should remain within a determined range. To broaden the gain bandwidth of an EDFA around 1550 nm, we employed an EDF with a high alumina co-doped silica core [4-6]. The gain bandwidth of this EDF within 0.1 dB variation at the flat gain area is 1543 nm through 1558 nm, which is 15 nm wide. Figure 2 shows the gain characteristics of a 4-wave amplifying EDFA by the variation of pump power which is experimentally measured. The input power of each channel is -35 dBm and the wavelength of each channel is located at 1548 nm, 1551 nm, 1554 nm and 1557 nm which is in the flat-gain area. From this figure, we noted that the linear gain slope characteristics is maintained within the pump power variation range. Also note that the gain slope ($dG/d\lambda$) varies from positive ($dG/d\lambda>0$) to negative ($dG/d\lambda<0$) according to the increase in the pump power, and that there is an optimum pump power for flat-gain characteristics. It is also possible to maintain the gain characteristics by keeping the average gain level, which is the AGC, against the input power variation [7]. To adjust the output channel level, some methods other than pump-power controlling of EDFA must be introduced, because the pump power is adjusted for the gain characteristics of EDFAs. A variable optical attenuator has very small wavelength dependence of the attenuation, which simplifies the control of output level of each channel. Therefore, we introduced the variable optical attenuator as the key device in the EDFA for WDM systems.

2.2 Experiments for a single stage configuration

Several possible configurations for EDFAs derived from the discussion above are shown in Fig. 3, including the proposed configuration. They are experimentally compared as follows. In a 4-channel WDM system, we have assumed the output power of each channel of the amplifier to be controlled at +7 dBm. The minimum input power is set at -25 dBm for each channel. Figure 3(a)

shows the experimental setup of the EDFA, which is a single stage (type-A). The EDF is pumped forward and backward by 980nm LDs, which provide a maximum of 160 mW into the EDF. The signal gain flatness is maintained by the AGC against variations in the input power. The automatic output power level control (ALC) is implemented by the variable optical attenuator at the end of the EDF. The EDF length was determined when the input power was -25 dBm/ch and had a flat gain. In spite of the 980 nm pump scheme, the noise figure is rather high (7 dB) in Fig. 4. As the input power increases, so much pump power is required that the input power range is restricted to only 2 dB , which means that -23 dBm/ch is the maximum input power to achieve both a flat gain and the desired output power. The total insertion loss of the optical modules located in the front of EDF is 1.7 dB, and that of the optical modules located in the back of EDF is 2.0 dB. This indicates that the required optical gain of the EDF alone is 35.7 dB, which is so high that the EDF noise figure degrades due to backward ASE.

2.3 Experiments for a two-stage configuration

A two-stage EDFA can suppress the backward ASE by an isolator and the 1530 nm ASE peak by a 1530 nm rejection filter which are located between the both stages [8,9]. This allows a low noise operation in the preamplifier section and an efficient conversion in the postamplifier section, which is the second stage. Thus the two-stage EDFA is expected to operate at a low noise figure with a wide input power range.

Taking into account the power distribution along the EDF, we set the negative slope gain ($dG/d\lambda<0$) in the first stage for a low noise figure because of a high inversion population, and the positive slope gain ($dG/d\lambda>0$) in the second stage for a high pump power conversion. The gain slope of the second stage is adjusted to compensate for the negative slope gain of the first stage. We set a 20 dB gain and a 1.4 dB gain tilt between both end signals (1548 nm and 1557 nm) of the first stage, and compensated for the tilt in the second stage.

The position of the variable attenuator for the ALC operation is also important in a two-stage EDFA. Figure 3(b) shows one of the two-stage EDFA configurations (type-B) which has an attenuator at the end (rear-attenuator). The first stage of type-B has the same configuration as type-A. The second stage is pumped backward by 1480 nm LDs which provide the maximum of 100 mW into the EDF. Both stages are controlled by the AGC, and the output power is adjusted by the optical variable attenuator. Figure 5 shows the noise figure of each channel in the configuration of type-B. The noise figure was considerably improved to around 5.3 dB. It is 3.6 dB in the case of the EDF alone. This is a 1.7 dB improvement over the single stage configuration type-A. However, this configuration still does not realizes a wide input power range. For a high input power, the signal output power before the variable attenuator is estimated to be so high that the required pump power for the second stage exceeds the limit level of the present setup. Thus, the input power range with this configuration was 4 dB.

Figure 3(c) shows the setup of the other two-stage EDFA configurations (type-C) with an attenuator between the two stages (mid-attenuator). This is the proposed configuration. The mid-attenuator controls the input power of the second stage, and the pump power of the second stage is fixed. The whole amplifier is thus automatic-level-controlled. With this configuration, the pump power of the second stage is independent of the input signal power, and cannot be the limit factor of the input power dynamic range. Figure 6 shows the noise figure of the proposed configuration against the input power. As the input power increased, the increasing loss of the attenuator slightly affected the noise figure of this type of EDFA. But the deterioration in the noise figure was only 0.3 dB from 5.3 dB to 5.6 dB, for a 10 dB input power range. Figure 7 shows the output power variation of each channel against the input power range. For each input power level, the gain flatness achieved is within 0.2 dB. So, for each channel, there is only a maximum of 0.2 dB variation for a 10 dB input power range.

3. Conclusion

We proposed a novel configuration of EDFA which is suitable for WDM in-line repeaters. This EDFA configuration realizes gain flatness, a low noise figure, a wide input dynamic range, and a high pump power conversion efficiency. The gain flatness is within 0.2 dB. The noise figure

of this configuration is at worst 5.6 dB. The deterioration in the noise figure is 0.3 dB for a wide input power dynamic range of 10 dB, that is, -25 dBm to -15 dBm.

Acknowledgments

We thank Dr. H. Kuwahara for his guidance and encouragement. We also thank Mr. Suyama and Mr. Inagaki for discussions and for offering EDFs.

References

[1] C. R. Giles et al., IEEE Photon. Technol. Lett., 2, 866 (1990).
[2] T. Sugawa et al., IEEE Photon. Technol. Lett., 2, 475 (1990).
[3] W. J. Miniscalco, IEEE J. Lightwave Technol., 9 , 234 (1991).
[4] M. Suyama et al., OSA'94, ThK2 (1994).
[5] C. G. Atkins et al., Electron. Lett., 25, 910 (1989).
[6] T. Kashiwada et al., OAA'93, MA6-1 (1993).
[7] E. Desurvire et al., Opt. Lett., 15, 547 (1990).
[8] J. F. Marcerou et al., OAA'91, ThE1-1 (1991).
[9] M. Suyama et al., OAA'93, MB5-1 (1993).

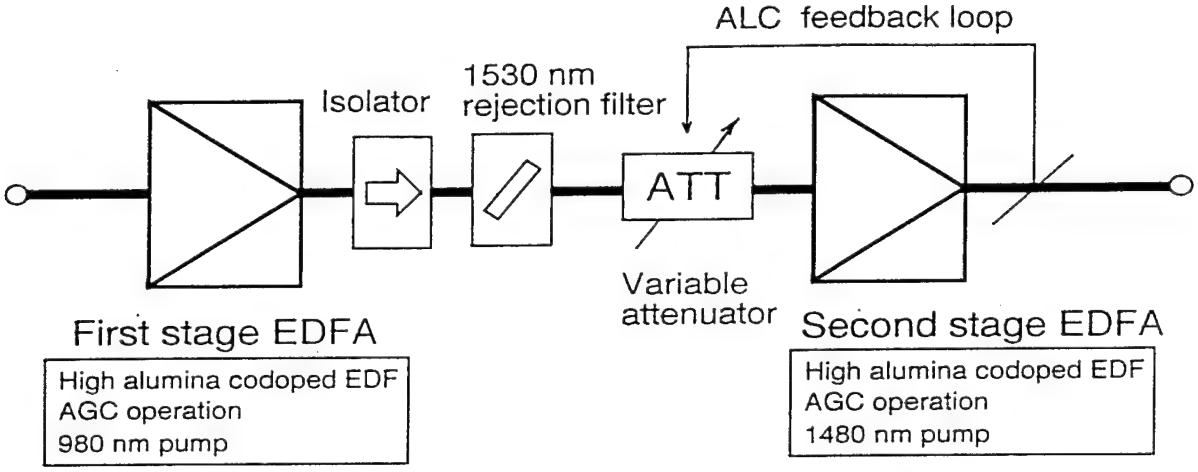

Fig. 1 Configuration of the proposed EDFA.

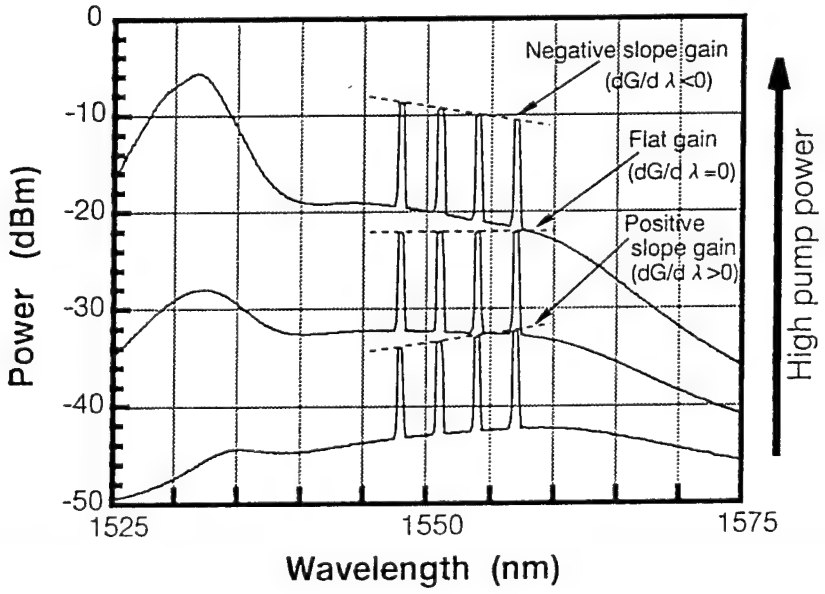

Fig. 2 Gain characteristics by the variation of the pump power.

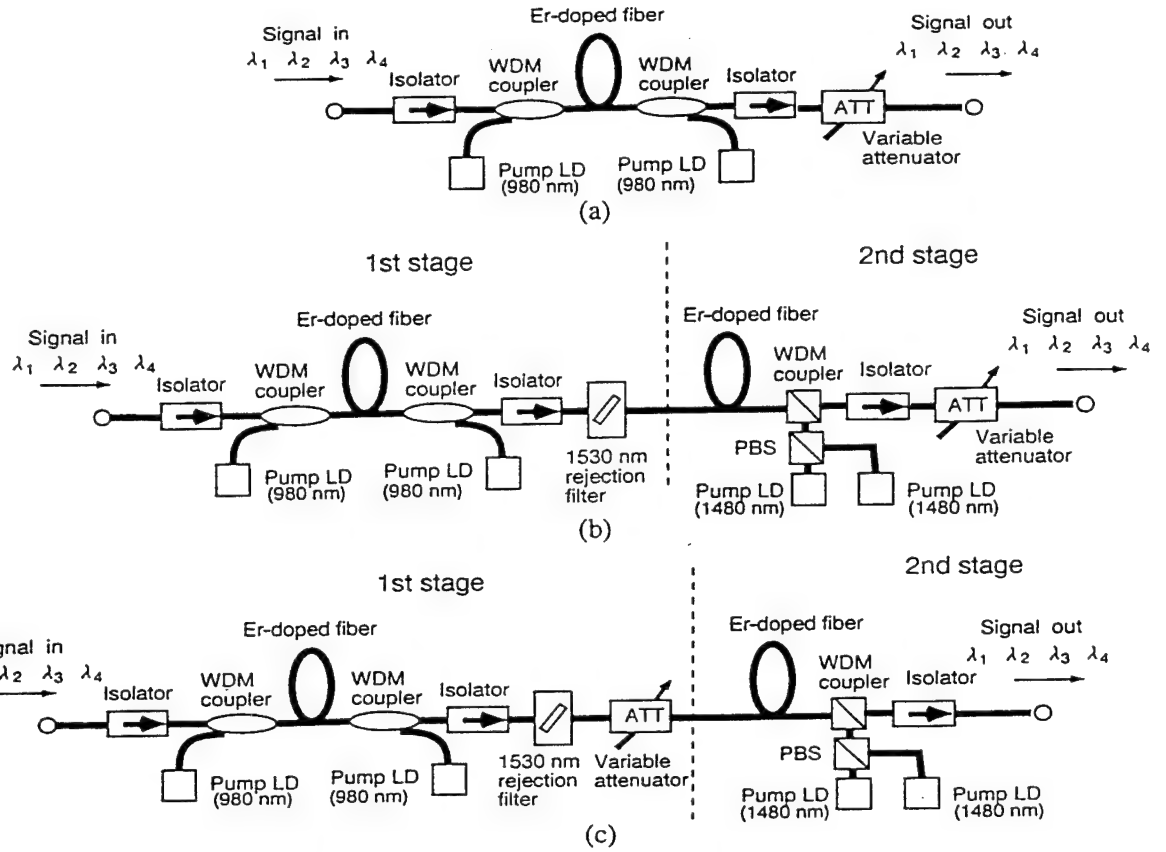

Fig. 3 Experimental setups for (a) type-A (single stage), (b) type-B (two stage with rear-attenuator) and (c) type-C, the proposed configuration (two stage with mid-attenuator).

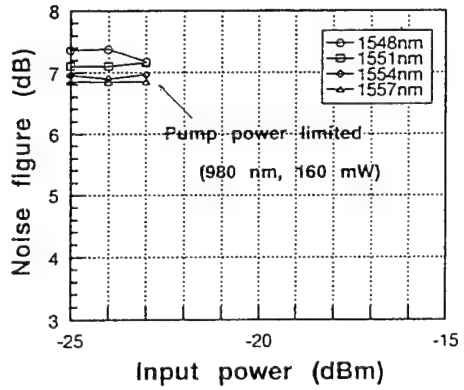

Fig. 4 Noise figure characteristics of type-A EDFA

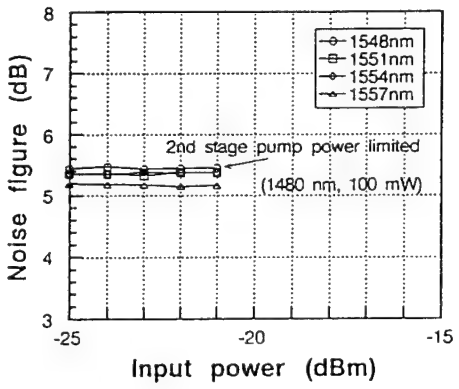

Fig. 5 Noise figure characteristics of type-B EDFA

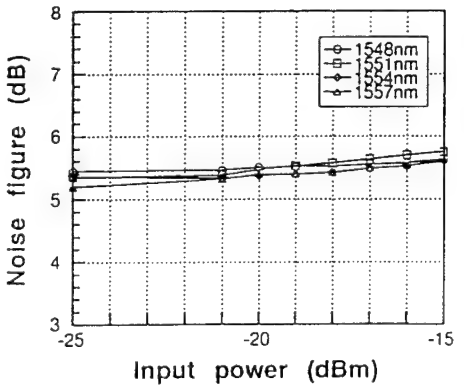

Fig. 6 Noise figure characteristics of the proposed EDFA

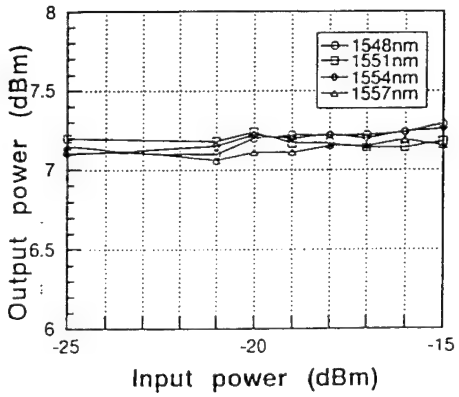

Fig. 7 Gain flatness and gain stability against input power dynamic range

Single-Stage Booster Amplifier with Two 980 nm Pumps Stabilized by Fiber Grating

G. R. Jacobovitz-Veselka , P. Wysocki, A. M. Vengsarkar, T. Erdogan*, V. Mizrahi+ and J. Borick. AT&T Bell Laboratories, 600 Mountain Ave. Murray Hill, NJ 07974-0636. Tel: (908)582-2928, Fax: (908) 582-2422. S. W. Granlund, AT&T Bell Laboratories STC, 9999 Hamilton Blvd., Breinigsville, PA 18031.Tel: (610)391-2469.
*Presently at the Institute of Optics, University of Rochester, Rochester, NY 14627 ,Tel: (716) 275-7227.+Presently at CIENA Corporation Optical Communications, 1340-C Ashton rd., Hanover, MD 21076, Tl:(410) 684-3939

Optical amplifiers using 980 nm pumps are desirable because of the inherent low amplifier noise figure, in some cases flatter amplifier gain and the high electrical-to-optical conversion efficiency of the strained quantum well InGaAs pump lasers. Simulations we have performed, show that the most cost effective design for an erbium-doped fiber (EDF) booster amplifier is the co- and counter-pumped single-stage amplifier. Also, for reliability reasons, pump redundancy is desirable. However, an amplifier in this configuration allows the two pumps to interact with each other, shifting their peak emission wavelengths. The 980 nm pump lasers are very sensitive to reflections. Weak reflections can shift the wavelength from 970 nm to 1040 nm, out of the erbium doped fiber absorption spectrum [1]. Isolators could be used to prevent the pumps from interacting; but, 980 nm isolators are expensive and have high insertion loss.

Here we describe a high output power erbium-doped fiber amplifier (EDFA) pumped in the co- and counter-propagating directions, with pump-redundancy, where isolators are not used and the peak pump emission wavelength is stable. Instead of isolators to stabilize the pump wavelengths we used a fiber grating reflector that simultaneously locks both pump lasers and a band-stop fiber filter to attenuate long emission wavelengths. Locking the two pumps with the same grating makes their wavelength the same. This configuration is less costly and has higher output power than a dual stage amplifier (with the same operating conditions) because of the lower cost and insertion loss of the gratings. Also, to obtain the desired performance, many amplifier designs require a particular pump emission wavelength. Selecting lasers with the desired pump emission wavelength decreases significantly the pump yield. Alternately, temperature tuning the pump unit to obtain the desired emission wavelength increases the pump power consumption and packaging complexity. Since, in our design, the emission wavelength of the pumps is selected by the fiber grating reflector, the pump yield is improved lowering the cost. Also, with the right arrangement of grating reflectors and band-stop filters, temperature control is not needed. Therefore, power consumption and packaging complexity are reduced.

Figure 1.a shows the EDFA design for a single stage booster amplifier pumped with two 980 nm laser diodes. Pump-redundancy is provided by splicing the two pumps to the two inputs ports of a 4 port 3 dB coupler. A short-period fiber grating reflector [2] is spliced to one of the 3dB coupler output port. This output port pigtail is then spliced to the A port of the wavelength division mutiplexer (WDM) 1 located at the input of the doped fiber. Another port of the two WDM's is a 1% tap that allows us to monitor the pump power and spectrum. The other output port of the 3dB coupler is spliced to WDM 2. The WDM's are spliced to the input and output ports of the 36-m-long erbium doped fiber (EDF) used as the amplifier medium. The pumps interact due to the pump-path-loop; from the output of the 3dB coupler, to WDM 1, to the EDF, to WDM 2 and finally to the other output port of the 3dB coupler.

In our experiment we used two pump lasers whose spectrum, without optical feedback from a fiber grating, were centered at 977 nm and 978 nm. Figure 1.b shows the pump spectrum when using the two pumps and a weak fiber grating reflector (R=9.8%) with reflectivity centered at 978 nm. The pump laser facets have < 5% reflections. The emission spectrum shows one peak at 978 nm, forced by the grating, and a stronger peak jumping around in the range from 990 nm < λ < 1040 nm. The unstable longer pump emission wavelength is generated because of the low absorption loss in the EDF, and amplifier components, at $\lambda > 1\mu m$ and bandfilling allow that the emission band move to longer wavelengths [1].

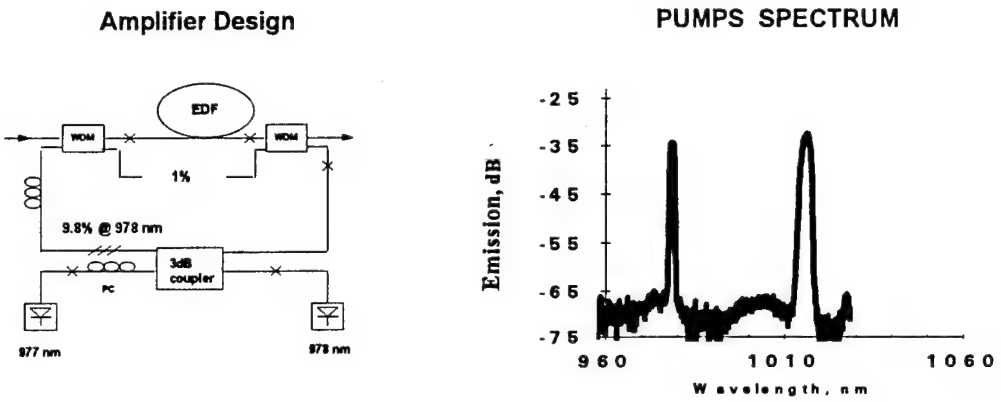

Figure 1: a) Amplifier design. b)Pump spectrum when using a 9.8% fiber grating reflector.

The EDF and components in the pump path have little absorption loss at $\lambda > 1$ μm; therefore, the longer wavelength component is not attenuated and keeps feeding itself through the pump-path loop. The pump-path-loop is an effective broadband reflector [1] which reflectivity is higher than the 9.6% reflection at 978 nm. To avoid this problem a stronger reflection grating or strong attenuation at $\lambda > 978$ nm is necessary.

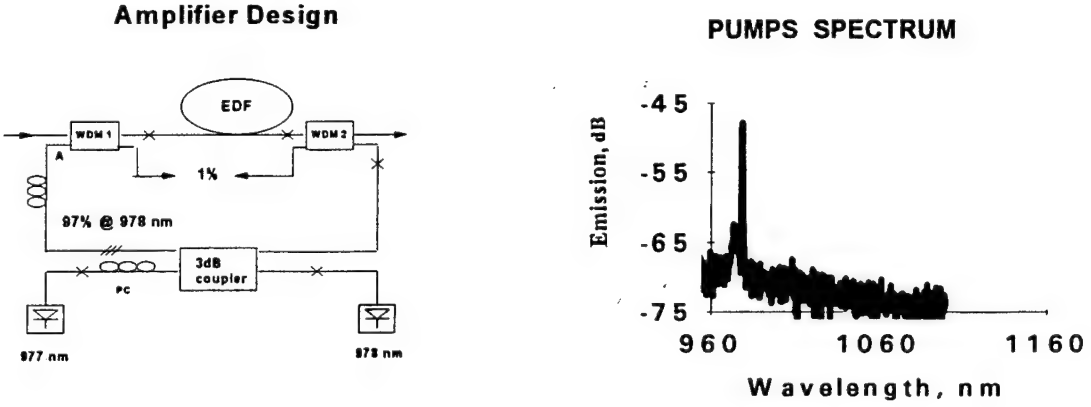

Figure 2: a) Amplifier design. b)Pump spectrum when using a 97% fiber grating reflector.

Figure 2b shows the emission spectrum when using a 97% reflectivity grating. The grating is centered at 978 nm and the same 36 m long EDF is used as the amplifying medium. The spectrum is very stable varying only 0.3 dB when the polarization is changed at two different points: between the pump and the 3 dB coupler and between the output of the 3 dB coupler and the WDM's. However, a 97% reflector introduces 15 dB pump insertion loss so a lower fiber grating reflector is much desired.

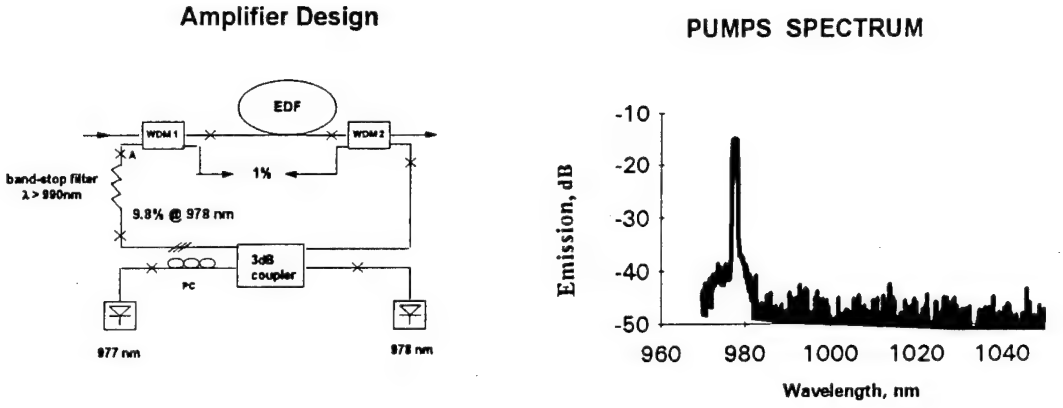

Figure 3: a) Amplifier design. b)Pump spectrum when using a 9.8% fiber grating reflector and band-stop filter for λ> 990 nm.

In order to use a less reflective fiber grating, a band-stop fiber grating filter [3] that attenuates wavelengths longer than 978 nm was added to the pump path between the low reflectivity fiber grating reflector and the input WDM 1. The band-stop filter is a long-period fiber grating that couples light from the guided mode to the forward propagating cladding mode. The band-stop filter breaks the loop avoiding emission at longer wavelengths and introduces no insertion loss at 978 nm. Using a band-stop fiber filter for $\lambda > 990$ nm with $\cong$ 5 dB attenuation no pump emission at wavelength longer than 978 nm was seen as shown in Figure 3b.

We constructed and measured the performance of another amplifier. This amplifier consists of the 9.8% fiber grating reflector centered at 978 nm, a 45 m long EDF and a long wavelength ($\lambda >$ 990 nm) band-stop fiber filter with $\cong$ 12 dB attenuation. Figure 4 shows the EDFA output power and NF as a function of wavelength. A minimum output power of 13.8 dBm and noise figure of 4.9 dB were achieved at co- and counter-propagating pump powers 13.34 dBm and 16.67 dBm and -12 dBm input signal. The large signal output power varies 0.47 dB over the entire spectrum (1530 nm $< \lambda <$ 1565 nm). These output power results are 0.5 dB lower than simulation results for the erbium fiber alone. We believe that this difference is due to component and splice losses added to the built amplifier.

Temperature controlling the pump laser increases the power consumption and complexity of the laser packaging. Pump laser temperature control is not necessary when using a strong reflection grating or a strong band-stop filter. In the EDFA described in the previous paragraph, changing the pump module temperature a few degrees induced a strong pump emission peak at 1

μm as well as at 978 nm, since the band-stop filter attenuation at 1 μm is 6 dB lower than at 1.006 μm. Changing the temperature moved the semiconductor pump laser emission peak wavelength away from the reflectivity peak of the grating reflector, reducing the grating effectiveness in locking the pumps at 978 nm. The reflection at 980 nm is then decreased

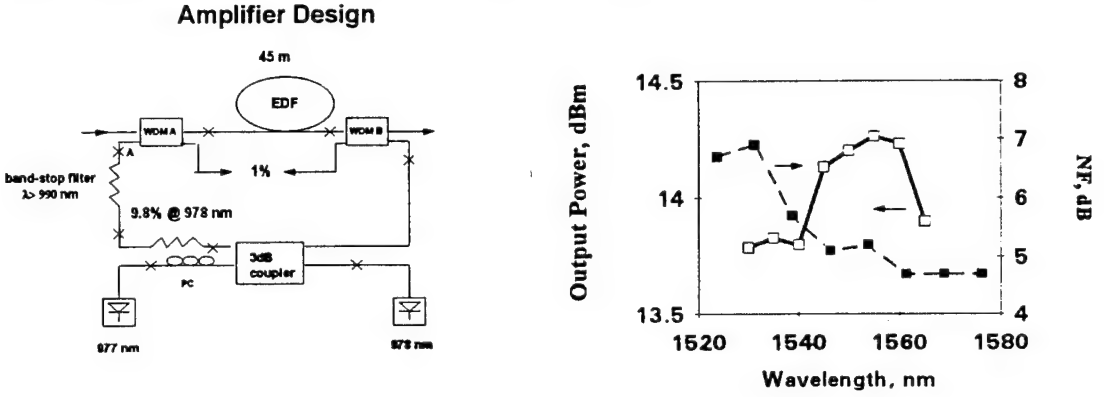

Figure 4: a) amplifier design. b) Amplifier performance using a 9.8% fiber grating reflector and a band-stop fiber for λ> 990 nm. The output power as a function of wavelength is represented by the straight line and the NF by the dotted line.

relative to that at 1 μm. Therefore, to operate the pumps without temperature control we should increase the grating reflectivity or increase the attenuation at 1 μm. Using a stronger reflection grating, 49.3%, centered at 980 nm we varied the temperature on the pump laser package by 26 ^{0}C, from 16 ^{0}C to 42 ^{0}C, without observing the 1 μm pump emission peak. However, increasing the reflectivity of the grating reflector increases the pump path insertion loss. A better solution is to use a stronger band-stop filter that does not add to the pump insertion loss. The 980 nm peak emission wavelength remained stable with respect to temperature and polarization.

Simulations show that a co- and counter-propagating 980 nm pumped amplifier is one of the most cost effective designs for a booster amplifier. However, this configuration allows interaction between the pumps shifting the emission peak to wavelengths out of the EDF absorption band. We have presented a low cost way to avoid this problem by using fiber grating reflectors and fiber grating band-stop filters instead of adding isolators to the pump path. This design also allows pump redundancy and no need for temperature controlling the pump laser, reducing the power consumption and complexity of the laser packaging.

References:

[1] C. R. Giles et. al. IEEE Photon Tech. Lett., vol.6, Aug. 1994.
[2] G. Meltz et.al. Opt. Lett. vol 14, 1989.
[3] A. M. Vengsarkar et.al. to be presented at OFC'95, Feb. 1995, San Diego, CA.

Suppression of Residual Amplitude Modulation using Highly Saturated Erbium-Doped Fiber Amplifiers

P. B. Hansen, L. Eskildsen, J. Alphonsus, D. Truxal

AT&T Bell Laboratories
101 Crawfords Corner Road
Holmdel, NJ 07733
Tel.: (908) 949-1384
Fax.: (908) 834-6943

Optical systems relying on launching high optical powers into fiber, such as repeaterless transmission systems are typically forced to employ artificial broadening of the spectrum to avoid Stimulated Brillouin Scattering [e.g. 1, 2]. Superimposing a small-signal sinusoid with a frequency of 5 kHz to 10 kHz onto the DC bias current of the laser diode is an efficient method for broadening the time-averaged optical spectrum [3]. Launch powers of up to 24 dBm, which have proven advantageous for maximizing the transmission distance of repeaterless systems, requires a spectral width on the order of 10 GHz [4]. This level of artificial broadening of the spectrum typically implies significant residual amplitude modulation, which translates into degradation of system performance.

In this paper, we experimentally demonstrate efficient suppression of the residual amplitude modulation in a highly saturated Erbium-doped fiber amplifier (EDFA) with a 25-kHz cut-off frequency. Transmission experiments show that a power penalty of 3.5 dB for a bit error rate of 10^{-9} can be reduced to as little as 0.2 dB.

The AM-suppressing amplifier, which was used to demonstrated the principle, is a two-stage Erbium-doped fiber amplifier bi-directionally pumped by six 1480-nm laser diodes. Wavelength multiplexing was employed to allow 4 lasers to pump the first stage of the amplifier. The two stages are separated by an optical isolator and a 10-nm bandpass filter. Figure 1 shows the measured gain versus output power. The maximum output power is 23.3 dBm. The optical-to-optical small-signal response of the EDFA is shown in Fig. 2. A 3-dB cut-off frequency as high as 25 kHz is utilized to dampen AM at frequencies in the 5 to 10 kHz range. The suppression at 5 kHz, 7 kHz and 10 kHz are 14.9 dB, 12.2 dB, and 9.2 dB, respectively.

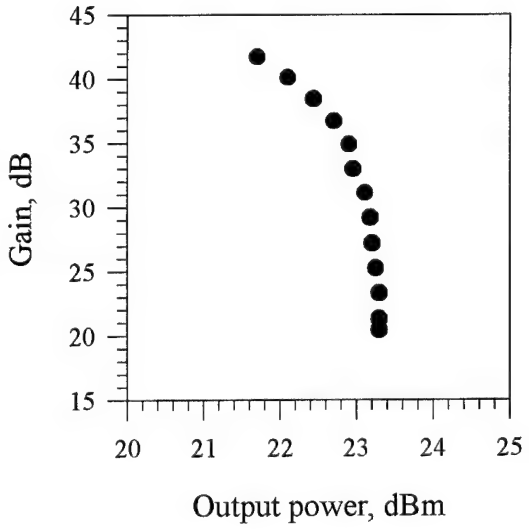

Fig. 1 Measured gain versus output.

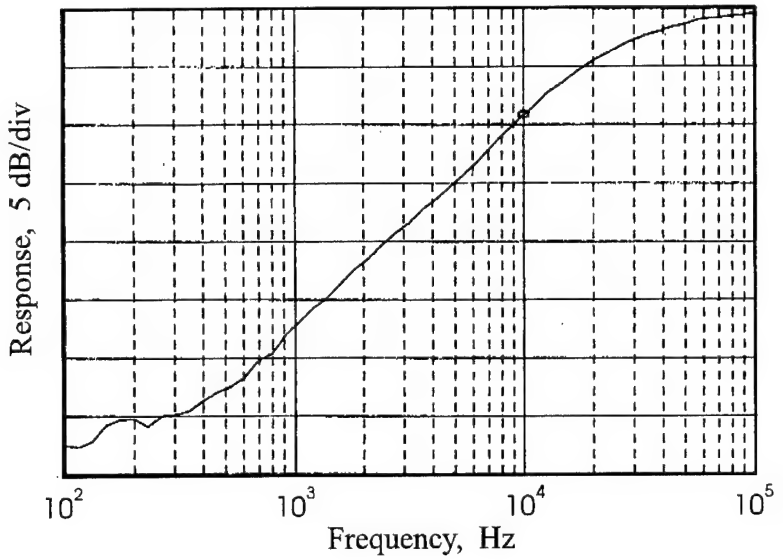

Fig. 2 Small-signal response of the highly saturated EDFA.

A transmission experiment was conducted to demonstrate the potential advantages in a repeaterless transmission system. The laser source is a multi-quantum well DFB laser biased by a sinusoid (24 mA peak-to-peak) superimposed on a DC current (62.5 mA). The spectral width and modulation index of the residual amplitude modulation at each of the frequencies are given in Table 1. Data (a 2^{31}-1 pseudo-random bit sequence) is encoded at a rate of 2.488 Gb/s by means of an external $LiNbO_3$ Mach-Zehnder modulator. The signal level is then boosted to 23.3 dBm by the AM-suppressing EDFA. The input power to the EDFA is 4.0 dBm. The receiver is a commercially available PIN detector.

The eye-pattern of a 10-kHz wavelength dithered signal measured on the output of the transmitter (without the AM suppressing EDFA) is shown in Fig. 3(a). Eye closure due to residual AM is evident. Figures 3(b-d) are the measured eye patterns at dither frequencies of 10 kHz, 7 kHz, and 5 kHz, respectively, when the signal is amplified by the EDFA. The eye closure is reduced significantly by the EDFA is all three cases. As indicated by the small-signal response measurement, Fig. 2, the improvement is larger at lower frequencies. In the case of 5 kHz

Dither frequency	Spectral width	Residual AM
5 kHz	7.7 GHz	0.42
7 kHz	8.1 GHz	0.42
10 kHz	8.7 GHz	0.44

Table 1 Spectral width and residual AM measured at dither frequencies of 5 kHz, 7 kHz and 10 kHz. The spectral width is the time averaged width.

dithering, the eye closure is nearly eliminated. For comparison, Fig 3(e) shows the eye-pattern without dithering.

Figure 4 shows the measured bit error rate performance for three wavelength dither frequencies - 5 kHz, 7 kHz, and 10 kHz - with and without the highly-saturated EDFA. The crosses (+) are the back-to-back bit error rate when no wavelength dithering is applied and the launch power for a data encoded signal therefore cannot exceed ~9 dBm. The open symbols indicate the measured bit error rates with 5 kHz (○), 7 kHz (Δ) and 10 kHz (□) wavelength dithering, respectively. The power penalties are 3.5 ± 0.1 dB independent of the dither frequency. The corresponding filled symbols show the bit error rate performance when the AM-suppressing EDFA is employed as a booster amplifier. The received optical power required to maintain a bit error rate of 10^{-9} has clearly been reduced. The power penalties are reduced to 0.2 dB, 0.5 dB, and 1.0 dB for the frequencies of 5 kHz, 7 kHz, and 10 kHz, respectively. As expected the improvement is the highest for the lowest dither frequency.

In conclusion, we have demonstrated efficient suppression of residual amplitude modulation originating from artificial broadening of the time averaged laser spectrum at frequencies in the range of 5 kHz to 10 kHz. In this experiment the residual AM resulted in a power penalty of 3.5 dB. Employing a highly saturated EDFA with a cut-off frequency of the small-signal response as high as 25 kHz to suppress the AM, the power penalties were reduced to 0.2 dB, 0.5 dB and 1.0 dB at dither frequencies of 5 kHz, 7 kHz, and 10 kHz,

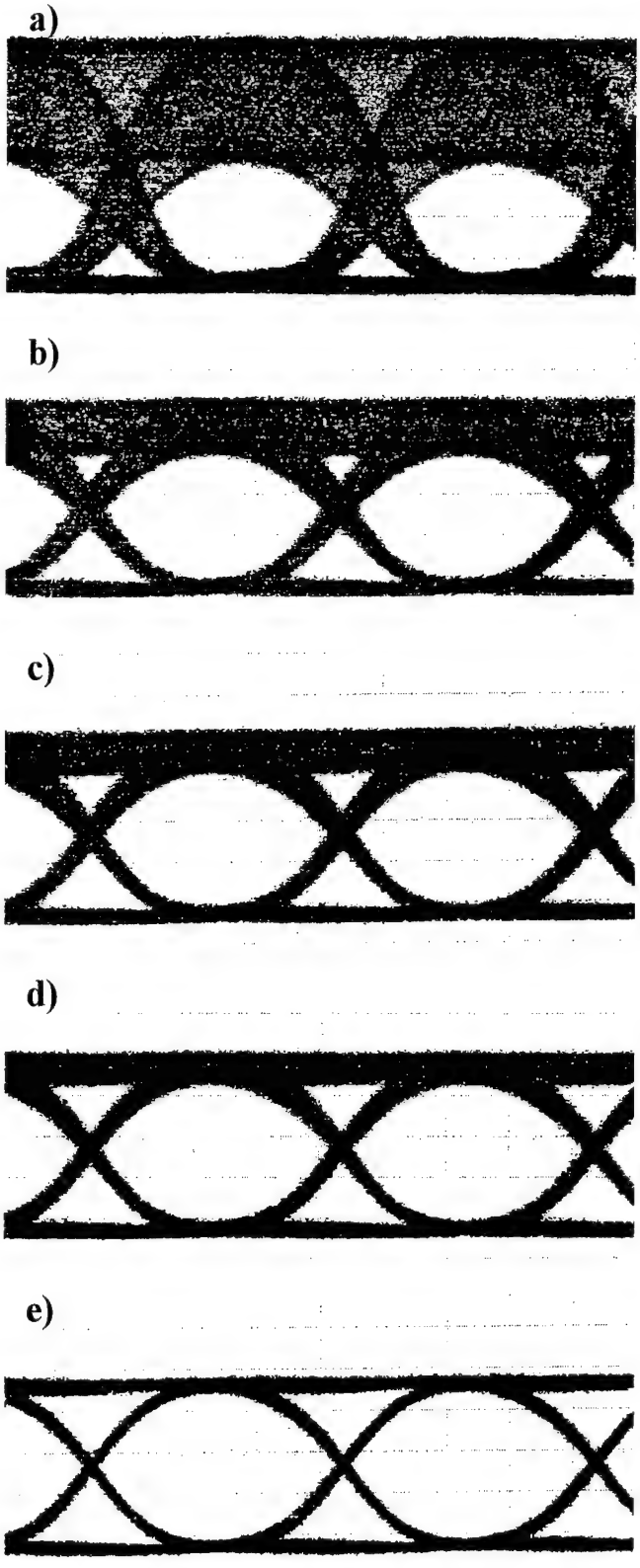

Fig. 3 Eye-patterns. a) 10-kHz dithered signal without AM suppression. Dithered signal with AM suppression at b) 10 kHz, c) 7 kHz, and 5 kHz. e) Eye-pattern of signal without dithering.

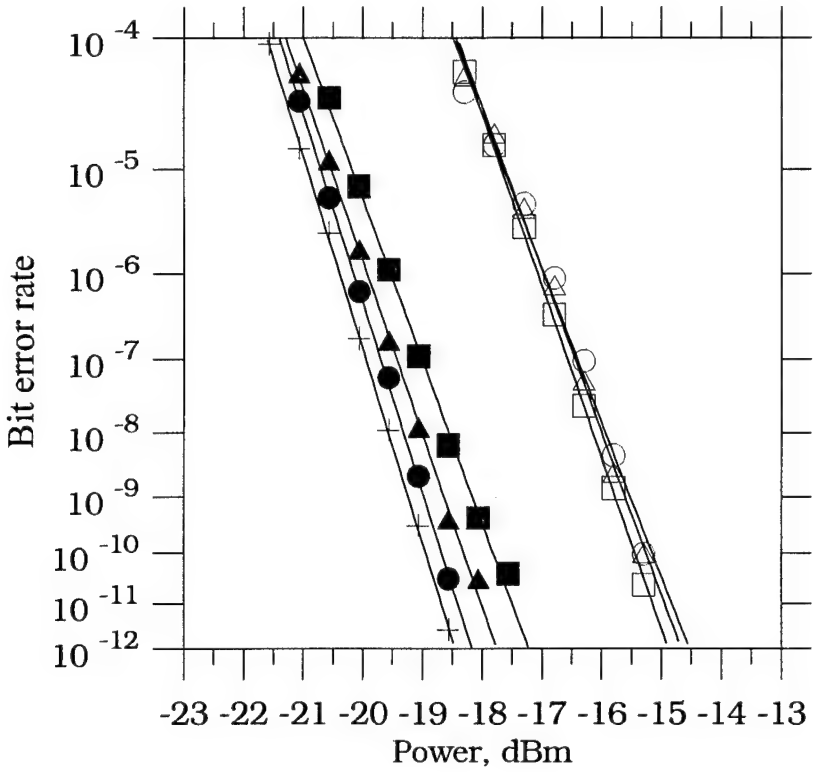

Fig. 4 Measured bit error rate with and without the AM suppressing EDFA.

respectively. Careful design of the booster amplifier ensuring a high cut-off frequency offers significant advantages for transmission system employing high launch powers, such as unrepeatered communication systems.

References

1. Y. Aoki, K. Tajima, and I. Mito: "Input power limits of single-mode optical fibers due to stimulated Brillouin scattering in optical communication systems," J. Lightwave Technol., vol. 6, no. 5, pp. 710-719, 1988.
2. Y. K. Park, O. Mizuhara, L. D. Tzeng, J. -M. P. Delavaux, T. V. Nguyen, M. -L. Kao, P. D. Yeates, and J. Stone: "A 5 Gb/s repeaterless transmission system using Erbium-doped fiber amplifiers," IEEE Photon. Technol. Lett., vol. 5, no. 1, pp. 79-82, 1993.
3. D. A. Fishman and J. A. Nagel: "Degradations due to stimulated Brillouin scattering in multigigabit intensity-modulated fiber-optic system," J. Lightwave Technol., vol 11, no. 11, pp. 1721-1728., 1993.
4. P. B. Hansen, V. L. da Silva, L. Eskildsen, S. G. Grubb, V. Mizrahi, W. Y. Cheung, T. Erdogan, T. A. Strasser, J. E. J. Alphonsus, G. Nykolak, D. L. Wilson, D. J. DiGiovanni, D. Truxal, A. M. Vengsarkar, S. G. Kosinski, P. F. Wysocki, J. R. Simpson, and J. D. Evankow: "423-km repeaterless transmission at 2.488-Gb/s using remotely pumped post- and pre-amplifiers," 20th European Conf. on Optical Communication, Post-deadline Proc., Sept. 1994, pp. 57-60.

Polarization-Maintaining Erbium-Doped Optical Fiber Amplifier

T. Sakai, K. Himeno, S. Okude, A. Wada & R. Yamauchi
Opto-electronics Laboratory
FUJIKURA Ltd.
1440 Mutsuzaki, Sakura-shi, Chiba 285
Phone: +81-43-484-3941, Fax: +81-43-484-3988

1. Introduction

Optical fiber amplifiers using an erbium doped fiber (EDF) have rapidly progressed in recent years and some transmission systems are already using erbium doped fiber amplifiers.

In the optical transmission equipments, it is sometimes required to amplify an optical signal in a constant state of the polarization. For example, a booster amplifier in an optical circuit using polarization dependent optical components like an external modulator requires such a polarization maintaining fiber amplifier. A ring laser[1] also needs a polarization maintenance. We have developed a polarization maintaining Erbium doped fiber (PM-EDF) based on the PANDA fiber technique[2]. In this paper, we report amplification and polarization characteristics of the PANDA type PM-EDF for the first time.

2. Fiber structure

The PM-EDF has the same core/cladding structure as the high efficiency EDF that has already been developed [3]. It has a germanium, erbium and aluminum co-doped core and a fluorine doped cladding. The fiber parameters are listed in Table 1 and the refractive index profile is shown in Fig. 1.

The polarization modal birefringence and the transmission loss are strongly affected by polarization maintaining fiber(PMF) structure namely a diameter (d) and a separation (s) of stress applying parts.

There is an optimum diameter of the stress applying parts to maximize the modal birefringence. On the other hand, the separation is determined by a trade-off between the modal birefringence and the loss are. We have selected 33 μm as a diameter of the stress applying part, and 16 μm as a separation. The separation 16 μm is slightly smaller than that of conventional PMF to increase the modal birefringence. The modal birefringence of 5.2×10^{-4} has been obtained in this structure. This value is 30 % better than conventional one.

3. Measurement Setup

Figure 2 shows the measurement setup for gain, noise figure and polarization extinction ratio. A signal light of 1555 nm wavelength and a pump light of 1480 nm are linearly polarized by passing a polarization dependent isolator. These lights are combined at a 3 dB coupler and launched to the PM-EDF. All the optical fibers and components after the isolators are polarization maintaining ones. Plain PMF and the PM-EDF are spliced by using an arc fusion splicer designed for PANDA fiber (FSM-20PM®). An arc fusion time is adjusted to minimize mode field mismatch[3]. The output light is divided into two orthogonal polarization axes by a polarization beam splitter (PBS). The amplified signal is clearly

distinguished above the amplified spontaneous emission level on an optical spectrum analyzer.

4. Amplification Characteristics

Figure 3 and 4 show the dependence of gain and noise figure on the input signal power and the pump power. The results include splicing losses between the PMF and the PM-EDF. In Fig. 3, gain over 30 dB is obtained for the pump power more than 25 mW in a small signal input condition. A pumping threshold of gain is approximately 4 mW. The noise figures are less than 5 dB for the pump power more than 15 mW. The performance of the fabricated PM-EDF is no way inferior to that of conventional high efficiency EDF.

In the PM-EDF, the difference of mode propagation may affect the gain in each polarization axes. So the gain characteristics are measured for four combinations of the signal and pump polarizations. The signal and pump lights are launched into the slow or fast axes in parallel or orthogonal to each other. As a result, no gain difference is observed among the four combinations within a splice loss deviation of 0.3 dB.

5. Polarization Characteristics

An external stress to a PMF degrades a polarization extinction ratio. The polarization extinction ratio become smaller for a longer fiber length and a smaller coiling diameter. In order to evaluate an extinction ratio of the PM-EDF with a practical fiber length and bending diameter, we measured fiber length dependence and bending diameter dependence. Figure 5 shows the measured length dependence of the polarization extinction ratio. We see that the extinction ratio decreases exponentially on the fiber length. The deviation of the measured values is due to polarization axis misalignment between the PMF and PM-EDF. An extinction ratio over 30 dB are achievable for the PM-EDF spliced with PMF pigtails, because a PM-EDF length required for a practical amplification is as short as 20 m. Figure 6 shows bending diameter dependence of the extinction ratio for a PM-EDF 2 m long. An extinction ratio higher than 35 dB is obtained for a PM-EDF 2 m long with 25 mm diameter coiling.

6. Conclusion

We have developed a PM-EDF as a polarization maintaining amplification medium, and have evaluated its characteristics. It has been confirmed that the PM-EDF has the amplification characteristics equal to the conventional high efficiency EDF. Gain characteristics have no dependence on the signal and pump polarization within a error of 0.3 dB. An extinction ratio of 30 dB is achievable for the PM-EDF with a coiling diameter of 35 mm.

7. References

[1] H. Takara, S. Kawakami, M. Saruwatari and K. Noguchi, Electronics Letters 22nd October 1992 Vol.28 No.22

[2] J. Noda, K. Okamoto and Y.Sasaki, Journal of Lightwave Technology, Vol. LT-4, No. 8, August 1986

[3] A. Wada, T. Sakai, D. Tanaka, T. Nozawa, R. Yamauchi, Optical Amplifiers and their Applications (OAA), paper FD3 (1991).

Table 1. Fiber parameters

Relative Refractive Index Difference	1.8%
Core Diameter	4.0 μ m
Erbium Concentration	870 wt.ppm
Aluminum Concentration	6700 wt.ppm
Mode Field Diameter (λ =1.55 μ m)	4.5 μ m
Cutoff Wavelength	1.36 μ m
Modal Birefringence (λ =1.55 μ m)	5.1×10^{-4}

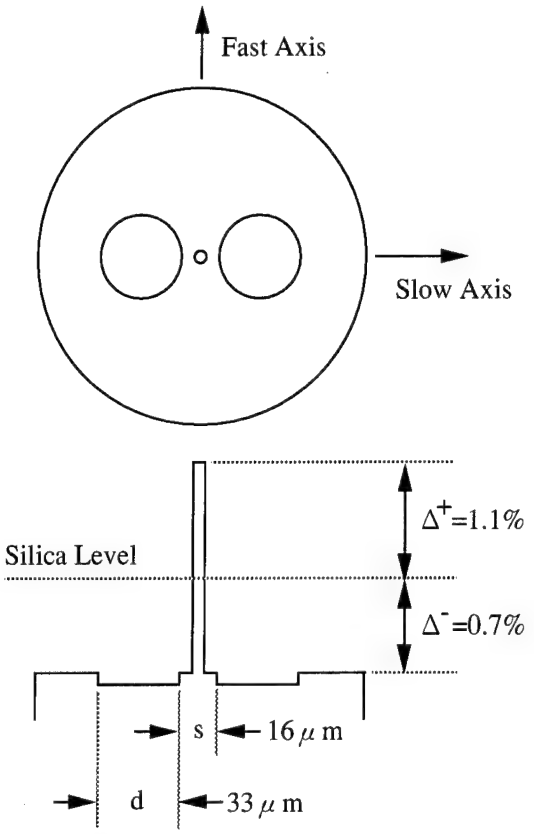

Figure 1. Refractive index profile

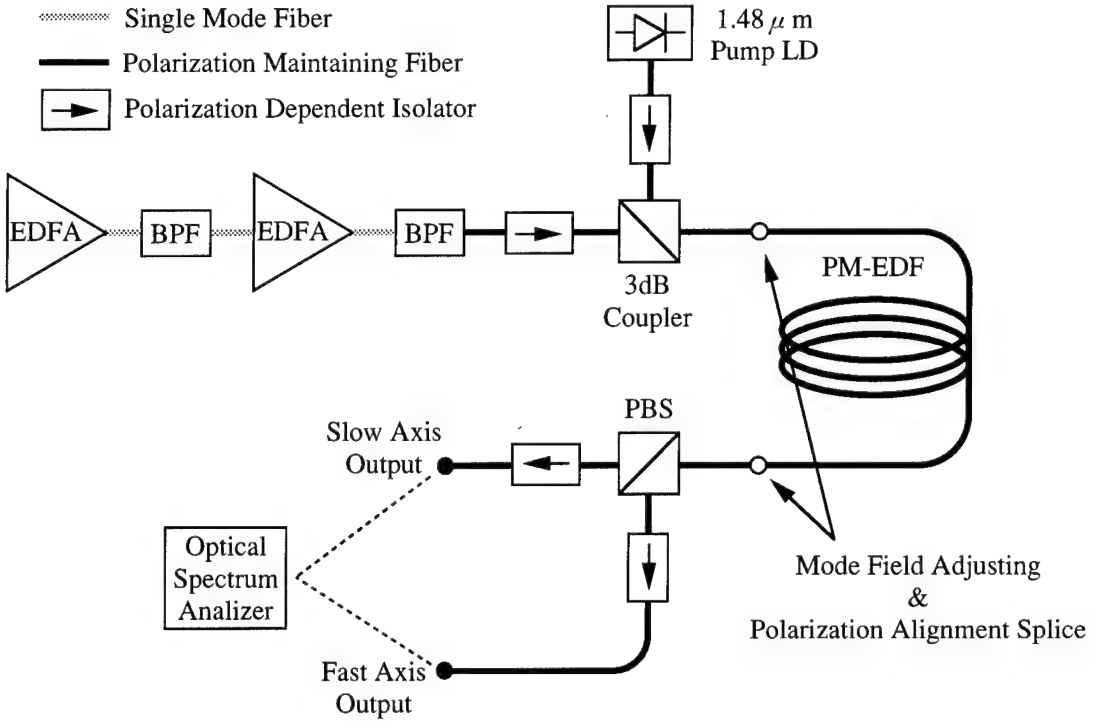

Figure 2. Measurement setup for gain, noise figure and extionction ratio

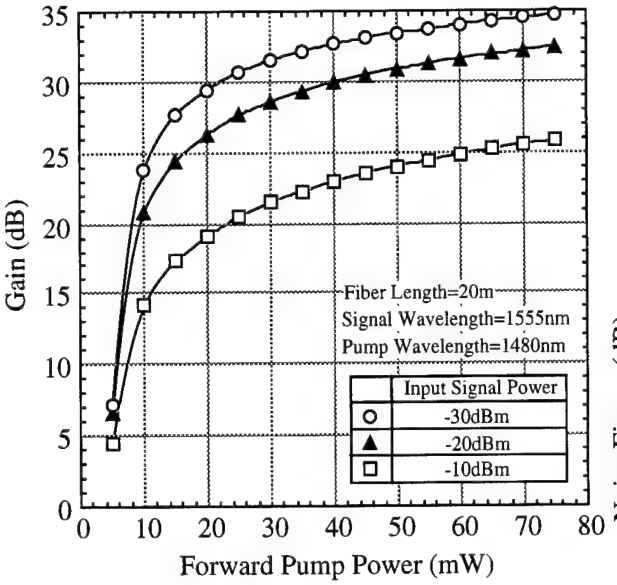

Figure 3. Pump power dependence of gain for different input signal powers

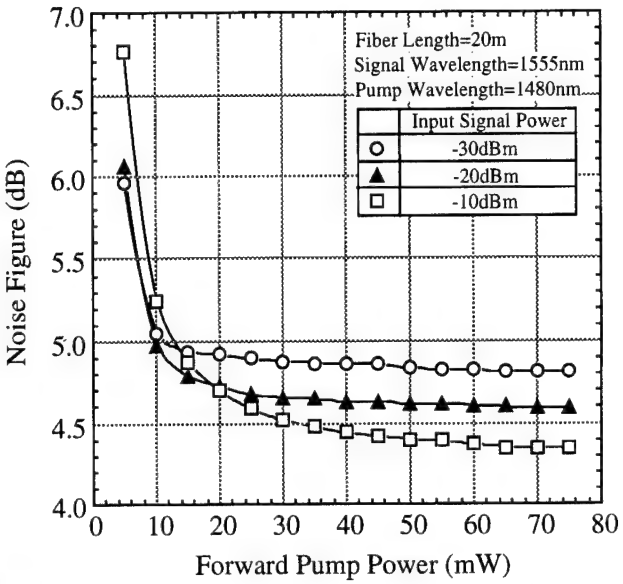

Figure 4. Pump power dependence of noise figure for different input signal powers

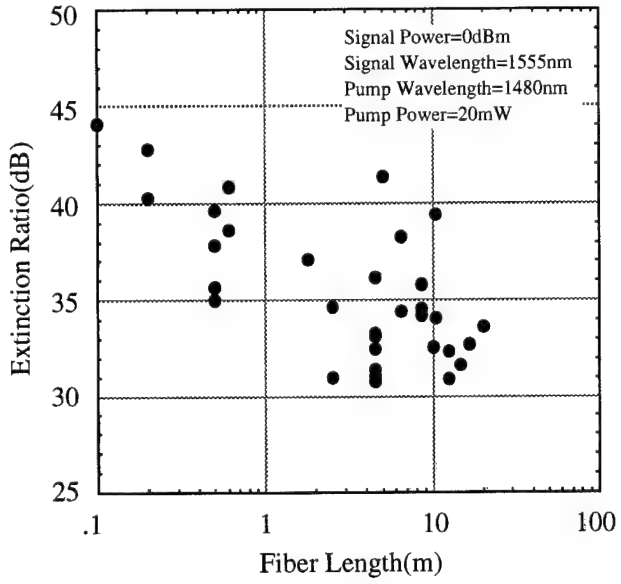

Figure 5. Fiber length dependence of polarization extionction ratio

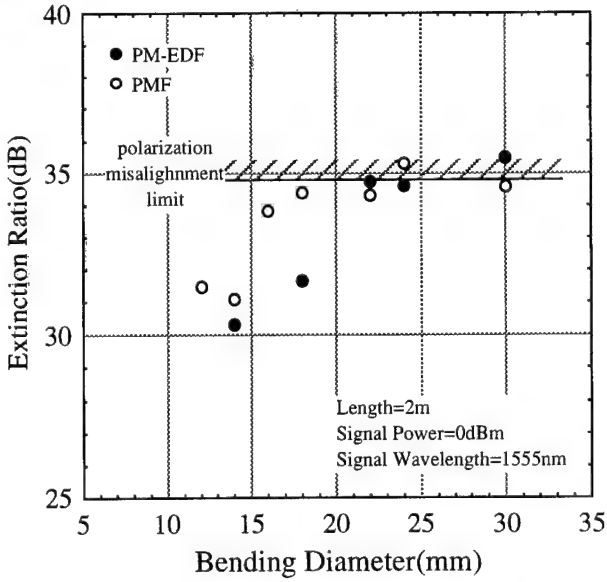

Figure 6. Bending diameter dependence of polarization extinction ratio

Planar Waveguides

FD 17:00-17:45
Theatersaal

Kevin Malone, *Presider*
NIST, U.S.A.

The Erbium-Doped Planar Amplifier: from Laboratory to Local Loop

Martin Hempstead
Optoelectronics Research Centre, University of Southampton, Southampton SO17 1BJ, UK
Tel: +44 1703 592825; Fax: +44 1703 593149

Introduction

The erbium-doped fibre amplifier (EDFA) was invented at the University of Southampton in 1987 [1], and rapidly recognised as a very significant advance. The first commercial EDFAs were available only four years later, making possible fully transparent transoceanic cables with unprecedented bandwidth and expanding the scope of land-based optical networks. Despite their unsurpassed performance, however, EDFAs remain expensive components whose cost must usually be shared among hundreds or even thousands of customers in order to make their use economically viable. They are thus to be found as head-end power amplifiers or booster amplifiers in trunk lines and submarine cables, but not in applications in the local loop.

It is to the local loop that integrated optical components are potentially well-suited. All-optical communication systems demand a variety of functions at the user end, for which the main requirement is low cost, and moderate performance is acceptable. For high-volume, complex, multichannel components such as multiplexers and splitters, integrated optics offer the advantages of mass production through photolithographic techniques and highly reproducible performance. These devices can benefit from incorporation of gain to offset insertion and splitting losses.

Research into erbium-doped planar amplifiers (EDPAs) is underway at a number of industrial and academic laboratories, and publications date from 1990. However, no commercial device exists and none seems imminent. Possible reasons might include technical problems or lack of suitable markets. I will examine these possibilities, and discuss one project aimed at developing practical devices for use in the local loop.

The Status of Research into Erbium-Doped Planar Amplifiers

It is still possible to summarise world-wide EDPA research in a few pages; table I shows the approaches which have been used to make waveguide amplifiers. Other systems are under investigation but have not progressed beyond planar waveguides or spectroscopic studies. Elaborate lasers and amplifiers have been made [2] using flame-hydrolysis-deposited SiO_2-on-Si or Er^{3+}-diffused $LiNbO_3$, but here I consider only simple, broadband single-pass amplifiers.

In comparison to EDFAs, EDPAs have tended to require rather high pump power levels, but otherwise their performance is good. EDPA optical path lengths are shorter than those in EDFAs and their propagation losses higher, so that erbium concentrations are necessarily greater. High dopant levels lead to problems of clustering and uniform upconversion, which degrade the performance. This continues to preclude the short lengths of highly doped amplifier which would have great appeal for use in integrated optics.

Host material	Waveguide Fabrication	Papers
Bulk-doped phosphate glass	Ion-exchange	11
Flame-hydrolysis SiO_2-on-Si	Reactive ion etching	10
Erbium-diffused $LiNbO_3$	Ti-diffusion/Proton exchange	10
Bulk-doped silicate glass	Ion-exchange	9
Sputtered silicate glass	Reactive ion etching	5
Sputtered Y_2O_3 films	Ion beam etching	4
PECVD SiO_2-on-Si	Reactive ion etching	4
Ion-implanted sputtered Al_2O_3	Reactive ion etching	3

Table I: Experimental EDPA systems

While there has been much discussion of the fabrication and performance of EDPAs, little has been written about the technical specifications for practical devices, and the research generally lacks specified technological goals. This perhaps reflects an expectation that the technology will not enter the market place anytime soon. Nevertheless, some existing EDPA systems appear to be capable of meeting the technical specifications for the applications discussed below. This is in contrast to semiconductor optical amplifier devices, which suffer from high insertion and polarization-dependent losses and short excited state lifetimes.

The Status of the Optoelectronics Market

In so far as integrated optics based on insulating dielectrics are concerned, market demand is rather limited. Several companies offer passive devices such as 1xN splitters based on silica-on-silicon waveguides or ion-exchanged waveguides in bulk glasses, and a well-developed range of high frequency signal-processing devices is available in lithium niobate.

While fibre optic trunk lines and EDFAs have been installed piecemeal into existing telecommunications networks, EDPAs can be an economic proposition competitive with "bulk" spliced fibre solutions only if there is a large demand for highly functional devices. For such demand to materialise 1550 nm photons must be present in the local loop. It is not cost-effective to replace existing copper coax networks with fibre, given the limited current demand for truly broadband services which renders the huge potential bandwidth increase irrelevant. On greenfield sites, however, the costs of fibre and coax are comparable, and the enhanced service quality of optical systems makes them the obvious choice. The optical access line project (OPAL) in the former East Germany is making extensive use of fibre networks, and represents a major market for passive integrated optics - some thousands of ion-exchanged splitters have been ordered for deployment over the next few years.

Government support, in the promotion of the "information superhighway" in the United States,

in the European Union RACE programme and in other projects in countries such as Singapore and Japan, will doubtless bring enhanced opportunities for the deployment of integrated optical components, and may encourage companies to develop products they would otherwise see as too risky for backing with scarce research funds.

Ultimately, the future of EDPAs will probably be tied closely to the development of fully optical broadband networks, and the need for compact, loss-compensated components in the local loop and in all-optical switching matrices. The availability of EDPAs will facilitate provision of enormous bandwidth to individual consumers, and play an important part in making the information revolution a reality. However, if these devices are not forthcoming, decisions on operating wavelengths and system designs may close the window of opportunity. The challenge facing EDPA developers is to adapt their already successful technologies to meet immediate needs (which may not exploit the full EDPA potential) cost-effectively.

The RACE 2109 LIASON project: targetted development of an EDPA

Within the European Union RACE programme (Research and technology development in advanced communications technologies in Europe), project LIASON has been funded to develop lossless 1xN splitters for use in the subscriber loop of optical networks. Applications are envisaged in analog CATV and digital PONs. In current CATV scenarios, the optical network power budget runs out at the kerb; incorporation of a lossless splitter allows the optical line to run onto the customer premises. For PONs system in OPAL, a 1x2 "lossless splitter" permits exploitation of the full capacity of optical line terminations in rural areas.

Technical and cost specifications for some of these applications are shown in table II [3]. Note the demanding 0.05 dB PDL requirement for CATV, which is unlikely to be met easily in any system, whether based on fibre or integrated optics. The cost requirements are also rather stringent; for large production volumes (in multiples of 10000 to 100000) they are feasible, but will depend crucially upon the availability of high power pump laser diodes (coupled pump powers 60-70 mW) at moderate cost. Although the PONs application demands the simplest device from a technical point of view, it is unclear whether the demand from the OPAL system can be high enough to bring the price down to a competitive level.

The LIASON concept builds on the extensive experience of its various partners in systems applications of optical networks, EDFAs and rare-earth spectroscopy in glasses and the commercial development and fabrication of high performance passive ion-exchanged splitters and multiplexers. The LIASON devices will be ion-exchanged waveguides in silicate glass hosts, with an upstream erbium-doped section to compensate the power reduction due to splitting up to 16 ways in a downstream, undoped section of cascaded y-junctions.

The LIASON realisation is handicapped by the bulk doping, which gives rise to deleterious reabsorption losses in the 3-level erbium system, lowering the gain and increasing the noise figure. However, careful host selection and characterization in combination with detailed modelling indicate that the required performance is attainable for at least some of the applications. This is provided the modal sizes and propagation losses in the amplifier section can be made small enough; good progress is being made in this direction.

The level of integration in the generation of LIASON devices under development is quite

	PON 1x2	CATV 1x16
Splitting "loss"	3 dB	12 dB
Noise figure at given fibre-to-fibre gain	< 10 dB (5dB gain)	<5.3 dB (0dB gain)
Internal reflection	<-23 dB	<-49 dB
Gain slope	-	<0.1 dB/nm
Polarisation-dependent loss	-	<0.05 dB
Unit cost/kECU	<2.6	<4.2

Table II: Specifications for Lossless Splitters

modest, but still represents a major simplification over a fibre-based solution, incorporating as it will on one chip pump/signal multiplexer, amplifier, pump/signal demultiplexer and 1xN splitter. Potential enhancements to take advantage of the integration and photolithographic fabrication technique include gain-flattening and provision for bidirectional operation, perhaps involving additional signals in the 1300 nm band.

Conclusion

While EDFAs have achieved technological maturity and commercial success, EDPAs remain a matter for laboratory research. EDPAs are potentially highly competitive for large-volume applications where economies of scale and the advantages of easy mass production become significant, and they can make significant contributions to the "information revolution". Technically, they can probably meet or exceed the relevant specifications for applications such as lossless splitters. EDPAs are thus suitable for deployment in the local loop, but at present pump laser costs they will be viable only in volumes of many thousands. Major programmes such as OPAL currently provide the kind of market necessary to make EDPAs a commercial reality; in the future, various national "information superhighways" may help move them from the laboratory to the local loop.

Acknowledgements

This work was supported by the RACE Programme in project R2109. The Optoelectronics Research Centre is an Interdisciplinary Research Centre supported by the UK EPSRC.

References

[1] R.J. Mears, L. Reekie, I.M. Jauncey, D.N. Payne, *Electronics Letters*, 23, 1026 (1987).

[2] See, for example, H. Suche, *Proceedings 7th European Conference on Integrated Optics, Delft, The Netherlands*, 565-570, April 1995.

[3] A.M.J. Koonen, F.W. Willems, R. Ries, C. Lerminiaux, *Proceedings 7th European Conference on Integrated Optics, Delft, The Netherlands*, 479-482, April 1995.

Selected References for Table I

Bulk-doped phosphate glass:

"Yb/Er integrated optics amplifiers in phosphate glass in single and double pass configurations," D. Barbier, J.M. Delavaux, A. Kevorkian, P. Gastaldo, J.M. Jouanno, *OFC '95*, postdeadline paper PD3-1.

"Erbium-doped composite glass waveguide amplifier," W.J. Wang, S.I. Najafi, S. Honkanen, Q. He, C. Wu, J. Glinski, *Electronics Letters*, 28, 1872 (1992).

Flame-hydrolysis SiO_2-on-Si:

"Erbium-doped silica-based waveguide amplifier integrated with a 980/1530 nm WDM coupler," K. Hattori, T. Kitagawa, M. Oguma, Y. Ohmori, M. Horiguchi, *Electronics Letters*, 30, 856 (1994).

Erbium-diffused lithium niobate:

"Erbium-doped single-pass and double-pass Ti:$LiNbO_3$ waveguide amplifiers," R. Brinkmann, I. Baumann, M. Dinand, W. Sohler, H. Suche, *IEEE J. Quantum Electronics*, 30, 2356 (1994).

Bulk-doped silicate glass:

"Ion-exchanged waveguide amplifier in erbium-doped glass for broad-band communications," P. Camy, J.E. Román, M. Hempstead, P. Laborde, C. Lerminiaux, *Topical Meeting on Optical Amplifiers and Their Applications, paper FD2, Davos, Switzerland*, June 1995.

"Erbium-doped ion-exchanged waveguide laser in BK-7 glass," T. Feuchter, E.K. Mwarania, J. Wang, L. Reekie, J.S. Wilkinson, *IEEE Photonics Technology Letters*, 4, 542 (1992).

Sputtered silicate glass:

"Systems evaluation of an Er^{3+}-doped planar waveguide amplifier," G. Nykolak, M. Haner, P.C. Becker, J. Shmulovich, Y.H. Wong, *IEEE Photonics Technology Letters*, 5, 1185 (1993).

Sputtered Y_2O_3 films:

"Sputter-deposited erbium-doped Y_2O_3 active optical waveguides," T.H. Hoekstra, P.V. Lambeck, H. Albers, T.J.A. Popma, *Electronics Letters*, 29, 581 (1993).

PECVD SiO_2-on-Si:

"Erbium-doped phosphosilicate glass waveguide amplifier fabricated by PECVD," K. Shuto, K. Hattori, T. Kitagawa, Y. Ohmori, M. Horiguchi, *Electronics Letters*, 29, 139 (1993).

Ion-implanted sputtered Al_2O_3:

"Optical gain in erbium-implanted Al_2O_3 waveguides," G.N. van den Hoven, E. Snoeks, A. Polman, C. van Dam, J.W.M. van Uffelen, M.K. Smit, *Proceedings 7th European Conference on Integrated Optics, Delft, The Netherlands*, 229, April 1995.

Ion-Exchanged Waveguide Amplifier in Erbium-Doped Glass for Broad-band Communications

Patrice Camy
Corning Europe Inc., 7 bis, Avenue de Valvins, 77210 Avon, France
Tel: +33 1 64 69 74 00; Fax: +33 1 64 69 74 54
José E. Román, Martin Hempstead
Optoelectronics Research Centre, University of Southampton, Southampton SO17 1BJ, UK
Tel: +44 1 1703 593088; Fax: +44 1 1703 593149
Pascale Laborde, Christian Lerminiaux
Corning Europe Inc., 7 bis, Avenue de Valvins, 77210 Avon, France

Introduction

Integrated optical circuits have the potential to be inexpensive devices suitable for mass manufacture, with complex functionality and reproducible properties. In optical networks such as those envisioned for digital telephony in Germany and for CATV services, optical power is exhausted at the curb, and the signal from an optical channel termination must be carried electrically to a number of end users. The EU RACE project R2109 LIASON has proposed a "lossless splitter," combining an upstream amplifier section and a downstream splitter to extend the optical network into customer premises [1]. The combination of stringent fabrication tolerances and a large potential market makes an integrated optical circuit an ideal solution. In the LIASON project this circuit will be realised using ion-exchanged waveguides in a dual glass substrate, one portion - the amplifier section - doped with erbium and the other undoped. The most stringent requirements arise from the 1x16 CATV lossless splitter [1], which demands a gain of about 13 dB and a noise figure of better than 5.4 dB for a coupled 980 nm pump power of 70 mW. We describe here the status of our development of the amplifying portion of this device.

Design considerations

Compared to fiber devices, planar waveguides have high propagation losses, so that an erbium amplifier must be relatively highly doped and short in order to perform well. Given this requirement for high doping levels, we need a glass host that minimises the well-known problems of clustering and uniform upconversion.

The erbium-doped amplifier employs a quasi-3-level energy level structure, so that the use of a bulk host incurs reabsorption losses which reduce the net gain and increase the noise figure. For this reason, most planar erbium-doped devices reported to date [2,3] utilize the etching of thin doped films to define waveguides in which the erbium ions are confined to the core. However, the effect of reabsorption may be greatly mitigated by using very tightly confined waveguide modes. Moreover, with the ion-exchange technique we have fabricated waveguides with propagation losses below 0.05 dB cm^{-1} in undoped waveguides. This is significantly lower than for etched guides with inherently higher roughness.

Amplifier Fabrication and Waveguide Characterization

We used as substrates polished borosilicate glass wafers doped with 0.5 wt% Er_2O_3 ($3.95x10^{19}$ Er^{3+} cm^{-3}). We have studied a number of candidate host materials; this glass has been selected because it showed no tendency to clustering or phase separation, and the uniform upconversion coefficient is expected to be low [4].

The waveguides were fabricated by a 2-step diffusion process in molten salt baths. In the first step, Tl^+ indiffusion through a mask produced waveguide structures, which were then buried by a second field-assisted and maskless exchange to improve the propagation loss and mode profile. The maximum refractive index difference is approximately 1.5%, which permits a waveguide bend radius as low as 10 mm without significant additional losses.

Waveguides of length 23 cm, with the layout shown in fig. 1, and 45 cm were made. The 23 cm guide had a cutoff at 1240 nm, and an insertion loss of 4.3 dB (including coupling losses) as measured at 1310 nm with standard monomode SMF28 fibers. The 45 cm guide had an insertion loss of 7.3 dB at the same wavelength. This indicates propagation losses of about 0.15 dB cm^{-1} and coupling losses of the order of 0.5 dB per interface.

The erbium aborption spectrum in the 1450-1570 nm range was determined by two methods; from the absorption of the emission from a tunable laser diode and from the transmission spectrum of white light as measured with a monochromator. The two methods were in good agreement, and the peak absorption at about 1537 nm was 23.5 dB in the 23 cm guide.

The mode profiles of the waveguides were measured by imaging the near-field; at 1550 nm (980 nm), the diameter at $1/e^2$ intensity was 8.5 μm (7 μm) in the direction parallel to the surface, and 6 μm (5μm) in the depth direction.

Amplifier performance

We have measured the gain of the 23 cm device at 1537 nm for pump wavelengths of 980 nm and 1480 nm. Fig. 2 shows the internal gain (ratio of signal intensity with and without pump minus signal absorption without pump) versus transmitted 980 nm pump power (for 40 mW of transmitted power the incident power was 230 mW). We obtained a maximum internal gain of about 10 dB, corresponding to about 6 dB net gain. Pumping with 50 mW incident power at 1480 nm, we observed approximately 5 dB internal gain, for a negligible net gain.

Modelling the amplifier performance

We have developed a comprehensive numerical model for the amplifier, which includes the effects of uniform upconversion and clustering, as well as forward and backward ASE and pump and signal saturation. It accounts for the mode profiles, assuming Gaussian intensity distributions. Uniform upconversion is incorporated as a quadratic term in the rate equations.

As inputs to this model, we have determined the appropriate absorption and emission spectra,

and estimated the uniform upconversion coefficient σ_{UC} from spectroscopic measurements [4]. In the context of the pair-induced-quenching model [5], we have an upper limit for the clustering fraction f_c of less than 0.1 (i.e. <10% of ions are in clusters).

We have indicated on fig. 2 the modelled gain when pumping at 980 nm, under different assumptions about the uniform upconversion coefficient and the level of clustering. These differing assumptions reflect our uncertainty about these quantities, but it must be noted that some of the other parameters, such as waveguide losses at 980 nm and the exact modal profiles, also have non-negligible uncertainty. Given these uncertainties, we conclude that the model is in reasonable agreement with the data, although its predictions are reliable only to within about ±2 dB at the highest pump powers used.

Conclusion

For the first time in an ion-exchanged waveguide format, we have fabricated long, low-loss guides which show appreciable net gain when pumped at 980 nm. This performance is comparable with 10 dB for 280 mW of pump power in sputtered guides [2] but inferior to the 27 dB for 264 mW of pump achieved in flame-hydrolysis deposited guides [3].

Although promising, the performance as yet falls far short of that required for the intended CATV application. We are currently working to make substantial improvements by exploiting the high index change - up to 0.1 - possible with Tl^+ ion exchange to make much more tightly confined modes. We also anticipate that detailed study of the fabrication conditions, combined with the use of an overlay, will enable us to reduce the signal propagation losses towards the values we have achieved in undoped guides, of less than 0.05 dB cm^{-1}.

Acknowledgements

This work was supported by the RACE Programme in project R2109. The Optoelectronics Research Centre is an Interdisciplinary Research Centre supported by the UK EPSRC.

References

[1] "System requirements and opportunities for lossless active splitters," A.M.J. Koonen, F.W. Willems, R. Ries, C. Lerminiaux, to be presented at ECIO, Delft, Holland, April 1995.

[2] "Systems evaluation of an Er^{3+}-doped planar waveguide amplifier," G. Nykolak, M. Haner, P.C. Becker, J. Shmulovich, Y.H. Wong, IEEE Photon. Technol. Lett., 5, 1185 (1993).

[3] "Erbium-doped silica-based waveguide amplifier integrated with a 980/1530 nm WDM coupler," K. Hattori, T. Kitagawa, M. Oguma, Y. Ohmori, M. Horiguchi, Electron. Lett., 30, 856 (1994).

[4] "Anomalously high uniform upconversion in an erbium-doped waveguide amplifier," M. Hempstead, J.E. Román, C.C. Ye, J.S. Wilkinson, P. Camy, P. Laborde, C. Lerminiaux, to be presented at ECIO, Delft, Holland, April 1995, paper TuC4.

[5] "Modelling of pair-induced quenching in erbium-doped silicate fibers," E. Delevaque, T. Georges, M. Monerie, P. Lamouler, J.-F. Bayon, IEEE Photon. Technol. Lett. 5, 73 (1993).

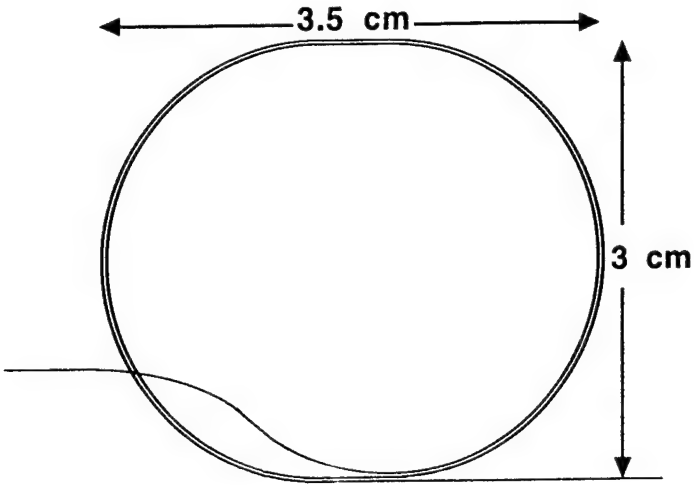

Fig. 1: Scheme of 23 cm waveguide layout

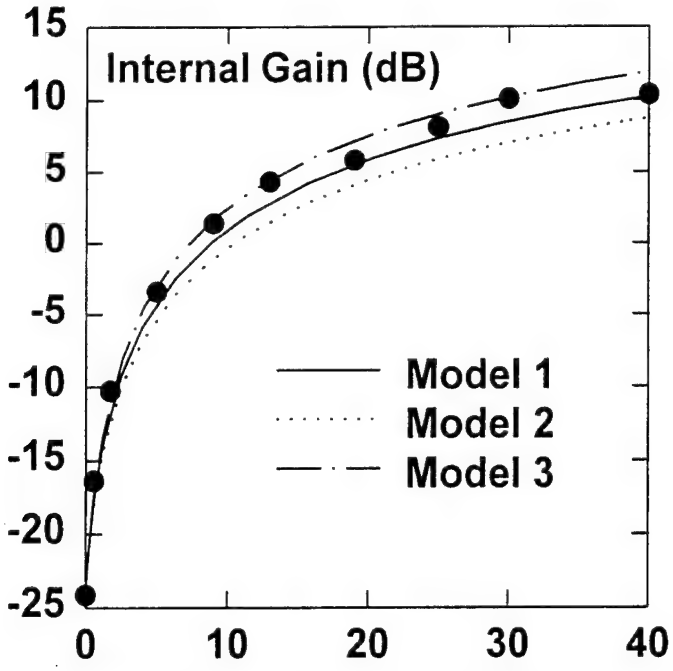

Fig. 2: Internal gain. Model parameters:

1: f_c= 0.05, σ_{UC}=2x10^{-18} cm^3 s^{-1}

2: f_c= 0.1, σ_{UC}=3x10^{-18} cm^3 s^{-1}

3: f_c= 0.0, σ_{UC}=1x10^{-18} cm^3 s^{-1}

Alternative Fiber Amplifiers

SaA 8:45-10:30
Theatersaal

Thierry Georges, *Presider*
France Telecom

1.3 μm Cascaded Raman Amplifiers

S.G. Grubb
AT&T Bell Laboratories
600 Mountain Avenue
Murray Hill, NJ 07974

Abstract: A novel cascaded Raman resonator approach has been used to utilize high-power, fiber-coupled pump sources in the 1-μm region to amplify signals at 1.3 μm in germanosilicate fibers. Gains of 40 dB and output powers of +24.6 dBm have been achieved. The first successful digital transmission test of a 1.3 micron cascaded Raman amplifier has also been completed.

Introduction: Prior to the advent of the Er^{3+} fiber amplifier, there was considerable work on Raman fiber amplifiers for optical amplification in the 1.5 μm transmission window.[1] There are currently no rare-earth-doped silica-fiber-based amplifier options in the 1.3 μm region. Pr^{3+}-doped fluoride fiber amplifiers already require substantially increased pump powers relative to Er^{3+} fiber amplifiers. Fluoride fibers also suffer the disadvantage of the inability to fusion splice to normal silica transmission fiber. Given the recent emergence of high-power, diffraction-limited, diode-based, cladding pumped fiber lasers (up to 5 Watts CW)[2] and other diode-pumped solid state lasers, Raman amplifiers merit a re-investigation for application in the 1.3 μm transmission window. The ability to fabricate low -loss Bragg grating resonators directly in germanosilicate fibers also leads to the possibility of constructing nested highly reflecting gratings. In this way, each intermediate Raman Stokes order can be resonated and thereby efficiently converted to the next higher Stokes order until the cascade is terminated by suitable output coupling at the desired order. Others have reported Raman amplifiers at 1.3 microns in germanosilicate fibers but without the use of resonant cavities. Gains coefficients comparable to Pr^{3+} -doped fiber amplifiers have been achieved in high-delta germanosilicate fibers[3] and gains of 39 dB have been obtained using germanosilicate fibers in a ring configuration with WDM couplers[4].

Two cascaded Raman configurations have to used to amplify signals at 1.31 μm in silica fibers. The first is to generate the third Stokes order at 1240 nm in a cascaded Raman laser pumping with a Nd^{3+} fiber laser at 1060 nm and then subsequently pump a separate section of silica fiber to amplify at 1.3 μm. This has the advantage of separate optimization of the Raman laser and amplifier sections, choosing between co- and counter-propagating amplification, and the ability to achieve distributed amplification in a standard silica transmission fiber. The second configuration is to write highly reflecting gratings through the first three orders, thereby increasing the circulating power at the third Stokes frequency, and inject a 1.3 μm signal (4^{th} Stokes) through this resonant structure. This configuration is again possible through the use of fiber Bragg gratings which can be made to be highly reflecting at any given Stokes order, but transparent to light at the other

circulating Stokes orders, and have negligible backreflection at the signal wavelength of 1.3 μm.

The germanosilicate fibers used in these experiments were slightly modified from the AT&T Accutether design. The fiber was H_2 sensitized prior to UV exposure to increase the photosensitivity[5]. The pump source was a diode-pumped, cladding-pumped Nd^{3+} fiber laser at 1060 nm. The rectangular silica fiber was then fusion spliced to a standard 125 μm circular fiber.

A 1060 nm-pumped, third-order-cascaded Raman laser was constructed using 800 meters of germanosilicate fiber. With a 20% output coupler at the third Stokes frequency of 1240 nm, a threshold of 175 mW and a slope efficiency of 53% have been obtained. Another laser with 4% output coupling resulted in a threshold of 450 mW, a slope efficiency of 61%, and a total output of 1.2 Watts at 1240 nm. A 10 km section of germanosilicate fiber was then pumped with a third order Stokes laser and the resultant pump on/off ratio was found to be 40 dB. The loss of the 1.3 μm signal through the unpumped amplifier is merely the passive loss of the silica fiber and any WDM's or isolator, and hence can be as low as 3 dB. The intracavity pumped version, using 1.5 km of fiber between the highly reflecting Stokes gratings (shown in Figure 1b), was then constructed. When operating the third-Stokes, intracavity configuration as a power amplifier, a +24.7 dBm output power was obtained for a signal input power of 0 dBm.

The first systems demonstration of a cascaded Raman amplifier at 1.3 microns has been achieved at 2.5 Gb/s.[6] A 1.3 micron signal was amplified and followed by a 42 km span of convention 1.3 micron zero dispersion fiber. No noise floor was evident in the BER measurements. The performance of the Raman amplifier was found to be highly dependent on the noise sources in the 1240 nm third-order cascaded Raman laser, particularly any residual ASE at 1.3 microns which is injected into the amplifying section. The dependence of systems performance on pump noise will be further discussed.

In conclusion, we have reported the first demonstration of a CW, diode-pumped, silica fiber amplifier at 1.3 μm. A cascaded, resonant Raman laser cavity utilizing intracavity Bragg gratings has been utilized to efficiently convert high-brightness, CW, fiber laser sources at 1060 nm to the third Stokes frequency at 1240 nm which in turns acts as a pump for a Raman amplifier at 1.31 μm. A gain of 35 dB and an output power of +24.7 dBm have been demonstrated. This amplifier has the advantage of using low-loss, fusion spliceable, germanosilicate fibers and being transparent when unpumped. The Raman amplification process is a strong function of decreasing fiber effective area and loss, hence substantially improved results are expected from optimized high-delta, low-loss germanosilicate fibers.

References:

1. Y. Aoki, J. Lighwave Technology, 6(7), 1225, 1988.

2. H. Po et. al. , Electr. Lett., 29(17), 1500, 1993.

3. E. Dianov, D. Fursa, A. Abramov et. al., Quantum Electronics, 24(9), 749, 1994.

4. S.V. Chernikov, Y. Zhu, J.R. Taylor, and R. Kashyap, Proc, CLEO '95, paper CMB7, Baltimore, MD May 21-26, 1995.

5. P.J. Lemaire, R.M. Atkins, V. Mizrahi, and W.A. Reed, Elect. Lett., 29, 1191 (1993).

6. D.R. Dykaar, S.G. Grubb, J. Simpson, T. Strasser, A. Vengsarkar, J.M. Borick, W.Y. Cheung, and S.B. Darack, Proc. OFC '95, paper PD1, San Diego, CA, February26-March 3, 1995.

Raman Amplifier For 1.3 μm On The Base Of Low-Loss High-Germanium-Doped Silica Fibers

E.M.Dianov, A.A.Abramov, M.M.Bubnov, A.V.Shipulin,
S.L.Semjonov, A.G.Schebunjaev

Fiber Optics Research Center at the General Physics Institute
Russian Academy of Sciences
38 Vavilov Street, Moscow 117942, Russia
Phone:(095)135 05 66. Fax:(095)135 81 39.

A.N.Guryanov, V.F.Khopin

Institute of Chemistry of High-Purity Substances,
Russian Academy of Sciences
49 Tropinin Street, N.Novgorod 603600, Russia

1. Introduction.

There is currently a great deal of interest in the development of 1.3 μm fiber amplifiers. Up to now the majority of cases Pr-doped fluoride fibers have been used in order to achieve high gain characteristics [1,2,3]. But fluoride fibers suffer the number of disadvantages, such as comparatively high level of the required pump powers and also the difficulties of the fabrication of silica-to-fluoride splices. Besides, there is a problem of fluoride fibers' strength and reliability. In this paper we report the results of our experiments using stimulated Raman scattering in the low-loss high-germanium-doped silica fibers for signal amplification in 1.3 μm transmission window.

The ability to fabricate high-germanium-content silica fibers with the reduced optical losses [4,5] has allowed us to achieve high gain coefficients at Raman amplification, which turned out to be comparable with the same ones of the conventional Pr-doped fiber amplifiers and at least two times higher than in the Raman amplifier using silica fiber with low germanium concentration [6]. Moreover, the application of 1.24 μm CW third Stokes radiation in high-germanium-doped fiber from 1.064 μm CW Nd:YAG laser as a pump source for the Raman

amplifier, proposed to our knowledge for the first time in paper [4], and the subsequent development of this method by using fiber Bragg grating resonators [6], allow to examine Raman amplifier as an alternative to a Pr-doped fiber amplifier.

2. Experimental and numerical results

The co-directional configuration has been used for the signal amplification in the vicinity of 1.31 μm, as shown in Fig.1. The third Stokes component was generated in the 0.5-km fiber with high germanium content. The increase of the germanium concentration generally should lead to the increase in gain, which is largely the result of the reduction in the fiber mode field diameter and of an enhancement in the stimulated Raman scattering gain coefficient. But the problem is to decrease the higher level of the germanium-induced excess losses, which reduce the gain efficiency.

High-aperture single-mode fibers with GeO_2 concentration of 12-32 mol.% for gain measurements were fabricated by the MCVD technique. The loss decrease in them was obtained due to the methods described in [7]. In spite of the essential progress in loss reduction, the exponential growth of loss dependence was observed at GeO_2 concentrations exceeding 15 mol.% in comparison with usual theoretical linear approximation of the minimum possible Rayleigh losses (Fig.2).

In order to estimate the possible Raman gains the numerical analysis has been done for real values of losses in fabricated fibers and also for losses in "ideal" fibers with minimum Rayleigh losses.

The experimental and calculated results for the maximum net small signal gain at 1.309 μm and pump power of 400 mW are shown in Fig.3. The maximum net gain which was achieved today turned out to be 24.4 dB in a fiber of about 4-km length with 25 mol.% GeO_2. The gain measurements for the fibers with other GeO_2 concentrations are in progress and will be presented. It is seen from Fig.3 that the possible gain level in fabricated fibers with GeO_2 concentration of about 13 mol.% may be higher than 40 dB at the proper fiber length.

The pump power dependences of gains were measured and computed for fibers with GeO_2 concentrations of 25 mol.% and 13 mol.% (Fig.4). The quite satisfactory agreement between them is observed at least for pump powers of up to 400 mW. The values of gain coefficient which were achieved in a fiber with 25 mol.% GeO_2 turned out to be 0.1 dB/mW and may reach 0.15 dB/mW in a fiber with 13 mol.% of GeO_2. These values of gain coefficients are comparable with the same ones of the conventional Pr-doped fiber amplifiers and considerable exceed the values for the low GeO_2 content fibers [6] (Fig.5).

The efficiency of the Raman amplifier is dependent on the fiber length. The computed values of the optimum fiber lengths, at which the gain may reach the maximum are shown in Fig.6 for the fabricated fiber and for the "ideal" fibers with the minimum Rayleigh losses as a function of GeO_2 concentration and different pump powers.

3. Conclusion

We have shown that Raman amplifiers for 1.3 μm based on the high-germanium-doped silica fibers with the reduced excess losses allow to reach high gain level of up to 40 dB with gain coefficients of 0.1-0.15 dB/mW. Further progress may be expected from the application of the improved high-aperture silica-germanium fibers and the amplifier configuration with fiber Bragg grating resonators.

4. References

1. T.Whitley, ECOC'94, Firenze, Proc.vol.2, pp.939-946, 1994.
2. E.Taufflieb, D.Joulin, H.Lefevre et al., OFC'94, San Jose, Tech.Digest, PD-4, pp.27-30, 1994.
3. M.Shimizu, T.Kanamori, J.Temmyo et al., OFC'93, San Jose, Tech.Digest, PD-12, pp.52-55, 1993.
4. E.Dianov, D.Fursa, A.Abramov et al., Quantum Electronics, vol.24(9), pp.749-751, 1994.
5. E.Dianov, D.Fursa, A.Abramov et al., ECOC'94, Firenze, Proc.vol.1, pp.427-430, 1994.
6. S.Grubb, T.Erdogan, V.Mizrahi et al., OAA'94, Breckinridge, PD3, 1994.
7. A.Abramov, M.Bubnov, E.Dianov et al., OFC'95, San Diego, Tech.Digest, WP4, 1995.

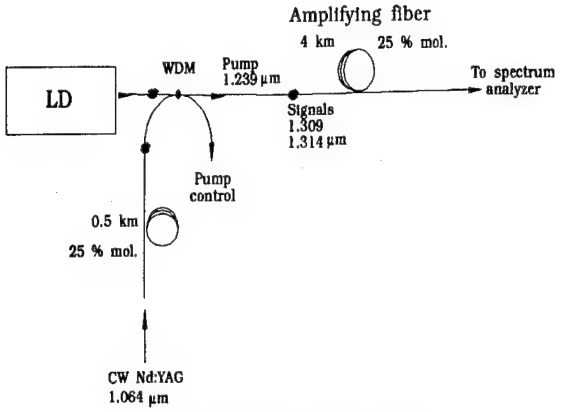

Fig 1. Experimental set up.

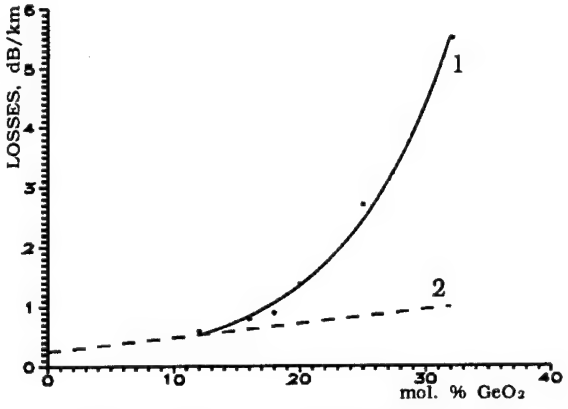

Fig 2. Losses vs. concentration of GeO_2 at 1.31 μm for fabricated fibers (1); linear approximation of the minimum Rayleigh losses (2).

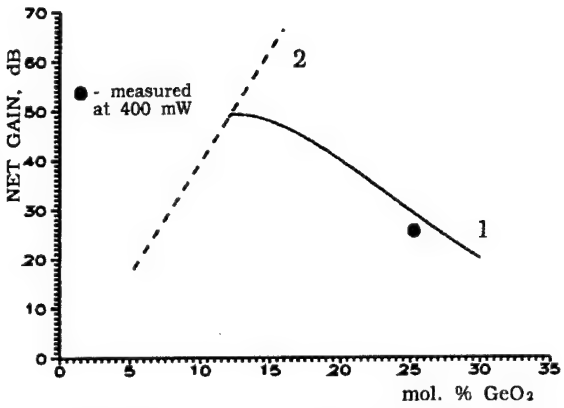

Fig 3. Net small signal gain for 400 mW pump power vs. concentration of GeO_2 for fabricated fibers (1) and for "ideal" fibers with the minimum Rayleigh losses (2).

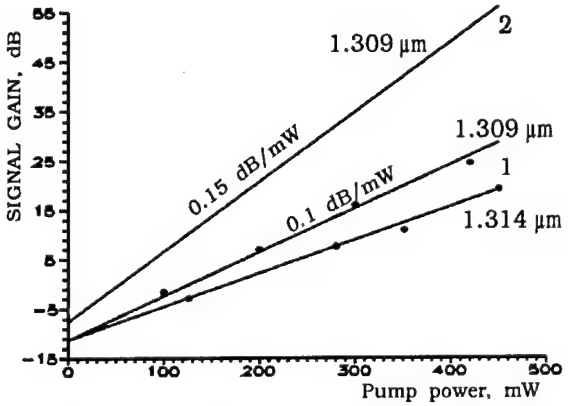

Fig 4. Comparison of measured (data points) and computed small signal gains vs. pump power for fibers with 25 mol. % (1) and 13 mol. % (2) GeO_2 .

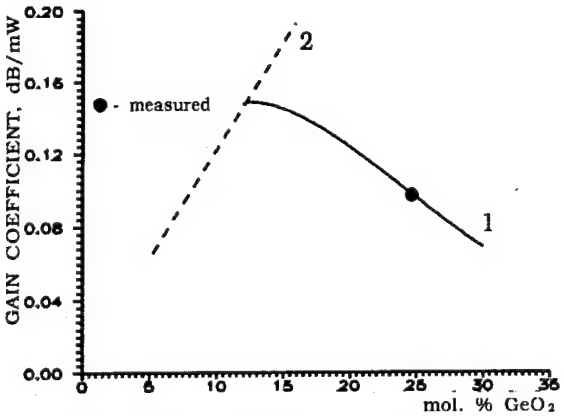

Fig 5. Gain coefficient vs. concentration of GeO_2 for fabricated fibers (1) and for "ideal" fibers with the minimum Rayleigh losses (2).

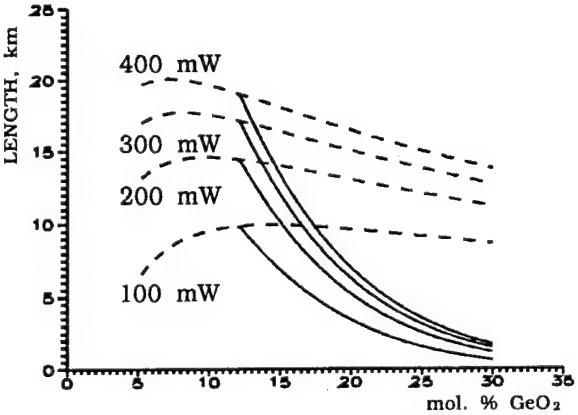

Fig 6. Fiber length for the maximum gain vs. concentration of GeO_2 at different pump powers for the fabricated fibers (solid lines) and for "ideal" fibers (dashed lines) with the minimum Rayleigh losses.

Fiber Optical Parametric Amplifier Operating Near Zero-Dispersion Wavelength

N. Kagi, T. K. Chiang, M. E. Marhic, and L. G. Kazovsky

Department of Electrical Engineering, Stanford University
Durand 202, Stanford, CA 94305-4055

Phone: 415-725-6932, Fax: 415-723-9251

Introduction: Erbium-doped fiber amplifiers (EDFAs) have many attractive features including high pump efficiency, immunity to saturation-induced crosstalk, and easy coupling to transmission fibers. However, the gain bandwidth of EDFAs is limited to 35 nm. In addition, the gain spectrum of the doped-fiber amplifiers is primarily determined by the dopant, and is thus difficult to change. Fiber optical parametric amplifiers (OPAs) do not suffer from these limitations, as they can in principle operate at any nominal wavelength, corresponding to the zero-dispersion wavelength λ_0 of a fiber [1], and a large bandwidth can be obtained by setting the pump wavelength close to λ_0. Although fiber OPA power gains over 30 dB have been demonstrated [2] [3] [4], to our knowledge the gain spectrum and the saturation characteristics have not been investigated. In this paper, we investigate theoretically and experimentally these features for a fiber OPA operating near λ_0.

Theory: Consider collinearly polarized pump and signal optical waves at frequencies f_P and f_S, respectively. When the two waves copropagate through an optical fiber, four-wave mixing generates a third wave at $2f_P - f_S$ (idler). The complex amplitudes of the three waves – pump A_P, signal A_S, and idler A_I – are governed by the following equations [5]:

$$\begin{aligned}
\frac{dA_P}{dz} &= i\gamma\left(|A_P|^2 + 2|A_S|^2 + 2|A_I|^2\right)A_P + 2i\gamma A_P{}^* A_S A_I \exp(i\Delta k z) - \frac{\alpha}{2}A_P, \\
\frac{dA_S}{dz} &= i\gamma\left(2|A_P|^2 + |A_S|^2 + 2|A_I|^2\right)A_P + i\gamma A_P{}^2 A_I{}^* \exp(-i\Delta k z) - \frac{\alpha}{2}A_S, \\
\frac{dA_I}{dz} &= i\gamma\left(2|A_P|^2 + 2|A_S|^2 + |A_I|^2\right)A_I + i\gamma A_P{}^2 A_S{}^* \exp(-i\Delta k z) - \frac{\alpha}{2}A_I,
\end{aligned} \tag{1}$$

where γ is the nonlinear coupling coefficient [1], Δk is the low-power propagation-constant mismatch, and α is the loss coefficient of the fiber. The first, second and third terms in Eqs. (1) correspond to the nonlinear refractive index change, four-wave mixing, and intrinsic fiber loss, respectively. In the zero-dispersion wavelength region, Δk can be written as [6]:

$$\Delta k = -\frac{2\pi c}{\lambda^2}\frac{dD}{d\lambda}(\lambda_S - \lambda_P)^2(\lambda_P - \lambda_0), \tag{2}$$

where λ_S and λ_P are the signal and pump wavelengths, respectively; $dD/d\lambda$ is the dispersion slope of the fiber. Using Eqs. (1) and (2), one can calculate OPA's gain spectrum and saturation characteristics.

Experiment: Fig. 1 shows the experimental setup. Since the parametric amplifier needs high pump power, a pulsed pump source was used in our experiments. A tunable DBR laser diode was driven with a train of 80-nsec square pulses with a duty cycle of 1/32. The laser output was amplified by an EDFA and used as a pump. A tunable external-cavity laser diode (ECL) was used as a signal light source. The pump and signal wavelengths were monitored by an optical spectrum analyzer (OSA). The intensity of the signal light was modulated at 400 MHz to allow AC measurements. A variable optical attenuator (ATT) was used to adjust the signal power. The pump and signal were launched into the OPA medium – a dispersion-shifted fiber (DSF), of length $L = 12$ km. The DSF had a zero-dispersion wavelength of 1557.9 nm, a dispersion slope of 0.067 ps/km•nm^2, and a loss coefficient of 0.23 dB/km. The peak pump power launched into the DSF was 180 mW. We confirmed that stimulated Brillouin scattering in the DSF was negligible by measuring the transmitted and reflected pump powers. At the end of the DSF, a tunable optical bandpass filter (OBPF) was used to select either signal or idler light. The output from the filter was detected by an O/E converter and sent to an oscilloscope. No optical isolator was needed because the parametric gain is unidirectional. The parametric gain in the DSF was measured by comparing the 400 MHz component of the output signal (or idler) with that of the input signal. The polarization of the signal light was adjusted using a polarization controller (PC) to obtain the maximum parametric gain.

Results: Eqs. (1) were integrated numerically using $\gamma = 2\times10^{-3}\,\mathrm{m^{-1}W^{-1}}$ and the above experimental parameters. Fig. 2 (a) shows the gain spectra calculated for four different values of $\lambda_P - \lambda_0$. The input signal power is -12 dBm. The solid lines show the signal power gain $G_S = |A_S(L)|^2 / |A_S(0)|^2$ and the broken lines show the idler power gain $G_I = |A_I(L)|^2 / |A_S(0)|^2$. From Eqs. (1), it can be shown that the relationship $G_S = G_I + \exp(-\alpha L)$ holds [7].

The shape of the gain spectrum depends on the sign of $\lambda_P - \lambda_0$. The reason is as follows. Because of the nonlinear refractive index change, the effective propagation-constant mismatch κ at high pump power and low signal power is given by $\kappa = \Delta k + 2\gamma P_P$ [1], where P_P is the pump power. The optimum gain occurs at $\kappa = 0$. Because $dD/d\lambda > 0$, the pump wavelength is in the normal dispersion region when $\lambda_P - \lambda_0 < 0$. In this case, $\Delta k \geq 0$ holds (see Eq. (2)) and κ is always positive since $\gamma > 0$ for silica fibers. Thus phase matching ($\kappa = 0$) cannot be achieved and the gain is maximum when $\lambda_S - \lambda_P = 0$; this gives the minimum value of κ (but not zero).

On the other hand, when the pump wavelength is in the anomalous dispersion region ($\lambda_P - \lambda_0 > 0$), $\Delta k \le 0$ holds and the gain is maximum at the signal wavelengths yielding $\kappa = 0$. Accordingly, larger gain can be obtained when $\lambda_p - \lambda_0 > 0$. Since Δk is proportional to $(\lambda_S - \lambda_P)^2(\lambda_P - \lambda_0)$, the gain bandwidth is proportional to $(\lambda_P - \lambda_0)^{-1/2}$.

Fig. 2 (b) shows the gain spectra obtained experimentally. The signal and idler gains were measured for the cases where $\lambda_S - \lambda_P < 0$ and $\lambda_S - \lambda_P > 0$. Although the general trend is similar to Fig. 2 (a), there are some discrepancies between the theoretical and experimental results. This is probably because λ_0 is not constant over the entire fiber length. For example, a 6-km long DSF has a deviation of λ_0 of about 0.1 % (~1.5 nm) along the fiber [8].

Fig. 3 shows the signal gain as a function of input pump power for $\lambda_P - \lambda_0 = 0.4$ nm and $\lambda_S - \lambda_P = -6.2$ nm. The output saturation power of 8.4 dBm was obtained experimentally at the 3 dB gain-compression point. The gain bandwidth decreases with increasing input signal power. Therefore the amplifier saturates faster at larger $|\lambda_S - \lambda_P|$.

Summary: We investigated theoretically and experimentally the gain spectrum and the saturation characteristics of a fiber optical parametric amplifier operating near zero-dispersion wavelength. The gain spectrum of the OPA is very sensitive to the difference between the pump and zero-dispersion wavelengths and the gain is larger when the pump wavelength is in the anomalous dispersion region (i.e. $\lambda_P - \lambda_0 > 0$ when $dD/d\lambda > 0$). We have experimentally demonstrated a gain of 12 dB and an output saturation power of 8.4 dBm for $\lambda_P - \lambda_0 = 0.4$ nm and $\lambda_S - \lambda_P = -6.2$ nm, with a pump power of 180 mW.

References

[1] G. P. Agrawal, *Nonlinear Fiber Optics*, Academic Press, San Diego, 1989.

[2] K. Washio, K. Inoue, and S. Kishida, *Electron. Lett.*, Vol. 16, pp. 658-660, 1980.

[3] M. Ohashi, K. Kitayama, Y. Ishida, and N. Uchida, *Appl. Phys. Lett.*, Vol. 41, pp. 1111-1113, 1982.

[4] J. P. Pocholle, J. Raffy, M. Papuchon, and E. Desurvire, *Optical Engineering*, Vol. 24, pp. 600-608, 1985.

[5] G. Cappellini and S. Trillo, *J. Opt. Soc. Am. B*, Vol. 8, pp. 824-838, 1991.

[6] K. Inoue, *J. Lightwave Technol.*, Vol. 10, pp. 1553-1561, 1992.

[7] S. Watanabe and T. Chikama, *Electron. Lett.*, Vol. 30, pp. 163-164, 1994.

[8] K. Inoue, *Opt. Lett.*, Vol. 19, pp. 1189-1191, 1994.

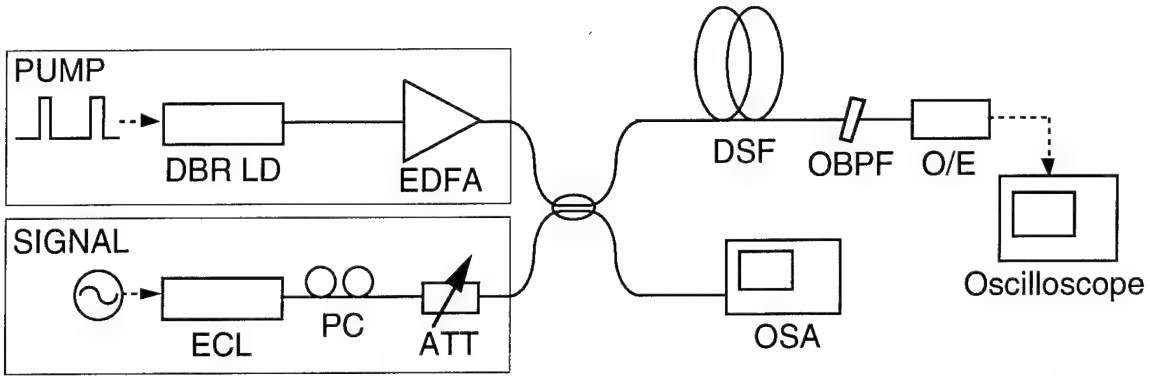

Fig. 1 Experimental setup. ECL – external-cavity laser diode; PC – polarization controller; ATT – optical attenuator; OBPF – optical bandpass filter; OSA – optical spectrum analyzer.

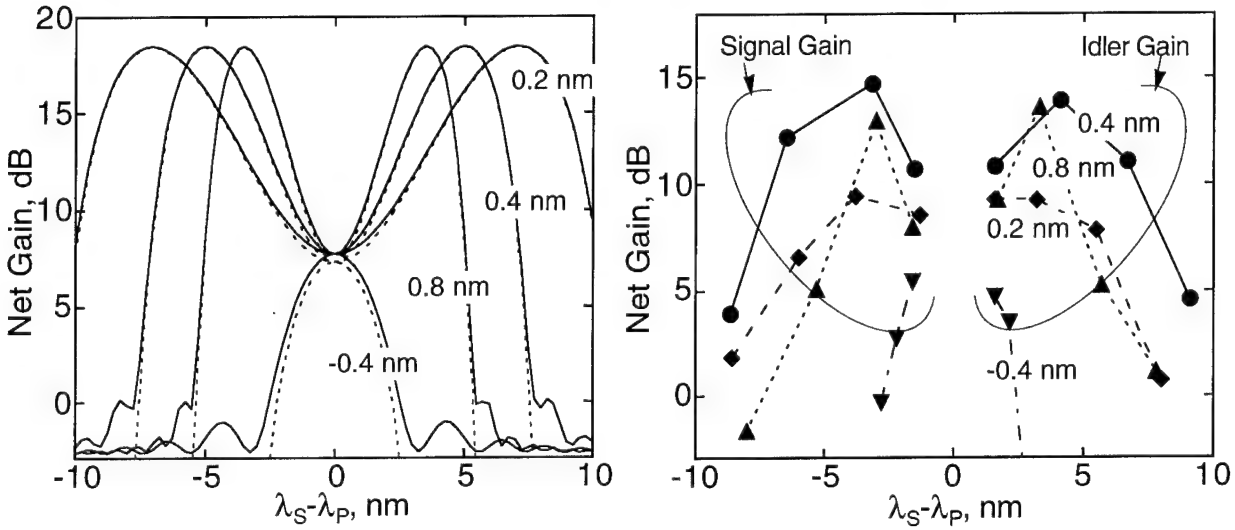

Fig. 2 Gain spectrum. (a) theoretical results (solid lines: signal gain, broken lines: idler gain), (b) experimental results. Numbers inside the graphs denote the values of $\lambda_p - \lambda_0$. The input signal power is -12 dBm in both cases.

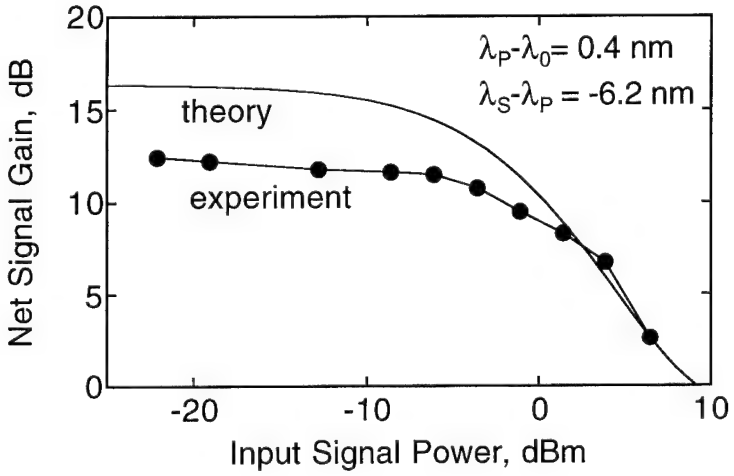

Fig. 3 Saturation characteristics.

High-Power 1.48 μm Cascaded Raman Laser in Germanosilicate Fibers

S.G. Grubb, T. Strasser, W.Y. Cheung, W.A. Reed, V. Mizrahi, T. Erdogan, P.J. Lemaire, A.M. Vengsarkar, and D.J. DiGiovanni

AT&T Bell Laboratories
600 Mountain Avenue
Murray Hill, NJ 07974

D.W. Peckham
AT&T Bell Laboratories
2000 NE Expressway
Norcross, GA 30071

B.H. Rockney
Polaroid Corporation
38 Henry Street.
Cambridge, MA 02139

We report CW, diode-pumped fiber laser output at 1.48 μm from a multiple order cascaded Raman laser. An output power of 1.5 Watts has been obtained when pumping with a diode-pumped Yb^{3+} cladding-pumped fiber laser.

Recently, the concept of a resonantly cascaded Raman laser and amplifier was introduced for amplification in the 1.3 μm transmission window.[1,2] The recent emergence of high-power, diffraction-limited, cladding pumped fiber lasers (up to 5 Watts CW)[3] and other diode-pumped solid state lasers around 1 μm has prompted interest in high-power pump and amplifier sources for telecommunications. We have found that it is possible to efficiently convert these high-power, CW, fiber-coupled sources as many as six Raman orders by utilizing nested highly-reflecting Bragg gratings written directly in germanosilicate fibers. In this way, each intermediate Raman Stokes order can be resonated and thereby efficiently converted to the next higher Stokes order until the cascade is terminated by suitable output coupling at the desired order. We are thus able to obtain high-output powers at 1.48 μm which can be used to pump high-power and remotely-pumped erbium amplifiers.

High-delta germanosilicate fibers were used as the Raman gain medium in these experiments. The fiber was H_2 sensitized prior to exposure in order to increase the photosensitivity[4]. The Bragg gratings were written sequentially in the two fiber ends, as shown schematically in Figure 1. The pump source was an 973 nm diode-pumped, cladding-pumped Yb^{3+} fiber laser at 1117 nm. The slope efficiency of the cladding pumped fiber laser was measured to be 70% relative to incident diode laser power.

A 1117 nm-pumped, fifth-order cascaded Raman laser was constructed using 800 meters of germanosilicate fiber. With a 20% output coupler at the fifth Stokes frequency of 1484 nm, a threshold of 660 mW and a slope efficiency of 46% have been obtained as shown in Figure 2. An output of 1.5 W at 1484 nm has been obtained with this diode-pumped source. The spectral output, as shown in Figure 3, is approximately 2 nm FWHM, considerably narrower than high-power 1.48 μm diode lasers. We have also constructed sixth order cascaded Raman lasers starting from either a 1064 nm Nd^{3+} cladding-pumped fiber laser or a Nd:YAG laser. When using a flashlamp-pumped Nd:YAG laser as the pump source, we have obtained an output power of 2.6 Watts at 1488 nm for 6.4 Watts of coupled pump power.

In conclusion, we have demonstrated efficient conversion of CW, high-power, diode-pumped fiber laser sources at 1 μm by Raman shifting to 1.48 μm by utilizing a cascaded, resonant Raman laser cavity. With a fifth-order Raman laser operating at a 46% slope efficiency, a diode-pumped output of 1.5 W was obtained at 1484 nm. An output power of 2.6 Watts has been obtained when pumping with a flashlamp-pumped Nd:YAG laser. These results demonstrate that efficient, CW, high-power, diode-pumped fiber laser or amplifier operation is obtainable over a significant range of infrared wavelengths.

References:

1. S.G. Grubb, T. Erdogan, V. Mizrahi, T. Strasser, W.Y. Cheung, W.A. Reed, P.J. Lemaire, A.E. Miller, S.G. Kosinski, G. Nykolak, P.C. Becker and D.W. Peckham, Proc. Optical Amplifiers and Their Applications, paper PD-3, August 3-5, Breckenridge, CO (1994).

2. W.A, Reed, W.M. Coughran, and S.G. Grubb, Proc. Optical Fiber Communications Conf., OFC '95, paper WD1, (1995).

3. H. Po et. al. , Electr. Lett., 29(17), 1500, (1993).

4. P.J. Lemaire, R.M. Atkins, V. Mizrahi, and W.A. Reed, Elect. Lett., 29, 1191 (1993).

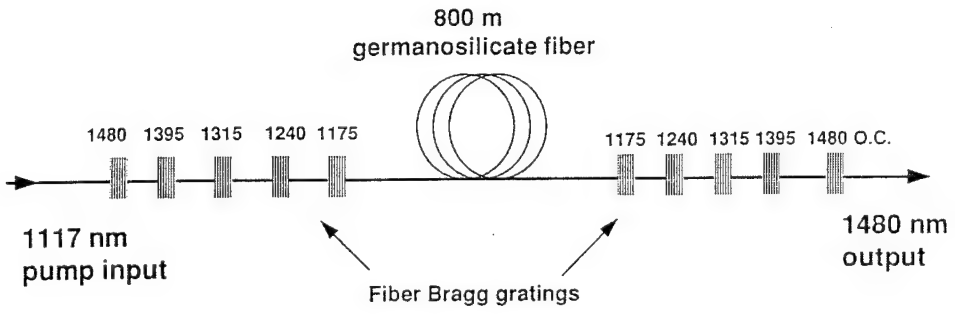

Figure 1: Schematic of 5th-order cascaded Raman laser.

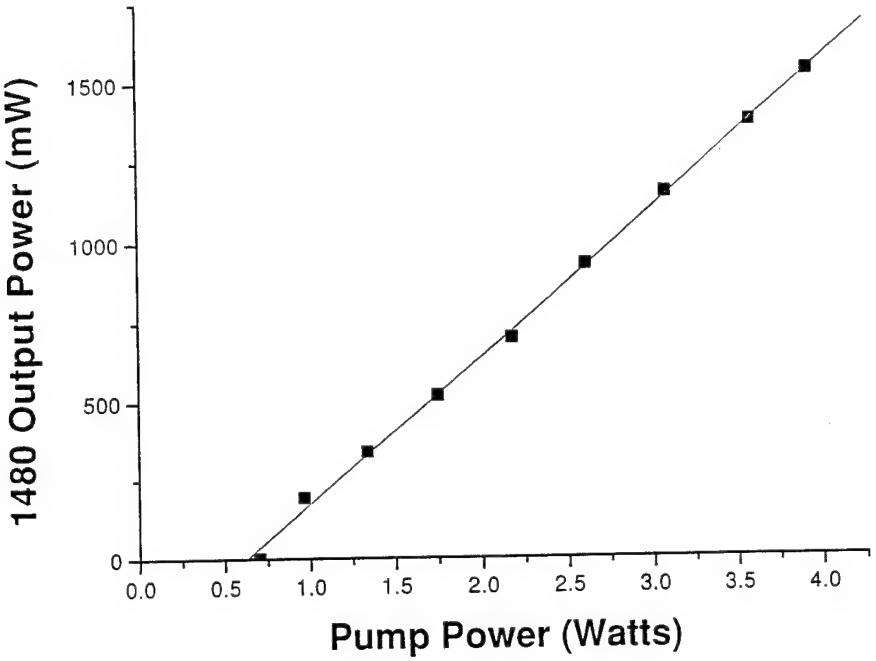

Figure 2: Laser characteristic for a 1117 nm-pumped 5th-order cascaded Raman laser.

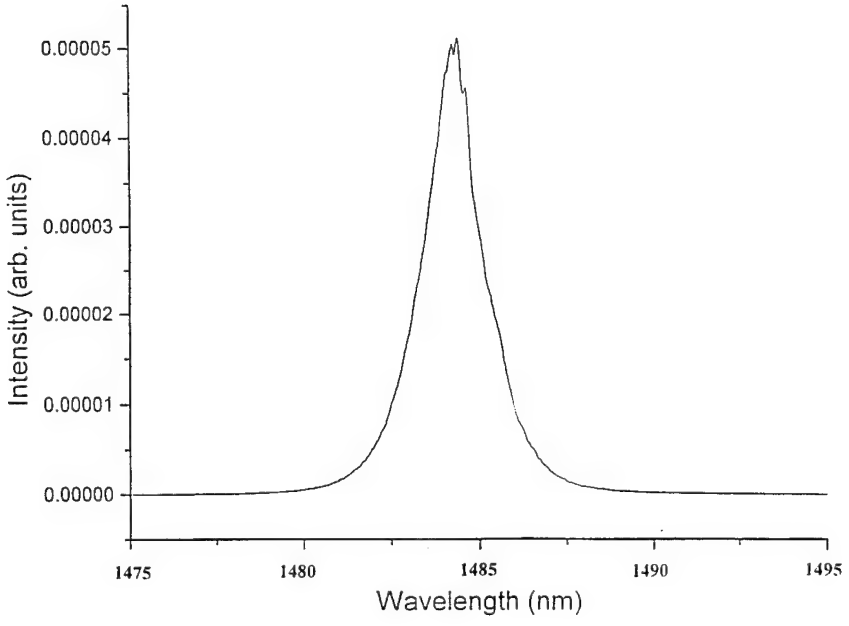

Figure 3: Spectral output from the 5th-order cascaded Raman laser.

Towards pump-efficient 1.3μm fibre amplifiers

D N Payne, R I Laming and D W Hewak

Optoelectronics Research Centre

University of Southampton

SO17 1BJ, UK

The optical amplifier became a realistic prospect for telecommunications after the demonstration of the erbium-doped fibre amplifier (EDFA), operating at 1.5μm, in 1987 [1]. Subsequent demonstrations of the diode-pumped device [2] led to the first commercial products in 1990 and installation of optically-amplified systems followed in 1993. However, the installed base of fibre is designed for 1.3μm operation and thus the early success of the EDFA spurred the search for a 1.3μm fibre amplifier. First efforts focused on neodymium (Nd^{3+}) and a diode-pumped device exhibiting 10dB gain for 50mW of pump power was demonstrated in a ZBLAN fibre in 1991 [3]. However, performance of Nd^{3+} in ZBLAN is limited in several respects, the most important of which, signal excited-state-absorption (ESA), limits the operating wavelength to more than 1.32μm, longer than ideal for zero dispersion in telecoms systems. Current research shows that alternative fluoride glasses can allow operation down to ~1310nm, which appears to be adequate for most installed systems which have a dispersion zero around 1315nm. Care must also be taken to suppress the large amplified spontaneous emission which results from the more-favoured 1.06μm transition [4].

More recently [5], a gain of 23dB for 124mW gain coefficient 0.16dB/mW of pump power has been achieved from Pr^{3+} doped ZBLAN-based fibre amplifier (PDFA) module pumped by a laser diodes. Unfortunately, the pump efficiency in the Pr^{3+} system is limited owing to a high non-radiative decay rate from the metastable to an intermediate level which dominates the 1.3μm emission even in a low phonon-energy glass such as that based on fluorides. Nevertheless, at least for a power amplifier, many would argue that the level of performance already achieved is adequate with a 250mW (24dBm) output obtained for 1.8W of pump from a Nd:YLF laser (an 18% slope efficiency) [7]. This approaches the performance of commercial erbium:ytterbium 1.5μm power amplifiers, but is a long way from EDFA line and pre-amplifier performance.

The problem of pump efficiency is being addressed with the identification and development of new host glasses, namely mixed-halides such as CdF_2:$CdCl_2$[7] and sulphides such as Ga_2S_3:La_2S_3 and GeS_2. The lattice vibration (phonon) energy of these glasses is significantly lower than that of ZBLAN (~400cm^{-1} cf 580cm^{-1}), which reduces phonon-mediated, nonradiative effects. As a result, spectroscopic analysis of Pr^{3+} in these glasses has revealed increased lifetimes of 325μs for the mixed halide and 290μs for GLS compared with 110μs for ZBLAN. In addition, the radiative quantum efficiency was correspondingly increased to 12% and 53% respectively in the new glasses (c.f. ~4% in ZBLAN). Unfortunately, the improved efficiency of the mixed halide has been achieved at the expense of stability, being hygroscopic and with a melting point of only 305°C.

The Ga_2S_3:La_2S_3 system is a much more promising host. The glass has a higher melting point than ZBLAN (A cf B) and is not hygroscopic. In addition, defined compositions are less prone to crystallization than ZBLAN. A potential drawback with Ga_2S_3:La_2S_3 based glasses is their longer wavelength Urbach edge, which leads to increased loss at the pump wavelength. This is potentially a serious problem for Pr^{3+} in which the maximum concentration for efficient operation is limited to ~500ppm. However, intrinsic losses of <0.1dB/m at the pump wavelengths are predicted for the latest glasses and since single-mode chalcogenide fibres with losses less than 1dB/m at 1μm have already been drawn[11], a 1.3μm GLS amplifier appears a realistic possibility.

In conclusion, many opportunities exist for the development of a practical 1.3μm amplifier, although many obstacles remain to be overcome before the device will find widespread application. The key to pump-efficient operation is the continued development of new low-phonon energy glasses, with chalcogenides looking most promising.

References

1. Mears et al. Electron. Lett., 23, 1987. p. 1026.
2. Nakazawa et al. Appl. Phys. Lett., 54, 1989. p. 295.
3. Miyajima et al, Proc. Opt. Amp. and their Appl., Snowmass, 1991, p. 16.
4. Pedersen et al, Proc. Opt. Amp. and their Apl., Santa Fe, 1992, p. 16.
5. Ohishi et al, Proc. OFC'91, San Diego, 1991. PD 2.
6. Yamada et al, Proc. Opt. Amp. and their Appl., Yokohama, 1993, . 240.
7. Whitley et al, BT Technol. J., 11 (2). 1993.
8. Newhouse et al, Proc. Opt. Amp. and their Appl., Santa Fe, 12, PD 16.
9. Samson et al. Proc. Opt. and their Appl., Yokohama, 1993, p. 240.
10. Becker et al. Proc. Opt. Amp. and their Appl., Santa Fe, 1992, PD 5.
11. Hewak et al, Electron. Lett., 29, 1993, p. 237.
12. Asobe et al, Electron. Lett., 29, 1993, p. 1966.

WDM Networks and Systems

SaB 11:00-12:30
Theatersaal

Paul Morkle, *Presider*
STC Submarine Systems, U.K.

WAVELENGTH DIVISION MULTIPLEXED NETWORKS

Hiromu Toba, Kazuhiro Oda and Kyo Inoue
NTT Optical Network Systems Laboratories
1-2356, Take, Yokosuka, 238-03 Japan
Phone +81-468-59-3226, Fax +81-468-55-1282

1. Introduction

Wavelength-division-multiplexing (WDM) or optical frequency-division-multiplexing (OFDM) based transport networks are being intensively studied because they are expected to support broadband services [1-4]. Both transmission line capacity and processing node capacity will be increased by the simple node configuration. In addition, they are transparent to signal format and bit rate. One of the main features of the WDM network is its "scalabilty" against node number and geographic span, which means WDM signals can be transmitted end-to-end without O/E E/O conversion [2]. It is important to evaluate the network scale taking the optical amplifier, fiber nonlinearity and interchannel crosstalk into consideration. This paper describes the technological issues for constructing WDM based transport networks. A recently developed WDM ring network demonstrator is also reported.

2. Network configuration

The nation-wide physical network is considered to be divided into the national and regional tier [3] as shown in Fig. 1. In the national tier, the physical network topology is ladder or mesh and an optical crossconnect (OXC) is installed in each node. Wavelengths are assigned to the connection between nodes. The wavelength path (WP) / virtual wavelength path (VWP) concept have been introduced for wavelength assignment [4]. Network size exceeds 1000 km and the node spacing is several hundreds of km. On the other hand, the ring topology is introduced to the regional tier, whose circumference is less than hundreds of km, and a simple optical add/drop multiplexer (OADM) can be set in the node. In this figure, the national tier and each regional tier are partitioned by electronic termination and wavelengths are re-used. Fig. 2 shows the optical node configuration. The OXC consists of multiwavelength optical amplifier, wavelength multi/demultiplexers, signal level and dispersion equalizers, space switching fabrics, and wavelength converters. Basic configuration is similar to the MWTN node in RACE II project [3]. The wavelength converter supports not only the VWP function, but also the optical regenerator function [5, 6]. Although the introduction of O/E and E/O converters is an alternative, this simple configuration and transparency is attractive. OADM has a simple configuration based on the optical amplifiers and passive devices.

3. Technological issues

One of the key issues is transmission distance (regenerative repeater span) for the WDM in-line amplifier system. Fig. 3 shows the calculation results for a 10 Gb/s WDM system with the channel spacing of 0.8 nm (100 GHz). Major factors are the noise figure and the output power of the optical amplifier and fiber four wave mixing (FWM) induced crosstalk. Total distance increases as the amplifier output power increases and the number of channels decreases. FWM severely limits the transmission distance with dispersion-shifted fiber (DSF), whose zero dispersion wavelength coincides with the center wavelength of the WDM signals. The limitation is remarkably relaxed by employing dispersion management [7] or 1.3 μm dispersion single-mode fiber (SMF) with dispersion compensating fiber (DCF) at each amplifier span [8]. In these cases, regenerative repeater span increases to thousands of km for the amplifier spacing of 40 km and several hundreds of km for 80 km spacing. Interchannel crosstalk is another factor affecting WDM network performance. In particular, beat induced crosstalk, so called "coherent crosstalk", severely restricts the number of channels and nodes [9, 10]. It occurs in OADM filters or space switches between the same wavelength signals as shown in Fig. 4. Crosstalk induced penalty for the beat induced crosstalk and the adjacent channel crosstalk is shown in Fig. 5. Interchannel crosstalk should be less than -12 dB for the adjacent channel crosstalk induced penalty of less than 0.5 dB, while it should be less than -22 dB for the beat induced crosstalk.

4. WDM ring network test bed

Figure 6 shows the photograph of the WDM based ring network test bed [11]. A center node (CN) and two remote nodes (RNs) are connected by two fibers, in which WDM signals are always transmitted in clockwise and counter clockwise directions for route diversity. Each RN is assigned a unique wavelength for transmission to and receiving from the CN. Configuration of the 15-channel ADM filter is shown in Fig. 7 [12]. The ADM filter consists of 100 GHz-spaced arrayed waveguide grating (AWG) 16 x 16 multiplexer with loop-back fibers connecting each output port with its opposite input port. Each fiber is connected to a 2 x 2 optical switch, which is used for the "add/drop" or "through" mode. Successful signal transmission and route switching performance have been confirmed.

5. Conclusion

WDM based transport network configurations were reviewed and the major technological issues that determine the network scale were described. It is expected that WDM based networks will be implemented in both national and regional tiers to support broad band services.

Acknowledgment

The authors would like to thank Dr. Takao Matsumoto and Dr. Kiyoshi Nosu for their continuous encouragement and useful discussion.

References

[1] K. Nosu et al., *J. Lightwave Technol.*, vol. 11, pp. 764-776, 1993.

[2] C.A. Bracket et al., *ibid.*, pp. 736-753.

[3] G. R. Hill et al., *ibid.*, pp. 667-679.

[4] K. Sato et al., *IEEE J. Selected Areas in Commun.*, vol. 12, pp. 159-170, 1994.

[5] K. Inoue et al., *Electron. Lett.*, vol. 30, pp. 438-439, 1994.

[6] K. Weich et al., in Proc. *ECOC'94*, pp. 643-646.

[7] A. H. Gnauck et al., in Tech. Digest *OFC'94*, PD19, 1994.

[8] M. Fukui et al., submitted to *IOOC'95*.

[9] E. L. Goldstein et al., *IEEE Photon. Technol. Lett.*, vol. 6, pp. 657-660, 1994.

[10] M. J. O' Mahony, in Proc. *ECOC'94*, pp. 907-913.

[11] H. Toba et al., in Proc. *ECOC'94*, pp. 263-266.

[12] Y. Tachikawa et al., *Electron. Lett.*, vol. 29, pp. 2133-2134, 1993.

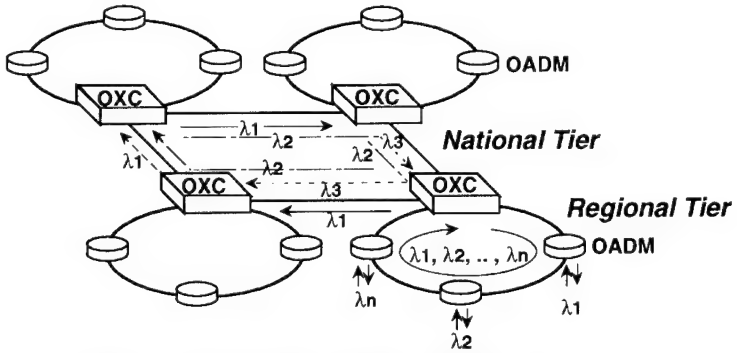

Fig. 1 WDM based Optical Network

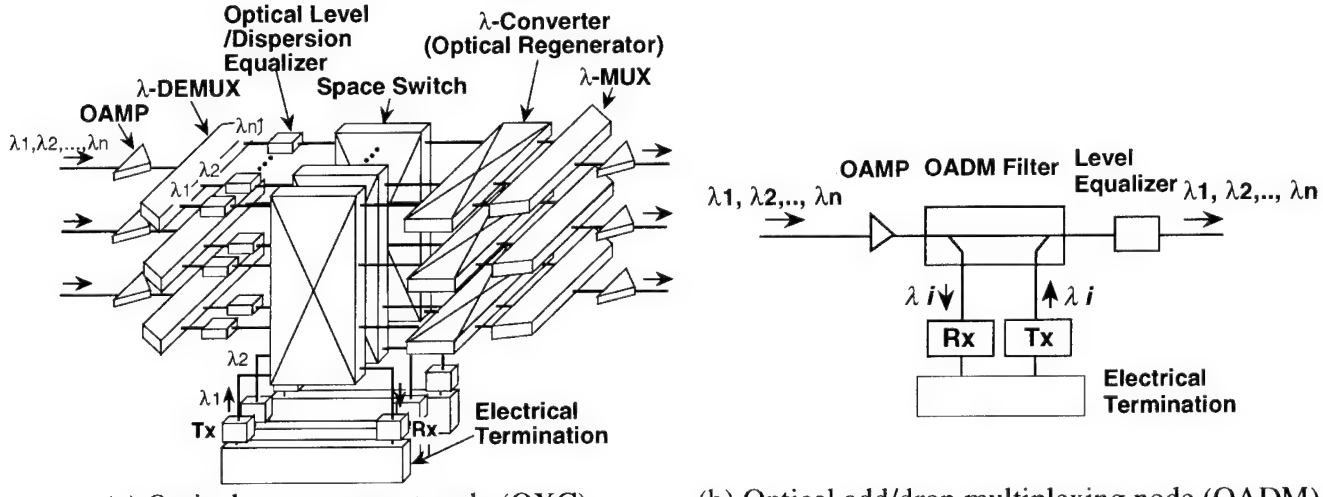

(a) Optical cross-connect node (OXC) (b) Optical add/drop multiplexing node (OADM)

Fig. 2 Optical node configuration

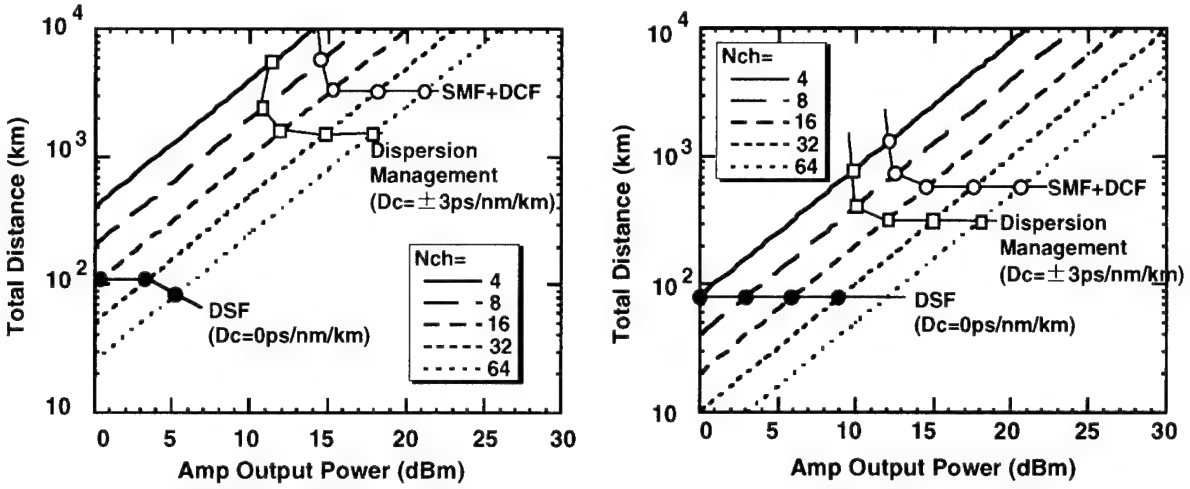

(a) OAMP Spacing : 40 km (b) OAMP Spacing : 80 km

Fig. 3 Muximum transmission distance (regenerative repeater span) for in-line amplified WDM transmission. o ,□ and ● show the FWM limitation. Channel spacing : 0.8 nm (100 GHz), noise figure of OAMP : 6 dB. (SMF: conventional single-mode fiber, DCF: dispersion compensating fiber, DSF: dispersion-shifted fiber)

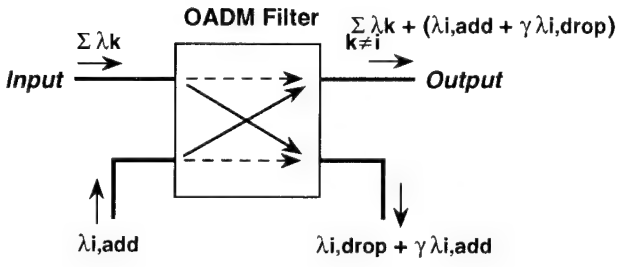

Fig. 4 Mechanism of beat-induced crosstalk generation in the OADM filter. (γ : crosstalk of the filter)

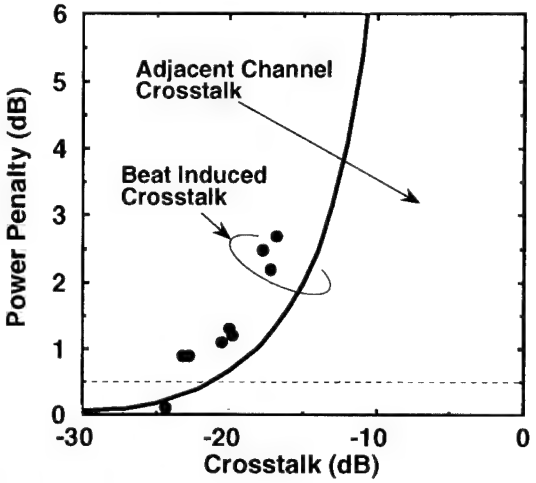

Fig. 5 Power penalty due to interchannel crosstalk. Black and gray line show the calculation results for beat induced crosstalk and adjacent channel crosstalk, respectively. Filled circles show the experimental result for beat induced crosstalk.

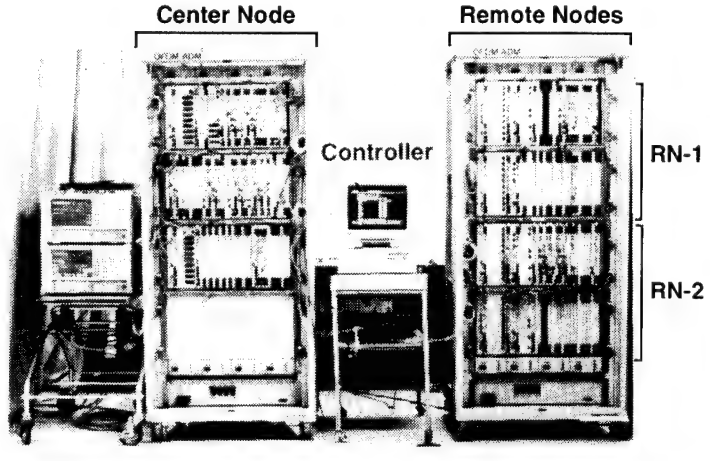

Fig. 6 Photograph of the WDM based ring network test bed.

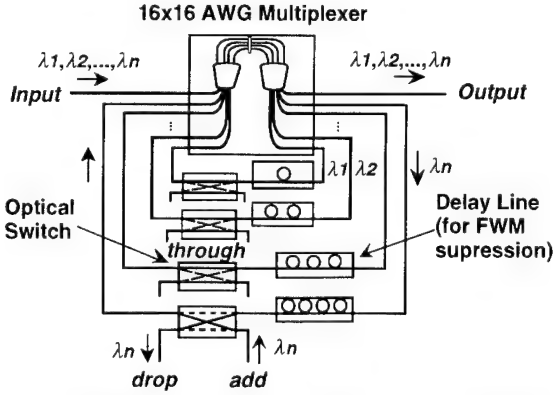

Fig. 7 100GHz-spaced 15 channel OADM filter

EFFECT OF AMPLIFIER GAIN SHAPE ON OPTICAL NONLINEARITY PENALTIES

Fabrizio Forghieri, R. W. Tkach, A. R. Chraplyvy and J. A. Nagel

AT&T Bell Laboratories
Crawford Hill Laboratory
Holmdel, NJ 07733
phone: (908) 888–7286
fax: (908) 888-7190
e-mail: biccio@big.att.com

The advent of erbium-doped-fiber amplifiers (EDFA) has revolutionized the field of optical communications in two ways. First, their large optical gain allows long-haul unregenerated systems with optical repeaters spaced more than 100 km. Second, their large bandwidth permits to increase the capacity by an order of magnitude by wavelength-division multiplexing (WDM) several high bit rate channels.

The main remaining problem of EDFAs is their non-flat frequency response, that limits the usable optical bandwidth for a given length. The nonuniform wavelength-dependent gain leads to optical signal-to-noise (SNR) degradation of some of the channels. A simple technique to circumvent this problem has been proposed [1] and demonstrated [2]. The optical SNR at the output can be equalized by adjusting the input powers of each channel according to a simple algorithm. The requirement is to transmit more power in the channels where the gain is lower, keeping the total power constant.

This pre-emphasis method works remarkably well in systems for which the impairment due to optical nonlinearities is negligible, but the need for transmitting high powers in some of the channels could give rise to additional penalties for systems in which nonlinearities are important.

Here, computer simulations of the performance of WDM systems are reported that include both optical fiber nonlinearities and amplifier gain shape. The problem of nonlinear penalties in presence of nonuniform amplifier gain is studied by comparing the performance of three systems. In the first the EDFAs have flat gain, in the second they have nonuniform gain and in the third the EDFAs have nonuniform gain and pre-emphasis is used. It is found that, as already known for linear systems, pre-emphasis considerably improves the performance of systems otherwise severely degraded by nonuniform gain. However, when the power required for the pre-emphasis becomes too large, some of the channels suffer penalties arising from optical nonlinearities.

The system under consideration is shown in Fig. 1. It consists of ten spans of 100 km of conventional fiber (CF), followed by a repeater with 10 km of dispersion compensating fiber (DCF) and an amplifier with excess noise factor equal to 2. Table 1 summarizes the physical parameters of the fiber. The DCF has a figure of merit of 200 ps/nm/dB.

The computer simulator is based on the split-step Fourier method to solve the nonlinear

Fig. 1. Schematic diagram of system in computer simulations.

Schrödinger equation [3] and includes amplifier gain shape at each repeater. Fig. 2 shows the gain shape of the EDFA used in the simulations.

The WDM system has ten 10-Gb/s channels centered around 1552.4 nm and equally spaced by 2 nm. The total power at the transmitter and after each repeater is 13 dBm. Two different pseudo-random sequences of 64 bits are alternatingly used in adjacent channels. The two sequences and further details on the simulator can be found in [4], [5].

Fig. 3(a) shows the output spectrum when the EDFAs are assumed to have flat gain. The SNR in the signal bandwidth is more than 20 dB. The dashed line in Fig. 4(a) shows the penalties of all ten channels due to nonlinearities only (the simulation was rerun without noise). Penalties are computed as the ratio between maximum eye opening and twice the average power. The penalty is around 2 dB for all channels and is mainly due to self-phase modulation. Due to the large channel spacing, multichannel nonlinear effects do not play an important role. The small fluctuations from channel to channel are attributable to four-wave mixing and are caused by the short bit sequences used.

Fig. 3(b) shows the output spectrum when the gain curve of Fig. 2 is used without any pre-emphasis. The outer channels have a SNR lower than 14 dB, insufficient for satisfactory performance. Furthermore, the channels close to the gain peak have penalties higher than 3 dB, as shown by the dash-dotted line in Fig. 4(a), because of their larger power at the end of the system.

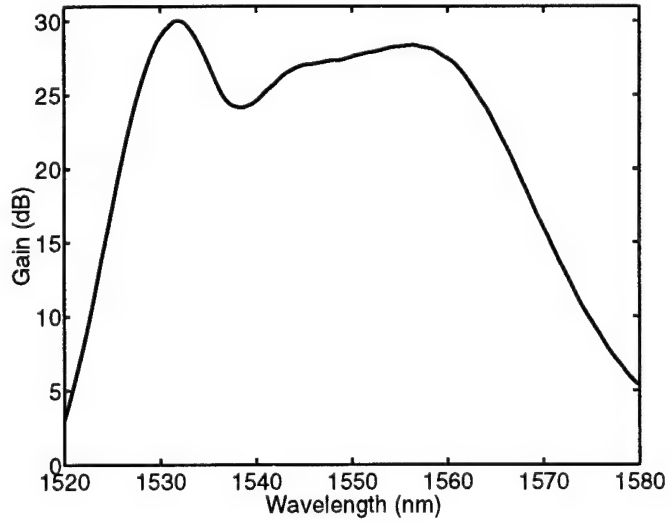

Fig. 2. EDFA gain spectrum.

		CF	DCF	
Dispersion	D	16	-160	ps/nm/km
Dispersion slope	$dD/d\lambda$	0.08	-0.8	ps/nm^2/km
Loss	α	0.2	0.8	dB/km
Effective area	A_e	80	20	μm^2

Table 1. Physical parameters of the fibers

Fig. 3(c) shows the spectrum at the transmitter if pre-emphasis is used, applying the algorithm in [1], to equalize the output SNR for all channels. In this case, as shown in Fig. 3(d), all the channels at the receiver have the same SNR of about 20 dB, but the outer channels have larger nonlinear penalties, as shown by the continuous line in Fig. 4(a), due to their high launched power.

This effect is even more clear if unequally spaced channels are used to completely suppress any

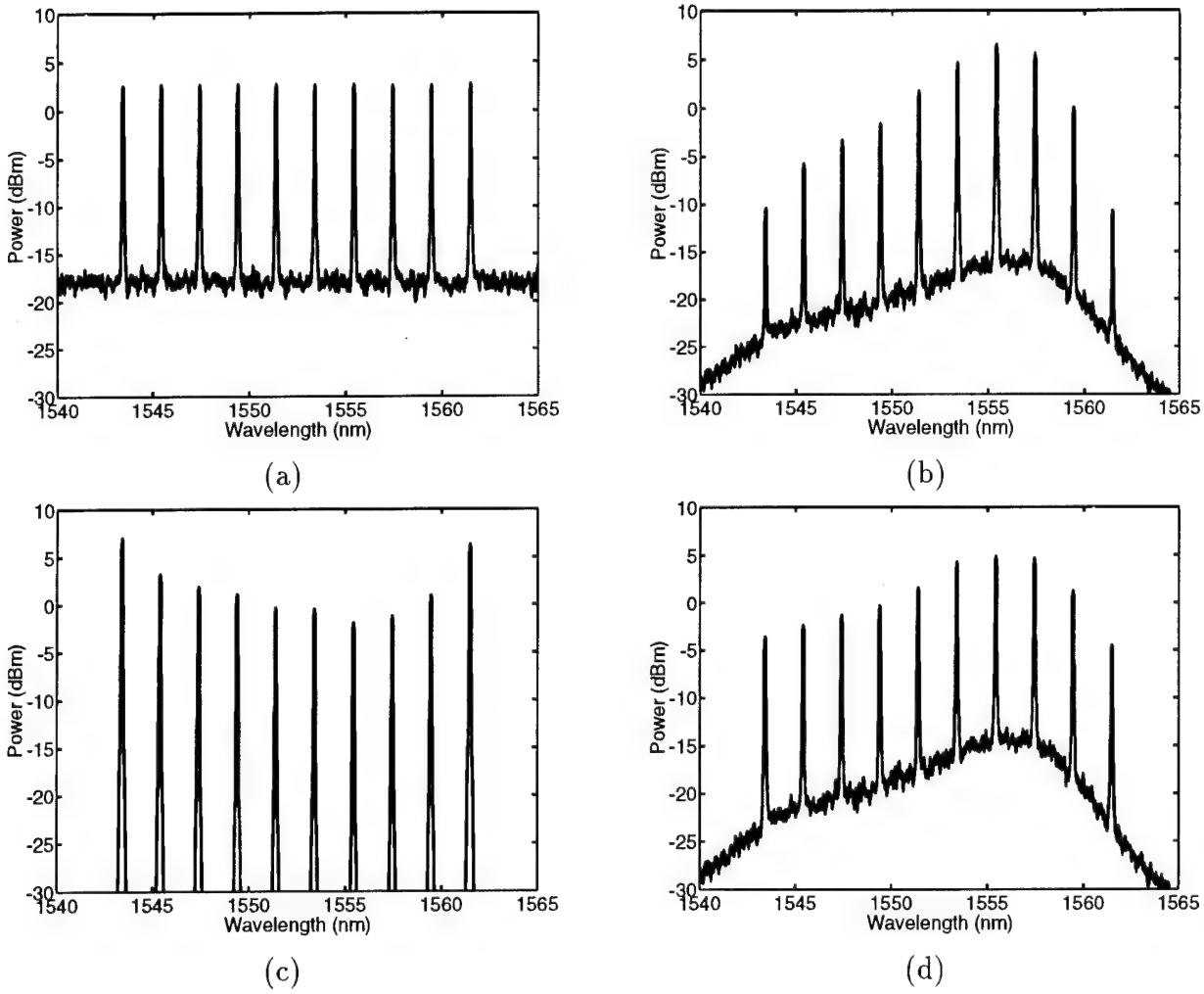

Fig. 3. (a) Output spectrum with flat gain. (b) Output spectrum with gain shape. (c) Input spectrum with pre-emphasis. (d) Output spectrum with gain shape and pre-emphasis. All spectra are computed with a resolution bandwidth equal to the bit-rate.

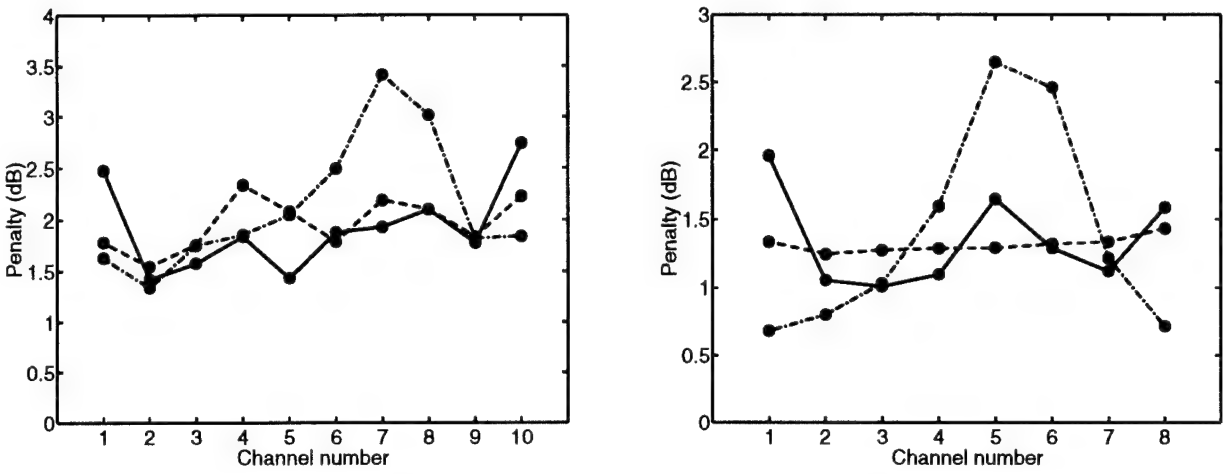

Fig. 4. Nonlinear penalties with (a) equal and (b) unequal channel spacing. Shown are systems with flat gain (dashed) and with nonuniform gain with (continuous) and without (dash-dotted) pre-emphasis. The average launched per channel is 3dBm in both cases.

mixing effect [5], [6]. Results for simulations with eight channels unequally spaced with a minimum spacing of 2 nm, total bandwidth of 18.2 nm and same power per channel are shown in Fig. 4(b), for the same three cases detailed above.

In conclusion, it has been shown by simulation that nonuniform amplifier gain can severely degrade both outer channels, due to linear SNR, and middle channels, due to nonlinearities. Using pre-emphasis of the signal powers at the transmitter, as shown in [1], [2], can completely restore the SNR but can introduce nonlinear penalties in the outer channels due to the high powers required to balance the SNR. Therefore there is a limit to what pre-emphasis can do when nonlinearities are important. The outer channels are trapped between error rate floors due to low optical SNR and increasing penalties due to nonlinearities. In these cases gain equalization at each amplifier might be necessary.

References

[1] A. R. Chraplyvy, J. A. Nagel and R. W. Tkach, "Equalization in amplified WDM lightwave transmission systems," *IEEE Photon. Technol. Lett.*, vol. 4, pp. 920–922, Aug. 1992.

[2] A. R. Chraplyvy, R. W. Tkach, K. C. Reichmann, P. D. Magill, and J. A. Nagel, "End-to-end equalization experiments in amplified WDM lightwave systems," *IEEE Photon. Technol. Lett.*, vol. 4, pp. 428–430, Apr. 1993.

[3] G. P. Agrawal, *Nonlinear Fiber Optics.* New York: Academic, 1989.

[4] D. Marcuse, A. R. Chraplyvy, and R. W. Tkach, "Dependence of cross-phase modulation on channel number in fiber WDM systems," *J. Lightwave Technol.*, vol. 12, pp. 885–890, May 1994.

[5] F. Forghieri, R. W. Tkach, and A. R. Chraplyvy, and D. Marcuse, "Reduction of four-wave mixing crosstalk in WDM systems using unequally spaced channels," *IEEE Photon. Technol. Lett.*, vol. 6, no. 6, pp. 754–756, June 1994.

[6] F. Forghieri, R. W. Tkach, and A. R. Chraplyvy, "WDM systems with unequally spaced channels," *J. Lightwave Technol.*, vol. 13, May 1995.

SUPPRESSION OF RAMAN CROSSTALK IN WDM SYSTEMS

Fabrizio Forghieri, R. W. Tkach, and A. R. Chraplyvy

AT&T Bell Laboratories
Crawford Hill Laboratory
Holmdel, NJ 07733
phone: (908) 888–7286
fax: (908) 888-7190
e-mail: biccio@big.att.com

Stimulated Raman scattering (SRS) crosstalk has been recently shown to severely limit ultra-high-capacity long-haul optical communication systems [1]. In this paper SRS crosstalk in intensity-modulated WDM systems is analyzed including modulation statistics of multiple channels in presence of chromatic dispersion. It is found that the depletion caused by SRS on a given channel has an average, deterministic component that is the dominant source of SNR degradation, and a statistical contribution that depends on the bits transmitted in the other channels. Power equalization at amplifiers can completely suppress the average part of SRS crosstalk, exploiting its deterministic nature. The residual degradation caused by the statistical component is analytically evaluated, assuming that pulses propagate without distortion and neglecting all other nonlinear effects. The proposed technique increases the number of channels that can be transmitted by about an order of magnitude.

The effect of SRS on a WDM system is to deplete the shortest-wavelength channels that act as pumps for the longer-wavelength channels [1]. The fractional power lost by the shortest-wavelength channel (the most degraded one) is a random variable since it depends on the bits transmitted in the other channels. For more than ten channels and with zero-dispersion fiber, the depletion is well approximated by a truncated gaussian with average value in dB that depends only on the average transmitted power [2]. The effect of fiber chromatic dispersion, neglecting pulse shape distortion, is to introduce a walk-off between pulses transmitted in different channels, causing more (independent) bits to interact, therefore its effect is similar to an increase in the number of channels. In [3] the effect of dispersion on Raman crosstalk has been evaluated for the case of a 2-channel system and for some binary sequences. Here, the statistical approach used in [2] has been extended to analyze systems with arbitrary number of channels and random modulation, and an

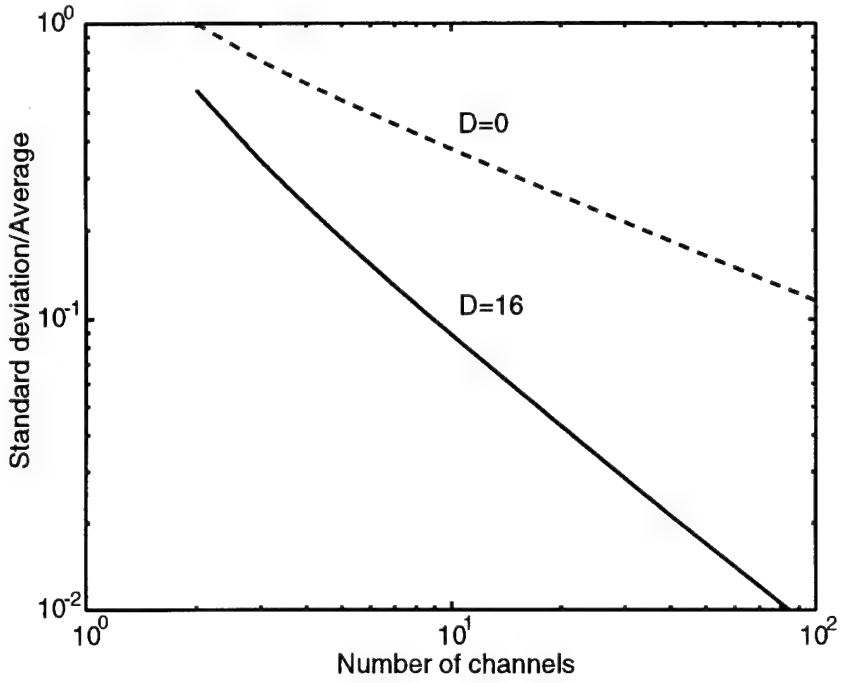

Fig. 1. Ratio between standard deviation and mean of shortest-wavelength-channel power depletion versus number of channels for zero-chromatic dispersion (dashed line) and conventional fiber with dispersion of 16 ps/nm/km (solid line). The other parameters are: channel spacing 0.5 nm; bit rate 10 Gb/s; fiber length 50 km; fiber loss 0.2 dB/km.

analytical expression has been found for this case. The result is summarized in Fig. 1, where the ratio between standard deviation and mean of the shortest-wavelength channel depletion is given versus the number of channels for zero-chromatic dispersion (dashed line) and conventional fiber with dispersion of 16 ps/nm/km (solid line). When this ratio is less than 0.1 the truncated gaussian is essentially a gaussian distribution, since the tails extend below 10^{-20}.

In the limit of infinitely many channels, the probability density function of the depletion converges to a delta function and the effect of SRS becomes completely deterministic. In this limit and assuming ideal amplifiers with flat gain, the depletion can be in principle exactly compensated by using a filter after each in-line amplifier that provides an attenuation linearly varying in wavelength and with the correct slope to undo the SRS depletion. This post-amplifier wavelength-dependent loss does not introduce any SNR degradation.

With a finite number of channels, only the average depletion can be suppressed by the filters. The residual statistical fluctuations of the depletion cause a SNR degradation. Fig. 2 shows SNR degradation versus number of channels for a 5000 km-long WDM system with 50 km amplifier

spacing and 10 Gb/s bit rate per channel. In the calculations realistic system parameters have been assumed: amplifier noise figure 6 dB, fiber loss 0.25 dB/km, 10 dB margin at the receiver. The dotted line is the result of the worst-case analysis [1] which, for dispersion shifted fiber, is very close to the limit obtained with a statistical approach when power equalization is not used. The dashed line shows the improvement due to the chromatic dispersion of conventional fiber. The solid line corresponds to a system with proper filters placed after each amplifier and conventional fiber, and is obtained under the assumption that bits in different channels are uncorrelated at each amplifier. The power equalization provided by the filters allows the number of channels to be increased tenfold.

Fig. 3 shows number of channels at which a 0.5 dB SNR degradation is introduced versus system length. The dotted line is the result of the worst-case analysis without filters, the solid line shows the improvement achievable with the proposed technique, with the same assumptions as in Fig. 2. There is a substantial increase in the maximum number of channels when the deterministic component in

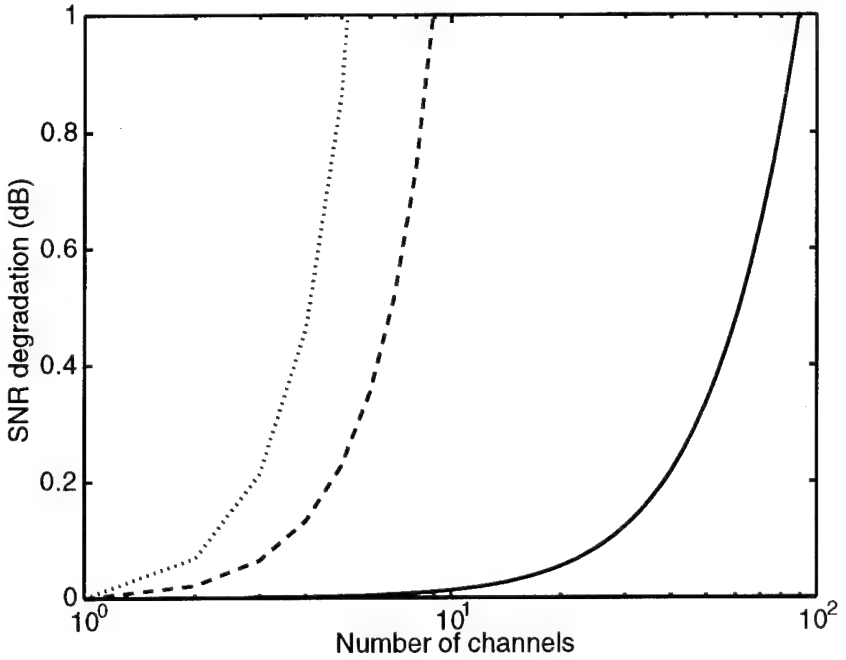

Fig. 2. SNR degradations versus number of channels for a 5000 km-long WDM system obtained with worst-case analysis and zero-dispersion fiber (dotted line), statistical analysis and conventional fiber (dashed line) power equalization at amplifiers and conventional fiber (solid line). The WDM system has 50 km amplifier spacing, 10 Gb/s bit rate per channel, 0.5 nm channel spacing, amplifier noise figure 6 dB, fiber loss 0.25 dB/km, 10 dB of margin at the receiver.

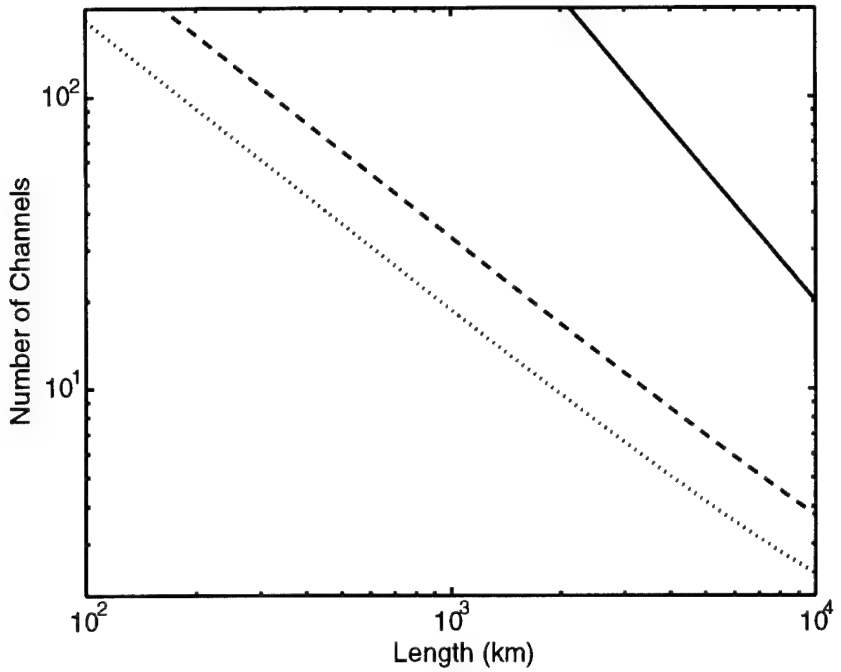

Fig. 3. Number of channels versus system length for a 0.5 dB SNR degradation. Other parameters are the same as in Fig. 2. Worst-case analysis and zero-dispersion fiber (dotted line), statistical analysis and conventional fiber (dashed line) power equalization at amplifiers and conventional fiber (solid line).

the SRS crosstalk is suppressed with the power equalization technique. The improvement depends on system parameters; using lower receiver margin or better amplifiers rapidly increases the benefit of using power equalization. The theory relies on the small gain linearization of SRS, therefore the average depletion between filters should not exceed 1 dB.

In conclusion, a simple, passive technique to suppress SRS crosstalk in WDM systems has been presented. This technique allows an increase of the number of channels by at least an order of magnitude even at transoceanic distances.

References

[1] A. R. Chraplyvy and R. W. Tkach, "What is the actual capacity of single-mode fibers in amplified lightwave systems?," *IEEE Photon. Technol. Lett.*, vol. 5, pp. 666–668, June 1993.

[2] F. Forghieri, R. W. Tkach and A. R. Chraplyvy, "Effect of modulation statistics on Raman crosstalk in WDM systems," *IEEE Photon. Technol. Lett.*, vol. 7, pp. 101–103, Jan. 1994.

[3] D. Cotter and A. M. Hill, "Stimulated Raman crosstalk in optical transmission: effects of group velocity dispersion," *Electron. Lett.*, vol. 20, pp. 185–187, Feb. 1984.

Optimum Gain Equalization for WDM In-line Multistage Amplifier Systems

Mitsunori Fukutoku, Kazuhiro Oda and Hiromu Toba
NTT Optical Network Systems Laboratories
1-2356 Take, Yokosuka, 238-03 Japan
Phone: +81-468-59-3103, Fax: +81-486-55-1282

I. Introduction

Optical wavelength-division-multiplexing (WDM) is attractive to realize large capacity optical communication systems and networks [1]-[3]. Er^{3+}-doped fiber amplifiers (EDFAs) will play a major role in such systems. The EDFAs are required to have wide and flat gain bandwidth to simultaneously amplify several WDM channels. If a small gain imbalance exists, it accumulates across the amplifier stages and seriously degrades the optical signal to noise ratio (OSNR). As a result, the transmission distance is restricted. Optimization of optical amplifiers for WDM systems has been studied [4]-[6]. However, it is impossible to obtain completely flat gain over the entire wavelength region occupied by WDM channels. Therefore, optical gain equalizers (GEQ) are indispensable to compensate for the gain imbalance in cascaded amplifier systems. This paper proposes a simple method to obtain optimum optical gain equalization for multistage in-line amplifier systems that employ the GEQs and confirms its effectiveness with a numerical simulation.

2. Principle

Figure 1 shows the block diagram of the typical multistage in-line amplifier system. The GEQ is inserted after every n-th EDFA, which is used to compensate the insertion loss of each GEQ including its excess loss. The output power of each channel after each GEQ is adjusted to the same power at the first EDFA input. We make three assumptions as follows.
(1) All EDFAs have the same characteristics.
(2) The wavelength dependence of the noise figure is negligible over the operation wavelength region.
(3) The loss of each fiber span is equal to the mean gain of WDM channels at each EDFA.
Under these assumptions, the OSNR for the i-th channel after the n-th EDFA is given by

$$\mathrm{OSNR}_i = \frac{G_0 \alpha_i^{\,n} Pin}{\sum_{j=1}^{n} \alpha_i^{\,(j-1)} G_i F h \nu B} \qquad (1)$$

with

$$\alpha_i = \frac{G_i}{G_0} \quad . \qquad (2)$$

Subscript i denotes the i-th channel and Pin is the input signal power. G_0 is the mean gain of all WDM channels at each EDFA, F is the noise figure, h is plank's constant, ν is optical signal frequency, B is the optical bandwidth of measured amplified spontaneous emission (ASE), G_i is the gain of the i-th channel, α is the gain imbalance factor, n is equalization interval i.e. the number of EDFAs between two neighboring GEQs.

Figure 2 shows the OSNR of three cases as a function of number of span.

(1) gain imbalance factor $\alpha = 0$ dB without GEQ (ideal condition)

(2) gain imbalance factor α = -1 dB without GEQ

(3) gain imbalance factor α = -1 dB with GEQ after every 6 th EDFA

We define OSNR degradation as the ratio of the OSNR for the case that gain imbalance exists to the OSNR under ideal condition. In Fig. 2, although the OSNR degradation increases span by span in case (2), the OSNR degradation does not depend on the number of spans in case (3). When GEQs are employed, the reduction of OSNR degradation was estimated to be 9.5 dB. The calculation results clearly show the effectiveness of GEQs.

Next, we describe the method of optimizing the gain equalization. The optical power of the minimum gain channel decreases with the multistage amplification within the GEQ interval. As a result, the OSNR of the minimum gain channel is degraded. To reduce this degradation, pre-emphasis of the input power, i.e. weighting of the input power into the first EDFA is introduced [7]. We assumed that the weighted input of the i-th channel Pin_i was proportional to the m-th inverse power of gain imbalance factor α_i as follows.

$$Pin_i \propto \alpha_i^{-m} \tag{3}$$

Using Eq. 1 and 3, the OSNR degradation with weighted input after each GEQ is given by

$$\Delta\mathrm{SNR}_i = \frac{\sum_{j=1}^{n} \alpha_i^{(j-1)}}{(n-1)\alpha_i^{(n-m-1)}} = \frac{\alpha_i^{(m-n+1)}(1-\alpha_i^{n})}{(n-1)(1-\alpha_i)}. \tag{4}$$

Equation 4 is the convex function of α at the condition of $0 < m < n$-1 and the maximum OSNR degradation occurs at the minimum or maximum gain channel. Therefore, we can determine the optimum weighting factor m such that the maximum and minimum gain channels have the same OSNR degradation. Next, we determine the optimum equalization interval n taking the excess loss of the GEQ and output level imbalance of the amplifier into account.

3. Numerical simulation

A numerical simulation was carried out to verify the optimization method just mentioned. The calculations were based on Giles's model [8]. The EDFA model assumes an Al co-doped fiber whose cross-section data is the same as in [9]. In the calculation, 16 WDM channels were assumed with wavelength ranging from 1530 nm to 1560 nm with 2 nm channel spacing; the total signal input power into the EDFA was -3 dBm. All amplifiers were co-pumped at 980 nm with 50 mW. When the input power of all channels was set to -15 dBm, the mean gain of all channels was 16.7 dB, the maximum gain was 20.3 dB at 1530 nm and the minimum gain was 15.6 dB at 1542 nm. The maximum gain imbalance factor and the minimum gain factor were 3.6 dB and -1 dB, respectively. The transmission loss of one span was 16.7 dB which correspond to about 60 km of dispersion shifted fiber.

Using the proposed optimization method, the OSNR degradation and the optimum weighting factor, m, as a function of equalization interval, n, is shown in Fig. 3. When the equalization interval is short, the OSNR degrades due to the increased number of EDFAs for GEQ loss compensation. When the equalization interval is long, the OSNR degrades due to more power imbalance. As clearly shown in Fig. 3, the optimized equalization interval n and weighting factor m are 5 and 1.5, respectively; they yield the minimum OSNR degradation of 1.7 dB.

Figure 4 shows calculated optical spectra with and without the proposed equalization and loss characteristic of the GEQ for 8 fiber spans, which corresponds to 480 km transmission. The number of EDFAs with and without GEQs were 10 and 8, respectively.

GEQs were inserted after the 5 th and 10 th EDFA. Figures 4 (a)-(b) show the spectra with no equalization. The input power into the first EDFA of all channels was set to -15 dBm as shown in Fig. 4 (a). The spectrum after 8 EDFAs is shown in Fig. 4 (b) and the power difference is estimated to be more than 30 dB between the maximum and minimum gain channel. Figure 4 (c)-(e) show the optical spectra with optimized equalization and GEQ loss curve. In Fig. 4 (c), the input power into the first EDFA was weighted by optimum weighting factor m=1.5 and the power difference was set to about 7 dB. The output spectrum of the 10-th EDFA is shown in Fig. 4 (d). Compared to Fig. 4 (b), the equalized OSNR was obtained over the whole wavelength region in Fig. 4(d). In Fig. 4 (e), the allowable insertion loss at the minimum gain channel, i.e. excess loss of GEQs was 9.8 dB. Such GEQs will be realized by waveguide type demultiplxers and variable attenuators [10], [11].

Figure 5 shows the calculated OSNR degradation for the same conditions as Fig. 4. Without GEQs, the maximum OSNR degradation was 12 dB at the minimum gain wavelength. It reduced to 5 dB when using only GEQs and 2.5 dB when using both GEQ and pre-emphasis. The optimum equalization, which combines pre-emphasis and GEQs, significantly reduces the optical SNR degradation.

4. Conclusion

A simple method of optimizing optical gain equalization has been proposed. The optimization method focuses on the equalizer insertion interval and weighting factor of the input power of the first EDFA to minimize the OSNR degradation.

A numerical simulation was carried out to verify the effectiveness of the optimization method. Using the optimizing method, the OSNR degradation was reduce to 2.5 dB after 8 fiber spans for 16 WDM channels with 30 nm wavelength bandwidth, the degradation was 12 dB without equalization case.

Acknowledgment

The authors wish to thank Dr. Takao Matsumoto and Dr. Masaki Fukui for their continuous encouragement and fruitful discussions.

Reference

[1] K. Nosu et al., *IEEE J. Lightwave technol,* Vol.11, pp. 764-776, 1993.
[2] K. Oda et al., *Electron. Lett.*, Vol. 30, pp. 982-984, 1994.
[3] A. R. Chraplyvy et al., *OFC'94* Post deadline paper PD19, pp. 92-95, 1994.
[4] M. A. Ali et al., *IEEE Photon. Technol. Lett.*, Vol. 6, pp. 1039-1042, 1994.
[5] B. Clesca et al., *Electron. Lett.*, Vol. 30, pp. 1308-1309, 1994.
[6] C. G. Atkins et al. , *Electron. Lett.*, Vol. 25, pp. 910-911, 1989.
[7] A. R. Chraplyvy et al.,*IEEE Photon. Technol. Lett.,* Vol. 4, pp. 920-922, 1992.
[8] C. Randy Gliles et al., *IEEE J. Lightwave technol,* Vol.9, pp. 217-283, 1991.
[9] William L. Brames et al., *IEEE J. Quantum Electron.*, Vol. 27, pp. 1004-1010, 1991.
[10] A. F. Elrefaie et al., *IEEE Photon. Technol. Lett.,* Vol. 5, pp. 1026-1028, 1993.
[11] Hiroshi Takahashi et al., *IEEE J. Lightwave technol,* Vol. 12, pp. 989-995, 1994.

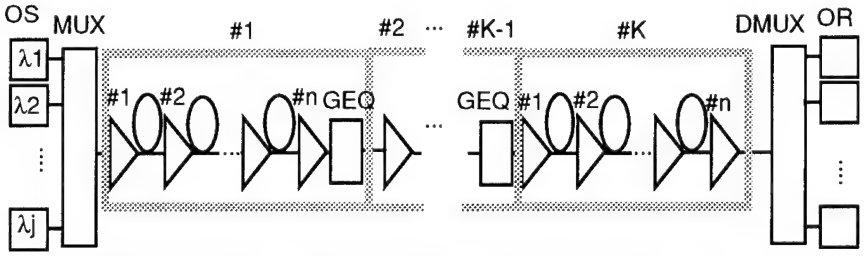

Fig. 1 Block diagram of the multistage in-line amplifier system.

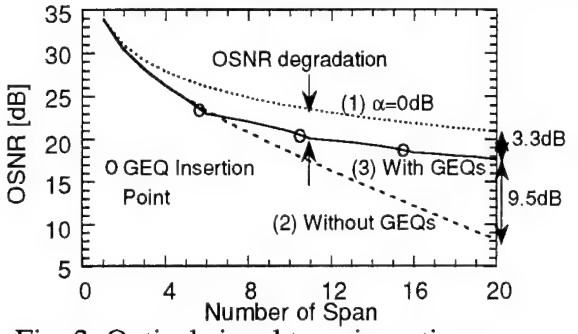

Fig. 2 Optical signal to noise ratio as a function of number of span. Input power: -15 dBm, noise figure: 6 dB, Optical band width: 0.2 nm.

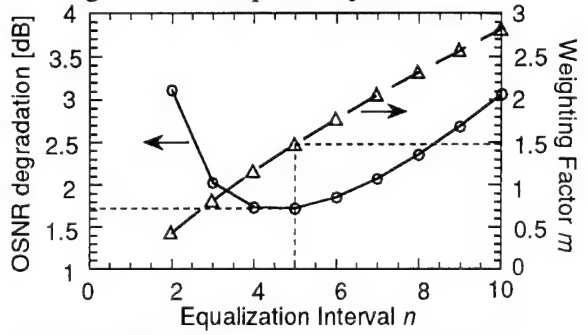

Fig. 3 OSNR degradation and weighting factor m against equalization interval n.

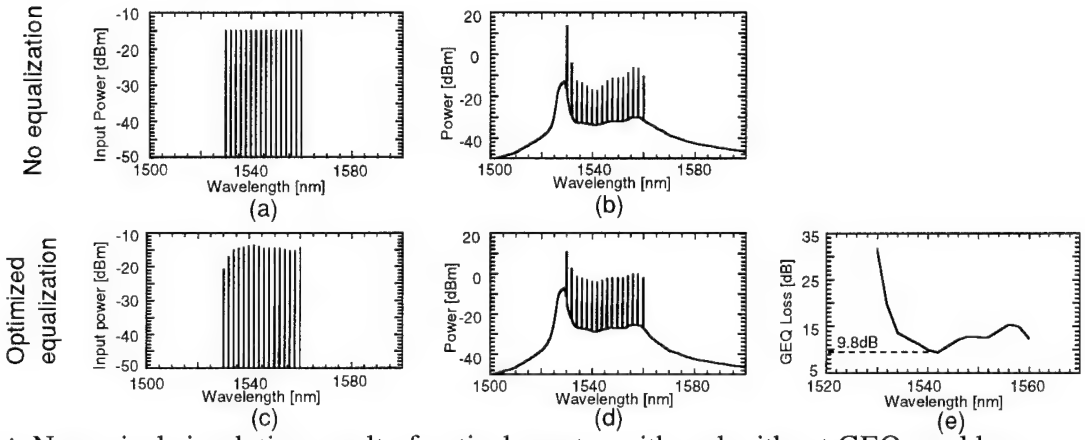

Fig. 4 Numerical simulation result of optical spectra with and without GEQs and loss characteristic of GEQ. Optical band width: 0.2 nm. (a) Input spectra without GEQ, (b) Output spectra of 8 th EDFA without GEQ, (c) Input spectra with optimized equalization, (d) Output spectra of 10 th EDFA with optimized equalization, (e) Loss characteristic of GEQ.

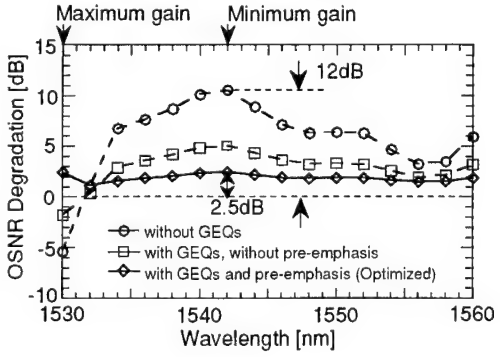

Fig. 5 Numerical simulation result of OSNR degradation after 8 fiber spans against wavelength.

8 x 10 Gbit/s Repeaterless Transmission over 150 km of Dispersion-Shifted Fiber Using Fluoride-Based Amplifiers

B. Clesca°, S Artigaud, L. Pierre*, and J.-P. Thiery*

Alcatel Alsthom Recherche, Route de Nozay, 91460 Marcoussis, France
* Alcatel CIT, 91 625 Nozay Cedex, France
° Present address : Alcatel CIT, 91 625 Nozay Cedex, France
Telephone number: 33.1.64.49.25.33
Telefax number: 33.1.64.49.43.69

Introduction

The wavelength-division multiplexing (WDM) technique opens up new vistas in ultra high-capacity digital transport systems: the use of several optical channels tuned at different wavelengths and launched simultaneously into the same fiber enables one to achieve high aggregate bit rate [1, 2]. The total capacities reported in Refs. [1, 2] are well beyond the capacity allowed by single-channel systems. Wavelength multiplexing effectively lifts up the bit rate limit usually encountered in systems based upon a single carrier supporting the data stream. This limit is imposed by direct electronic modulation in semiconductor components or opto-electronic circuits and by the various distorsions experienced by short non-return-to-zero pulses through the fiber.

However, depending on the number and spacing of channels, new limitations related to optical amplification and propagation over the fiber may arise within WDM transport systems. Concerning the amplification of wideband multiplexes, fluoride-based erbium-doped fiber amplifiers (EDFAs) have proved to date to be the most effective way to achieve amplification over bandwidths as large as 28 nm [3]. Over standard fibers (i.e., non-dispersion-shifted fibers), no significant limitation caused by cross-phase modulation has been reported so far in WDM system experiments [1]. On the other hand, dispersion-shifted fibers (DSFs) result in small limitations caused by dispersion but also in high four-wave mixing (FWM) efficiency. The efficiency is enhanced by low channel spacing and near-zero local chromatic dispersion [4].

Two approaches have surfaced to reduce the potentially significant system impairments caused by FWM: nonuniform channel spacing [5] and dispersion-managed fiber routes [6]. Here, we take advantage of the large bandwidth offered by fluoride-based EDFAs to increase the channel spacing with a subsequent decrease in FWM efficiency. Following the description of the characteristics of fluoride-based amplifiers designed as power and pre-amplifiers, we present the experimental results of an 8 x 10 Gbit/s repeaterless transmission experiment over 150 km of dispersion-shifted fiber.

Fluoride-based EDFA characteristics

Because of the different spectroscopic behavior of erbium ions within fluoride materials, fluoride-based amplifiers offer improved gain flatness in comparison with their silica-based counterpart [7]. The guidelines, in terms of degree of inversion and doped fiber length, have been provided in Ref. [8] for designing flat-gain amplifiers with a given gain level. By way of illustration, Fig. 1 shows the output spectrum of a fluoride-based EDFA for a total input power of -6 dBm. The input multiplex is composed of 8 wavelength-multiplexed channels with channel spacing of 4 nm (λ = 1532-1560 nm) and identical powers. For about 2 x 60 mW 1480-nm pump power launched into the doped fiber,

+17 dBm output power and signal-to-noise ratio in excess of 37 dB are observed while the gain excursion is as small as 1.2 dB.

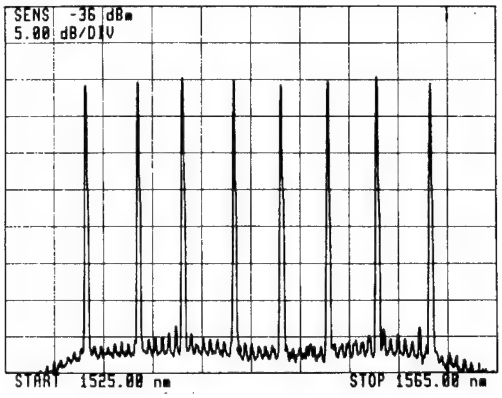

Fig. 1: Fluoride-based amplifier output spectrum for -6 dBm total input signal power with an 8-channel multiplex (spacing 4 nm) (full span: 1525-1565 nm, 0.1-nm resolution bandwidth, 5 dB/div).

Figure 2 shows the experimental setup used to assess the sensitivity performance of a fluoride-based EDFA designed as a preamplifier for multichannel operation. At the amplifier input, all the 8 channels support one 10 Gbit/s data stream and have identical power. Bit-error-rates (BERs) are measured versus the power per channel received at the input of the preamplifier. Figure 3 shows the BERs for each channel when the whole multiplex is coupled into the preamplifier. At the receiver level, the fluoride-based preamplifier is followed by a 40-GHz optical filter and a 10 Gbit/s p.i.n. opto-electronic receiver. The 10 Gbit/s receiver is made of discrete components; it offers an 11 dB optical dynamic range and a sensitivity of -13.5 dBm for 10^{-10} BER and pseudorandom bit sequences of 2^{31}-1 length. The average sensitivity for 10^{-9} bit-error-rate is -33 dBm and the sensitivity excursion between channels is relatively low over 28 nm (1.5 dB). This sensitivity result is similar to the one obtained under single-channel operation with silica-based preamplifiers using 1480 nm pump sources and simple configuration [9].

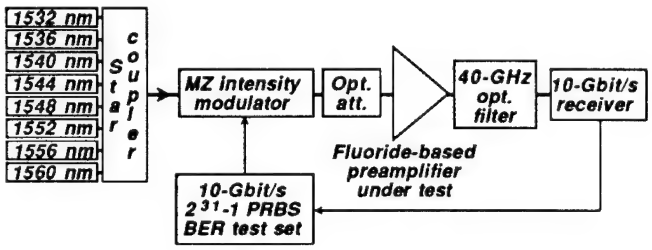

Fig. 2: Experimental setup used for the assessment of fluoride-based preamplifier performance.

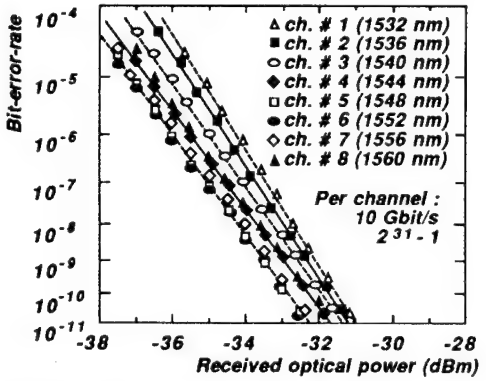

Fig. 3: BERs versus received power per channel for an 8 x 10-Gbit/s multiplex applied to a fluoride-based preamplifier.

These experimental results clearly demonstrate that fluoride-based fiber amplifiers can be fruitfully implemented in repeaterless wideband WDM systems without any gain equalization or flattening techniques.

8 x 10 Gbit/s transmission experiment over 150 km of DSF

Figure 4 shows the setup used to perform repeaterless transmission over 150 km of dispersion-shifted fiber. At the transmitter level, 8 wavelength-multiplexed channels ranging

over 28.6 nm (constant channel spacing of 512 GHz) are coupled into a first fluoride-based amplifier to compensate the loss caused by the external Mach-Zenhder intensity modulator. The polarization states of the 8 channels are identical at the modulator input polarizer. Identical channel spacings and polarisation states between channels maximize FWM efficiency. A second fluoride-based amplifier is used to enhance the signal power at the input end of the 150-km long dispersion-shifted fiber.

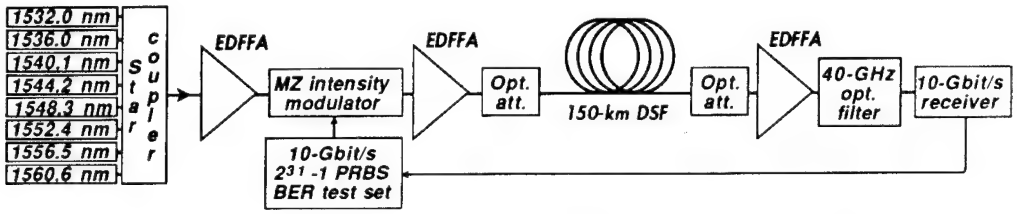

Fig. 4: Experimental setup for 8 x 10 Gbit/s transmission experiment. (EDFFA: erbium-doped fluoride fiber amplifier)

The DSF used in this work is a fiber designed for long-haul amplified submarine systems with the following characteristics: the zero-dispersion wavelength λ_0 is near $\lambda = 1557$ nm in the first effective length for nonlinearity (where most of FWM occurs); the attenuation and effective area are 0.2 dB/km and 50 μm^2, respectively.

The sensitivity for 10^{-9} BER measured at the preamplifier input is shown in Fig. 5 as a function of the channel wavelength, with and without the 150-km DSF span. The bit rate is 10 Gbit/s and pseudorandom bit sequences of 2^{31}-1 length are used. The results shown in Fig. 5 are obtained for +4 dBm power per channel launched into the fiber. The greatest sensitivity penalty is observed for channel 7 ($\lambda = 1556.5$ nm close to λ_0, 15 FWM intermodulation products under this carrier) and is only 0.6 dB. This experiment corresponds to a repeaterless 12-Tbit/s-km capacity-distance product. This result is slightly higher than the best performance previously reported for repeaterless DSF systems, in which unequal channel spacing was used for decreasing FWM efficiency [5].

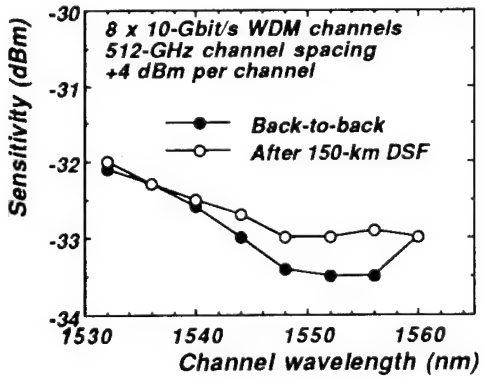

Fig. 5: Sensitivity for 10^{-9} BER versus channel wavelength for 8 channels without and with 150-km long DSF.

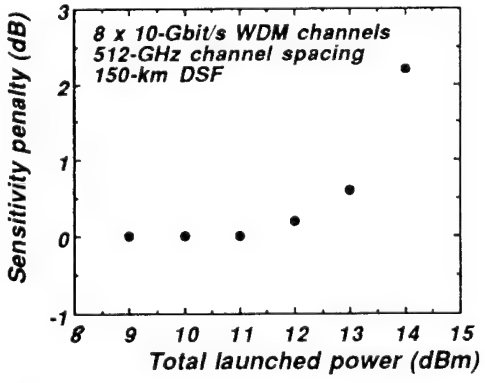

Fig. 6: Sensitivity penalty at 10^{-9} BER for channel 7 versus total power launched into the 150-km long DSF.

When the launched power is increased at the transmitter level, the sensitivity penalty for channel 7 increases as shown in Fig. 6. This is due to the corresponding increase of the FWM crosstalk. The crosstalk level caused by FWM is shown in Fig. 7 at the DSF output for a launched power of +14 dBm. The frequency of channel 7 is sligthly shifted in order to exhibit the FWM intermodulation products. The FWM crosstalk level measured in Fig. 7 for channel 7 is near -22 dB. This level corresponds to the sensitivity penalty of 2.2 dB

in Fig. 6. This penalty is consistent with results reported in Ref. [10]. It is worth noting that in actual embedded fiber route, attenuation is more likely to be near 0.3 dB/km rather than 0.2 dB/km in laboratory conditions. This larger fiber loss will lower FWM efficiency.

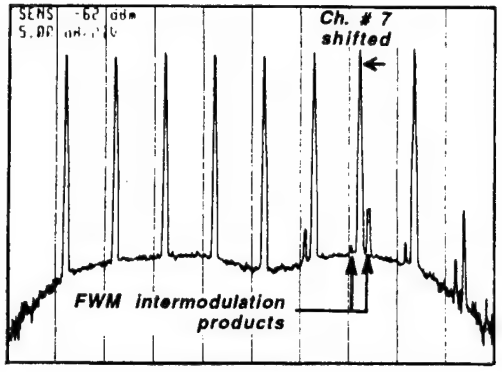

Fig. 7: Spectrum at the output of the 150-km long DSF for +14 dBm launched power; the frequency of channel 7 is slightly shifted (same scales as in Fig. 1).

Conclusion

With reasonnable pump power (2 x 60 mW at λ = 1480 nm), fluoride-based EDFAs were shown to exhibit greatly improved gain flatness under multichannel operation with respect to their silica-based counterparts. Their characteristics, such as +17 dBm output power with 1.2-dB gain excursion and sensitivity weakly spread around -33 dBm for 10 Gbit/s bit rate, demonstrate that fluoride-based amplifiers are most suitable to wideband WDM transmission.

These wideband performance enable us to achieve 8 x 10 Gbit/s repeaterless transmission over 150 km of dispersion-shifted fiber with moderate sensitivity penalty caused by four-wave mixing. This scheme is allowed by the large channel spacing offered by fluoride-based amplifiers (512 GHz, i.e. about 4 nm, for an 8-channel multiplex) and by the subsequent decrease in FWM efficiency. The transmission experiment reported in this paper corresponds to a capacity-distance product of 12 Tbit/s.km without any in-line amplifier.

Acknowledgments

This work was partly supported by the European Economic Community (RACE GAIN project n° 2018). Out of the fluoride-based amplifiers used in the work reported in this paper, one was provided by M. Fake from Hewlett-Packard Ipswich under the GAIN program.

References

[1] H. Onaka et al., "10 Gb/s, 4-wave 200 km and 16-wave 150 km repeaterless transmission experiments over standard single-mode fiber," *in Tech. Dig. ECOC '94*, Firenze, Italy, vol. 4, pp. 49-52, 1994.

[2] R. W. Tkach et al., "One-third Terabit/s transmission through 150 km of dispersion-managed fiber," *in Tech. Dig. ECOC '94*, Firenze, Italy, vol. 4, pp. 45-48, 1994.

[3] B. Clesca et al., "Multiwavelength gain flatness assessment of fluoride-based fibre-amplifiers using a circulating loop," *IEE Electron. Lett.*, vol. 30, n° 16, pp. 1308-1309, 1994.

[4] G. P. Agrawal, "Nonlinear fiber optics," Academic Press, San Diego, 1989.

[5] F. Forghieri et al., "Repeaterless transmission of 8 10-Gb/s channels over 137 km (11Tb/s-km) of dispersion-shifted fiber," *in Tech. Dig. OFC '94*, San Jose, USA, paper PD26, 1994.

[6] A. R. Chraplyvy et al., "8 x 10 Gb/s transmission through 280 km of dispersion-managed fiber," *IEEE Photon. Technol. Lett.*, vol. 5, n° 10, pp. 1233-1235, 1993.

[7] B. Clesca et al., "Gain flatness comparison between erbium-doped fluoride and silica fiber amplifiers with wavelength-multiplexed signals," *IEEE Photon. Technol. Lett.*, vol. 6, n° 4, pp. 509-512, 1994.

[8] D. Bayart et al., "Experimental investigation of the gain flatness characteristics for 1.55 µm fluoride-based erbium-doped fibre amplifiers," *IEEE Photon. Technol. Lett.*, vol. 6, n° 5, pp. 613-616, 1994.

[9] B. L. Patel et al., "High performance 10 Gbit/s optial transmission system using erbium-doped fibre preamplifier," *IEE Electron. Lett.*, vol. 27, n° 23, pp. 2179-2180, 1991.

[10] B. Clesca and S. Artigaud, "Experimental investigation of four-wave mixing in multichannel systems over dispersion-shifted fibre," submitted to *IEE Electron. Lett.*.

Nonlinearities in Semiconductor Optical Amplifiers

SaC 14:00-15:45
Theatersaal

Luuk F. Tiemeijer, *Presider*
Philips Optoelectronics Center, The Netherlands

Applications of high-speed non-linearities of semiconductor amplifiers

R. J. Manning, D. A. O. Davies, A. D. Ellis and D.M. Patrick
BT Laboratories,
Martlesham Heath,
Ipswich,
Suffolk
UK.
IP5 7RE
Tel: +44 1473-645362
Fax: +44 1473-646885
e-mail: r_j_manning@bt-web.bt.co.uk

Introduction

In the recent past, there has been unprecedented progress in the use of non-linear effects in semiconductor laser amplifiers (SLAs) for high-speed all-optical signal processing. Applications include all-optical demultiplexing (1-4), clock recovery (5,6), mid-span spectral inversion (7), wavelength conversion (8,9), and use as an ultrafast AND gate for optical packet processing (10).

This paper will concentrate on the use of SLAs for two of the basic functional blocks in optical time division multiplexed (OTDM) systems, namely gating (demultiplexing) and clock recovery. These may be combined to form an optical regenerator (11), or an all-optical routing device (12). These two functions have been demonstrated all-optically, exploiting cross-phase modulation in silica fibre. We have shown that the resonant nonlinearity in SLAs can be used in both functional blocks. Because of the very short length of SLAs (~500 μm), we can envisage making extremely compact units using current integration technology.

a) High speed demultiplexing

Contrary to what has been believed until recently, it is possible to perform demultiplexing using a SLA at a repetition rate much faster than its natural recovery rate of~1 GHz (1). This is due to the carrier dynamics, which we now consider. For interferometric switching, we require a differential phase shift of π, ie:

$$\Delta\phi \geq \pi$$

$$\text{ie } 2\pi\Delta n l/\lambda \geq \pi \text{ or } \Delta n \geq \lambda/2l$$

where Δn is the refractive index change, l is the amplifier length and λ is the wavelength. Hence, for a gain length of 500μm, at 1500nm we require $\Delta n = 1.5\times10^{-3}$. Assuming a refractive index change per carrier pair of ~ $2\times10^{-20}\text{cm}^3$, a total carrier density of $\approx 0.75\times10^{17}\text{cm}^{-3}$ has to be transferred from conduction to valence bands. The crucial point is that this is a small fraction of the typical inversion of $\approx 10^{18}\text{cm}^{-3}$ for SLAs . Hence we have a total phase change of many π available from the population inversion.

Figure 1 shows the dynamic behaviour when a regular 10 GHz gating pulse stream is applied to the SLA. A rapid change in the inversion, in sympathy with the injected pulses, is followed by a slower recovery due to the applied bias current. Because of the slow recovery time, the first few pulses progressively saturate the gain. A steady state is reached, where a partial recovery of π between the pulses is possible, and we see a regular 'sawtooth' phase change . Whilst the detailed carrier dynamics in SLAs are undoubtedly complex, a simple argument can

be used to explain this fast recovery. In steady state, with no optical input, the bias current must exactly balance the carrier recombination. In normal operating conditions, the carrier lifetime is typically ~500ps and the carrier density is $\approx 10^{18}cm^{-3}$, so the bias current supplies one tenth of the carrier density, $10^{17}cm^{-3}$ (equivalent to a phase change of π), in ~50-100ps.

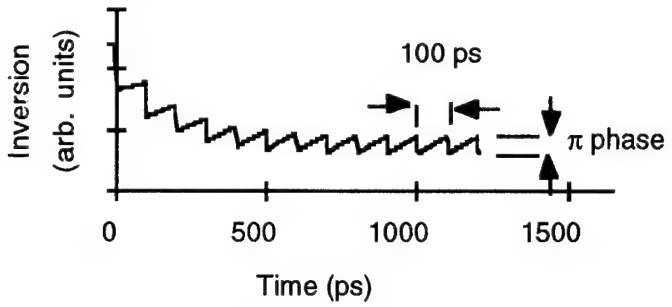

Figure1
Evolution of the population inversion with a regular gating pulse

If the gain is heavily depleted, ie we are far from equilibrium, the recovery rate is limited by the carrier injection rate. This qualitative description gives good agreement with experiment(1), and highlights that it is the control of the gain recovery via the bias current which is so important in the use of SLAs for high speed applications. We note that, by running at high bias currents (300-400 mA), we can expect up to an order of magnitude increase in the carrier injection rate, so giving a phase change of π in 10 ps, or 100 GHz operation as an upper limit.

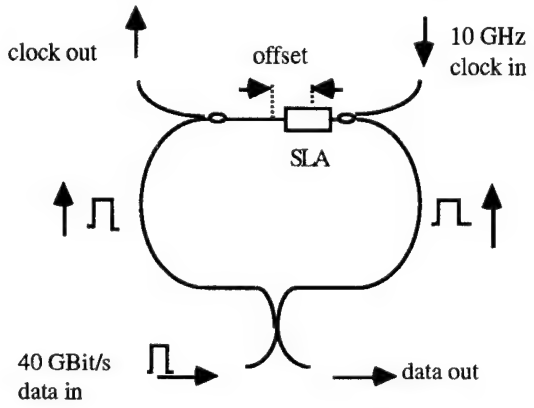

Figure 2
Experimental configuration for demultiplexing

Fig.2 schematically shows the set up used by Ellis and Spirit (1) to demultiplex a 10 Gbit/s data stream from a 40 Gbit/s train. A SLA is the nonlinear element in a loop mirror, and is placed slightly offset from the centre (4). Data injected into the loop mirror is split by a 50:50 coupler and the two streams arrive asynchronously at the SLA. The SLA is addressed by 10 GHz gating pulses which arrive after one data pulse but before its counter-propagating replica. This imparts a π relative phase change on to the replica, so the pulse is switched out at the coupler. The periodic sawtooth phase variation in Figure 1 is experienced by the subsequent pulses and their replicas. These pulses experience only a small phase difference and remain unswitched. Gating pulse energies of ~ 0.5 pJ at the SLA facet were required for switching. The SLA directly

replaces the many km of silica fibre that would normally be used (11).

b) All-optical clock recovery

The clock recovery circuit used is shown in Fig. 3 (5). Cross-phase and amplitude modulation in the SLA caused by the incoming data is used to mode-lock the ring laser at the line rate. The ring length is a multiple of the line rate, or of a word length if word recovery is required (12).

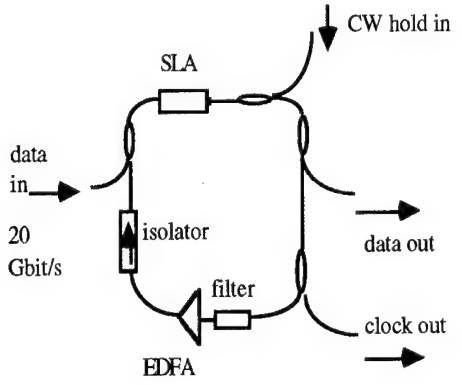

Figure 3
Experimental configuration for clock recovery

Non-uniform phase variations occur in the SLA when it is driven by data, rather than a regular clock These variations in the phase and amplitude corrupt the mode-locking process and lead to patterning in the recovered clock. For this reason, an intense holding beam is used, which saturates the gain and speeds the gain recovery via stimulated absorption/emission, so that such phase wander is prevented(13). Figures 4 and 5 illustrate this effect for a hypothetical 111110011011 data sequence without (Fig.4) and with (Fig.5) the holding beam:

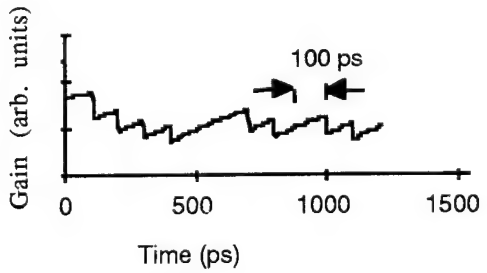

Figure 4
Gain variation of SLA when data-driven

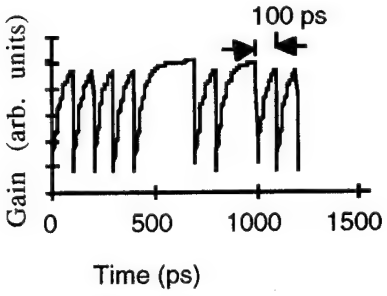

Figure 5
Gain variation with holding beam

This technique was used succesfully to demonstrate pattern-free clock recovery at 20 GHz (5). It is important to note that, whilst phase recovery should take place within a bit period, a phase window wider than the pulse is desirable to allow jitter tolerance, an essential requirement of clock recovery. Time-resolved phase and amplitude measurements of a SLA with a holding beam indicate that this requirement is easily satisfied for pulses < 10 ps (14).

c)Data switching in a SLA loop mirror

In order to perform regeneration, the recovered clock is injected into a SLA loop mirror gated by the 'old' data stream, to give a replica, but with jitter removed. This has been recently demonstrated with 10 Gbit/s data (15), where the same asynchronous arrangement is used as for demultiplexing. Again, because data is used to address the SLA, there is phase wander (Fig 4). It might be thought that a holding beam would be necessary to prevent patterning, as in clock recovery. However the phase wander in the loop is experienced by both clockwise and anti-clockwise propagating pulses, and is of little importance if the SLA is very close to the middle of the loop. Because of gain recovery in the presence of zeros, the next 'one' in the data sequence will cause a slightly larger phase shift. These height variations in phase differences are smoothed by the sinusoidal response of the loop mirror, and so switching is relatively insensitive to such changes, giving error-free modulation (15). Furthermore,the switching window is approximately square, giving a reasonable jitter tolerance.

Conclusions

We have shown that the carrier dynamics in SLAs play a crucial role in high-speed applications, such as OTDM. We have demonstrated the basic functions needed for all-optical regeneration using SLAs as non-linear elements, and that it should be possible to make a compact photonic regenerator.

References

1) A.D.Ellis and D.M.Spirit, Electron. Lett. 29(1993) 2115
2) K. Suzuki, K. Iwatsuki, S. Nishi and M. Saruwatari, Electron. Lett. 30,(1994) 660
3) M. Eiselt, Electron. Lett. 28,(1992) 1505
4) J.P.Sokoloff, I. Glesk and P.R. Prucnal, IEEE Phot. Tech. Lett. 6(1994) 98
5) D.Patrick and R.J.Manning, Electron. Lett. 30(1994) 151
6) O. Kamatani, S. Kawanishi and M. Saruwatari, Electron. Lett. 30(1994) 807
7) M.C.Tatham, X.Gu, L.D. Westbrook, G. Sherlock and D.M. Spirit, Electron. Lett. 30(1994) 1335
8) K.E. Stubkjaer, T. Durhuss, B. Mikkelsen et al, ECOC'94 Proceedings, p635
9) J.M. Wiesenfeld, B. Glance, J.S. Perino and A.H. Gnauck, IEEE Phot. Tech. Lett.,5(1993) 1300
10) D. Nesset, M.C. Tatham, L.D. Westbrook and D. Cotter, Electron. Lett. 30(1994) 1938
11) J.K. Lucek and K.Smith, Optics Lett. 18(1993) 1226
12) J.K.Lucek and K.Smith, CLEO '94 CPD7 postdeadline paper
13) R.J. Manning and D.A.O. Davies, Optics Lett., 19,(1994) 889
14) R.J.Manning, D.A.O. Davies, D. Cotter and J.K. Lucek, Electron. Lett. 30(1994) 787
15) D.A.O. Davies, A.D. Ellis, T. Widdowson and G.Sherlock, to be published in Electron. Lett.

Femtosecond Pulse Amplification and Cross-Phase Modulation in Semiconductor Laser Amplifiers–Theory and Experiment

A. Dienes, J. P. Heritage, M. Y. Hong, R. S. Grant
Dept of ECE, University of California, Davis, CA, 95616

P. J. Delfyett
CREOL, Orlando, FL, 32826

We have recently reported a theoretical model [1,2] for subpicosecond pulse amplification in semiconductor laser amplifiers (SLA). The model includes a variety of dispersive and nonlinear effects, and has been succesful in quantitatively describing [1,2] experimental results of spectral distortions, as well as time domain gain dynamics, during subpicosecond strong signal amplification in an SLA. Here, we present the results of two different experiments, each on a different device, and apply the theoretical model to explain the results. The purpose is not only to test the behavior of the devices with regard especially to the effects of fast nonlinearities and gain dispersion, but also to test the general applicability of the model and its range of validity. The model consists of a nonlinear propagation equation with auxilliary equations describing the slow and fast gain dynamics self-phase modulation and gain dispersion, as given in [1,2].

The first experiment was carried out on an angle stripe ridge guide Graded Index Separate Confinement (GRINSCH) Strained Layer InGaAs/AlGaAs laser diode. The single InGaAs active layer has a thickness of 10 nm. The graded index layers are composed of AlGaAs with the concentration of Al changing from 60% to 0%. The length of the device is 1mm and the width is about 5 μm. The angle of the stripe is 7 degrees. We performed strong signal amplification of femtosecond pulses and observed the spectral distortions at various input signal levels. The nearly transform limited 150 fs duration input pulses were derived from a mode-locked Ti:Sapphire laser. Figure 1 shows a typical experimental output spectra at an injection current of 75 mA which resulted in a linear gain of about 17 DB. The input spectrum (not shown) is 5.8 nm wide (FWHM), symmetric, and centered at 884 nm. Strong spectral distortions can be seen, especially at the higher input level. It is known that for subpicosecond pulses spectral distortions are caused by self-phase modulation (SPM) associated not only with slowly recovering gain saturation but also with fast gain compression owing to carrier heating [1,2,3]. For pulses of 150 fs duration the effects of dynamic gain dispersion are also important because the pulse spectrum occupies up to ~30% of the gain bandwidth. What is interesting about the distortions seen on Figure 1 is that they

are remarkably similar to those observed for much longer 2ps pulses, but dissimilar to those observed for 400 fs pulses in an earlier experiment [1,2]. Physically this can be explained by the fact that since the 150 fs pulse duration is much shorter than the recovery of the carrier heating, the gain compression by carrier heating also behaves like an integrating gain saturation. Thus, this gain compression also displays a characteristic step-like feature in time, and the resulting SPM only adds long wavelength spectral components. Only for pulses whose duration is comparable to the relaxation time of the carrier heating are more complex spectral distortion effects manifested, as is the case in the second experiment. The results shown in Figure 1 can be quantitatively explained by integrating the model equations (with a modified split-step Fourier transform method), using the known parameters of the experiment and varying the others within physically reasonable limits, as will be presented. It should be noted that for this experiment the effects of the gain dispersion also cause strong spectral shifts, in addition to the SPM.

The second experiment was cross-phase modulation and was carried out [4] on a wide area gain guided, angle stripe GaAs/AlGaAs SLA. Both the pump and the probe signals were derived from a hybrid mode-locked external cavity laser system with compression [2,4]. For signals of 450 fs duration very complex spectral changes were observed as a function of the pump-probe time delay. These owe mainly (but not exclusively) to the index changes by carrier depletion *and* by carrier heating. Since the probe pulse "sees" not only the onset, but also the recovery of the carrier heating, a complex combination of red shifted and blue shifted spectral distortions result. The experimental results are well described by our theoretical model as can be seen on Figure 2. To obtain the theoretical results, the propagation equation was integrated for the pump signal, using *the same device parameters* as for the previously matched experiments on this SLA [1,2]. The instantaneous net gain and phase functions for each segment of the amplifier was saved and the delayed probe signal was modified by these functions. All the salient features of the experimental set of curves are reproduced nicely on the theoretical set. For negative delays (i.e. probe arriving before pump, but with some overlap) the spectrum shifts toward longer wavelengths, an effect of the carrier depletion caused SPM. At zero delay, red shift still exists but the probe spectrum is actually narrowed, an effect not at all intuitively obvious. At small positive delays, double peaking occurs with the main peak rather suddenly shifting to the short wavelength side. These changes are brought about by the relaxation of the heated carriers which occurs on the tail of the pump pulse. Finally, the "blue" peak decays back into the original spectral shape as the pulses no longer overlap. While similar qualitative explanations for such effects have been offered previously [3,4] the good agreement on the details of the spectral features as well as on the size of the spectral shifts shows that our model gives a very satisfactory description of the phenomena observed.

The results of the these two experiments show the importance of the various ultrasfast nonlinearities and of gain dispersion on strong signal femtosecond pulse amplification in SLAs. Our theoretical model is able to describe the behavior of quite different devices. Additionally, it appears that the theory remains valid for pulses as short as 150 fs. This is in agreement with related theories based on similar assumptions [5].

References

1. M. Y. Hong, Y. H. Chang, A. Dienes, J. P. Heritage, and P. J. Delfyett, IEEE J. Quantum Electron. **QE-30**, 1122 (1994).
2. P. J. Delfyett, A. Dienes, J. P. Heritage, M. Y. Hong, and Y. H. Chang, Appl. Physics **B58**, 183 (1994).
3. C. T. Hultgren, D. J. Dougherty, and E. P. Ippen, Appl. Phys. Lett. **61**, 2767 (1992).
4. P. J. Delfyett, Y. Silberberg, and G. A. Alphonse, Appl. Phys. Lett. **59**, 10 (1991).
5. J. Mørk, J. Mark, and C. P. Seltzer, Appl. Phys. Lett. **64**, 2206 (1994).

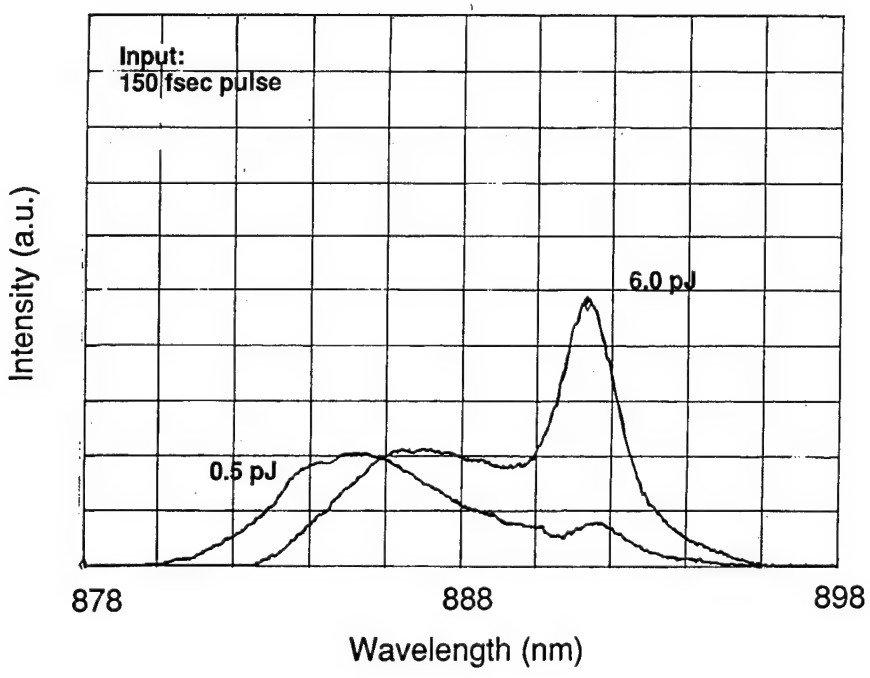

Figure 1. Experimental output spectra for 150 fs pulse amplification

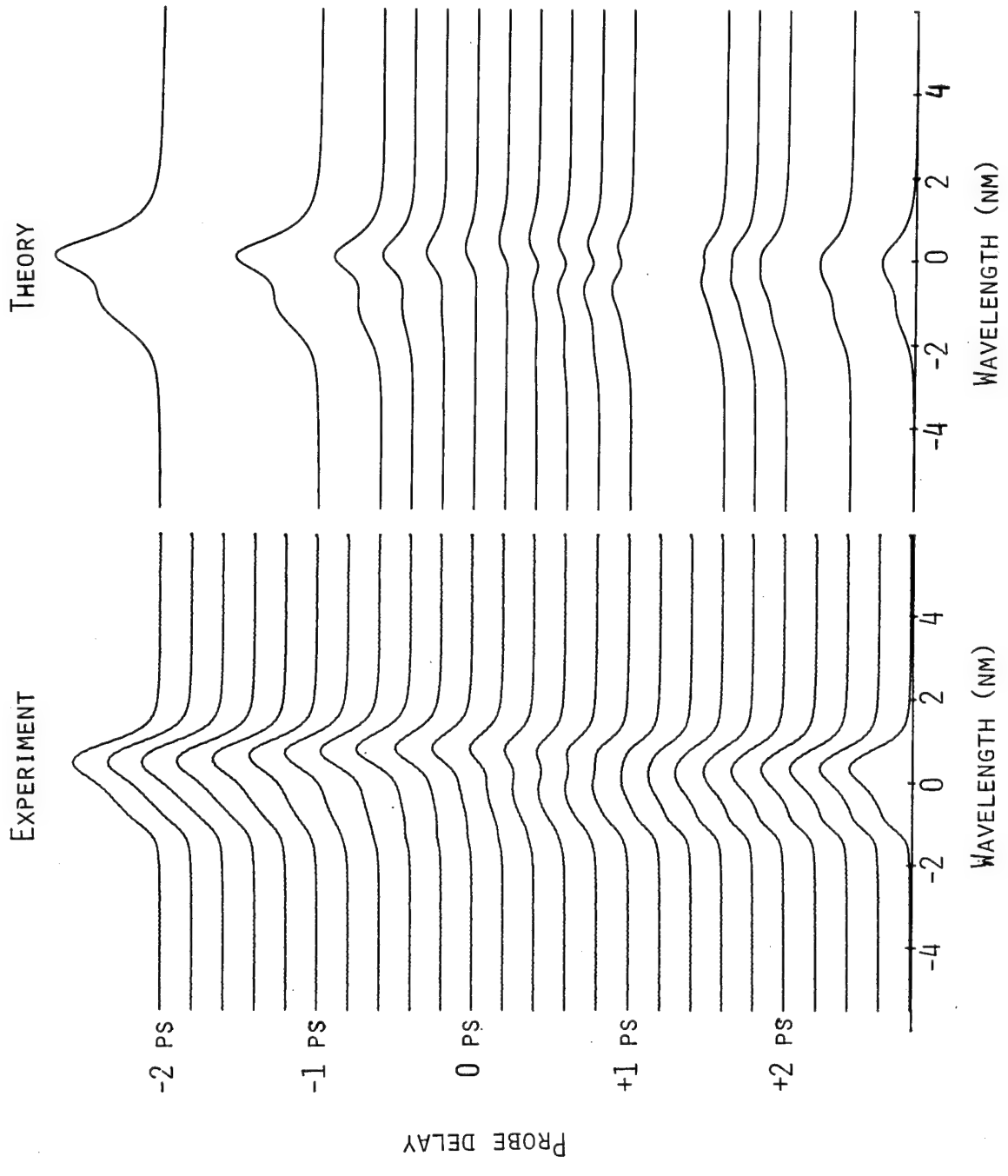

FIGURE **2.** CROSS-PHASE MODULATED SPECTRA

Saturation and Gain Dispersion Effects on Four Wave Mixing in Semiconductor Laser Amplifiers

I. Koltchanov, S. Kindt, K. Petermann
Institut für Hochfrequenztechnik, TU Berlin,
Einsteinufer 25, D-10587 Berlin, Germany
Tel. +049 30 314 22 628, Fax. +049 30 314 24 626

S. Diez, R. Ludwig, R. Schnabel, H.G. Weber
Heinrich-Hertz-Institut für Nachrichtentechnik,
Einsteinufer 37, D-10587 Berlin, Germany
Tel. +49 30 310 02 443, Fax. +49 30 310 02 241

R.Schimpe, G. Kristen
Siemens AG, Corporate Research and Development,
D-81739 Munich, Germany
Tel. +49 89 636 2742, Fax. +49 89 636 3832

Four-wave mixing (FWM) in semiconductor laser amplifiers (SLA) is presently a subject of intensive theoretical and experimental investigations. The high interest in this phenomenon is due to its potential applications, for example: wavelength conversion [1], compensation of signal distortions by mid-span phase conjugation [2] and demultiplexing of high bit rate data signals [3]. Moreover FWM is also of interest for spectroscopic investigations [4]. FWM experiments with detunings up to 4.3 THz [5] or even 5 THz [6] were reported recently.

The theoretical analysis of FWM in the SLA's should include considerations of wave propagation and saturation effects. There are several approaches to this problem in the literature. In [7] the propagation problem is solved, but gain saturation has not been taken into account. In [8] the nonlinear susceptibility $\chi^{(3)}(N)$ resulting from carrier density pulsations (CDP) and spectral hole burning (SHB) was assumed to be proportional to the gain coefficient $g(N)$. The non-proportionality of $\chi^{(3)}(N)$ to $g(N)$ was considered only concerning carrier heating (CH) in [8,9]. In all analytical approaches [7-9] the gain of the amplifier was assumed to be wavelength independent, having the same value for all waves participating in the FWM process. However, numerical calculations based on the density matrix formalism (DME) [10] show that the nonlinear susceptibility due to CDP and SHB is also not proportional with g(N). In this paper we discuss an analytical solution which takes into account a non-proportionality of $\chi^{(3)}(N)$ to $g(N)$ concerning CDP, CH and SHB, as well as a wavelength dependent gain . The theory is compared with DME based numerical calculations and experimental studies of FWM in a wide range of input powers (30 dB) and detunings (5 THz).

The arrangement for the theoretical and experimental investigations of the FWM process is as follows: Two optical fields, a pump wave E_2 (frequency f_2) and a probe wave E_1 (frequency f_1), are coupled into a SLA. Beating of both fields leads to modulation of various parameters of the gain medium at the beat frequency $\Delta f = f_2 - f_1$. The resulting dynamical index and gain grating causes the generation of new waves in particular of a signal wave E_3 (frequency $f_3 = f_2 + \Delta f$). This process of signal generation is accompanied by amplification of these waves during their propagation in the SLA (in contrast to the FWM in passive

devices). At high input powers the SLA is saturated, which results in a change of the gain coefficient and the nonlinear susceptibility due to their dependence on carrier density N.

In our experiments we have observed FWM sidelines up to 30 dB variation of input powers. This procedure was repeated for different detunings in the range of 0.2 ... 5 THz. The light sources were tunable external cavity InGaAsP-lasers. Pump and probe waves were amplified by Er-doped fiber amplifiers and filtered to reduce the input level of spontaneous emission. The input power into the polarization independent bulk InGaAsP amplifier (cross-section of the active stripe 0.45x0.9μm, length 500μm) [11] was varied by an attenuator. The output intensities of the pump $P_2(L)$, probe $P_1(L)$ and signal waves $P_3(L)$ as well as that of the amplified spontaneous emission (ASE) -signal $P_{ASE}(L)$ were measured by an optical spectrum analyser (Resoulution bandwidth: 0.08nm). A typical dependence of these values on the input power is shown in Fig.1. An increase of the input power causes gain saturation which results in a reduction of the ASE and an increase of P_3. Fig.1 reveals that saturation effects have to be taken into account to describe FWM in a wide range of input powers.

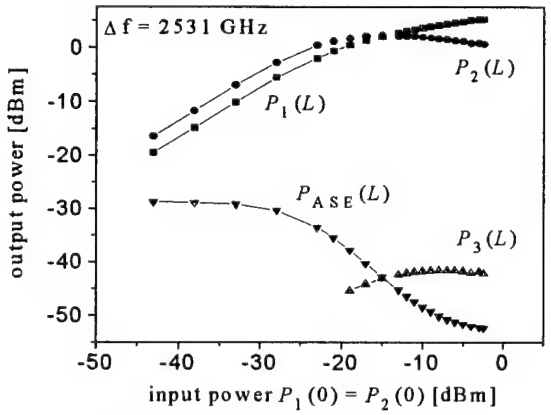

Fig. 1

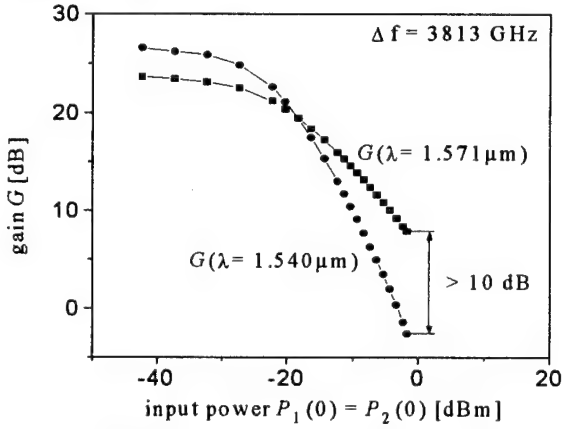

Fig. 2

In Fig.2, the gain for the pump and probe waves is shown vs. input power for detuning of about 4 THz. In this case the gain difference of the waves participating in the FWM (shown here E_1 and E_2) is more than 10dB and therefore represents an essential spectral effect. As can be seen in Fig.2, the gain saturation is not uniform. The gain difference changes the sign at a certain input power. This is due to the shift of the gain profile to longer wavelengths with saturation. It can be described theoretically with the assumption that the carrier density transparency is different for different wavelengths. In other words the gains as functions of carrier density at different wavelengths are not proportional to each other.

The neglection of the gain dispersion and non-proportional behaviour of $\chi^{(3)}$ and g leads to difficulties in the determination of the fitting parameters for the FWM detuning characteristics. These fitting parameters for FWM become dependent on the input power, which does not allow to characterise unambigously the nonlinear processes contributing to FWM. For example according to the theory of [7] the normalised efficiency of FWM $\eta = P_3/P_2^2P_1^*$ is independent of the input power. This contradicts the results in Fig.3 where the detuning characteristics are shown for input powers $P_1(0) = P_2(0)$ of -10 dBm and 0 dBm. Theoretical fits for these two input powers (solid lines) give different parameter sets. Calculations performed with the theory of [8] assuming that $\chi^{(3)}(N)$ is proportional $g(N)$ lead to an even stronger dependence on the input power.

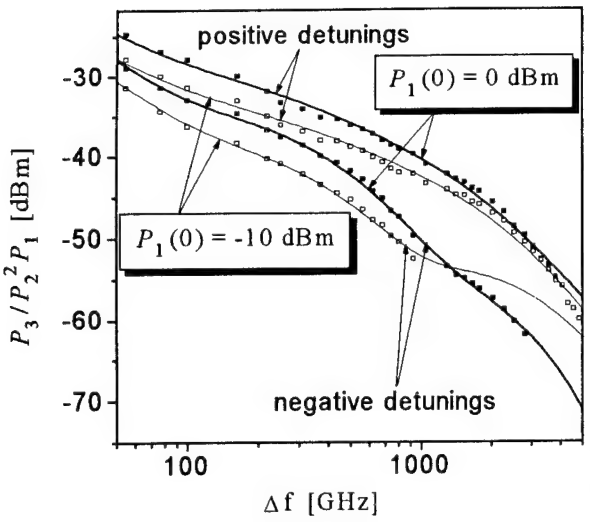

Fig. 3

In the present study we have developed a numerical and analytical theory of FWM which takes saturation and spectral effects into account. These effects include the difference of the unsaturated gain for the waves participating in the FWM, the non-uniform gain saturation at different wavelengths as shown in Fig.2 and the different dependencies of gain and nonlinear susceptibility on carrier density (not only due to *CH*). The full numerical model (based on DME-calculations) includes symmetrical and asymmetrical nonlinear gain suppression, and the exact dependence of the material parameters $\chi^{(3)}$ and g on carrier density, on frequency detuning and on pump wavelength. The approximations necessary for numerical theory are the same as in [10]. The analytical theory was developed assuming that $|E_2| > |E_1| > |E_3|$, which was accomplished in the experiment by choosing $P_2(0) = 10\ P_1(0)$.

The analytical result for the normalised efficiency of FWM is expressed as a function of the detuning, the normalised input power and the unsaturated gain of the pump wave. The difference in the unsaturated gain values is taken into account by the factor $\beta = 1+(g_{01}-g_{03})/2g_{02}$, and the non-uniform gain saturation is described by the factor $\sigma = (g_{01}-g_{03})/2g_{02} - (g_{N1}-g_{N3})/2g_{N2}$. Here g_{0i} is the small-signal gain coefficient and g_{Ni} is the differential gain of wave i. The factors β and σ can be determined from the saturation characteristics of the gain, as for instance shown in Fig.2. The effect of the non-proportionality of $\chi^{(3)}(N)$ and $g(N)$ is taken into account by the parameter $Q = \sum (g_{02}/g_{N2})(\chi_Y^{(3)}/g_2)_N$, where the summing occurs over the different nonlinear processes Y = *CDP,CH,SHB*. For small detunings $\Delta f << 1$ THz the gain dispersion effects can be neglected ($\sigma \to 0$, $\beta \to 1$) and our expression corresponds to the expression published in [9]. For large detunings the results of our analytical theory and of the approximated solution of [9] can be significantly different as shown in Fig. 4 (S_i in Fig.4 is photon density of wave i at the SLA output). If the assumption $\chi^{(3)}(N)$ proportional to $g(N)$ is made, then $Q \to 0$ and our analytical theory agrees with [8]. However, if $\chi^{(3)}$ and g have different dependences on the carrier density, the large discrepancy between our theory and [8] occurs also for small detunings.

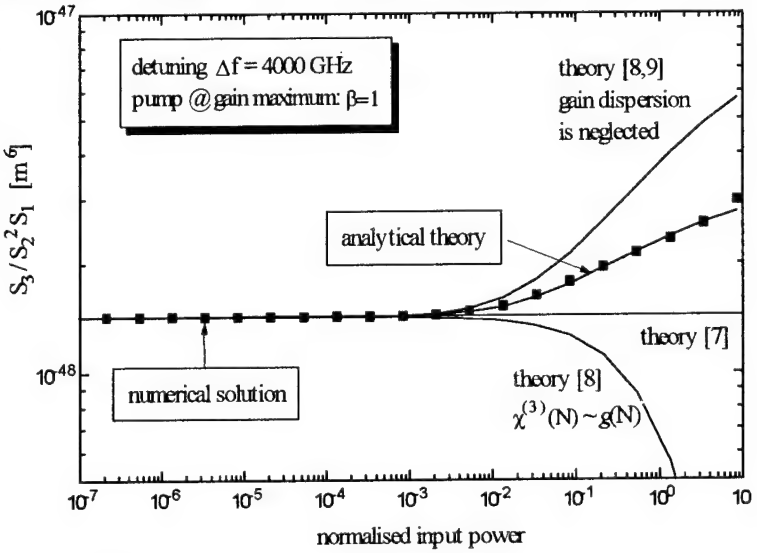

Fig. 4

As can be seen in Fig.4, the numerical calculations are in a good agreement with our analytical theory. Small deviations at high input powers were found to be due to the neglection of the nonlinear gain suppression.

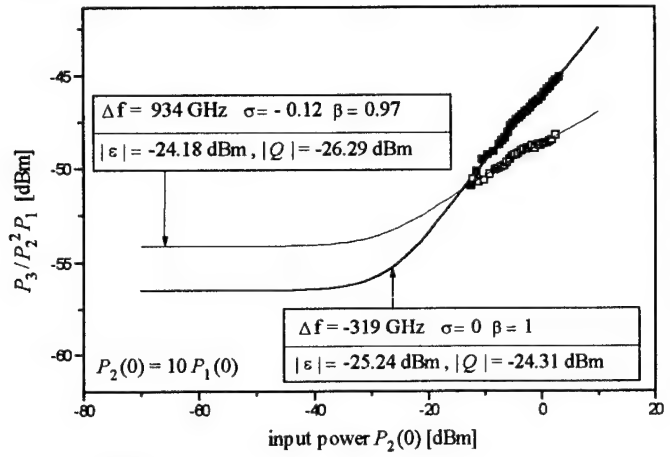

Fig.5

A comparison of the analytical theory and the experimental results is shown in Fig.5. A small ripple of the experimental data points is due to the residual facet reflections of the SLA. Fig.5 shows a fit of the calculated normalised efficiency η to the experimental results. From these fitting curves a factor $|\varepsilon|^2$ describing the limiting value of η at small input powers (in the unsaturated case) and the parameter $|Q|^2$ defined above could be reliably found for each detuning. Repeating the fit procedure for different detunings, we could obtain the detuning characteristic $|\varepsilon(\Delta f)|^2$ independent of input power, saturation and propagation effects.

In conclusion, we have studied the influence of gain dispersion and saturation on FWM in a semiconductor laser amplifier: by the gain difference of the participating waves due to the various differential gains and transparency points, and by the different dependencies of the nonlinear susceptibility and the gain on carrier density. The analytical theory is in good agreement with numerical results and experimental data. Based on our new analytical solution we obtained an input power independent detuning characteristic from the experimental data.

References

1. R. Schnabel, W. Pieper, M. Ehrhardt, M. Eiselt and H. G. Weber, Electron. Lett. **29**, 2047 (1993).
2. M. C. Tatham, G. Sherlock and L. D. Westbrook, in *Proceedings of ECOC'93*, Vol. 3, p. 61 (paper ThP 12.3), Montreux, Switzerland, Sept.1993 (Swiss Electrotechnical Association, Zurich, 1994).
3. R.Ludwig, G.Raybon, in *Proceedings of ECOC'93*, Vol. 3, p. 57 (paper ThP 12.3), Montreux, Switzerland, Sept.1993 (Swiss Electrotechnical Association, Zurich, 1994).
4. J. Zhou, N. Park, K. J. Vahala, M. A. Newkirk, and B. I. Miller, Appl. Phys. Lett. **63**, 1179 (1993).
5. A. D'Ottavi, E. Iannone, A. Mecozzi, S. Scotti, P. Spano, R. Dall' Ara, G. Guekos and J.Eckner, "Ultrafast gain and refractive index dynamics of semiconductor amplifiers measured by four-wave mixing," in *14-th International Semiconductor Laser Conference*, Maui, September 19-23, 1994, paper T2.3.
6. R. Schnabel et al. "Ultrafast, Multi-THz frequency conversion of a picosecond train using a 1.5 μm MQW seniconductor laser amplifier", PS 93', Palm Springs, paper PD1.
7. K. Kikuchi, M. Amano, C. E. Zah and T. P. Lee, Appl. Phys. Lett. **64**, 548 (1994).
8. A. Mecozzi, Optics Letters **19**, p.892 (1994).
9. A. Mecozzi, A. D'Ottavi, F. Cara Romeo, P. Spano, R. Dall'Ara, G. Guekos, J. Eckner, "High saturation behaviour of the four-wave mixing signal in semiconductor amplifiers," Appl. Phys. Lett., in press.
10. A. Uskov, J.Mørk, and J.Mark, IEEE J. Quantum Electron. **30**, p.1769 (1994)
11. R.Schimpe, B.Bauer, C. Schanen, G. Franz, G. Kristen, S.Pröhl, "1.5μm InGaAsP Tilted Buried-Facet Optical Amplifier", Conf on Lasers and Electro-Optics (CLEO '91), Baltimore, May '91, Paper CFK5

Wavelength conversion using interferometric structures containing semiconductor optical amplifiers

B. Mikkelsen, T. Durhuus, C. Joergensen, S.L. Danielsen,
R.J.S. Pedersen and K.E. Stubkjaer.

Center for Broadband Telecommunications, Technical University of Denmark
DK-2800 Lyngby, Denmark, Tel.: +45 42 88 14 44, Fax: +45 45 93 16 34

Introduction: Wavelength converters will be important for the development of wavelength division multiplexed (WDM) networks, as they allow for a flexible and distributed network management [1-2]. Furthermore, converters enable easy and fast dynamic routing in optical switches [3-7] as well as more advanced functionalities, i.e., optical buffering [7,8] and TDM to WDM conversion [9]. Therefore, much attention has been devoted to the realisation of all-optical wavelength converters. Considered techniques rely on mechanisms such as cross-gain and cross-phase modulation in semiconductor optical amplifiers (SOAs) [10-15], optical modulation of lasers [16-20] and four-wave-mixing in fibers and SOAs [21-22].

Particularly, integrated interferometric structures containing SOAs as optical phase shifters seem at present to be very attractive candidates for realisation of practical converters. This paper outlines the principle of operation and performance of such interferometric converters.

Interferometric structures: Wavelength conversion based on cross-phase modulation (XPM) in SOAs explores the dependency of the refractive index on the carrier density and hence an optical input signal. To make use of the XPM, the SOAs have to be placed in an interferometric configuration such as a Mach-Zehnder interferometer (MZI) [13] or a Michelson interferometer (MI) [10,14]. Both configurations, that are shown in Fig. 1, will be discussed in the following.

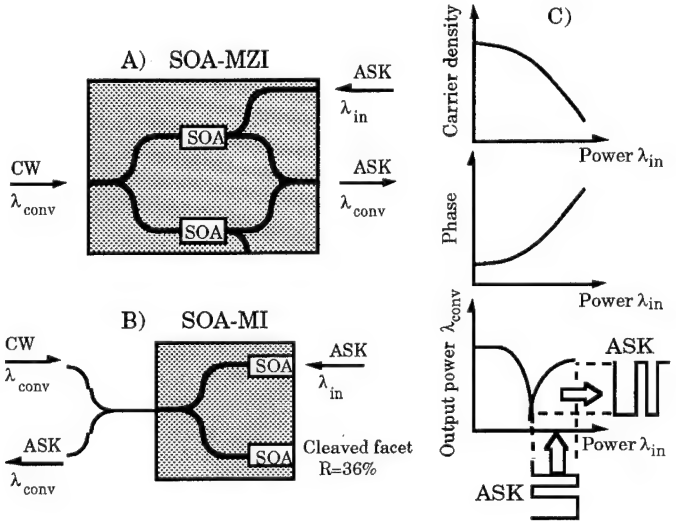

Fig. 1 Schematic of interferometric converters: (A) SOA-MI and (B) SOA-MZI, and (C) operation principle.

In the Mach-Zehnder configuration shown in Fig. 1a, the incoming signal to be converted at λ_{in} depletes carriers in one SOA and accordingly changes the phase difference between the two interferometer arms, thereby modulating the transfer function experienced by the CW-signal at λ_{conv}

(see Fig. 1c). The input arm used to couple the input signal into one of the SOAs might, however, be avoided by simply using asymmetric splitting ratios of the two couplers forming the interferometer [13,23]. The Michelson configuration is basically a folded version of the MZI, and the principle of operation is therefore very similar (see Fig. 1b). The two configurations will be compared later.

The possibility for wavelength conversion by use of the SOA-MZI and the SOA-MI configurations was first demonstrated by hybrid interferometers [10,13-14], however, both versions have recently been monolithically integrated resulting in compact converters with excellent stability. The fabrication of the SOA-MZI and the SOA-MI is described in [23-25] and [26-27], respectively.

The operation principle of the interferometric wavelength converters is clearly illustrated in Fig. 2, that gives the measured static characteristics of a monolithic integrated SOA-MI (two 500 μm long SOAs have been integrated with a 2.5 mm long passive power splitter). It is worth noticing that a variation of the power at λ_{conv} of more than 20 dB is possible for a 5-10 dB variation of the power at λ_{in}. Hence, the interferometric converters give the possibility for an extinction ratio improvement of the converted signal compared to that of the input signal. Note that when operated on the positive slope in Fig. 2, the converted data have the same polarity as the input data.

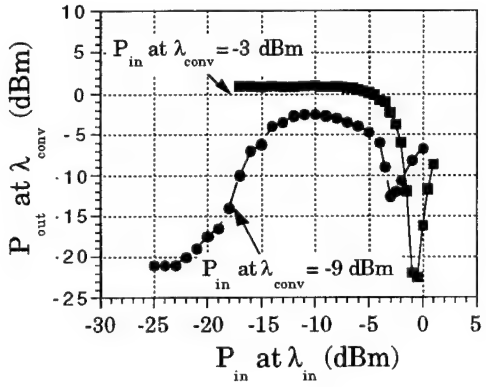

Fig. 2 Static characteristics of SOA-MI when λ_{conv} is 1570 nm and λ_{in} is 1556 nm. Bias current to the SOAs is 50 and 75 mA. The parameter is the coupled input power at λ_{conv}.

Performance of interferometric converters: Obviously, the maximum bit rate that can be converted is determined by the carrier dynamics of the SOAs. Penalty-free wavelength conversion at 10 Gbit/s has been reported by use of a SOA-MI [26-27] and at 5 Gbit/s by use of a SOA-MZI [23]. However, modulation bandwidths in excess of 20 GHz have been reported for discrete SOAs by operating at high optical power levels [10]. Moreover, the bandwidth increases strongly with increasing confinement factor and bias current [28]. Hence, the possibility for conversion of 40 Gbit/s data seems feasible although a high confinement factor might be difficult to realise with integrated structures.

One of the superior advantages of the interferometric structures compared to most conversion techniques is their ability to convert to longer and shorter wavelength with equal performance. This is because the differential refractive index of SOAs is almost wavelength independent [29]. The measured penalty for up- and down-conversion of 10 Gbit/s data is shown in Fig. 3 for the

SOA-MI. Note that penalty-free conversion is achieved over a wavelength range corresponding to the bandwidth of an EDFA.

Another attractive property of interferometric converters is that they can be made polarisation insensitive; the carrier depletion and hence the phase shift is independent of the polarisation of the signal to be converted as long as the gain of the SOA is polarisation insensitive. It should be emphasised, that today polarisation independent SOAs are made routinely in many laboratories [30-31].

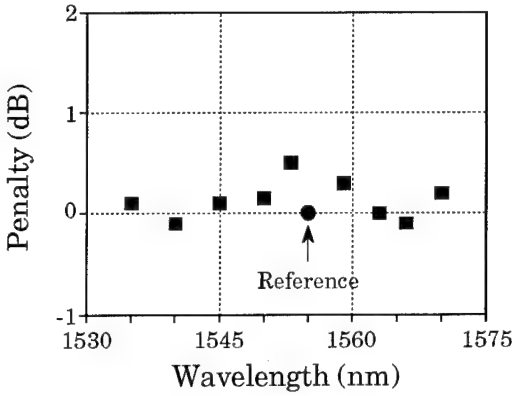

Fig. 3 Conversion with SOA-MI of 10 Gbit/s data to different wavelengths. P_{in} is -4 dBm and P_{conv} is -3 dBm.

Interferometric converters also feature converted signals with very high spectral purity, as shown in Fig. 4, where 10 Gbit/s converted data are transmitted over 60 km of non-dispersion shifted fiber. An additional feature, is the possibility to perform spectral cleaning and to improve the extinction ratio upon conversion, as also illustrated in Fig. 4. Moreover, interferometric converters can easily be cascaded because of both the high extinction ratio and a high signal-to-noise ratio for the converted signals [26].

The disadvantage of the interferometric converters are their sensitivity to the input signal power. As an example, with the operating conditions in Fig. 3 (for the SOA-MI), a 4 dB variation of the average power at λ_{in} results in a 3 dB reduction of the extinction ratio of the converted signal, corresponding to a 1 dB penalty. Therefore, the deployment of interferometric wavelength converters will generally require control of the operating conditions.

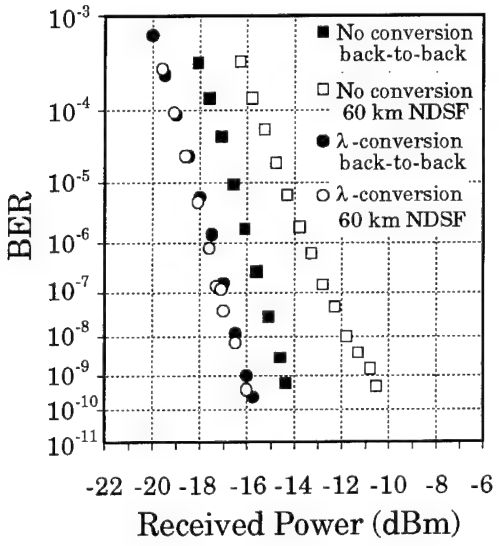

Fig. 4 Wavelength conversion of 10 Gbit/s data with simultaneous extinction ratio improvement and spectral cleaning (SOA-MI). Transmission is performed over 60 km of standard non-dispersion shifted fiber (NDSF).

Comparison of SOA-MZI and SOA-MI: Although the SOA-MZI and SOA-MI have almost identical performance, there are also some differences: the SOA-MZI allows the CW-signal and the input signal to be launched counter-directionally avoiding the need for optical filtering, whereas for the SOA-MI a part of the original signal will always pass through the converter and, hence, will be transmitted along with the converted signal if no filter is applied. This also prohibits the input and output wavelength for the SOA-MI to be identical. Wavelength conversion to the same wavelength might, however, be

possible simply by turning off the CW-signal allowing the SOA-MI to function as an ordinary amplifier. On the other hand, the SOA-MI allows the incoming signal to be coupled to only one SOA (interferometer arm) without using couplers. Therefore, the SOA-MI is expected to be less sensitive to the wavelength and the polarisation of the incoming signal. Moreover, since the converted signal in the SOA-MI passes the same 3-dB splitter twice, the attainable extinction ratio is relatively insensitive to a non-ideal splitting ratio in the splitter. Nevertheless, both types of converters seem at present to be very attractive for realisation of practical wavelength converters.

Conclusion: The principle of operation of wavelength converters based on interferometric structures containing SOAs as phase shifters is discussed. First versions of monolithic integrated Mach-Zehnder and Michelson interferometers have been realised and very promising results are obtained. By further device optimisation such as integration of interferometers with polarisation insensitive SOAs featuring high confinement factors, even better performance is envisaged.

Acknowledgement: Alcatel Alsthom Recherche, Thomson-CFS, France, Ericsson Components, Sweden and SEL-Alcatel, Germany are acknowledged for supplying the interferometric devices.

References

[1] K. Sato et al., J. Selected Areas in Com., Vol. 12, No. 1, pp. 159-170, Jan. 1994.
[2] A.A.M. Saleh, Techn. Dig. of OFC'95, paper ThE1, San Diego, Feb. 1995.
[3] M. Sotom et al.,in Proc. of ICC'93 Workshop on All-Optical Networks, Geneva, May 1993, paper 2.
[4] B. Mikkelsen et al., Proc. of Photonics in switching'95, paper PWE1, Salt Lake City, Marts 1995.
[5] F. Tillerot et al., Techn. Dig. of OFC'95, paper WJ5, San Diego, Feb. 1995.
[6] Jourdan et al., Techn. Dig. of OFC'95, paper ThI7, San Diego, Feb. 1995.
[7] S.L. Danielsen et al., Proc. of Photonics in switching'95, paper PWE2, Salt Lake City, Marts 1995.
[8] M. Calzavara et al., Techn. Dig. of ECOC'94, pp. 567-570, Florence, Sept. 1994.
[9] D. Norte and A.E. Wilner, Techn. Dig. of OFC'95, paper WJ6, San Diego, Feb. 1995.
[10] B. Mikkelsen et al., Techn. Dig. of ECOC'93, pp. 73-76, Montreux, Sept., 1993.
[11] C. Joergensen et al., Techn. Dig. of OFC '94, paper ThQ2, San Jose, California, Feb. 1994.
[12] J.M. Wisenfield et al., Electron. Lett., Vol. 30, pp. 720-721, 1994.
[13] T. Durhuus et al., Photon. Techn. Lett. , Vol. 6, pp. 53-55, Jan. 1994.
[14] B. Mikkelsen et al., Electron Lett., Vol. 30, pp. 260-261, Feb. 1994.
[15] A.D. Ellis et al., Techn. Dig. of ECOC'94, pp. 121-124, Florence, Sept 1994
[16] R.J. Pedersen et al., Techn. Dig. of OFC'94, paper ThQ3, San Jose, Feb. 1994.
[17] K. Weich et al., Techn. Dig. of ECOC'94, pp. 643-646, Florence, Sept 1994
[18] S. Gurib et al., Techn. Dig. of OFC'95, paper TuO3, San Diego, Feb. 1995.
[19] E. Lach et al., Techn. Dig. of ECOC'93, paper TuC5.4, Montreux, Sept., 1993.
[20] H. Yasaka et al., Electron Lett., Vol. 30, pp. 133-134, Jan. 1994.
[21] D.M. Patric and R.J. Manning, Electron Lett, Vol. 30, pp. 252-253, Feb. 1994.
[22] H.G. Weber et al., Techn. Dig. of OAA'94, paper FC1, Breckenridge, July 1994.
[23] T. Durhuus et al., Techn. Dig. of OFC'95, paper TuO6, San Diego, Feb. 1995.
[24] M. Schilling et al., Techn. Dig. of ECOC'94, pp. 647-650, Florence, Sept 1994
[25] N. Vodjdani et al., Techn. Dig. of ECOC'94, paper PD 95-98, Florence, Sept 1994
[26] B. Mikkelsen et al., Techn. Dig. of ECOC'94, PD-paper, pp. 67-70, Firenze, Sept. 1994.
[27[B. Mikkelsen et al., Techn. Dig. of OFC'95, paper TuD4, San Diego, Feb. 1993.
[28] B. Mikkelsen et al., To be puplished.
[29] N. Storkfelt et al., Electron Lett., Vol. 28, pp. 1774-1775, Sept. 1992.
[30] P. Doussiere et al., Techn. Dig. of OAA'92, p. 140 ,Santa Fe, New Mexicos, July 1992.
[31] L.F. Tiemeijer et al., Techn. Dig. of OAA'94, paper WD21, Breckenridge, July 1994.

Optical buffering at 10 Gbit/s employing a monolithically integrated all optical interferometric Michelson wavelength converter

S. L. Danielsen, B. Mikkelsen, C. Joergensen, T. Durhuus, K. E. Stubkjaer
Technical University of Denmark, Electromagnetics Institute, Bldg 348,
Center for Broadband Telecommunications, DK-2800 Lyngby,
Tlf.: +45 42 88 14 44, Fax: +45 45 93 16 34

Introduction: Future networks are likely to utilise optical switching to avoid the bottleneck of electronics [1]. Both optical cross connects operating in a circuit switched mode and optical packet switches could be implemented to achieve the highest degree of flexibility and transparency [2].

An important part of a packet (cell) switch is the buffer that is used for contention resolution. Optically, the buffer can be realised by fiber delay-lines [3]. However, to ensure a low cell loss probability the delay-line must have a length of 40-80 cell duration's which for an ATM cell corresponds to 1-3 km of fiber at 2.5 Gbit/s. Therefore, stability is of big concern. In [4] a multi wavelength fiber loop buffer architecture using tuneable filters and optical gates was proposed and successful storage of cells at 622 Mbit/s shown. Here, we report a novel buffer architecture operating at 10 Gbit/s. Based on the functionality of wavelength converters the wavelength domain is utilised to enable simultaneous storage of several cells in the same fiber loop. As a key device for controlling the buffering in the loop, we use a monolithically integrated Michelson interferometric converter [5], fabricated as the 4x4 gate switch array previously reported in [6]. Very efficient and stable wavelength conversion can be obtained with integrated interferometric converters using semiconductor optical amplifiers (SOA's) integrated in a Michelson or Mach Zehnder configuration [5,7]. We assess these qualities experimentally at 10 Gbit/s by successfully operating the novel memory configuration with one cell capacity.

Operating principle of the buffer: The all optical buffer architecture is shown schematically in Fig. 1. To illustrate an application, the buffer is placed at an outlet of a packet switch (other applications would be input buffering in a packet switch, use in time slot interchanges etc.). At the inlet of the packet switch, cells are wavelength converted to match the desired delay in the buffer and routed to the appropriate outlet. If a cell has to be stored for one cell period it is converted to λ_2 at the inlet of the switch and forwarded to the buffer for the desired outlet. In the buffer a wavelength demultiplexer routes the cell to a wavelength converter that converts the cell to λ_1. This will lead to one pass through the loop, since λ_1 is the output wavelength of the buffer. In case the cell has to be stored for two cell periods the cell is converted to λ_3 at the switch inlet. This leads to conversion to λ_2 followed by conversion to λ_1 in the buffer

resulting in a total of two trips through the loop. Following the above procedure, cells can be stored for n cell periods by use of n converters. It should be noted, that to minimise the required number of converters, variants of the buffer architecture that include additional loops with different lengths are possible but will not be discussed further in this paper.

Experiments and results: The buffer capability of the architecture is evaluated by a system experiment at 10 Gbit/s. The experimental setup is given in Fig. 2. Two wavelength channels at 1543 and 1556 nm are externally modulated by a MZI modulator. The modulating signal is a 2^9-1 PRBS sequence (approximately the length of an ATM cell) followed by a number of empty bits (guard band) matching the loop. Collision would occur if the two cells were coupled directly to the same fiber. Therefore, we demonstrate delay of one channel for one cell period.

The buffer experiment is operated in the following way : A wavelength demultiplexer consisting of two 1 nm filters selects the two channels. One channel (1543 nm) is coupled directly to a sampling oscilloscope while the other (1556 nm) is coupled into the loop. Here, the wavelength is converted to 1543 nm following the principle described in [5]. The converted signal is selected by a filter and stored in the fiber loop thereby avoiding collision of the original two cells. After two cell duration's both delayed and non-delayed cells will have passed the buffer, and arrive in sequence at the output where a sampling oscilloscope is used to assess the quality of the buffer.

The results of the experiments are given in Fig. 3 and 4. In Fig. 3.a, b and c time traces at different places in the setup are shown. Fig. 3.a gives the trace at the buffer output (1543 nm) for the cell routed directly through the buffer. The trace in Fig. 3.b originate from the cell at 1556 nm just before conversion. Converted pulses at the buffer output at 1543 nm are shown in Fig. 3.c. Due to the short fiber involved (compared to fiber lengths of 1-3 Km), stable storage of 10 Gbit/s cells with lengths of 511 bits is observed and in Fig. 4 cells at the buffer output are depicted. Fig. 4.a gives a trace of the non-delayed cells at 1543 nm while Fig. 4.b shows a converted cell delayed for one period through the loop. Finally, Fig. 4.c gives the total cell stream out of the buffer with suitable guard bands for setting up components. As illustrated in Fig. 3, data quality is preserved within the buffer and by using an EDFA and attenuater in the loop (not shown in the setup) equal signal levels of the cells is achieved. However, by further adjusting the power levels this amplifier could be avoided.

As presented in [5] the converter operates penalty free at 10 Gbit/s so that no penalty is associated with the buffering of the cells. The signal-to-spontaneous emission noise ratio for the converted signal (measured in an optical bandwidth of 1 nm) is more than 30 dB [5]. In addition to this, interferometric converters are able to improve the signal extinction ratio as well as to convert to all wavelengths within the EDFA window with

equal performance [5,7,8]. These features easily allows cascading of several converters (>10) thereby showing the potential for larger buffers by using this type of converter.

Conclusion: A simple and efficient multi wavelength all optical fiber loop buffer using optical wavelength converters has been proposed and experimentally tested at 10 Gbit/s. The wavelength converter is realised by SOA's monolithically integrated in a Michelson interferometer. Excellent operation for storing of one cell has been presented illustrating the feasibility of this buffer scheme. Hence, the proposed novel memory architecture is considered a promising candidate for high performance all optical cell storage.

Acknowledgement: The authors wish to thank Mats Gustavsson of Ericsson Components AB for supplying the wavelength converter.

References:

[1] P. Green et al., Jour. of Light. Technol., vol. 11, pp. 754-763, May 1993.
[2] A. Fioretti et al., in Proc. of ECOC '94, vol. 2, pp. 503-509, Florence, 1994.
[3] J. M. Gabriagues et al., in Proc. of ECOC '91, vol. 2, pp. 59-66, Paris, 1991.
[4] M. Calzavara et al., in Technic. Digest of OFC '93, vol. 4, pp. 19-20, San Jose, 1993.
[5] B. Mikkelsen et al., in Proc. of ECOC '94, PDP, pp. 67-70, Florence, 1994.
[6] M. Gustavsson et al., in Proc. of OA '92, PD9, Santa Fe, 1992.
[7] N. Vodjdani et al., in Proc. of ECOC '94, PDP, pp. 95-98, Florence, 1994.
[8] T. Durhuus et al., IEEE Photon Technol. Lett., vol. 6, pp. 53-55, Jan. 1994.

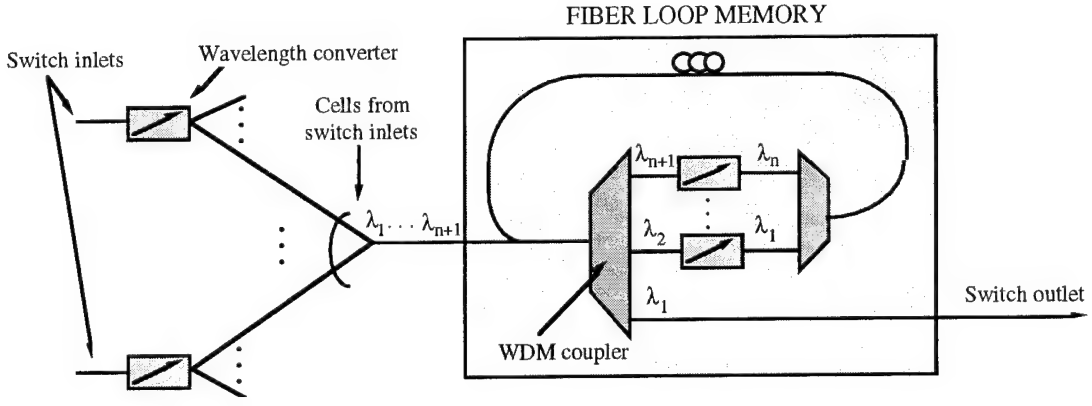

Fig.1 : Fiber loop memory employing all optical wavelength converters. At the switch inlet cells are wavelength converted. If a cell has to be stored for n cell periods it is converted to λ_{n+1} and in the buffer to λ_n,...,λ_2 and finally to λ_1 before it is directed to the output.

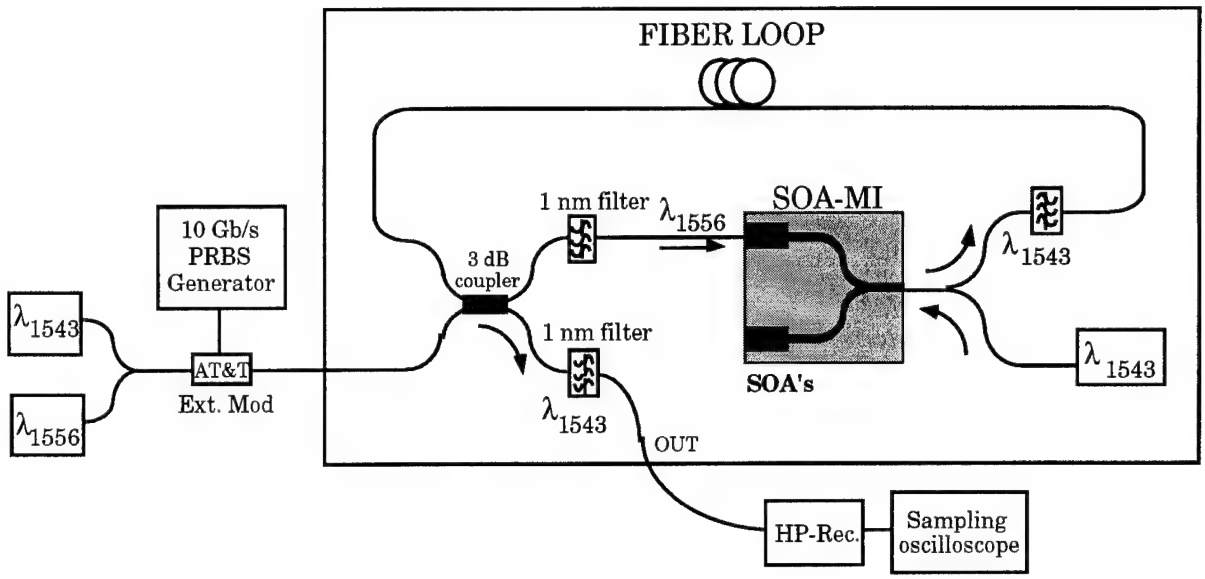

Fig.2 : Experimental setup for buffer experiment.

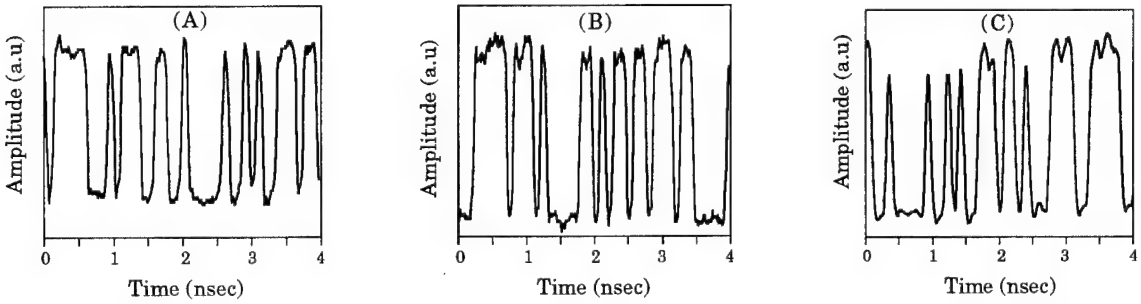

Fig.3 : 10 Gbit/s pulse traces taken within the cells at different places in the buffer. (A): Non-delayed cell at 1543 nm at the buffer output. (B): Cell at 1556 nm before the wavelength converter. (C): Delayed and converted cell at 1543 nm at the buffer output.

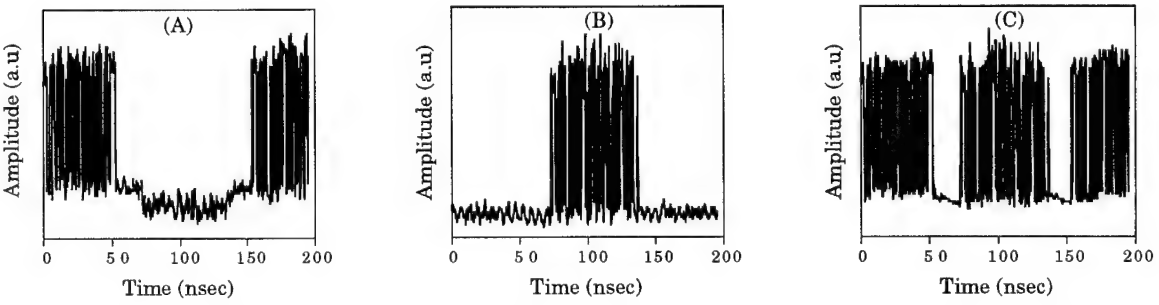

Fig.4 : Cell streams at the output of the buffer. (A): Non-delayed cells at 1543 nm routed directly through the buffer. (B): Converted and delayed cell at 1543 nm. (C): Total cell stream at the buffer output with suitable guard bands to clarify cell boundaries.

Abe, Haruo — FB5
Abramov, A. A. — SaA2
Aida, Kazuo — ThE2
Almström, Erland — FA2
Alphonsus, J. — FC5
Andrejco, M. J. — FC1
Andrekson, Peter A. — FB2
Antos, A. J. — FB2
Artigaud, S. — SaB5
Aspell, J. — FC1

Baney, Douglas M. — ThE
Basiev, T. T. — ThD6
Belov, A. V. — ThD1
Bergano, Neal S. — FB
Berglind, Eilert — FA2
Bertilsson, Kent — FB2
Besse, P. A. — FA3
Beylat, J. L. — ThD4
Billes, L. — ThD8
Borick, J. — FC4
Bousselet, P. — ThD4, FA4
Brillouet, Francois — FA
Bubnov, M. M. — SaA2

Camy, Patrice — FD2
Cheung, W. Y. — SaA4
Chiang, T.-K. — SaA3
Chikama, T. — FC3
Chiquet, F. — ThD4
Cho, S. H. — ThC2
Choe, W. H. — ThD1, FC2
Chou, H. — ThE1
Chraplyvy, Andrew R. — SaB2, SaB3
Chrostowski, J. — ThE3
Cinguino, P. — ThD9
Clesca, B. — SaB5
Conover, S. D. — ThC1

de Waardt, Hugo — FA5
Dagenais, M. — ThC2
Danielsen, S. L. — SaA4, SaC5
Davidson, C. R. — ThB2
Davies, D. A. O. — SaC1
Delfyett, P. J. — SaC2
Di Vita, Pietro M. — ThA2
DiGiovanni, D. J. — FC1, SaA4
Dianov, E. M. — ThD1, SaA2
Dienes, A. — SaC2
Diez, S. — SaC3
Doroshenko, M. E. — ThD6
Doussiere, P. — FA4
Duff, D. G. — ThB2
Durhuus, T. — SaC4, SaC5

Ellis, A. D. — SaC1
Epworth, Richard — ThD3
Erdogan, T. — FC4, SaA4
Eskildsen, L. — FC5

Fillion, T. — FA4
Forghieri, Fabrizio — SaB2, SaB3
Fox, S. — ThC2
Fraser, J. — ThE3
Fujiura, Kazuo — ThE4
Fukada, Youichi — ThD2
Fukutoku, Mitsunori — SaB4

Georges, Eric Saint — ThD5
Georges, Thierry — SaA
Giles, C. R. — ThD12
Gillner, Lars — FA2
Giuliani, G. — ThD9
Gnauck, A. H. — ThB4
Goix, M. — FA4
Goldstein, Evan — ThB
Gopalan, B. — ThC2
Goto, Koji — FB5
Granlund, S. W. — FC4
Grant, R. S. — SaC2
Grasso, Giorgio — ThB1
Grubb, S. G. — SaA1, SaA4
Guryanov, A. N. — ThD1, SaA2

Han, Jung-Hee — ThD11
Hansen, P. B. — FC5
Heim, P. J. S. — ThC2
Hempstead, Martin — FD1, FD2
Hewak, D. W. — SaA5
Heritage, J. P. — SaC2
Himeno, K. — FC6
Holtmann, Chris — FA3
Hong, M. Y. — SaC2
Hoshino, Koichi — ThE4
Huang, S.-H. — ThD14

Ichihashi, Yasutaka — ThD2
Inoue, Kyo — SaB1
Iwatsuki, Katsumi — FB3

Jacobovitz-Veselka, G. R. — FC4
Jennen, Jean G. L. — FA5
Jensen, R. A. — ThB2
Joergensen, C. — SaC4, SaC5
Jørgensen, Bo Foged — ThD15

Kagi, N. — SaA3
Kakui, Motoki — ThB3
Kanamori, Terutoshi — ThE4
Kareenahalli, S. — ThC2
Karpov, V. I. — ThD1
Kataoka, T. — FB4
Kawakami, H. — FB4
Kawazawa, Toshio — FB5
Kazovsky, L. G. — SaA3
Khopin, V. F. — ThD1, SaA2
Kim, Hyang-Kyun — ThD11
Kim, S. J. — ThD1, FC2
Kindt, S. — SaC3
Kinoshita, S. — FC3
Koltchanov, I. — SaC3
Koren, U. — FA1
Kristen, G. — SaC3
Kuramochi, Eiichi — ThC3
Kurkov, A. V. — ThD1

Laborde, Pascale — FD2
Laming, R. I. — SaA5
Larsen, Claus Popp — FA2

Laube, G. — FA4
Leclerc, D. — FA4
Lee, Chang-Hee — ThD11
Lee, Jae-Seung — ThD11
Lee, S. H. — FC2
Lee, Sang-Soo — ThD11
Lemaire, P. J. — SaA4
Lerminiaux, Christian — FD2
Lester, Christian — FB2
Liedenbaum, Coen T.H.F. — FA5
Ludwig, R. — SaC3
Lui, Wayne W. — ThD10

Maeda, Hideki — ThD2
Magari, Katsuaki — ThD10
Malone, Kevin — FD
Mamyshev, P. V. — FB1
Manning, R. J. — SaC1
Marhic, M. E. — SaA3
Marquant, A. — ThD4
Masuda, Hiroji — ThE2
McCormick, A. — ThD12
Mecozzi, Antonio — ThD13
Meier, Heinz — ThC
Melchior, Hans — FA3
Merritt, S. A. — ThC2
Midwinter, John E. — ThA1
Mikkelsen, B. — SaC4, SaC5
Mito, Ikuo — ThA
Mizrahi, V. — FC4, SaA4
Mollenauer, L. F. — FB1
Morkel, Paul R. — SaB
Myslinski, P. — ThE3

Nagel, J. A. — SaB2
Newhouse, Mark A. — FB2
Ngo, R. — FA4
Nilsson, J. — FC2
Nishi, Shigendo — FB3
Nishida, Yoshiki — ThE4
Nishimura, Masayuki — ThB3
Nishiya, Teruhiko — ThC3

Ó Cochláin, C. R. — ThC1
Oda, Kazuhiro — SaB1, SaB4
Okude, S. — FC6
Ohishi, Yasutake — ThE4
Osiko, V. V. — ThD6
Otani, Tomohiro — FB5

Papashvili, A. G. — ThD6
Park, E. — ThD14
Patrick, D. M. — SaC1
Payne, D. N. — SaA5
Peckham, D. W. — SaA4
Pedersen, Rune J. S. — ThD15, SaC4
Petermann, K. — SaC3
Pierre, L. — SaB5
Pommerau, F. — FA4
Protopopov, V. N. — ThD1

Reed, W. A. — SaA4
Reid, John J. E. — FA5
Riant, I. — ThD4
Risko, J. J. — ThB2
Rockney, B. H. — SaA4
Román, José E. — FD2
Rottwitt, Karsten — FB2

Sakai, T. — FC6
Schebunjaev, A. G. — SaA2
Scheffel, L. A. — ThC1
Schimpe, R. — ThD7, SaC3
Schnabel, R. — SaC3
Schweiker, W. — ThD7
Seano, V. — ThD9
Semjonov, S. L. — SaA2
Sharfin, W. F. — ThC1
Shigematsu, Masayuki — ThB3
Shin, Sang-Yung — ThD11
Shipulin, A. V. — SaA2
Sigachev, V. B. — ThD6
Simon, J. C. — ThD8
Stewart, Moira — ThD3
Stimple, J. — ThE1
Strasser, T. — SaA4
Stubkjaer, K. E. — SaC4, SaC5
Sudo, Shoichi — ThE4
Sugaya, Y. — FC3
Sugo, Mitsuru — ThC3
Suzuki, Ken-ichi — FB3

Tamamura, Toshiaki — ThC3
Tanaka, Masando — FB5
Temmyo, Jiro — ThC3
Thiery, J. P. — SaB5
Tiemeijer, Luuk F. — FA5, SaC
Tkach, R. W. — SaB2, SaB3
Toba, Hiromu — SaB1, SaB4
Truxal, D. — FC5
Tsvetkov, M. Yu — ThD1

Valiente, I. — ThD8
van der Plaats, J. C. — FC1
Vengsarkar, A. M. — FC4, SaA4
Vusirikala, V. — ThC2

Wada, A. — FC6
Wakabayashi, Hiroharu — FB5
Weber, H. G. — SaC3
Willems, F. W. — FC1
Willner, A. E. — ThD14
Wood, C. E. C. — ThC2
Wysocki, P. — FC1, FC4

Yamamoto, Hitoshi — FB5
Yamauchi, R. — FC6
Yokoyama, Kiyoyuki — ThD10
Yun, Tae-Yeoul — ThD11

Zervas, Michael N. — FC
Zou, X. Y. — ThD14

OPTICAL AMPLIFIERS AND THEIR APPLICATIONS 1995
TECHNICAL PROGRAM COMMITTEE

GENERAL CHAIRS

William J. Miniscalco, *GTE Laboratories, Inc., U.S.A.*
Ikuo Mito, *NEC Corporation, Japan*
John J. O'Reilly, *University College London, U.K.*

EUROPEAN CHAIR

Hans Melchior, *Swiss Federal Institute of Technology, Switzerland*

PROGRAM CHAIRS

Robert Jopson, *AT&T Bell Laboratories, U.S.A.*
Kristian Stubkjaer, *Technical University of Denmark, Denmark*
Masuo Suyama, *Fujitsu Ltd., Japan*

SUBCOMMITTEE 1: FIBER AND ACTIVE WAVEGUIDES

Yasutake Ohishi, *NTT, Japan, Subcommittee Chair*
Douglas Baney, *Hewlett Packard, U.S.A.*
Steven Frisken, *Photonic Technologies Pty. Ltd., Australia*
Thierry Georges, *CNET, France*
Stephen Grubb, *AT&T Bell Laboratories, U.S.A.*
Kevin Malone, *NIST, U.S.A.*
Mark Newhouse, *Corning, Inc., U.S.A.*
Masayuki Nishimura, *Sumitomo, Japan*
Bo Pedersen, *NKT Research Center, Denmark*
Akira Wada, *Fujikura, Japan*
Tim Whitley, *BT Laboratories, U.K.*
Michael Zervas, *University of Southampton, U.K.*

SUBCOMMITTEE 2: SEMICONDUCTOR DEVICES AND FUNCTIONAL CIRCUITS

Mats Gustavsson, *LM Ericsson, Sweden, Subcommittee Chair*
Shigehisa Arai, *Tokyo Institute of Technology, Japan*
Francois Brillouet, *Alcatel Alsthom Recherche, France*
Tatsuo Kunii, *Oki Electric Industry Company, Japan*
Shinya Sasaki, *Hitachi, Japan*
Wayne Sharfin, *Lasertron, U.S.A.*
Luuk F. Tiemeijer, *Philips, The Netherlands*
Kerry J. Vahala, *California Institute of Technology, U.S.A.*
Hans G. Weber, *Heinrich-Hertz-Institut, Germany*
Jay M. Wiesenfeld, *AT&T Bell Laboratories, U.S.A.*

SUBCOMMITTEE 3: SYSTEMS AND NETWORKS

Neal Bergano, *AT&T Bell Laboratories, U.S.A., Subcommittee Chair*
Stephen B. Alexander, *Ciena Corporation, U.S.A.*
Jan Conradi, *Telecommunications Research Laboratories, Canada*
Noboru Edagawa, *KDD R&D Laboratories, Japan*
K. Emura, *NEC, Japan*
Evan Goldstein, *Bellcore, U.S.A.*
Masahiko Jinno, *NTT, Japan*
Sonny Johansson, *Ellemtel Telecom Systems Lab., Sweden*
Paul R. Morkle, *STC Submarine Systems, U.K.*
Michael G. Taylor, *BNR Europe Ltd., U.K.*